

Wrocław University of Technology

Control in Electrical Power Engineering

Marek Michalik, Eugeniusz Rosołowski

Simulation and Analysis of Power System Transients

Simulation and Analysis of Power System Transients

Wrocław 2010

Copyright © by Wrocław University of Technology
Wrocław 2010

Reviewer: Mirosław Łukowicz

Project Office

ul. M. Smoluchowskiego 25, room 407
50-372 Wrocław, Poland
Phone: +48 71 320 43 77
Email: studia@pwr.wroc.pl
Website: www.studia.pwr.wroc.pl

CONTENTS

PREFACE	5
1. DISCRETE MODELS OF LINEAR ELECTRICAL NETWORK	7
1.1. Introduction	7
1.2. Numerical solution of differential equations	8
1.2.1. Basic algorithms	8
1.2.2. Accuracy of operation and stability	12
1.3. Numerical models of network elements	14
1.3.1. Resistance	14
1.3.2. Inductance	14
1.3.3. Capacitance	16
1.3.4. Complex RLC branches.....	17
1.3.5. Controlled sources	18
1.3.6. Frequency properties of discrete models	19
1.3.7. Distributed parameters model (long line model)	21
1.4. Nodal method	28
1.4.1. Derivation of basic nodal equations.....	28
1.4.2. Simulation algorithm	31
1.4.3. Initial conditions	33
1.5. Numerical stability of digital models.....	35
1.5.1. Numerical oscillations in transient state simulations.....	35
1.5.2. Suppression of oscillations by use of a damping resistance.....	37
1.5.3. Suppression of numerical oscillations by change of integration method	40
1.5.4. The root matching technique	41
Exercises.....	46
2. NON-LINEAR AND TIME-VARYING MODELS	49
2.1. Solution of non-linear equations.....	49
2.1.1. Newton method	49
2.1.2. Newton–Raphson method	52
2.2. Models of non-linear elements	53
2.2.1. Resistance.....	54
2.2.2. Inductance	57
2.2.3. Capacitance	59
2.3. Models of non-linear and time-varying elements	60
2.3.1. Non-linear and time-varying scheme	60
2.3.2. Compensation method.....	60
2.3.3. Piecewise approximation method.....	64
Exercises.....	66

3. STATE-VARIABLES METHOD	67
3.1. Introduction	67
3.2. Derivation of state-variables equations.....	69
3.3. Solution of state-variables equations	72
Exercises.....	74
4. OVER-HEAD LINE MODELS.....	75
4.1. Single-phase Line Model.....	75
4.1.1. Line Parameters.....	75
4.1.2. Frequency-dependent Model	77
4.2. Multi-phase Line Model	91
4.2.1. Lumped Parameter Model.....	91
4.2.2. Distributed Parameters Model.....	98
Exercises.....	111
5. TRANSFORMER MODEL.....	113
5.1. Introduction	113
5.2. Single-phase Transformer.....	114
5.2.1. Equivalent Scheme	114
5.2.2. Two-winding Transformer	117
5.2.3. Three-winding Transformer	123
5.2.4. Autotransformer Model.....	125
5.2.5. Model of Magnetic Circuit.....	126
5.3. Three-phase Transformer	132
5.3.1. Two-winding Transformer	132
5.3.2. Multi-winding Transformer.....	140
5.3.3. Z (zig-zag)-connected Transformer.....	145
Exercises.....	148
6. MODELLING OF ELECTRIC MACHINES.....	151
6.1. Synchronous Machines.....	151
6.1.1. Model in $0dq$ Coordinates	152
6.1.2. Model in Phase Coordinates.....	168
6.2. Induction Machines	169
6.2.1. General Notes.....	169
6.2.2. Mathematical Model	171
6.2.3. Electro-mechanical Model	176
6.2.4. Numerical Models	180
6.3. Universal Machine.....	181
Excercises	182
REFERENCES	183
INDEX	189

PREFACE

The availability of modern digital computers has stimulated the use of computer simulation techniques in many engineering fields. In electrical engineering the computer simulation of dynamic processes is very attractive since it enables observation of electric quantities which can not be measured in live power system for strictly technical reasons. Thus the simulation results help to analyse the effects which occur in transient (abnormal) state of power system operation and also provide the valuable data for testing of new design concepts.

In case of computer simulation the continuous models have to be transformed into the discrete ones. The transformation is not unique since differentiation and integration may have many different numerical representations. Thus the selection of the numerical method has the essential impact on the discrete model properties. The basic difference between continuous and discrete models is observed in frequency domain: the frequency spectrum of signals in discrete models is the periodic function of frequency and the period depends on simulation time step applied. Another problem is related to numerical instability of discrete models which manifests itself in undamped oscillations even though the corresponding continuous models are stable. The arithmetic roundup affecting digital calculation accuracy may also contribute to the discrete models instability.

In this book all the aforementioned topics are concerned for discrete linear and nonlinear models of basic power system devices like: overhead transmission lines, cable feeders, transformers and electric machines. The relevant examples are presented with special reference to ATP-EMTP software package application.

We hope that the book will come in useful for both undergraduate and postgraduate students of electrical engineering when studying subjects related to digital simulation of power systems.

Wroclaw, September 2010

Authors

1. DISCRETE MODELS OF LINEAR ELECTRICAL NETWORK

1.1. Introduction

The simulation of power networks is aimed at detailed analysis of many problems and the most important of them are:

- determination of power and currents flow in normal operating conditions of the network,
- examination of system stability in normal and abnormal operating conditions,
- determination of transients during disturbances that may occur in the network,
- determination of frequency characteristics in selected nodes of the network.

The network model is derived from differential equations that relate currents and voltages in network nodes according to Kirchhoff's law. The simulation models are usually based upon equivalent network diagrams derived under simplified assumptions (which sometimes can be significant) that are applied to the network elements representation. In this respect models can be divided into two basic groups:

1. Lumped parameter models. 3D properties of elements are neglected and sophisticated electromagnetic relations that include space geometry of the network are not taken into account.
2. Distributed parameter models. Some geometrical parameters are used in the model describing equations (usually the line length).

In classic theory relations between currents and voltages on the network elements are continuous functions of time. In digital simulations the numerical approach must be applied. Two ways are applied for this purpose:

- transformation of continuous differential relations into discrete (difference) ones,
- state variable representation in continuous domain and its solution by use of numerical methods.

Consequences of transformation from continuous to discrete time domain:

- problem of accuracy - discrete representations are always certain (more or less accurate) approximation of continuous reality,
- frequency characteristics become periodic according to Shannon's theorem,

- problem of numerical stability - numerical instability may appear even though the continuous representation of the network is absolutely stable.

1.2. Numerical solution of differential equations

1.2.1. Basic algorithms

In electric networks with lumped parameters the basic differential equation that describes dynamic relation between physical quantities observed in branches with linear elements (R, L, C) takes the form:

$$\frac{dy(t)}{dt} + \lambda y(t) = bw(t) \quad (1.1)$$

where $y(t)$, $w(t)$ denotes electric quantities (current, voltage) and λ , b are the network parameters. In case of a single network component (inductor, capacitor) (1.1) simplifies into:

$$\frac{dy(t)}{dt} = bw(t) \quad (1.2)$$

Laplace transformation of (2) yields:

$$sY(s) = bW(s) \quad (1.3)$$

To obtain discrete representation of (1.2) the continuous operator in s-domain must be replaced by the discrete operator z in z-domain ('shifting operator'). The basic and accurate relation between those two domain is given by the fundamental formula:

$$z = e^{sT} \quad (1.4)$$

where T - calculation step.

Approximate rational relations between z and s can be obtained from expansions of (1.4) into power series. Let's consider the following three most obvious cases:

$$1. \quad z = e^{Ts} = 1 + Ts + \frac{(Ts)^2}{2!} + \dots + \frac{(Ts)^n}{n!} + \dots \quad (1.5)$$

Neglecting terms of powers higher than 1 results in approximation:

$$z \cong 1 + Ts \quad (1.6)$$

and further:

$$s \cong \frac{z-1}{T} \quad (1.7)$$

$$2. \quad z = e^{Ts} \approx 1 + Ts + (Ts)^2 + \dots + (Ts)^n + \dots = \frac{1}{1 - Ts} \quad (1.8)$$

Again, if the higher power terms are neglected then:

$$z \cong \frac{1}{1 - Ts} \quad (1.9)$$

and

$$s \cong \frac{z-1}{Tz} \quad (1.10)$$

$$3. \quad z = e^{sT} \quad (1.11)$$

$$s = \frac{1}{T} \ln z = \frac{2}{T} \left[\frac{z-1}{z+1} + \frac{(z-1)^3}{3(z+1)^3} + \dots \right] \quad (1.12)$$

Again, if terms of power higher than 1 are neglected then:

$$s \cong \frac{2(z-1)}{T(z+1)} \quad (1.13)$$

The approximation (1.13) is the well known Bilinear Transformation or Tustin's operator.

Applying the derived approximations of s to differential equation (1.3) three different discrete algorithms for numerical calculation of $w(k)$ integral can be obtained.

Using the first approximation of s (1.7) in (1.3):

$$\frac{z-1}{T} Y(z) = bW(z) \quad (1.14)$$

and, in discrete time domain:

$$\frac{y(k+1) - y(k)}{T} = bw(k) \quad (1.15)$$

The obtained formula (1.15) is the *Euler's forward approximation* of a continuous derivative. The corresponding integration algorithm takes the form:

$$Y(z) = z^{-1}Y(z) + z^{-1}bTW(z) \quad (1.16)$$

and

$$y(k) = y(k-1) + bTw(k-1) \quad (1.17)$$

The algorithm (1.17) realizes iteration that within a single step T can be written as:

$$y(t_k) = y(t_{k-1}) + bT \int_{t_{k-1}}^{t_k} w(\tau) d\tau \quad (1.18)$$

The algorithm (1.17) is of *explicit* type since the current output in k -th calculation step depends only on past values of the input and output in $(k-1)$ instant.

Using the second approximation of s (1.6):

$$\frac{z-1}{zT} Y(z) = bW(z) \quad (1.19)$$

and

$$\frac{y(k) - y(k-1)}{T} = bw(k) \quad (1.20)$$

Now the obtained formula (1.20) is the *Euler's backward approximation* of a continuous derivative. The resulting integration algorithm takes the form:

$$Y(z) = z^{-1}Y(z) + bTW(z) \quad (1.21)$$

and

$$y(k) = y(k-1) + bTw(k) \quad (1.22)$$

This algorithm is of *implicit* type since the current output in k -th instant depends on present value of the input in the same instant.

The algorithm (1.9) which realizes integration within a single step T , can now be written as:

$$y(t_k) = y(t_{k-1}) + bT \int_{t_k}^{t_{k+1}} w(\tau) d\tau \quad (1.23)$$

Using the third approximation of s (1.7) in (1.3) we get:

$$\frac{2(z-1)}{T(z+1)} Y(z) = bW(z) \quad (1.24)$$

$$Y(z) = z^{-1}Y(z) + \frac{Tb(W(z) + z^{-1}W(z))}{2} \quad (1.25)$$

$$y(k) = y(k-1) + \frac{Tb(w(k) + w(k-1))}{2} \quad (1.26)$$

This algorithm (1.26) realizes numerical integration based upon trapezoidal approximation of the input function $w(k)$.

Graphical representation of all derived integrating algorithms is shown in Fig.1.1.

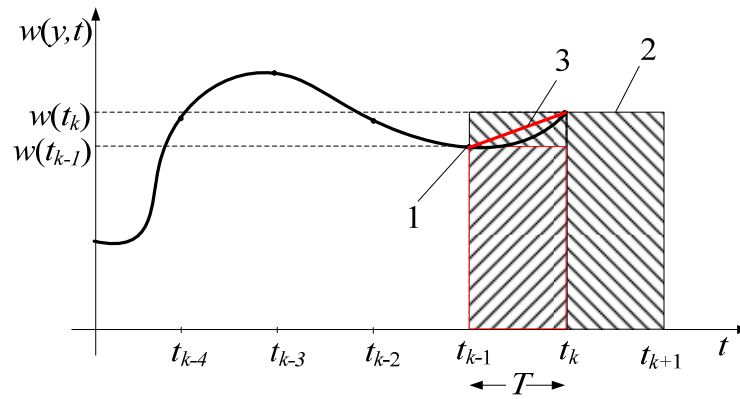


Fig.1.1. Numerical integration; 1 - Euler's 'step back' (explicit) approximation.; 2 - Euler's 'step forward' (implicit) approx.; 3 - trapezoidal approximation

Examination of Fig.1.1 leads to the following conclusions:

- Forward approximation of derivative results in 'step backward' (explicit) integrating algorithm and vice versa. The explicit algorithm tends to underestimate while the implicit one overestimates the integration result.
- The algorithm based on trapezoidal approx. reduces the integration error since its output $y_{TR}(k)$ (1.10) is an average of outputs of both aforementioned algorithms $y_E(k)$ (1.8), $y_I(k)$ (1.10) at any instant k , i.e.

$$y_{TR}(k) = \frac{y_E(k) + y_I(k)}{2} \quad (1.27)$$

In general, the numerical integration methods depend on approximations of continuous derivative (or integral) and can be divided into two groups, namely:

- single step integration methods (self-starting),
- multi-step methods.

All algorithms considered belong to the first group. As an example of a multi-step numerical integrator the 2-nd order Gear algorithm can be shown:

$$y(k) = \frac{4y(k-1) - y(k-2) + Tbw(k)}{3} \quad (1.28)$$

The algorithm is not self-starting one and must be started by use of a single step algorithm but reveals stiff stability properties.

1.2.2. Accuracy of operation and stability

Accuracy of numerical integration for the algorithms considered can be estimated from homogenous form of the eqn.(1.1), i.e.:

$$\frac{dy(t)}{dt} + \lambda y(t) = 0 \quad (1.29)$$

which yields the accurate solution:

$$y(t) = y(t_0)e^{-\lambda t} \quad (1.30)$$

where $y(t_0)$ – initial condition at t_0 ; $\lambda > 0$

Applying s approximations (1.7, 1.10, 1.13) to (1.29) the following numerical expressions are obtained [18]:

- Explicit Euler's method ('step backward') (1.7)

$$y(k) = (1 - \lambda T)y(k-1) \quad (1.31)$$

- Implicit Euler's method ('step forward') (1.10)

$$y(k) = \frac{y(k-1)}{1 + \lambda T} \quad (1.32)$$

- Trapezoidal approximation (1.13)

$$y(k) = \frac{2 - \lambda T}{2 + \lambda T} y(k-1) \quad (1.33)$$

Accurate result of integration at the instant $t_k = kT$ is:

$$y_{aL}(k) = y(k-1)e^{-\lambda T} \quad (1.34)$$

Thus the local integration error for one interval $T = t_k - t_{k-1}$ can be defined as:

$$\Delta_L = y_{aL}(k) - y(k) \quad (1.35)$$

This local error can easily be determined for each algorithm considered. Let's take for example the method (1.7):

$$\Delta_L = y(k-1)e^{-\lambda T} - (1 - \lambda T)y(k-1) = y(k-1)(e^{-\lambda T} - 1 + \lambda T) \quad (1.36)$$

Expansion of the exponential term into power series yields:

$$\Delta_L = y(k-1)\left(\frac{(\lambda T)^2}{2} - \frac{(\lambda T)^3}{3!} + \dots\right) \quad (1.37)$$

Putting the constraint $\lambda T < 1$ and using some mathematics the local error can be estimated by the approximate formula:

$$\Delta_L = \left| \frac{(\lambda T)^{p+1}}{(2)^{p-1}(2 + \lambda T)} \right| \quad (1.38)$$

where p is the order of the algorithm (in this case $p = 1$).

The global error Δ_G is defined as the difference between accurate and approximate integration result in a longer time span i.e. from the first step ($k = 1$) to the arbitrary step $k > 1$ so that:

$$\Delta_G = y_0 e^{-k\lambda T} - y(k) \quad (1.39)$$

The respective integration results of (1.29) for the algorithms considered are (order of presentation as in previous case):

- Explicit Euler's method ('step backward') (1.7):

$$y(k) = (1 - \lambda T)^k y_0 \quad (1.40)$$

- Implicit Euler's method ('step forward') (1.10):

$$y(k) = \frac{y_0}{(1 + \lambda T)^k} \quad (1.41)$$

- Trapezoidal approximation (1.13):

$$y(k) = \left[\frac{2 - \lambda T}{2 + \lambda T} \right]^k y_0 \quad (1.42)$$

Discussion of results

- Algorithms (1.31) and (1.40). The integration method is convergent and the algorithms remain stable if:

$$|1 - \lambda T| < 1 \quad (1.43)$$

Thus, the stability of the algorithms is ensured if:

$$T < \frac{2}{\lambda} \quad (1.44)$$

- The remaining algorithms are stable regardless of the value of T .
- If the algorithm is stable the global error tends to zero even though the local error may attain significant values.

Illustration of the errors discussed is shown in Fig.1.2. The plots presented have been calculated for: $y_0 = 10$; $\lambda = 2$; $T = 0.987$ [76].

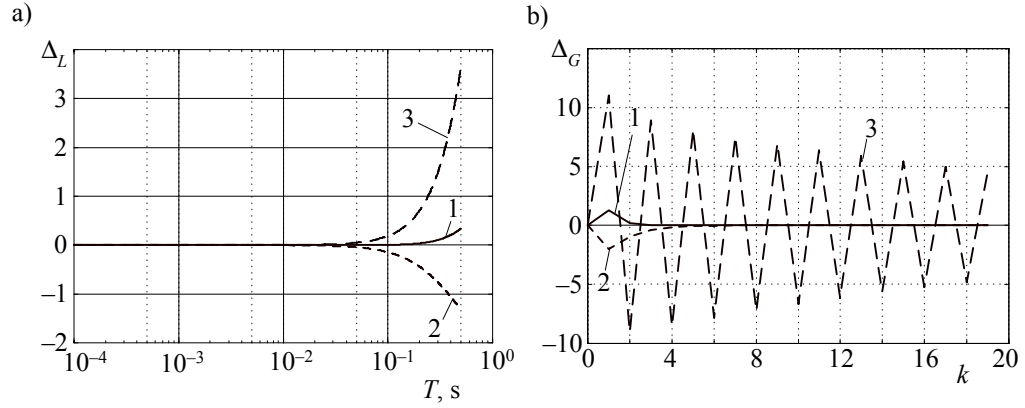


Fig. 1.2. Local Δ_L and global Δ_G error values for the algorithms considered: 1 – trapezoidal approx.; 2 – Euler's 'step forward' ; 3 – Euler's 'step backward'

1.3. Numerical models of network elements

1.3.1. Resistance

As the resistive elements do not have the energy storing capacity the discrete relation between current and voltage drop across resistance R can be obtained directly from the continuous relation and:

$$i(k) = \frac{1}{R} u(k) = Gu(k) \quad (1.45)$$

1.3.2. Inductance

The energy stored in magnetic field produced by current has the impact on voltage across the element so its continuous model is described by the equation:

$$\frac{di(t)}{dt} = \frac{1}{L} u(t) \quad (1.46)$$

Using the transformation (1.6) or (1.9) the Euler's implicit discrete model of the element is obtained:

$$i(k) = i(k-1) + \frac{T}{L}u(k) = i(k-1) + Gu(k), \quad G = \frac{T}{L} \quad (1.47)$$

Note that T/L has the conductance unit.

For the trapezoidal transformation (1.7) or eqn.(1.10) the discrete model takes the form:

$$i(k) = i(k-1) + \frac{T}{2L}[u(k-1) + u(k)] \quad (1.48)$$

or

$$i(k) = Gu(k) + i(k-1) + Gu(k-1), \quad G = \frac{T}{2L} \quad (1.49)$$

The eqn. (1.49) can be rearranged in the following way:

$$i(k) = Gu(k) + i(k-1) + Gu(k-1) \quad (1.50)$$

or

$$i(k) = Gu(k) + j(k-1) \quad (1.51)$$

where

$$j(k-1) = i(k-1) + Gu(k-1) \quad (1.52)$$

The calculations in step k employ the values calculated in step $k-1$ which are constant and can be considered as the constant current sources $j(k-1)$. Thus the inductance can be represented by equivalent numerical model corresponding to (1.52) which is shown in Fig.1.3.

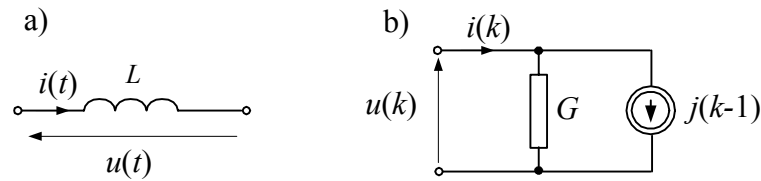


Fig. 1.3. Discrete model of inductance; a) symbol; b) numerical model

1.3.3. Capacitance

This element also reveals the energy storing capacity in form of electric charge and the relation between voltage and current in the element is given by the formula:

$$\frac{du(t)}{dt} = \frac{1}{C} i(t) \quad (1.53)$$

Using the same transformations as for the inductance the discrete models of capacitance can be derived:

$$u(k) = u(k-1) + \frac{T}{C} i(k) \quad (1.54)$$

Introducing the conductance notation (1.54) takes the form:

$$i(k) = Gu(k) - Gu(k-1), \quad G = \frac{C}{T} \quad (1.55)$$

and

$$i(k) = Gu(k) + j(k-1), \quad j(k-1) = -Gu(k-1) \quad (1.56)$$

Using the trapezoidal integration method the discrete model of capacitance takes the similar form:

$$u(k) = u(k-1) + \frac{T}{2C} (i(k-1) + i(k)) \quad (1.57)$$

The companion discrete model for capacitance can be derived as:

$$i(k) = Gu(k) + j(k-1) \quad (1.58)$$

$$j(k-1) = -i(k-1) + Gu(k-1), \quad G = \frac{2C}{T} \quad (1.59)$$

The respective representation is shown in Fig.1.4:

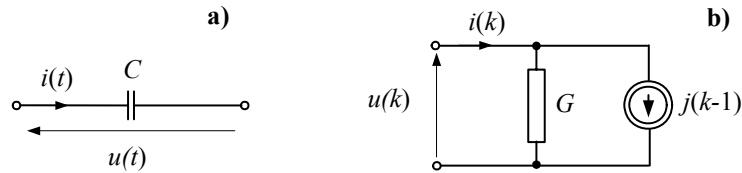


Fig. 1.4. Discrete model of capacitance; a) symbol; b) numerical model

In the very similar way the parameters of circuit representations for any integration method used can be derived. In Table 1.1 the example of those parameters for three selected methods are shown.

Table 1.1. Companion circuit parameters for selected numerical integration methods.

Integration method	Model of inductance L	Model of capacitance C
Euler's implicit method	$j(k-1) = i(k-1), \quad G = \frac{T}{L}$	$j(k-1) = -Gu(k-1), \quad G = \frac{C}{T}$
Trapezoidal approximation	$j(k-1) = i(k-1) + Gu(k-1), \quad G = \frac{T}{2L}$	$j(k-1) = -(i(k-1) + Gu(k-1)), \quad G = \frac{2C}{T}$
Gear's 2 nd order	$j(k-1) = \frac{1}{3}(4i(k-1) - i(k-2)), \quad G = \frac{2T}{3L}$	$j(k-1) = -G\left(2u(k-1) + \frac{1}{3}u(k-2)\right), \quad G = \frac{3C}{2T}$
Basic numerical algorithm: $i(k) = Gu(k) + j(k-1)$		

1.3.4. Complex RLC branches

The equivalent discrete model of in series connected RLC branch can be obtained by series connection of basic models of each particular element in the branch as it is shown in Fig.1.5b.

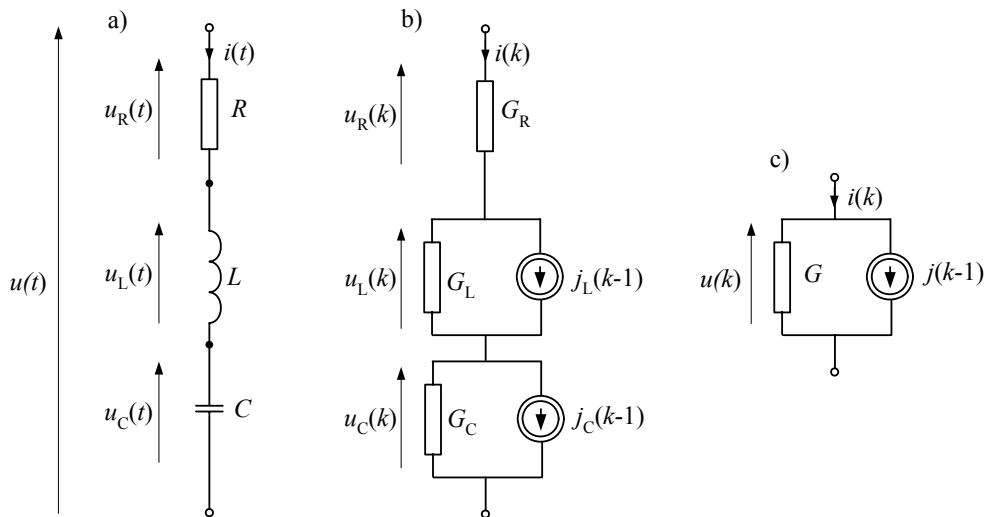


Fig. 1.5. Discrete model of RLC branch; a) the continuous model; b) discrete models of particular elements; c) the equivalent discrete model of the branch.

To derive the equivalent discrete model (Fig. 1.5c) of the overall circuit consider the basic equation for voltage across the branch (Fig. 1.5b):

$$u(k) = u_R(k) + u_L(k) + u_C(k) \quad (1.60)$$

in which the particular terms can be expressed by their basic models:

$$\begin{aligned} u_R(k) &= \frac{1}{G_R} i(k), \\ u_L(k) &= \frac{1}{G_L} (i(k) - j_L(k-1)), \quad u_C(k) = \frac{1}{G_C} (i(k) - j_C(k-1)). \end{aligned} \quad (1.61)$$

After substitution and appropriate rearrangement of (1.60) the equivalent model equation is obtained:

$$i(k) = Gu(k) + j(k-1) \quad (1.62)$$

in which, for trapezoidal approximation:

$$\begin{aligned} G &= \frac{G_R G_L G_C}{G_R G_L + G_R G_C + G_L G_C} = \frac{2CT}{4LC + 2RCT + T^2} \\ j(k-1) &= \frac{G_R G_C j_L(k-1) + G_R G_L j_C(k-1)}{G_R G_L + G_R G_C + G_L G_C} = \frac{G}{G_L} j_L(k-1) + \frac{G}{G_C} j_C(k-1), \end{aligned}$$

$$\text{and } G_R = \frac{1}{R}, \quad G_L = \frac{T}{2L}, \quad G_C = \frac{2C}{T}.$$

If capacitance C is not present in a branch then $C \rightarrow \infty$ must be put into the above equations. For missing R or L , $R = 0$ or $L = 0$ must be used, respectively. For example, in case of the RL branch the respective relations are:

$$G = \frac{T}{2L + RT}, \quad j(k-1) = \frac{2L}{2L + RT} j_L(k-1) = \frac{1 - RG_L}{1 + RG_L} i(k-1) + Gu(k-1) \quad (1.63)$$

1.3.5. Controlled sources

Controlled sources are used very often in electronic and electric network models. Generally there are four basic types of such sources (Fig. 1.6) [18, 70]:

- Voltage controlled current sources $j = ku_x$ controlled by voltage u_x applied to control terminals.
- Current controlled current sources $j = ki_x$ controlled by current i_x injected into control terminals.
- Voltage controlled voltage sources $u = ku_x$.

- Current controlled voltage sources $u = ki_x$.

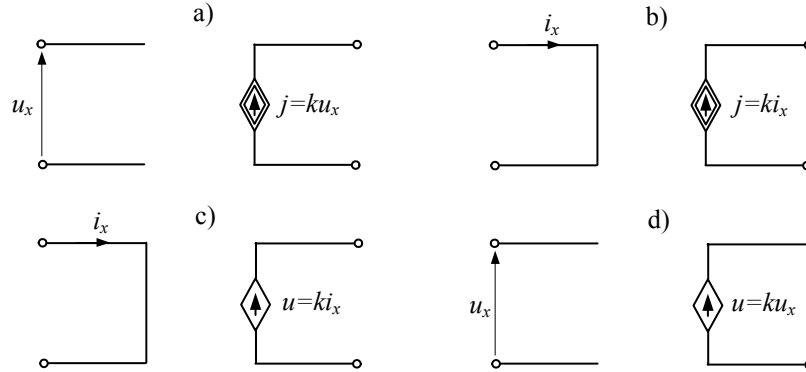


Fig. 1.6. Diagrams of controlled sources; a) voltage controlled current source;
b) current controlled current source; c) current controlled voltage source;
d) voltage controlled voltage network.

Models of controlled sources are very simple; however, their implementation in simulation programs may sometimes be cumbersome.

1.3.6. Frequency properties of discrete models

The frequency properties of discrete models are uniquely determined by the method used for approximation of derivatives that appear in the continuous model of a given element. Comparison of the continuous and the discrete models frequency properties provides very useful information on how to select the calculation period T in order to obtain the accurate enough transient component waveform of specified frequency f_{\max} which is present in the frequency spectrum of continuous transient voltages or currents.

As an example let's consider the discrete model of inductance obtained by use of trapezoidal approximation. Using the already known relations (1.46, 1.13) we get:

$$\frac{2(z-1)}{T(z+1)}i(z) = \frac{1}{L}u(z) \quad (1.64)$$

$$i(z) = \frac{T}{2L} \frac{z+1}{z-1} u(z) \quad (1.65)$$

Now using (1.4) and remembering that in frequency domain $s=j\omega$:

$$i(j\omega) = \frac{T}{2L} \frac{e^{j\omega T} + 1}{e^{j\omega T} - 1} u(j\omega) \quad (1.66)$$

Applying rudimentary trigonometry knowledge the magnitude of the equation (1.66) can be written in the following form:

$$|i(j\omega)| = \frac{\frac{T}{2}}{L \tan \frac{\omega T}{2}} |u(j\omega)| \quad (1.67)$$

Introducing the complex discrete admittances $Y_d(j\omega)$ and the continuous $Y_c(j\omega)$ we get:

$$|Y_d(j\omega)| = \frac{|i(j\omega)|}{|u(j\omega)|} = \frac{\frac{T}{2}}{L \tan \frac{\omega T}{2}} = \frac{\frac{T\omega}{2}}{L\omega \tan \frac{\omega T}{2}} = \frac{\frac{T\omega}{2}}{\tan \frac{\omega T}{2}} |Y_c(j\omega)| \quad (1.68)$$

where $Y_c(j\omega) = 1/jL\omega$ is the admittance of the continuous model of inductance.

Thus, the ratio of the discrete admittance to the continuous one is given by:

$$\frac{|Y_d(j\omega)|}{|Y_c(j\omega)|} = \frac{\frac{T\omega}{2}}{\tan \frac{\omega T}{2}} \quad (1.69)$$

and changes with frequency as it is shown in Fig. 1.7.

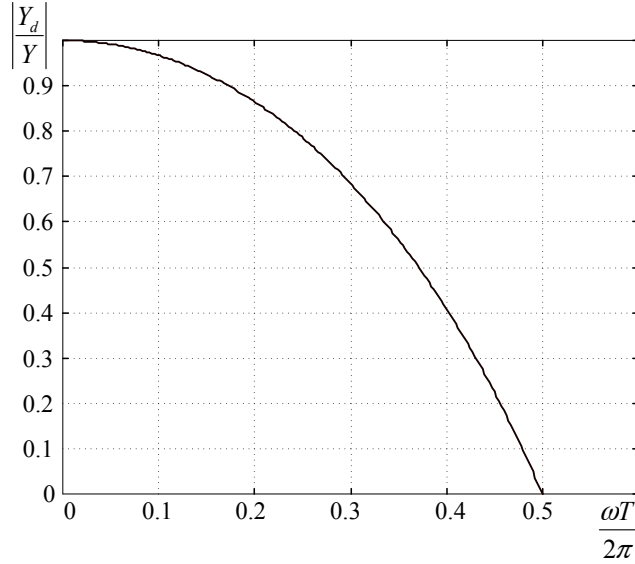


Fig. 1.7. Frequency response of discrete inductance model.

From eqn. (1.69) and from Fig. 1.7 one can notice that $Y_d(j\omega)$ reaches zero if $\tan \frac{\omega T}{2} \rightarrow \infty$. This limit is reached when:

$$\frac{\omega T}{2} = \frac{\pi}{2} \quad \text{or} \quad T = \frac{\pi}{\omega} = \frac{\pi}{2\pi f} = \frac{1}{2f} \quad (1.70)$$

So if f_{\max} is the frequency of the highest harmonic to be observed in current or voltage signals then the calculation step T should be small enough according to following condition:

$$T \ll \frac{1}{2f_{\max}} \quad (1.71)$$

Practically, if required number of data samples within the period $T_{\max} = \frac{1}{f_{\max}}$ is N then (1.71) implies:

$$T \leq \frac{1}{Nf_{\max}} \quad (1.72)$$

in which N must not be less than 2 (usually $N > 20$).

1.3.7. Distributed parameters model (long line model)

Distinction between lumped and distributed models of electric elements is made on the basis of mutual relation between three basic parameters of the environment in which the electromagnetic wave is propagated. These parameters are:

- specific electric conductivity γ
- relative magnetic permeability μ
- relative electric permittivity ε

In case of lumped elements it is assumed that only one of the above listed parameters is dominant and the remaining ones can be neglected. Thus particular elements are deemed as lumped under following conditions:

- $\mu = \varepsilon = 0$ – lumped resistance
- $\gamma = \varepsilon = 0$ – lumped inductance
- $\gamma = \mu = 0$ – lumped capacitance.

Additionally in case of lumped parameters model of an electric network the electromagnetic field must be quasi-stationary; it means that in each point of the network the electromagnetic field is practically the same or the differences are negligibly small. In this respect the length of the electric conductor l is considered as

the distinctive parameter. As the boundary value the length l_{gr} equal to $\frac{1}{4}$ of the electromagnetic wavelength propagated is assumed.

Thus, if the frequency of the propagated wave is f , than the l_{gr} can be estimated as:

$$l_{gr} = \frac{\lambda}{4} = \frac{c}{4f}, \quad (1.73)$$

where c is the velocity of light and $\lambda = \frac{c}{f}$ is the wavelength.

If $l \ll l_{gr}$ then the length of the line can be neglected and can be modelled as the lumped parameter element. Otherwise ($l \approx l_{gr}$) the line should be considered as the long one.

For example, if the transient harmonics of frequency $f = 1000$ Hz (the 20th harmonic) may appear in the line during faults then $l_{gr} = c/(4f) = 3 \cdot 10^5 / (4 \cdot 1000) = 75$ km. The lightning stroke may induce much higher harmonics in the line so in such case even a few kilometres long line should be represented by distributed parameters model.

To derive the continuous model of the long line the equivalent Δx long segment of the line shown in Fig.1.8 can be used. As Δx is assumed to be sufficiently short the circuit parameters can be considered as the lumped ones.

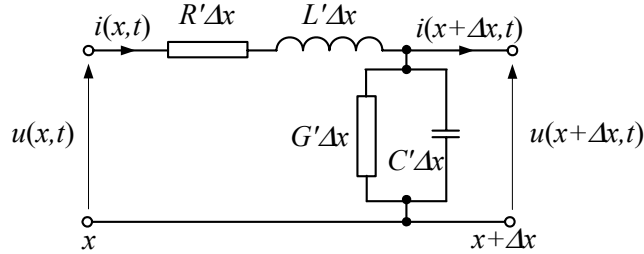


Fig.1.8. Elementary segment of a long line

The basic equations that describe the elementary line segment in Fig.1.8 are:

$$\begin{aligned} u(x,t) &= R' \Delta x \cdot i(x,t) + L' \Delta x \frac{\partial i(x,t)}{\partial t} + u(x + \Delta x, t), \\ i(x,t) &= G' \Delta x \cdot u(x + \Delta x, t) + C' \Delta x \frac{\partial u(x + \Delta x, t)}{\partial t} + i(x + \Delta x, t), \end{aligned} \quad (1.74)$$

where: R' , L' , G' , C' denote 'unit/ length' values of resistance, inductance and capacitance of the line, respectively.

Dividing both equations by Δx and taking the limes ($\Delta x \rightarrow 0$) the following relations are obtained:

$$\begin{aligned} -\frac{\partial u(x,t)}{\partial x} &= R' i(x,t) + L' \frac{\partial i(x,t)}{\partial t}, \\ -\frac{\partial i(x,t)}{\partial x} &= G' u(x,t) + C' \frac{\partial u(x,t)}{\partial t}. \end{aligned} \quad (1.75)$$

If the line is homogenous then (1.75) can be separated with respect to current and voltage (for simplicity: $u = u(x,t)$, $i = i(x,t)$):

$$-\frac{\partial u^2}{\partial x^2} = -R' G' u - R' C' \frac{\partial u}{\partial t} + L' \frac{\partial i^2}{\partial x \partial t} \quad (1.76)$$

and

$$\frac{\partial u^2}{\partial x^2} = R' G' u + (R' C' + G' L') \frac{\partial u}{\partial t} + L' C' \frac{\partial u^2}{\partial t^2} \quad (1.77)$$

Applying the same simplifying procedure to the second equation in (1.75) the respective relation for current can be obtained:

$$\frac{\partial i^2}{\partial x^2} = R' G' i + (R' C' + G' L') \frac{\partial i}{\partial t} + L' C' \frac{\partial i^2}{\partial t^2} \quad (1.78)$$

Both (1.75) and (1.76) are the second order hyperbolic partial differential equations known as telegraph equations [80].

a) Lossless (non-dissipating) long line

This case is obtained under assumption that $R'=0$ and $G'=0$ and the resulting simplification of (3.4) and (3.5) is:

$$\begin{aligned} \frac{\partial u^2}{\partial x^2} - \frac{1}{v^2} \frac{\partial u^2}{\partial t^2} &= 0, \\ \frac{\partial i^2}{\partial x^2} - \frac{1}{v^2} \frac{\partial i^2}{\partial t^2} &= 0. \end{aligned} \quad (1.79)$$

in which:

$$v = \frac{1}{\sqrt{L' C'}} \quad (1.80)$$

The general solution of (3.6) has been found by d'Alembert [24, 28]. For the following boundary conditions:

$$u(x, t)|_{x=0} = \varphi(t), \quad \left. \frac{\partial u(x, t)}{\partial x} \right|_{x=0} = \psi(t)$$

the solution of (1.79) takes the form:

$$u(x, t) = \frac{1}{2} (\varphi(t + x/v) + \varphi(t - x/v)) + \frac{v}{2} \int_{t-x/v}^{t+x/v} \psi(\alpha) d\alpha \quad (1.81)$$

The loci of points $(t - x/v) = \text{const}$ and $(t + x/v) = \text{const}$ known as propagation characteristics of (1.81) [6, 39] show the propagation mechanism of $\varphi(x, t)$ waves in a long line.

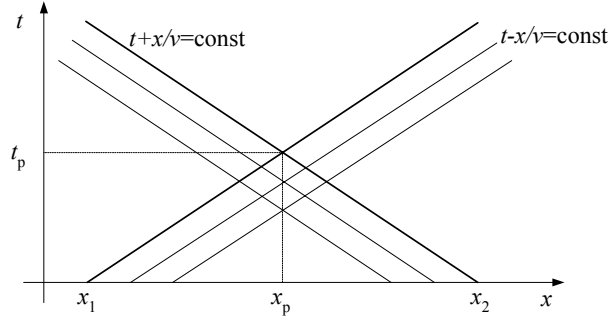


Fig. 1.9. Propagation characteristics of a lossless long line

The boundary conditions expressed in terms of voltage $u_1(t)$ and current $i_1(t)$ at the beginning of the lossless ($R' = 0$) line (1.75) yields:

$$\varphi(t) = u(0, t) = u_1(t), \quad \psi(t) = \frac{\partial u(0, t)}{\partial x} = -L' \frac{\partial i(0, t)}{\partial t} = -L' \frac{di_1(t)}{dt}$$

and the solution (1.81) takes the form:

$$u(x, t) = \frac{1}{2} (u_1(t + x/v) + u_1(t - x/v)) - \frac{1}{2} Z_f \int_{t-x/v}^{t+x/v} di_i(t) \quad (1.82)$$

where $Z_f = \sqrt{\frac{L'}{C'}}$ is the wave (surge) impedance of the line.

For $x = l$ (end of the line) solution of (1.82) is given by the equation:

$$u_2(t) = \frac{1}{2}(u_1(t+\tau) + u_1(t-\tau)) - \frac{1}{2}Z_f(i_1(t+\tau) - i_1(t-\tau)) \quad (1.83)$$

where: $\tau = l/v$ is the line propagation time.

Similarly, the wave equation for current can be obtained and:

$$i_2(t) = -\frac{1}{2}(i_1(t+\tau) + i_1(t-\tau)) + \frac{1}{2Z_f}(u_1(t+\tau) - u_1(t-\tau)) \quad (1.84)$$

Note that it was assumed that the current at the end of the line flows in reverse direction with respect to the current at the line beginning (see Fig.1.8) and that is why it bears the opposite sign.

Subtracting (1.83) from (1.84) the model of the long lossless line is obtained:

$$i_2(t) = G_f u_2(t) - G_f u_1(t-\tau) - i_1(t-\tau) \quad (1.85)$$

where: $G_f = \frac{1}{Z_f}$.



Fig.1.10. Assignment of variables in the lossless line

When the boundary conditions are assigned to the beginning and to the end of the line, the solution concerns these two points only. The propagation characteristics also comprise of 2 points: $x_1 = 0$ and $x_2 = l$. This simple model is called the Bergeron's model [24, 49].

The continuous model (1.85) of the lossless line can easily be converted into the discrete one. Assuming that wave propagation time is $mT = \tau$ then:

$$m = \frac{\tau}{T} = \frac{l}{vT} \quad (1.86)$$

and

$$i_2(k) = G_f u_2(k) - G_f u_1(k-m) - i_1(k-m) \quad (1.87)$$

By analogy the discrete model for the current at the beginning of the line can be derived, so the respective input and output line currents are:

$$\begin{aligned} i_1(k) &= G_f u_1(k) + j_1(k-m), \\ i_2(k) &= G_f u_2(k) + j_2(k-m), \end{aligned} \quad (1.88)$$

where

$$\begin{aligned} j_1(k-m) &= -G_f u_2(k-m) - i_2(k-m), \\ j_2(k-m) &= -G_f u_1(k-m) - i_1(k-m), \end{aligned} \quad (1.89)$$

The equivalent circuits corresponding to (1.88) and (1.89) are shown in Fig. 1.11.

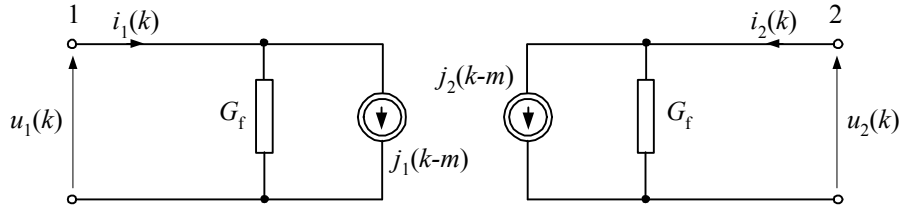


Fig.1.11. Equivalent circuit of the long line discrete model

b) The long line model with dissipation losses

The dissipation losses are uniquely attributed to heating of the line resistance which was neglected in derivation of the lossless line model. The inclusion of the resistance to the long line model is based upon assumption that its value is relatively small with respect to the line reactance. This assumption justifies the inclusion of the lumped resistance at both ends of the line as it is shown in Fig. 12.

When the resistance is connected as shown in Fig.1.12a the equations (1.88), (1.89) refer to voltages at nodes 1' and 2' for which the following relations are valid:

$$\begin{aligned} u'_1(k) &= u_1(k) - \frac{R}{2} i_1(k), \\ u'_2(k) &= u_2(k) - \frac{R}{2} i_2(k), \end{aligned} \quad (1.90)$$

where: $R = lR'$

As the result the conductance G_f and history of calculation changes so that:

$$\begin{aligned} j_1(k-m) &= -G_f u_2(k-m) - h_f i_2(k-m), \\ j_2(k-m) &= -G_f u_1(k-m) - h_f i_1(k-m), \end{aligned} \quad (1.91)$$

where:

$$G_f = \frac{1}{Z_f + R/2}, \quad h_f = \frac{2Z_f - R}{2Z_f + R}.$$

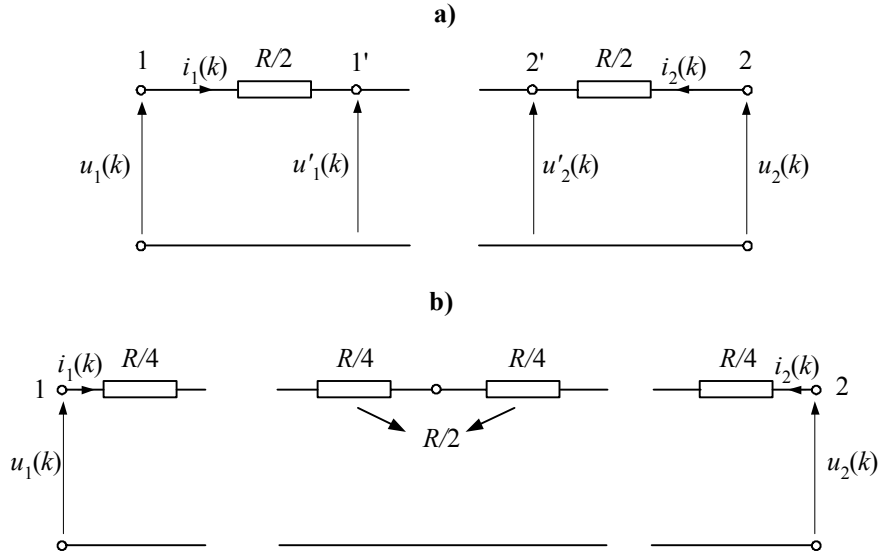


Fig.1.12. Inclusion of resistance into the long line model

More accurate model can be obtained when the resistance is connected into the line model as it is shown in Fig.1.12b. In this case all the line parameters connected to the middle node of the line can be eliminated and the resulting equations obtained are:

$$\begin{aligned} i_1(k) &= G_f u_1(k) + h_{fa} j_1(k-m) + h_{fb} j_2(k-m), \\ i_2(k) &= G_f u_2(k) + h_{fa} j_2(k-m) + h_{fb} j_1(k-m), \end{aligned} \quad (1.92)$$

where: $h_{fa} = Z_f G_f$, $h_{fb} = \frac{R}{4} G_f$, and $G_f = \frac{1}{Z_f + R/4}$.

In general the dissipating long line models can be written in the compact matrix form so that:

$$\begin{bmatrix} i_1(k) \\ i_2(k) \end{bmatrix} = \begin{bmatrix} G_f & \\ & G_f \end{bmatrix} \begin{bmatrix} u_1(k) \\ u_2(k) \end{bmatrix} + \begin{bmatrix} h_{fa} & h_{fb} \\ h_{fb} & h_{fa} \end{bmatrix} \begin{bmatrix} j_1(k-m) \\ j_2(k-m) \end{bmatrix} \quad (1.93)$$

and the matrixes $G_f = \{G_f\}$ and $h_f = \{h_f\}$.

The form of the matrixes depends upon the considered representation of the dissipating long line (as in Fig. 1.12a or as in Fig. 1.12.b).

1.4. Nodal method

The method is frequently used for network node equations formulation mainly because its application is easy and the algorithms of nodal equations solution are well known and fast. Below, the fundamentals of nodal method are presented which refer to the admittance representation of network branches with current and voltage controlled sources. Extension of the method for networks containing voltage and current controlled voltage sources branches is known as the modified nodal method and will not be considered here since the method is mainly applied to simulation of transients in electronic networks [8, 36].

1.4.1. Derivation of basic nodal equations

The equivalent diagram of the network branch typical for the nodal method is shown in Fig. 1.13. The mathematical model of the branch is described by the following equation:

$$i_a = G_a u_a + G_{ba} u_b + j_a = G_a (u_k - u_l) + G_{ba} (u_m - u_n) + j_a \quad (1.94)$$

where u_b is the current source controlling voltage with the control coefficient G_{ba} , located in the other network branch. It must be noted that j_a may refer to the independent current source as well as to the source related to the past values of current (history) in the branch.

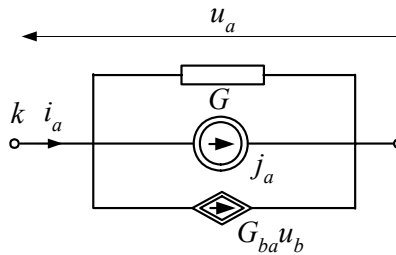


Fig. 1.13. Equivalent diagram of the conductance branch typical for nodal method

Let's consider a network comprising of n_g branches and $n_w + 1$ nodes with one of the nodes being the reference one. Such a network can be described by equation (1.94) written in matrix form:

$$\mathbf{i}_g = \mathbf{G}_g \mathbf{A}^T \mathbf{u} + \mathbf{j}_g \quad (1.95)$$

where:

- $\mathbf{G}_{g(n_g \times n_g)}$ is the conductance matrix which contains branch conductances G_a (at the diagonal) and conductances of controlled current sources G_{ba} (outside the diagonal);
- $\mathbf{A}_{n_w \times n_g} = \{a_{ij}\}$ is the incidence matrix which takes the following values : $a_{ij} = 1$ – if the branch j is connected to the node i and is directed to that node, $a_{ij} = -1$ – if the branch is of opposite direction, $a_{ij} = 0$ – if the branch j is not connected to the node i ;
- \mathbf{u} is the vector of potentials in n_w independent network nodes (it is the vector of voltage difference between particular nodes and the reference node);
- \mathbf{j}_g is the vector of nodal current sources.

Multiplication of (1.94) by the incidence matrix \mathbf{A} transforms the branch currents into the nodal ones. The sum of the branch currents in each node is always equal to zero (the first Kirchhoff's law) so that:

$$\mathbf{A} \mathbf{i}_g = 0 \quad (1.96)$$

and, for the right side of (1.94):

$$\mathbf{G} \mathbf{u} = \mathbf{i} \quad (1.97)$$

where: $\mathbf{G}_{n_g \times n_g} = \mathbf{A} \mathbf{G}_g \mathbf{A}^T$ is the matrix of nodal conductance , $\mathbf{i}_{n_w \times 1} = -\mathbf{A} \mathbf{j}_g$ is the vector of the nodal currents (positive sign is assigned to elements of the vector \mathbf{i} if the corresponding source is directed to the node).

Due to the matrix \mathbf{A} definition particular elements of the vector \mathbf{i} are the sum of branch currents which are directed to a given node.

Relation (1.97) is known as the equation of nodal potentials. For a given matrix \mathbf{G} and for the known excitation vector \mathbf{i} solution of (1.97) yields the vector \mathbf{u} which determines voltages between the independent nodes and the reference one. To facilitate the network transient calculations some modifications are applied to (1.97). Two such modifications are of extreme importance in power system networks calculations since they enable:

- inclusion of voltage sources connected to the reference node;
- improvement of calculation in case of parameter changes in selected branches.

If independent voltage sources connected in series with impedance appear in branches then they should be transformed into the equivalent current sources according to the Norton's theorem. In power networks the reference node is usually

assigned to earth. In such case all voltage sources connected to earth are no longer independent. To avoid this the following procedure can be applied [24, 87]:

- Select the set of nodes A (excluding the reference node) for which nodal voltages are not determined.
- Nodes with determined voltages belong to the set B . The sum of both set makes the total set of all independent nodes in the network: $n_w = n_A + n_B$.
- Vector of nodal voltages \mathbf{u} in (1.97) can now be presented as:

$$\mathbf{u} = \begin{bmatrix} \mathbf{u}_A \\ \mathbf{u}_B \end{bmatrix} \quad (1.98)$$

in which only the vector \mathbf{u}_A is to be determined.

- Now (1.97) can be written as:

$$\begin{bmatrix} \mathbf{G}_{AA} & \mathbf{G}_{AB} \\ \mathbf{G}_{BA} & \mathbf{G}_{BB} \end{bmatrix} \begin{bmatrix} \mathbf{u}_A \\ \mathbf{u}_B \end{bmatrix} = \begin{bmatrix} \mathbf{i}_A \\ \mathbf{i}_B \end{bmatrix} \quad (1.99)$$

where: \mathbf{G}_{AA} is the conductance matrix of that part of the network which has no nodes connected to the branches with voltage sources, \mathbf{G}_{BB} contains self and mutual conductances of nodes for which voltages are known, while \mathbf{G}_{AB} and \mathbf{G}_{BA} represent matrixes of mutual conductances of sets A and B ; node current vector is divided similarly.

- The unknown node voltage vector \mathbf{u}_A can be determined from the equation:

$$\mathbf{G}_{AA}\mathbf{u}_A = \mathbf{i}_A - \mathbf{G}_{AB}\mathbf{u}_B \quad (1.100)$$

while the node current vector in the set B can be found from the lower part of (1.99):

$$\mathbf{i}_B = \mathbf{G}_{BA}\mathbf{u}_A + \mathbf{G}_{BB}\mathbf{u}_B \quad (1.101)$$

Elements of the vector \mathbf{i}_B are the sum of sources current flowing into the respective nodes in the set B , including branches obtained for the voltage sources.

Another important issue related to calculation of transients is the possibility of an easy change of network configuration without necessity of matrix \mathbf{G} calculation. This problem appears, for instance, when switches in the network being analyzed change their positions. In such case any switch can be represented by the conductance branch for which the value of G_{wyl} depends upon the switch position: $G_{\text{wyl}} = F_{\text{max}}$ – the switch closed, $G_{\text{wyl}} = 0$ – the switch open; F_{max} – very big real value. Thus, when the switches change position the overall network configuration remains unchanged, only

the values of matrix \mathbf{G} elements change. That is why the nodes connected to the switch branches should be located in lower part of matrix \mathbf{G} [22]. The example illustrating the nodal method application is shown in [76].

In existing simulation programs the Gaussian elimination method is applied in versions which differ mainly in representation of elements with variable parameters (switches). It should be noted that the representation of a switch by the element of variable conductance may bring about some numerical problems when the conductance value is very small (closed switch) since the matrix may become singular.

1.4.2. Simulation algorithm

The detailed algorithm of transient simulation depends mainly upon how the numerical problems are solved. However, in general, all algorithms comprise of the three basic stages (Fig. 1.14):

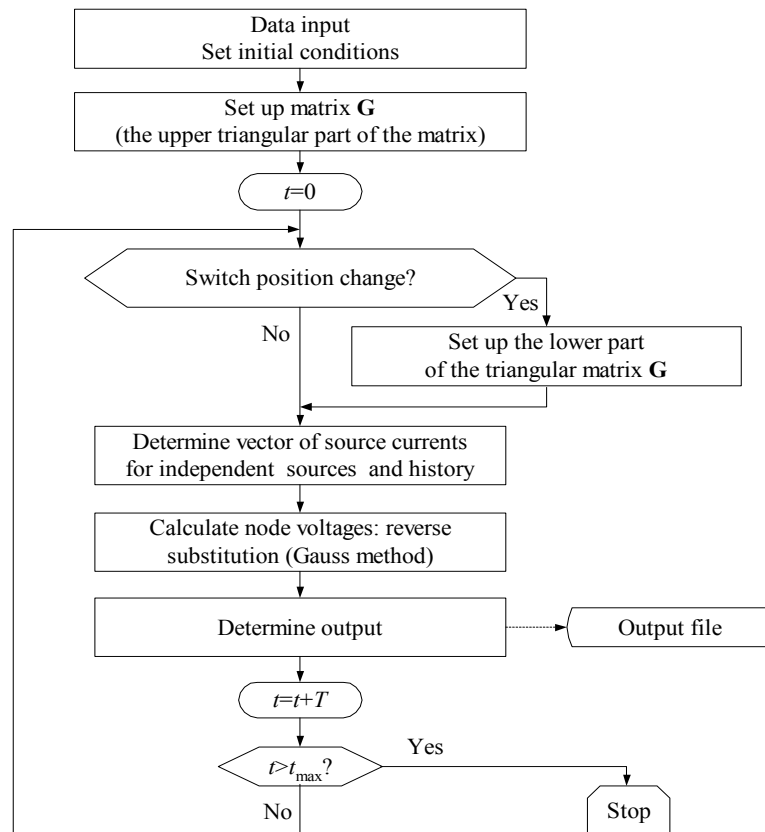


Fig. 1.14. Basic structure of algorithms for transient calculation using the nodal method

- Data and initial conditions setup
- Calculations
- Results record

The results of the algorithm operation can be illustrated by the following example.

Example 1.1. Simulate the transients generated in the network shown in Fig.1.15a which is the part of the 400 kV power system drawn for the positive sequence impedances. Assume that all current and voltage initial conditions for $(t < 0)$ are equal to zero.

System parameters: $E_s = 330$ kV, $Z_s = 0.5 + j10 \Omega$, $Z_1 = 4700 + j2800 \Omega$, $Z_2 = 415 + j200 \Omega$.

Line: $R' = 0.0288 \Omega/\text{km}$, $L' = 1.0287$ mH/km, $C' = 11.232$ nF/km, length $l = 180$ km.

Calculation step: $T = 5 \cdot 10^{-5}$ s.

Using the respective digital models for the system elements the equivalent network shown in Fig.1.15b is obtained. The switch W is closed ($G_W = 10^6$ S). Simulation starts ($t = 0$) when the voltage E_s is switched on.

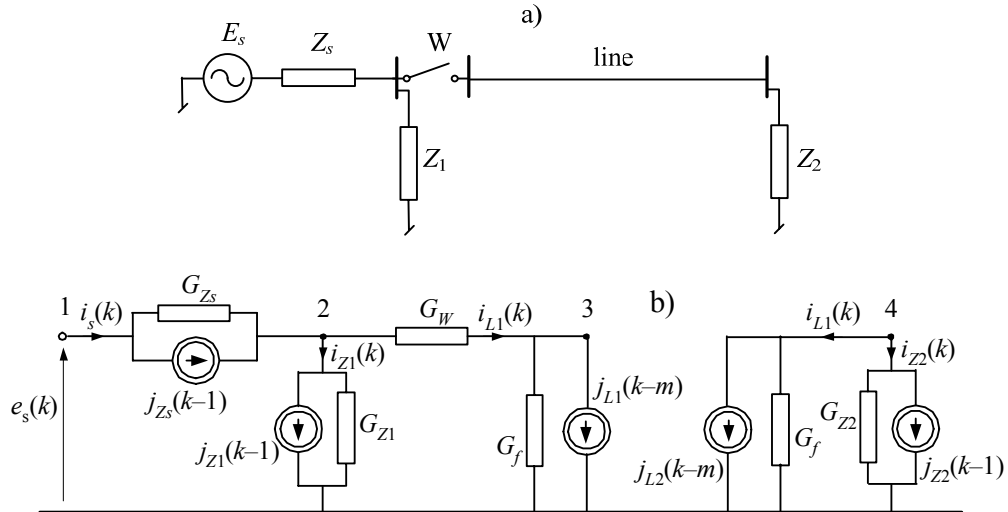


Fig.1.15. Illustration of the simulation algorithm operation; a) analyzed system; b) equivalent network of the analyzed system

Simulation is based on step by step solving of (1.100) and (1.101). The selected waveforms of currents and voltages in the network are shown in Fig. 1.16.

The intensive transient state caused by charging of the line can be noticed in the first period of fundamental frequency. The oscillation period is equal to the propagation time necessary for the electromagnetic wave to travel along the line in both directions. Relatively slow decay of those oscillations can partly be attributed applied trapezoidal integration method which is

sensitive to rapid changes of reflected current and voltage waveforms. Problem of digital simulations is analyzed in further part of this Chapter (sect. 1.5).

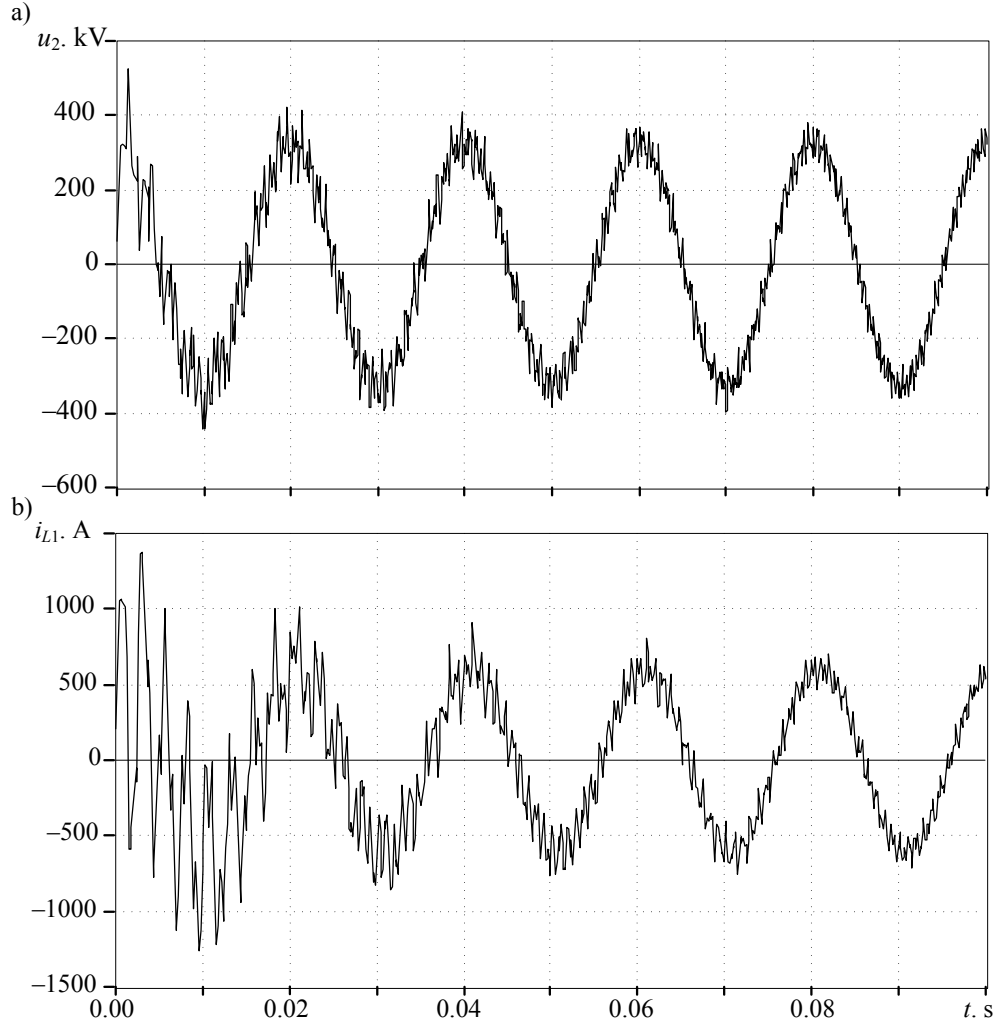


Fig.1.16. The voltage a) and current b) at the beginning of the line

1.4.3. Initial conditions

To start simulations according to the algorithm discussed initial conditions for currents and voltages in LC branches and in long (distributed parameters) line have to be fixed first. In case of AC networks the initial conditions refer to the steady state of the

network before calculation of transients starts. Thus, the initial conditions are determined for complex network model with sinusoidal excitation sources and with all switches set to positions corresponding to the network normal operating conditions.

If the network includes nonlinear elements then, initial conditions calculations are carried out for linear approximation of their nonlinear transition characteristics. In case of long lines which are modelled as elements of distributed parameters initial conditions are calculated using the simplified model in which the line is represented by a single Π cell as it is shown in Fig. 1.17.

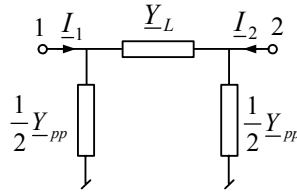


Fig. 1.17. Equivalent circuit of along line for steady state calculations

The values of admittances in the circuit shown in Fig. 1.17 can be determined from 'unit per length' parameters of the line according to the following equations:

$$\underline{Y}_L = \frac{1}{\underline{Z}_L}, \text{ where: } \underline{Z}_L = l(R' + j\omega L') \frac{\sinh \gamma l}{\gamma l}, \quad \gamma = \sqrt{(R' + j\omega L')(G' + j\omega C')} \quad (1.102)$$

$$\frac{1}{2} \underline{Y}_{pp} = \frac{l}{2} (G' + j\omega C') \frac{\tanh \frac{\gamma l}{2}}{\frac{\gamma l}{2}} \quad (1.103)$$

where l – line length. Complex parameter γ is the line propagation constant.

The steady state equation of the network in Fig. 1.17 takes the following form:

$$\begin{bmatrix} \underline{Y}_L + \frac{1}{2} \underline{Y}_{pp} & -\underline{Y}_L \\ -\underline{Y}_L & \underline{Y}_L + \frac{1}{2} \underline{Y}_{pp} \end{bmatrix} \begin{bmatrix} \underline{U}_1 \\ \underline{U}_2 \end{bmatrix} = \begin{bmatrix} \underline{I}_{12} \\ \underline{I}_{21} \end{bmatrix} \quad (1.104)$$

The admittances located in the matrix diagonal can be simplified so that:

$$\underline{Y}_L + \frac{1}{2} \underline{Y}_{pp} = \underline{Y}_L \cos \gamma l \quad (1.105)$$

In case of the long and lossless line ($R' = G' = 0$) the respective values of admittances in boundary conditions are:

$$\underline{Z}_L = j\omega L' \frac{\sin(\omega l \sqrt{L'C'})}{\omega l \sqrt{L'C'}}, \quad \frac{1}{2} \underline{Y}_{pp} = \frac{j\omega C l}{2} \frac{\tan\left(\frac{\omega l}{2} \sqrt{L'C'}\right)}{\frac{\omega l}{2} \sqrt{L'C'}} \quad (1.106)$$

The short line, for which the related functions ($\sinh x/x$, $\tanh x/x$, $\sin x/x$, $x \rightarrow 0$) take the values close to 1, can be considered as an element of lumped parameters so that:

$$\underline{Y}_L = \frac{1}{R + j\omega L}, \quad \underline{Y}_{pp} = G + j\omega C \quad (1.107)$$

where $R = lR'$ similarly to the rest of the line parameters.

The results of steady state calculations are in general complex numbers. If the real part of the obtained result is taken as the initial condition for transients calculation then all excitation current and voltage sources should be of cosine type.

1.5. Numerical stability of digital models

Numerical models used for simulation of transient processes in power networks can be deemed as satisfactory if the simulation results are adequate to processes observed in real networks. There are two basic sources of errors that can make the simulation results inadequate, namely,

- omission of the elements which are essential for the network operation
- application of numerical methods that are inadequate to calculation of analyzed effects.

The problems concerned may appear in some specific situations only. For example, the ideal switch that is represented by two limit values of conductance (0 and ∞) can be used as a circuit breaker if the values of the current to be broken are relatively low. Similar problems may occur due to application of inadequate numerical methods resulting in numerical instability.

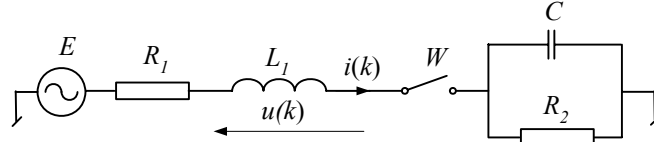
Numerical instability appears when the errors caused by numerical round up of calculation results sum up in each calculation step.

Practically, the both considered types of errors are related very closely as the further analysis shows.

1.5.1. Numerical oscillations in transient state simulations

As the typical illustration of the problem let's consider the following example.

Example 1.2. Simulate the transient effects that appear in the network shown in Fig. 1.18 when the switch opens at $t_{\text{open}} = 0.012\text{s}$. Assume that the models of elements used are companion to trapezoidal approximation method.



The element parameters: $R_1 = 1\Omega$, $L_1 = 100\text{mH}$, $R_2 = 1000\Omega$, $C = 4.7\mu\text{F}$, $E = 100\cos(100\pi t)$.

Fig.1.18. The simulated network

The respective waveforms of the current flowing through the switch and the voltage drop across the inductance L_1 are shown in Fig. 1.19.

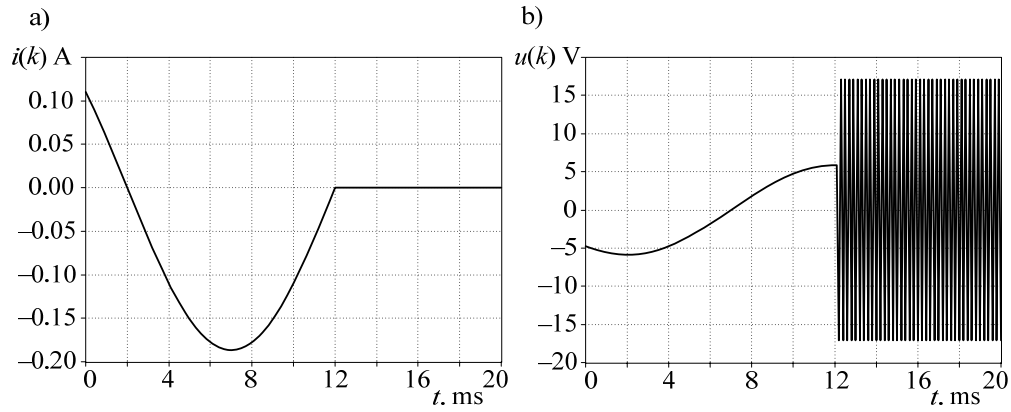


Fig. 1.19. The results of simulation; a) the current in the switch; b) the voltage across the inductance L_1

As one can see the network current drops to zero when the switch opens but the voltage across inductance oscillates with constant non-decaying amplitude of relatively small value since the value of the current at the breaking moment is also very small. A closer look at the oscillating voltage (Fig. 1.20) reveals that it changes its sign in each calculation step.

The oscillations appear since the energy stored in the coil cannot be dissipated (the circuit is broken). Thus the observed error in simulation result can be credited to inadequate model applied. Such errors may appear in less obvious situations (some model parameters drastically change their values within one calculation step).

To analyze the described numerical effect let's consider the voltage drop across the inductance which, in case of numerical model derived for trapezoidal approximation, can be expressed as (*derive this equation*):

$$u(k) = \frac{1 + RG_L}{G_L} i(k) - \frac{1 - RG_L}{G_L} i(k-1) - u(k-1) \quad (1.108)$$

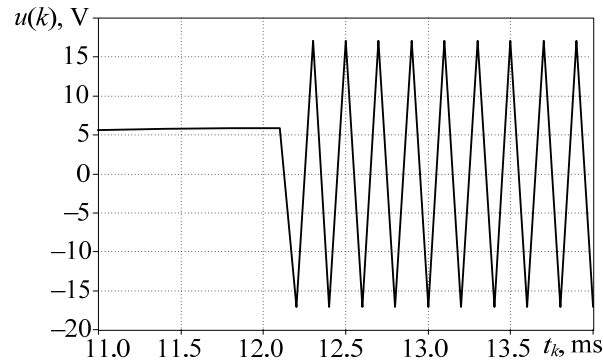


Fig.1.20. Oscillating inductance voltage

When the switch opens at $k-1$ instant the current attains zero in two consecutive steps ($i(k) = i(k-1) = 0$). Thus, $u(k) = -u(k-1)$ for all further calculation steps.

There are many methods that can be applied to damp such oscillations; they are known as critical damping adjustment methods (CDA) [56, 59].

1.5.2. Suppression of oscillations by use of a damping resistance

The most obvious way of oscillation suppression is the use of nonlinear model that matches reality. However, sometimes this approach may be very difficult or even impossible to apply. In such cases the use of linear resistance can bring the satisfactory effects.

The analysis of the network in Fig. 1.19 immediately brings to the conclusion that the use of resistance connected in parallel with the coil should result in suppression of voltage oscillations. In such case the modified inductance model takes the form (Fig. 1.21):

$$i(k) = \frac{T}{2L} (u(k) + u(k-1)) + i(k-1) + \frac{1}{R} (u(k) - u(k-1)) \quad (1.109)$$

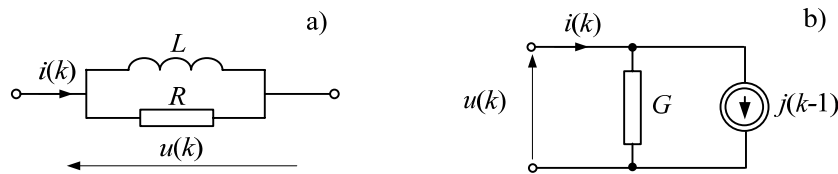


Fig. 1.21. Modified inductance model

In standard notation it is:

$$i(k) = Gu(k) + j(k-1) \quad (1.110)$$

where:

$$G = \frac{TR + 2L}{2LR}, \quad j(k-1) = i(k-1) + \frac{TR - 2L}{2LR} u(k-1).$$

Voltage across the modified inductance is:

$$u(k) = \frac{1}{G} (i(k) - i(k-1)) - \alpha u(k-1) \quad (1.111)$$

where: $\alpha = \frac{R - \frac{2L}{T}}{R + \frac{2L}{T}}$

The coefficient α is responsible for damping of oscillations. If $R = \infty$, $\alpha = 1$. The lower the value of R the lower the value of α . The oscillations on inductance in the example circuit for different values of α are shown in Fig. 1.22.

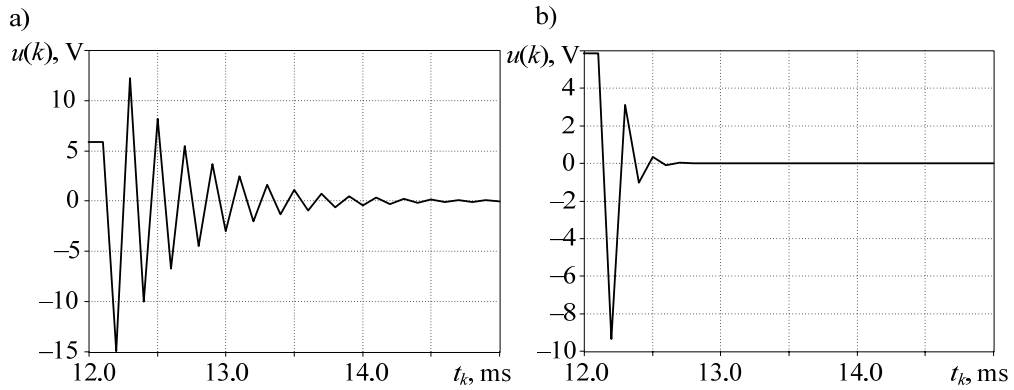


Fig.1.22. Oscillations on the inductor for different values of α . $\alpha=0.818$ (a) and $\alpha=0.333$ (b)

The similar effects can be observed on capacitances in case of rapid decrease of the capacitance voltage. In such case the modified capacitance model takes the form as in Fig. 1.23.

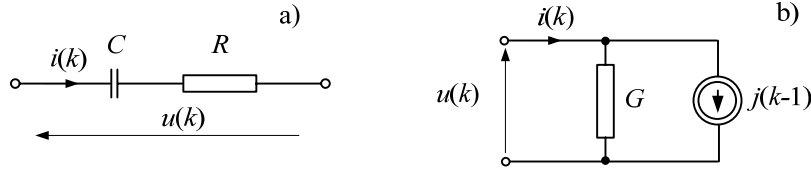


Fig. 1.23. Series RC model.

The respective relations are:

$$i(k) = \frac{2C}{T}(u(k) - Ri(k)) - i(k-1) - \frac{2C}{T}(u(k-1) - Ri(k-1)) \quad (1.112)$$

$$i(k) = G(u(k) - u(k-1)) - \alpha i(k-1) \quad (1.113)$$

where: $G = \frac{2C}{T + 2RC}$, $\alpha = \frac{\frac{T}{2C} - R}{\frac{T}{2C} + R}$.

In this case the oscillations of current occur for $\alpha = 1$ ($R=0$) at the moment when $u(k)=u(k-1)=0$.

It must be noted that the damping resistor changes the frequency response of the model considered. For example, in case of inductance, the eqn. (1.66) now takes the form:

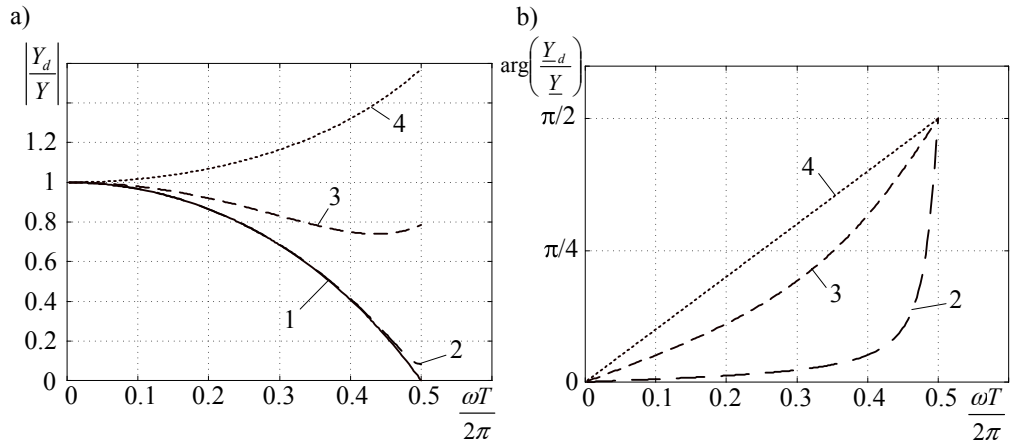


Fig. 1.24. Frequency response for magnitude and argument of the relation $\underline{Y}_d / \underline{Y}_c$; 1 - $\alpha = 1$, 2 - $\alpha = 0.818$, 3 - $\alpha = 0.333$, 4 - $\alpha = 0$.

$$i(j\omega) = G \frac{e^{j\omega T} + \alpha}{e^{j\omega T} - 1} u(j\omega) = \underline{Y}_d \underline{U}_d(j\omega) \quad (1.114)$$

and G and α are as in (1.110) and (1.111), respectively.

The relation between the digital \underline{Y}_d and continuous \underline{Y}_c admittances for different values of α are shown in Fig. 1.24.

1.5.3. Suppression of numerical oscillations by change of integration method

The analysis carried out above shows that numerical oscillations are related directly to the method of continuous derivative approximation.

Using the three different approximations considered, namely:

- $u(k) = \frac{L}{T} (i(k) - i(k-1))$ implicit Euler's method,
- $u(k) = \frac{2L}{T} (i(k) - i(k-1)) - u(k-1)$ trapezoidal approximation,
- $u(k) = \frac{L}{2T} (3i(k) - 4i(k-1) + i(k-2))$ Gear's 2nd order.

for the same network model (example) different intensity of numerical oscillations can be observed. It is shown in Fig. 1.25.

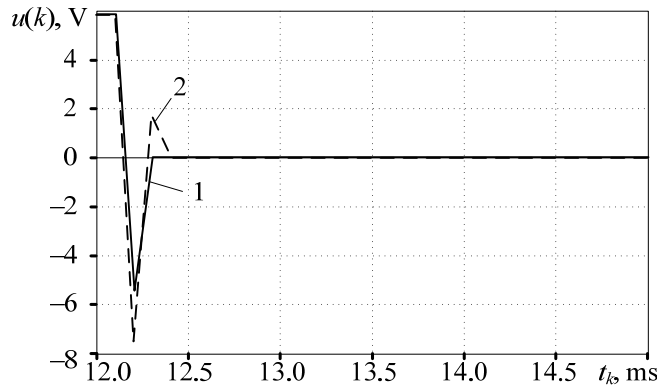


Fig.1.25. Oscillations at the inductor (sample network); 1 – implicit Euler's method, 2 – Gear's 2nd order

The Euler's method reveals the best oscillation damping property since they are suppressed in one calculation step (critical damping). The Gear's method is slightly worse. On the other hand the trapezoidal method that is least stable offers simplicity and good accuracy of calculations in steady state (no rapid changes of the network parameters) [2].

Thus, in practice, the combination of Euler's and trapezoidal methods are applied in the following way:

- if step there are no rapid changes of the network parameters in the current calculation the trapezoidal method is used;
- otherwise the Euler's implicit method takes the calculations over for 2 consecutive steps but of twice shorter duration ($T/2$) to avoid the model parameter change.

1.5.4. The root matching technique

Another approach to the numerical network representation that results in suppression of numerical oscillation is the use of the root matching technique [88, 89]. In this approach the network model is based on the continuous transfer function relating current and voltage in the network considered. In general such a transfer function has the form:

$$H(s) = \frac{(s - s_{z1})(s - s_{z2})...(s - s_{zM})}{(s - s_{p1})(s - s_{p2})...(s - s_{pN})} \quad (1.115)$$

Transformation to the discrete domain is obtained by replacement of continuous zeros and poles by their discrete counterparts:

$$z_i = e^{s_i T} \quad i - \text{the number of respective zero and pole} \quad (1.116)$$

so that:

$$H_d(z) = \frac{D(z - e^{s_{z1}T})(z - e^{s_{z2}T})...(z - e^{s_{zM}T})}{(z - e^{s_{p1}T})(z - e^{s_{p2}T})...(z - e^{s_{pN}T})} \quad (1.117)$$

This operation is called a *matched Z transform* [42].

The constant D is determined by comparison of steady state response for specified excitation which should be the same for the continuous and the discrete system.

Since the calculations are carried out in off-line mode the input signals can be represented (sampled) in many different ways. Some of them are shown in Fig. 1.26.

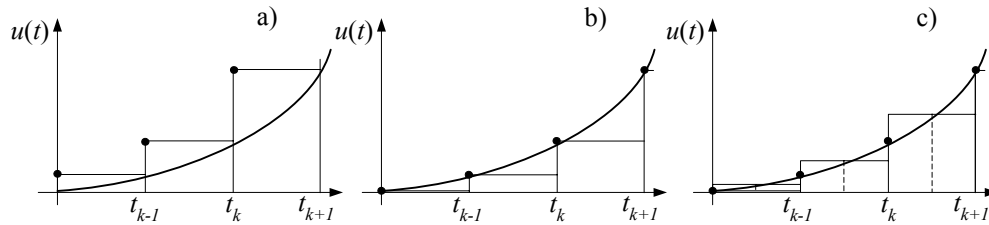


Fig.1.26. The ways of the continuous input signal representation (sampling).

Thus the final discrete transfer function $H(z)$ must be corrected accordingly by use of the sampling function $H_s(z)$ related to the applied signal sampling operation:

$$H(z) = H_d(z)H_s(z) \quad (1.118)$$

and

$$H_s(z) = z \text{ for Fig. 1.26a}$$

$$H_s(z) = 1 \text{ for Fig. 1.26b}$$

$$H_s(z) = \frac{1}{2}(z+1) \text{ for Fig. 1.26c}$$

Thus the algorithm of the *matched Z transform* application can be summarized as follows:

- determine the continuous transfer function $H(s)$ of the network considered,
- transform $H(s)$ into $H(z)$ replacing all continuous zeros and poles by use of (1.116),
- determine the constant D so that $\mathcal{L}\{y(t)\}_{t \rightarrow \infty} = \mathcal{Z}\{y(k)\}_{k \rightarrow \infty}$ for specified input signal - y denotes the output variable (current or voltage).

Example 1.3. Using the root matching technique determine the digital model of the circuit shown Fig. 1.27a

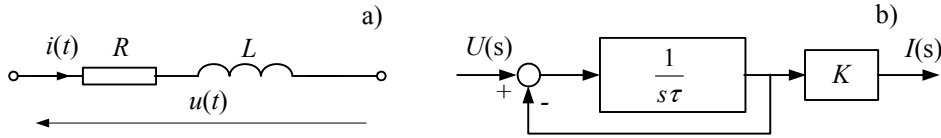


Fig.1.27. The network considered a) and its equivalent block diagram b)

The network considered is described in continuous Laplace domain by the following equation:

$$U(s) = (R + sL)I(s)$$

and its transfer function is like below:

$$H(s) = \frac{I(s)}{U(s)} = \frac{\frac{1}{R}}{1 + s\frac{L}{R}} = \frac{K}{1 + s\tau}$$

and can be represented by the block diagram like in Fig. 1.27b.

The transfer function obtained has no finite zeros and only one pole $s_{p1} = -1/\tau = -R/L$.

Assuming that the input signal (voltage) is sampled as in Fig. 1.27a and using the transformation (1.118) the resulting discrete transfer function is obtained:

$$H(z) = \frac{D}{(z - e^{-TR/L})} z = \frac{Dz}{(z - e^{-TR/L})}$$

To determine D let's assume that $u(t)$ is a unit step function $u(t) = 1[t]$ for which $U(s) = 1/s$, and:

$$i(s) = \frac{K}{s(1 + s\tau)}.$$

The steady state response is now:

$$i(t)\big|_{t \rightarrow \infty} = \lim_{s \rightarrow 0} sI(s) = \lim_{s \rightarrow 0} \frac{K}{1 + s\tau} = K.$$

Similarly for $u(k) = 1(k)$ and $Z\{1(k)\} = z/(z-1)$:

$$I(z) = \frac{Dz^2}{(z - e^{-TR/L})(z-1)}$$

and

$$i(k)\big|_{k \rightarrow \infty} = \lim_{z \rightarrow 1} (z-1)I(z) = \lim_{z \rightarrow 1} \frac{Dz^2}{z - e^{-TR/L}} = \frac{D}{1 - e^{-TR/L}}.$$

By comparison of steady state responses we get:

$$D = (1 - e^{-TR/L})K.$$

So, finally:

$$H(z) = \frac{I(z)}{U(z)} = \frac{(1 - e^{-TR/L})z}{R(z - e^{-TR/L})}.$$

Now in few steps the numerical algorithm for calculation of $i(k)$ can be written:

$$RI(z)(1 - e^{-TR/L}z^{-1}) = U(z)(1 - e^{-TR/L})$$

$$i(k) = Gu(k) + j(k-1),$$

where:

$$G = \frac{(1 - e^{-TR/L})}{R}, \quad j(k-1) = e^{-TR/L}i(k-1).$$

It can be noted that the past history of the algorithm depends upon the current only so the voltage oscillations on inductance due to the rapid change of current will not occur. In the similar way the numerical algorithms corresponding to the typical first and the higher order transfer functions and related to them electrical elements can be developed.

It also must be noted that the method considered can be applied to the transfer functions that have at least one zero or pole located outside the origin of the s plane. Thus the single L , C elements must be modelled using the trapezoidal method.

The comparison of oscillation suppression properties for the root matching and the trapezoidal method is shown Fig. 1.28. The obtained current waveforms are evidently in favour of the root-matching algorithm.

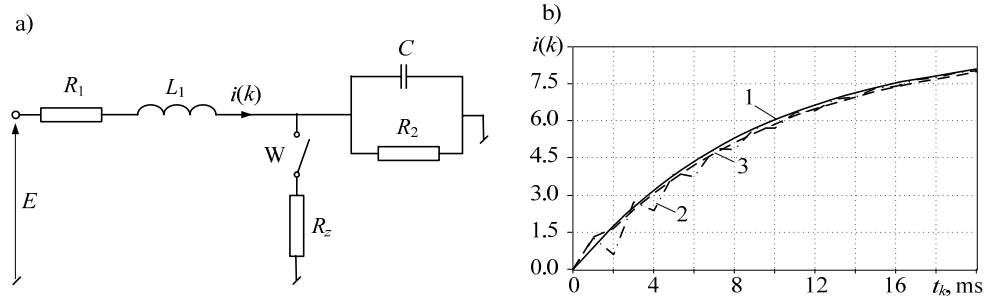


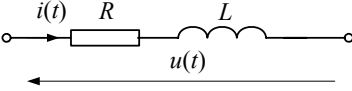
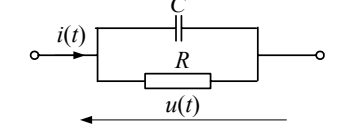
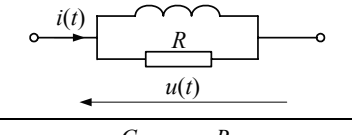
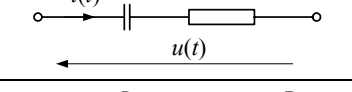
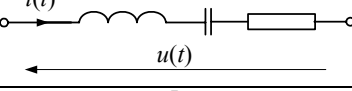
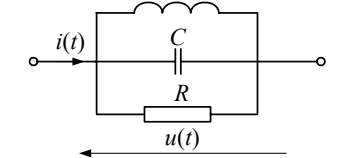
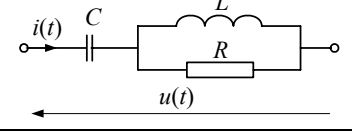
Fig. 1.28. The current $I(k)$ waveform after closing of W; 1- accurate values; 2- trapezoidal method; 3 - the root matching method.

Table 1.2. Parameters of digital models obtained by use of root matching method [88]

Nr	Element transmittance: $H(s) = I(s)/U(s)$	Model parameters $i(k) = Gu(k) + j(k-1)$
1	$H(s) = K/(1+s\tau)$	$G = K(1 - e^{-T/\tau})$, $j(k-1) = e^{-T/\tau}i(k-1)$
2	$H(s) = K(1+s\tau)$	$G = K/(1 - e^{-T/\tau})$, $j(k-1) = -e^{-T/\tau}Gu(k-1)$
3	$H(s) = Ks/(1+s\tau)$	$G = K(1 - e^{-T/\tau})/T$, $j(k-1) = e^{-T/\tau}i(k-1) - Gu(k-1)$
4	$H(s) = K(1+s\tau_1)/(1+s\tau_2)$	$G = K(1 - e^{-T/\tau_1})/(1 - e^{-T/\tau_2})$, $j(k-1) = e^{-T/\tau_2}i(k-1) - e^{-T/\tau_1}Gu(k-1)$
5	$H(s) = K\omega_n^2/(s^2 + 2\xi\omega_n s + \omega_n^2)$	$G = K(1 - A + B)$, $j(k-1) = Ai(k-1) - Bi(k-2)$
6	$H(s) = K\omega_n^2 s/(s^2 + 2\xi\omega_n s + \omega_n^2)$	$G = K(1 - A + B)/T$, $j(k-1) = Ai(k-1) - Gu(k-1) - Bi(k-2)$
7	$H(s) = K\omega_n s/(s^2 + 2\xi\omega_n s + \omega_n^2)$	$G = T/(K(1 - A + B))$, $j(k-1) = i(k-1) - AGu(k-1) + BGi(k-2)$
The coefficients A i B depend upon roots of the transmittance characteristic equation:		
$\xi > 1$: $A = 2e^{-\xi\omega_n T} \left(e^{T\omega_n \sqrt{\xi^2 - 1}} + e^{-T\omega_n \sqrt{\xi^2 - 1}} \right)$, $B = e^{-2\xi\omega_n T}$		
$\xi = 1$: $A = 2e^{-\omega_n T}$, $B = e^{-2\omega_n T}$		
$\xi < 1$: $A = 2e^{-\xi\omega_n T} \cos\left(\omega_n T \sqrt{1 - \xi^2}\right)$, $B = e^{-2\xi\omega_n T}$		

The root matching method lends itself very well to networks described by transmittances. The examples of digital models corresponding to typical transmittances are shown in Table 1.2 while the examples of electric circuits related to transmittances in Table 1.2 are shown in Table 1.3.

Table 1.3. Examples of electric circuits of transmittances shown in Table 1.2

Nr	Diagram	Parameters of digital model	Model w Table 1.2
1a		$K = 1/R, \tau = L/R$	1
1b		$K = R, \tau = RC$	1, inverse
2a		$K = L, \tau = L/R$	3
2b		$K = C, \tau = RC$	3, inverse
3a		$K = C, \omega_n^2 = \frac{1}{LC}, \xi = \frac{R}{2} \sqrt{\frac{C}{L}}$	6
3b		$K = RL, \omega_n^2 = \frac{1}{LC}, \xi = \frac{R}{2} \sqrt{\frac{C}{L}}$	6, inverse
3c		$K = L, \omega_n^2 = \frac{1}{LC}, \xi = \frac{1}{2R} \sqrt{\frac{L}{C}}$	6, inverse

Term 'inverse' in the last column means, current and voltage in the transmittance $H(s) = U(s)/I(s)$ in the corresponding numerical algorithm in Table 1.2, should be inverted. In such case G in the equivalent circuit denotes resistance and $j(k-1)$ corresponds to voltage.

Exercises

- 1.1. Solution of differential equation:

$$\frac{dy(t)}{dt} = f(y, t)$$

by use of the second order Adams–Bashforth’s numerical method is as follows:

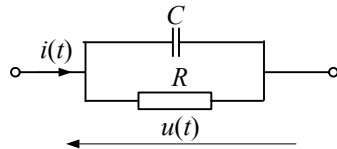
$$y(k) = y(k-1) + \frac{T}{2} (3f(y(k), t_k) - f(y(k-1), t_{k-1})).$$

Using this method determine numerical models of:

- inductance L ,
- capacitance C ,
- in series connected R and the L .

- 1.2. Using the trapezoidal integration method determine the numerical models of the following branches:

a)



b)

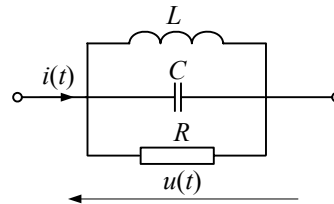


Fig. Z1.1

- 1.3. Consider the single phase long line (1.93) and, assuming that the line is supplied by an ideal voltage source, derive the respective numerical models for the line output being:
- a) short-circuited, b) open.
- 1.4. Prove that the use of bilinear transformation:
- $$s = \frac{2}{T} \frac{z-1}{z+1}$$
- in transmittance $H(s)$ of the first order system is equivalent to application of trapezoidal integration method.
- 1.5. Using the root matching technique determine the numerical models of the circuits shown in Fig.Z1.2. Assume the signal sampling like in Fig. 1.25a.

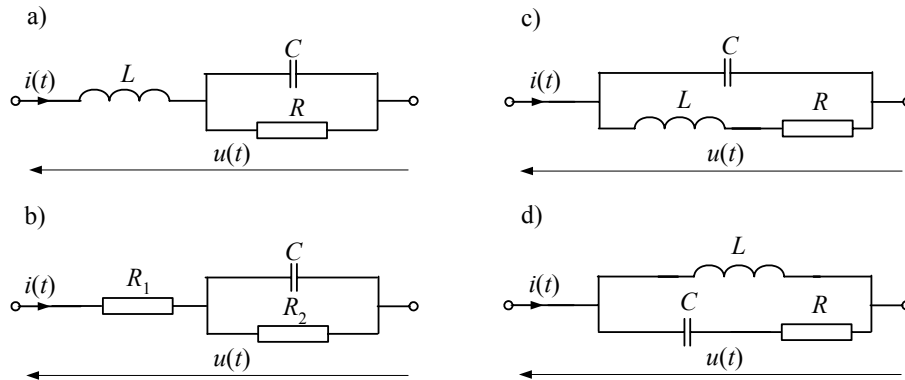


Fig. Z1.2

1.6. In steady state the circuits shown in Fig. Z1.3a, b are supplied by: $u(t) = 100 \cos(\omega t + \varphi)$, $\omega = 100\pi$, $\varphi = \pi/3$ and the switches W are open. Simulate transients for switches being closed at the instant $t_z = 0.02$ s in the following steps:

- determine the equivalent numerical model of the circuit considered like in Fig. Z1.3c, using the Euler explicit method (rectangular integration method). Hint: the switch can be represented as variable resistance R_2 or R_3).
- determine the initial conditions (the values of $j(0)$);
- simulation time: 0.1 s;

Repeat the simulation for model derived by use of trapezoidal integration method.

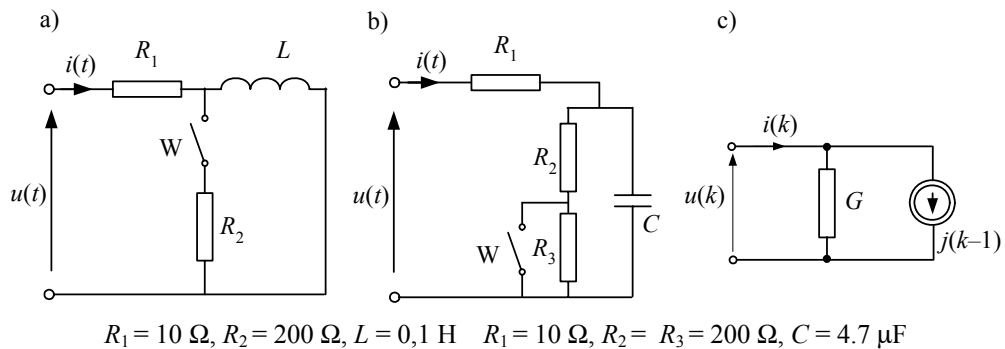


Fig. Z1.3

1.7. Simulate the transient overvoltages generated when the switch W in the d.c. circuit (Fig. Z1.4) opens. Calculate the initial conditions from the circuit node equation and for this purpose assume that the input is a low frequency a.c. voltage (instead of $u = U$ use $u = U \cos(2\pi f t)$, $f = 5\text{--}10$ Hz).

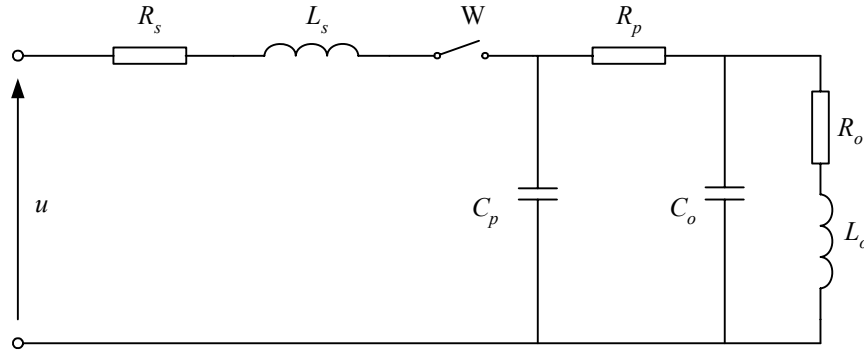


Fig. Z1.4

Solve the node equations using MATLAB or similar program.

The circuit parameters:

$U = 24 \text{ V}$, $R_s = 1 \text{ } \Omega$, $L_s = 64 \text{ mH}$, $R_p = 0,5 \text{ } \Omega$, $R_o = 10 \text{ } \Omega$, $L_o = 95 \text{ mH}$, $C_o = 0,5 \text{ } \mu\text{F}$, $C_p = 0,2 \text{ } \mu\text{F}$. The switch opens at $t_w = 0$.

- 1.8. Determine the numerical model of the network shown in Fig. Z1.4 for trapezoidal integration method. Write the node equations for the numerical model obtained. Show the equations describing the nodal current vector in each calculation step. Simulate transients when the switch W opens (use MATLAB program). Assume the calculation step $T = 1 \text{ } \mu\text{s}$. Calculate the initial conditions as in problem 1.7.

2. NONLINEAR AND TIME-VARYING MODELS

2.1. Solution of nonlinear equations

Elements of electric networks are said to be nonlinear if their physical parameters R , L or C are not constant but depend on either currents flowing through or voltage drop across them. Additionally, if their parameters also change in time such elements are said to be the time varying ones. Generally, digital modelling of the nonlinear elements is much more sophisticated than modelling of the time varying ones.

The numerical models of on nonlinear elements are described by nonlinear differential equations which must be solved in each calculation step by simulation programs in the process of transients' calculation. There are many methods by which the nonlinear equations can be solved but, excluding some rare cases, all that methods yield approximate solutions which are obtained by use of iterative procedures. Below the short description of the method for single variable nonlinear equation solution known as the Newton's method is presented along with extension of the method to multivariable case

2.1.1. Newton's method

If a function is smooth enough it can be represents by a straight line tangent to the function (linear approximation of the higher order functions).

If the variable x_1 is located in vicinity of the root α of the function $f(x)$, then its value can be determined from the Taylor's series [32, 83]:

$$f(\alpha) = f(x_1) + f'(x_1)(\alpha - x_1) + \frac{1}{2}f''(x_1)(\alpha - x_1)^2 + \dots \quad (2.1)$$

Limiting the above series to the first two terms determination of the root can be obtained by solution of the following equation:

$$f(x_1) + f'(z)(\alpha - x_1) = 0 \quad (2.2)$$

Using (2.2) the iteration formula can be derived under assumption that α is the better approximation of the solution sought (subsequent n -th solution) than the one

obtained for z in previous $n-1$ iteration. Generalizing, the following formula can be obtained:

$$x^n = x^{n-1} - \frac{f(x^{n-1})}{f'(x^{n-1})} \quad (2.3)$$

Formula (2.3) is known as the Newton's method of nonlinear equation solution [31, 32, 83] and is advantageous to the other methods used for the purpose since, in particular:

- the method is strongly convergent,
- it covers the wide class of functions for which the iteration process is convergent as compared to the methods using direct iteration.

Application of the method discussed can be explained by the following example:

Example 2.4. Using the Newton's method determine the current flowing in the circuit shown in Fig. 2.1a.

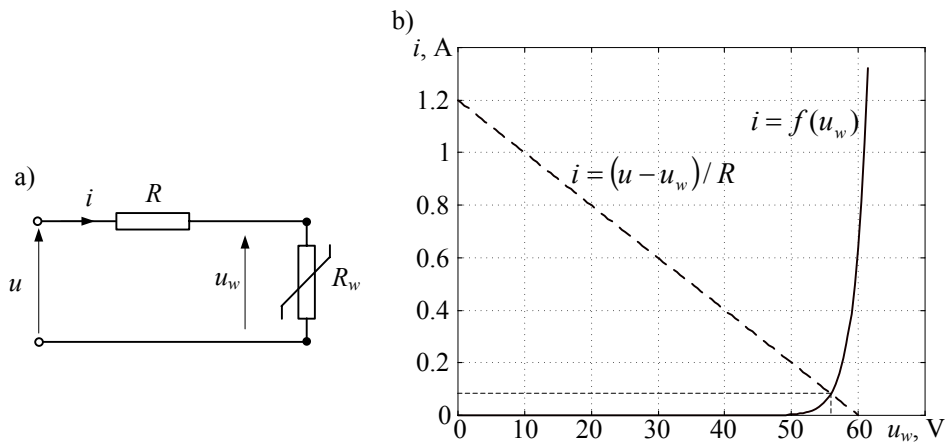


Fig 2.1. Example of the nonlinear network: a) the diagram and b) graphical method of the working point estimation

The nonlinear resistor represents a varistor whose v - i characteristic is given by the following equation:

$$i = k_i \left(\frac{u_w}{u_{ref}} \right)^q \quad (2.4)$$

For which: $k_i = 0.001$ A, $u_{ref} = 48$ V, $q = 29$, $R = 50$ Ω . Supply voltage $u = 60$ V.

Let's discuss the Newton's method for current and voltage equations which describe the circuit shown in Fig.2.1a. Note that in Newton's method the function considered must take the form:

$$f(x) = 0 \quad (2.5)$$

so (2.4) can be written in the following voltage form:

$$f(u_w) = u - Rk_i \left(\frac{u_w}{u_{ref}} \right)^q - u_w \quad (2.6)$$

The resulting iterative algorithm is:

$$u_w^n = u_w^{n-1} - \frac{f(u_w^{n-1})}{f'(u_w^{n-1})}, \text{ where: } f(u_w^{n-1}) = u - Rk_i \left(\frac{u_w^{n-1}}{u_{ref}} \right)^q - u_w^{n-1}, \quad f'(u_w^{n-1}) = -\frac{qRk_i}{u_{ref}} \left(\frac{u_w^{n-1}}{u_{ref}} \right)^{q-1} - 1.$$

The result of calculations is shown in Fig. 2.2a. The iteration process is convergent. For the current equation we get:

$$f(i) = u - Ri - u_{ref} \left(\frac{|i|}{k_i} \right)^{\frac{1}{q}} \quad (2.7)$$

$$\text{from which: } i^n = i^{n-1} - \frac{f(i^{n-1})}{f'(i^{n-1})},$$

$$\text{where: } f(i^{n-1}) = u - Ri^{n-1} - u_{ref} \left(\frac{|i^{n-1}|}{k_i} \right)^{\frac{1}{q}}, \quad f'(i^{n-1}) = \frac{-u_{ref}}{q|i^{n-1}|} \left(\frac{|i^{n-1}|}{k_i} \right)^{\frac{1}{q}} - R.$$

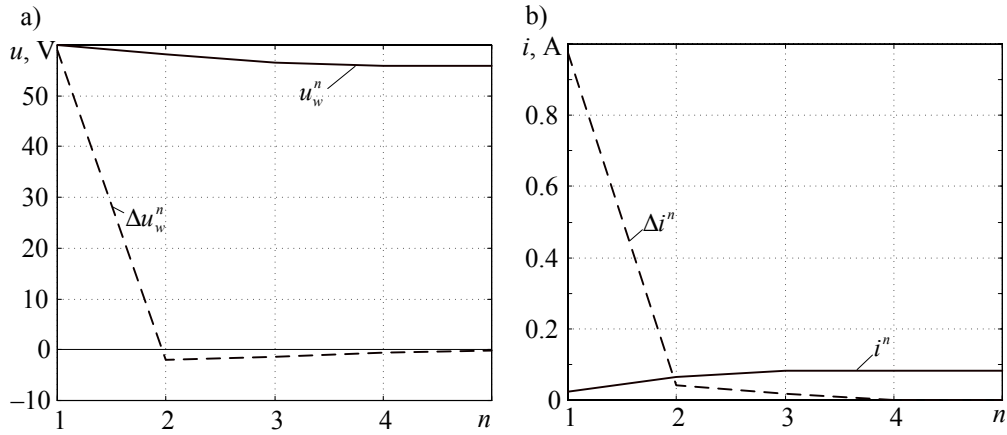


Fig. 2.2. Iteration process according to the Newton's method: a) for the voltage equation and b) for the current equation

The calculation process is shown in Fig. 2.2b. Again, the iteration process is convergent.

The Newton's method is very effective tool in numerical solution of nonlinear equations and is widely applied to iterative algorithms designs which are used in simulation programs.

2.1.2. Newton–Raphson's method

In general any set of nonlinear equations can be written as follows:

$$f(\mathbf{x}) = \begin{bmatrix} f_1(x_1, x_2, \dots, x_m) \\ f_2(x_1, x_2, \dots, x_m) \\ \dots \\ f_m(x_1, x_2, \dots, x_m) \end{bmatrix} = 0 \quad (2.8)$$

in which at least one function is nonlinear.

Solution of this set is obtained by determination of vector $\mathbf{x} = [x_1 \ x_2 \ \dots \ x_m]^T$ for which (2.5) is satisfied. The solution can be obtained by means of the method used for a single nonlinear equation extended to a multi-variable case. Thus the equation (2.1) can be now written as:

$$f(\xi) \approx f(\mathbf{x}^0) + (\xi - \mathbf{x}^0) f'(\mathbf{x}^0) + \dots = 0 \quad (2.9)$$

where the vector ξ represents coordinates of the point in multivariable space for which (2.8) is satisfied.

Matrix which determines the derivative $f'(\mathbf{x}^0)$ is known as Jacobean (Jacoby's matrix) and:

$$\mathbf{J}(f(\mathbf{x})) = f'(\mathbf{x}) = \frac{\partial f(\mathbf{x})}{\partial \mathbf{x}} = \begin{bmatrix} \frac{\partial f_1}{\partial x_1} & \frac{\partial f_1}{\partial x_2} & \dots & \frac{\partial f_1}{\partial x_m} \\ \frac{\partial f_2}{\partial x_1} & \frac{\partial f_2}{\partial x_2} & \dots & \frac{\partial f_2}{\partial x_m} \\ \vdots & \vdots & \dots & \vdots \\ \frac{\partial f_m}{\partial x_1} & \frac{\partial f_m}{\partial x_2} & \dots & \frac{\partial f_m}{\partial x_m} \end{bmatrix} \quad (2.10)$$

By analogy to (2.2) expansion of (2.9) leads to the following iterative procedure which can be applied to solution of the set (2.8):

$$\mathbf{x}^n = \mathbf{x}^{n-1} - \mathbf{J}^{-1}(f(\mathbf{x}^{n-1})) f(\mathbf{x}^{n-1}) \quad (2.11)$$

providing $\det[\mathbf{J}(f(\mathbf{x}^{n-1}))] \neq 0$, and $\mathbf{J}(f(\mathbf{x}^n)) = \mathbf{J}(f(\mathbf{x}))|_{\mathbf{x}=\mathbf{x}^n}$.

The algorithm (2.11) is known as Newton–Raphson’s method and is widely used for iterative solving of nonlinear equation sets. In computer programs the procedure (2.11) is realized according to the following sequence:

- calculate $f(\mathbf{x}^{n-1})$,
- calculate $\mathbf{J}(f(\mathbf{x}^{n-1})) = f'(\mathbf{x}^{n-1})$,
- solve the set on resulting linear equations: $\mathbf{J}(f(\mathbf{x}^{n-1}))\mathbf{z}^{n-1} = f(\mathbf{x}^{n-1})$,
- determine the subsequent approximation $\mathbf{x}^n = \mathbf{x}^{n-1} - \mathbf{z}^{n-1}$.

Conversion of the process is determined on the basis of vector \mathbf{z}^{n-1} norm related to the norm of \mathbf{x}^{n-1} :

$$\frac{\|\mathbf{z}^{n-1}\|}{\|\mathbf{x}^{n-1}\|} < \varepsilon \quad (2.12)$$

Due to the limited accuracy of function $f(\mathbf{x}^{n-1})$ and Jacobean $\mathbf{J}(f(\mathbf{x}^{n-1}))$ determination the overall accuracy of the algorithm is also limited. It is manifested by further increase of vector \mathbf{z}^{n-1} norm after reaching the minimum value. It is the indication that further calculations should be ended and the algorithm terminating calculations has the form:

$$\|\mathbf{z}^n\| > \rho \|\mathbf{z}^{n-1}\| \quad (2.13)$$

where the value of the ρ coefficient is close to one.

In the similar way the other methods of the nonlinear equations solution can be extended to multi-variable case. In general each model of any electric network comprises of both linear and nonlinear elements. So, in overall model, the set of known linear elements must be complemented by the nonlinear models of resistances, inductances and capacitances. Below the general rules of the combined model setup are presented. Similarly to the linear models the nonlinear ones are expressed in current- conductance form which matches the nodal method.

2.2. Models of non-linear elements

The typical nonlinear i - v transition characteristics encountered in electric networks are shown in Fig. 2.3. The most typical one is show in Fig.2.3a: resistance (conductance) of such an element is positive and unique in the entire voltage domain. The characteristics in Fig. 2.3b, c reveal the intervals of negative resistance (conductance) while the case in Fig.2.3d, typical for nonlinear magnetic elements (hysteresis), is not a function but relation.

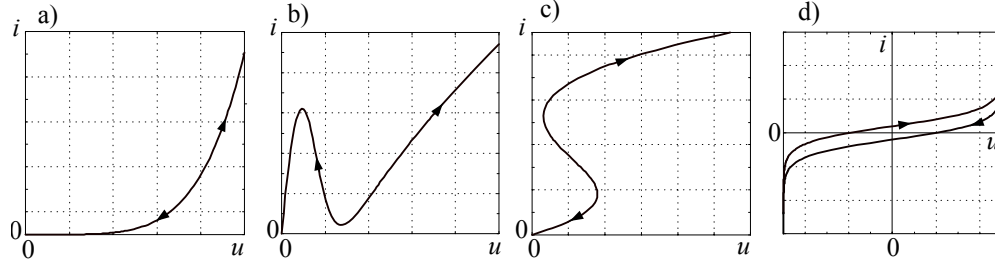


Fig. 2.3. Characteristics $i = f(u)$ of nonlinear electric elements :
a) monotonic, b) type N, c) type S, d) with hysteresis

2.2.1. Resistance

Functional relation between current and voltage is valid for characteristics show in Fig. 2.3a,b,c. The basic way of the respective numerical model formulation for such elements is shown in Fig. 2.4.

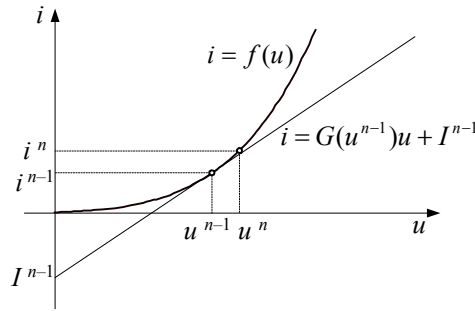


Fig. 2.4. The idea of iterative model formulation for nonlinear conductance

The considered characteristic $i = f(u)$ is the continuous and smooth function. In the point of coordinates u^{n-1}, i^{n-1} conductance of the element can be determined by the following relation:

$$G(u^{n-1}) = G^{n-1} = \left. \frac{di}{du} \right|_{u=u^{n-1}} = \left. \frac{df(u)}{du} \right|_{u=u^{n-1}} \quad (2.14)$$

The straight line tangent to the function considered in the point u^{n-1}, i^{n-1} (Fig. 2.4) is described by the equation:

$$i = G^{n-1}u + I^{n-1} \quad (2.15)$$

The value of $i^n = f(u^n)$ can be estimated for small change of voltage to the value u^n according to (2.15):

$$i^n = G^{n-1}u^n + I^{n-1} \quad (2.16)$$

in which the value of the current I^{n-1} in $n-1$ calculation step is:

$$I^{n-1} = i^{n-1} - G^{n-1}u^{n-1} \quad (2.17)$$

where: $i^{n-1} = f(u^{n-1})$.

Relations (2.16) and (2.17) determine the iterative model of nonlinear conductance. The corresponding equivalent circuit is like in Fig. 2.5.

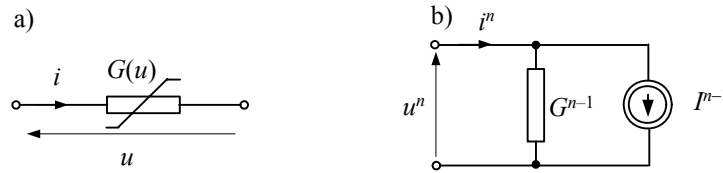


Fig. 2.5. Iterative model of conductance: a) conductance branch; b) equivalent diagram

The method shown can be used for calculations in nonlinear networks if the mapping of u^n across conductance in subsequent calculation step, made on the basis of the current i^{n-1} estimation, is correct. It can be illustrated by the following example.

Example 2.5. Apply model (2.16) to the circuit considered in Example 2.1.

The principle of electric diagrams formulation for linear and nonlinear elements is the same as in previous case. So, in the circuit (Fig. 2.1a) the voltage source is converted into the equivalent current one and the nonlinear element is replaced by circuit shown in Fig. 2.5b. The resulting diagram is shown in Fig. 2.6. It is a 2-node network with the reference node earthed.

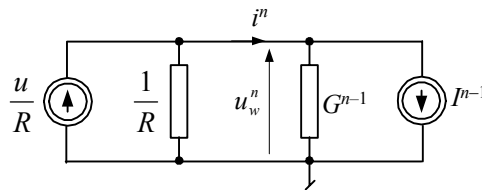


Fig. 2.6. Equivalent diagram of the circuit in Fig. 2.1a

Using the nodal method the following circuit equation can be obtained:

$$(G^{n-1} + 1/R)u_w^n = u/R - I^{n-1} \quad (2.18)$$

where: $I^{n-1} = i^{n-1} - G^{n-1}u_w^{n-1}$, $i^{n-1} = k_i \left(\frac{u_w^{n-1}}{u_{ref}} \right)^q$ (see (2.3) and $G^{n-1} = \frac{di}{du_w} \Big|_{u_w=u_w^{n-1}} = \frac{qk_i}{u_{ref}} \left(\frac{u_w^{n-1}}{u_{ref}} \right)^{q-1}$.

Calculations are carried out in the following way:

1. Set initial conditions: $u_w^0 = u_{w0}$, $n = 0$.
2. Put $n = n + 1$.
3. Calculate: i^{n-1} , G^{n-1} , I^{n-1} .
4. Calculate u_w^n from (2.18): $u_w^n = \frac{u/R - I^{n-1}}{G^{n-1} + 1/R}$.
5. If $|u_w^n - u_w^{n-1}| > \varepsilon$, go to 2.

The algorithm is equivalent to the Newton's method which was used in Example 2.4 [18] since in both cases the same results are obtained.

In case of characteristic like in Fig. 2.3c the solution for the specified voltage may not be unique. Therefore resistance related to the function $u = f(i)$ should be considered instead of conductance (Fig. 2.7). Again, assuming that the function $u = f(i)$ is smooth and continuous, the value of u is obtained in n -th approximation from the equation of the straight line which is tangent to the curve in $n-1$ -th point so that:

$$u = R(i^{n-1})i + U^{n-1} = R^{n-1}i + U^{n-1} \quad (2.19)$$

in which: $U^{n-1} = u^{n-1} - R^{n-1}i^{n-1}$, $R^{n-1} = \frac{df(i)}{di} \Big|_{i=i^{n-1}}$.

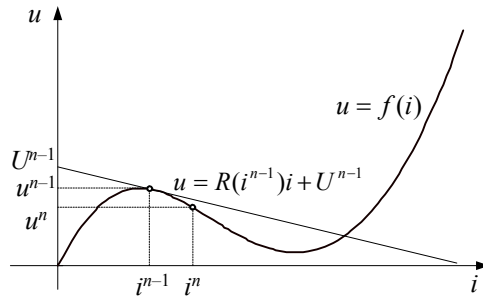


Fig. 2.7. The idea of iterative model formulation for nonlinear conductance

Using (2.19) the following approximation for subsequent iteration is obtained:

$$u^n = R^{n-1}i^n + U^{n-1} \quad (2.20)$$

which can be transformed into (like in (2.16)):

$$i^n = G^{n-1}u^n + I^{n-1} \quad (2.21)$$

where: $G^{n-1} = \frac{1}{R^{n-1}} = \frac{1}{\left. \frac{df(i)}{di} \right|_{i=i^{n-1}}}$, $I^{n-1} = i^{n-1} - G^{n-1}u^{n-1}$.

As it can be seen the nonlinear conductance model expressed in current-conductance form is independent of the nonlinear characteristic shape. The difference only concerns the way in which the equivalent conductance is calculated.

2.2.2. Inductance

Basic mathematical model of inductance is determined by the equation:

$$u(t) = \frac{d\psi(t)}{dt} \quad (2.22)$$

where: ψ is a magnetic flux.

Alternative form of (2.22) is:

$$u(t) = L(i) \frac{di(t)}{dt} \quad (2.23)$$

where: $L(i) = \frac{d\psi(i)}{di}$ and $\psi(t) = L(i)i(t)$.

If $\psi(i)$ is nonlinear then inductance is a function of current then $L = L(i)$.

In order to obtain the digital model of inductance related to (2.23) the numerical model (1.31) can be used:

$$i(k) = Gu(k) + j(k-1) \quad (2.24)$$

in which, for trapezoidal method: $j(k-1) = i(k-1) + Gu(k-1)$, $G = \frac{T}{2L}$.

In this case, however, the conductance G is not constant:

$$G(i(k)) = \frac{T}{2L(i(k))} \quad (2.25)$$

and the equation (2.24) should be written as:

$$i(k) = \frac{T}{2L(i(k))} u(k) + i(k-1) + \frac{T}{2L(i(k-1))} u(k-1) \quad (2.26)$$

In k -th calculation step inductance $L(i(k-1))$ is known along with history of the process which is determined by the current $j(k-1)$. The first term of (2.26) is the model of nonlinear resistance $R(i(k)) = \frac{2L(i(k))}{T}$ so that:

$$i(k) = \frac{1}{R(i(k))} u(k) + j(k-1) \quad (2.27)$$

where: $j(k-1) = i(k-1) + \frac{1}{R(i(k-1))} u(k-1)$, $R(i(k-1)) = \frac{2L(i(k-1))}{T}$.

To solve this equation the iterative method (2.21) can be applied and the value of $j(k-1)$ in the k -th calculation step is:

$$i^n(k) = G(i^{n-1}(k)) u^n(k) + I^{n-1}(k) + j(k-1) \quad (2.28)$$

where: $I^{n-1}(k) = i^{n-1}(k) - G(i^{n-1}(k)) u^{n-1}(k)$, $G(i^{n-1}(k)) = \frac{T}{2L(i^{n-1}(k))}$ (for trapezoidal integration method).

It can be noted that modelling of nonlinear inductance comprises of two calculation processes: digital integration which is denoted by calculation step number k and iterative approximation of solution carried out in each calculation step which is denoted in (2.28) by index n . As the initial value of the current in current calculation step the value calculated in the previous step can be taken i.e.: $i^0(k) = i(k-1)$. Equation (2.28) represents the iterative model of nonlinear inductance in which the selected method of numerical integration is arbitrary.

The equivalent circuit of the nonlinear inductance is shown in Fig. 2.8.

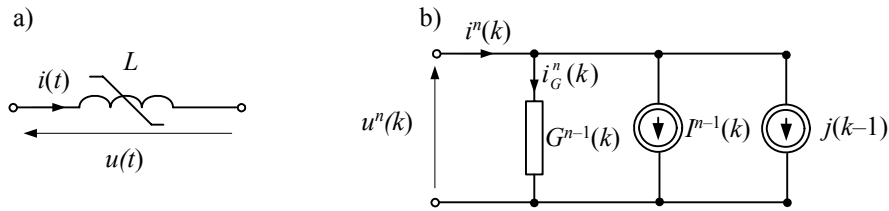


Fig. 2.8. Digital iterative model of the nonlinear inductance a) symbol of nonlinear inductance, b) the equivalent diagram of the digital model

2.2.3. Capacitance

In the similar manner the numerical model of a nonlinear capacitance can be derived. Starting from the fundamental equations:

$$i(t) = \frac{dq(t)}{dt} \quad (2.29)$$

where q is the electric charge: $q(t) = C(u)u(t)$, and:

$$\frac{du(t)}{dt} = \frac{1}{C(u)} i(t) \quad (2.30)$$

where: $C(u) = \frac{dq(u)}{du}$,

the numerical model for trapezoidal integration method (1.37) takes the form:

$$i(k) = G(u(k))u(k) + \frac{G(u(k))}{G(u(k-1))} j(k-1) \quad (2.31)$$

in which: $G(u(k)) = \frac{2C(u(k))}{T}$, $j(k-1) = i(k-1) + G(u(k-1))u(k-1)$.

Since the conductance is now a function of voltage solution of this equation can be obtained by use of the iterative method (2.16) and in such case:

$$i^n(k) = G(u^{n-1}(k))u^n + I^{n-1}(k) \quad (2.32)$$

where: $I^{n-1}(k) = i^{n-1}(k) - G(u^{n-1}(k))u^{n-1}$.

It should be noted that solution of (2.31) calls for application of the iterative method like it was done for solution of (2.27) (in his case voltage and current must be mutually altered). The equivalent diagram of the nonlinear capacitance model is shown in Fig. 2.9.

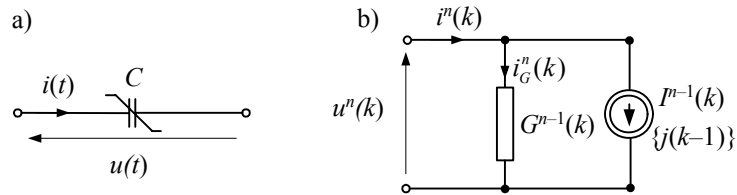


Fig. 2.9 Equivalent diagram: a) nonlinear capacitance and b) digital iterative model

2.3. Models of non-linear and time-varying elements

2.3.1. Non-linear and time-varying scheme

Any electric network becomes nonlinear if at least one of the network elements is nonlinear. In such case the network can be analyzed by use of Newton–Raphson’s algorithm rather than by direct use of the nodal method. In this approach the network equations should be written in form of (2.8) and the resulting calculation algorithms become very complex.

The nodal method can be applied if the network is represented by discussed above linear and nonlinear models. The method, in case of linear network, leads to the general equation (1.97) which for the nonlinear network can be written as:

$$\mathbf{G}^{n-1} \mathbf{u}^n = \mathbf{i}^n \quad (2.33)$$

The set of matrix \mathbf{G}^{n-1} elements comprises of linear conductances (constant values from linear network models) and the variable ones which are updated in each calculation step by iterative procedures. The elements of vector \mathbf{i}^n are: independent current sources ($I(k)$ – constant with respect to the iteration step n), equivalent current sources of linear network models L , C ($j_L(k-1)$, $(j_C(k-1)$ and equivalent current sources related with nonlinear network models: $I_R^{n-1}(k)$, $I_G^{n-1}(k)$, $I_L^{n-1}(k)$ so that in general form:

$$\mathbf{i}^n = f(I(k), j_L(k-1), j_C(k-1), I_R^{n-1}(k), I_G^{n-1}(k), I_L^{n-1}(k), I_C^{n-1}(k)) \quad (2.34)$$

If some network elements are time-varying then fundamental equation of the nodal method takes more general form:

$$\mathbf{G}^{n-1}(k) \mathbf{u}^n(k) = \mathbf{i}^n(k, k-1) \quad (2.35)$$

The double index indicates that vector in the right side of the equation comprises of independent sources determined in k -th calculation step and in the previous ones (history of calculations).

Solution of (2.35) is cumbersome; matrix $\mathbf{G}^{n-1}(k)$ cannot be factorized since it contains variable elements. Thus the method considered is ineffective in application to vast nonlinear and time-varying networks.

2.3.2. Compensation method

The compensation method is directly related to the Thevenin theorem concerning representation of selected fragment of electric network by equivalent voltage source and the source impedance [23, 52].

a) Network with one non-linear element

The idea of the method considered is presented for the network with a single nonlinear element (Fig. 2.10).

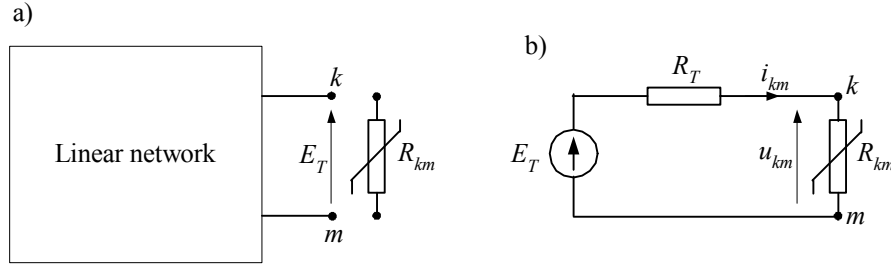


Fig. 2.10 Compensation method: a) linear network with removed branch km and b) the equivalent circuit

The linear part of the network, excluding the branch km (Fig. 2.10a), is transformed into the equivalent circuit according to the Thevenin theorem (Fig. 2.10b). The equations describing the equivalent network are easy to derive:

$$i_{km} = \frac{E_T}{R_T + R_{km}}, \quad u_{km} = E_T - R_T i_{km}, \quad (2.36)$$

where $R_{km} = g\left(i_{km}, \frac{di_{km}}{dt}, \dots\right)$.

In case of nonlinear inductance or capacitance the equivalent circuit model is complemented by the current or voltage sources which come from the numerical models of the nonlinear element used. The nonlinear element can also be represented by the model with voltage dependent conductance G_{km} . If the function determining resistance R_{km} (conductance G_{km}) is given explicitly then the above equations can be solved by use of Newton's method. Sometimes the nonlinear characteristic is given in a piece-wise form (Fig. 2.11). In such case the solution is linear for the segment which is intersected by the linear characteristic of the equivalent circuit.

In order to solve (2.36) the parameters of the equivalent circuit E_T and R_T have to be determined first. E_T can be calculated by means of the nodal method applied to the circuit in which the branch km has been removed (that implies that $G_{km} = 0$ in the conductance matrix \mathbf{G}) [23]. Let's denote this matrix by \mathbf{G}_{km}^0 . The voltage source E_T can be obtained by solution of the following equation:

$$\mathbf{G}_{km}^0 \mathbf{u}^0 = \mathbf{i} \quad (2.37)$$

in which: $E_T = u_k^0 - u_m^0$, and u_k^0, u_m^0 are elements of vector \mathbf{u}^0 related to nodes k and m , respectively ; \mathbf{i} is the vector of nodal currents in the equivalent circuit.

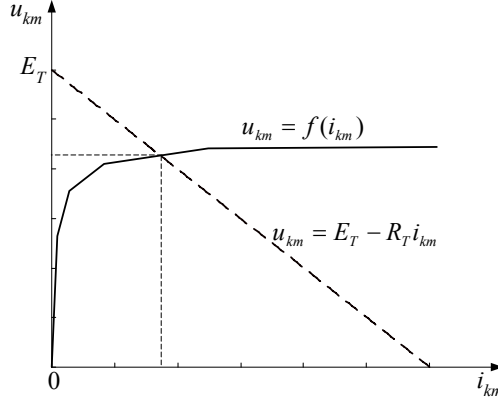


Fig. 2.11. The meth of the nonlinear equation solution for piece- wise approximation of the nonlinear characteristic

Resistance R_T is calculated by subtraction of vector \mathbf{r} elements k and m and the vector \mathbf{r} is obtained by subtraction of columns k and m in matrix $(\mathbf{G}_{km}^0)^{-1}$ [23]. The vector \mathbf{r} can also be determined by solution of the following equation:

$$\mathbf{G}_{km}^0 \mathbf{r} = \mathbf{p} \quad (2.38)$$

where the vector \mathbf{p} elements are:

$$p_l = \begin{cases} 1 & \text{if } l = k \\ -1 & \text{if } l = m \\ 0 & \text{otherwise} \end{cases}$$

and the condition $l = m$ is important only when voltage in m -th node is not defined (or is not the reference node).

Finally the vector of node voltages in the nonlinear network is determined by solution of the following equation [23]:

$$\mathbf{u} = \mathbf{u}^0 - \mathbf{r} i_{km} \quad (2.39)$$

Calculations according to the compensation method are carried out in each calculation step in the following order:

1. Calculation vector \mathbf{u}^0 and voltage E_T according to (2.37).
2. Calculation vector \mathbf{r} and resistance R_T according to (2.38).

3. Calculation the current i_{km} solving the nonlinear equation (2.36).
4. Calculation the corrected vector of node voltages according to (2.39).

The second step of the algorithm is repeated only if the configuration of the linear part of the network has been changed. The only difference in numerical calculations for linear and nonlinear network concerns the step 3 (calculation of i_{km} in the nonlinear branch). That is why the compensation method is advantageous to the Newton-Raphson's one.

b) General non-linear network

The presented algorithm can also be applied with certain limitations to networks comprising of more than one nonlinear element. Let's assume that the number of nonlinear elements in the network is M . In the first step of the algorithm vector \mathbf{u}^0 is determined according to (2.37) for the matrix \mathbf{G}_{km}^0 in which all elements related to M branches connected to nodes $k_1 - m_1, k_2 - m_2, \dots, k_M - m_M$ are removed. As a result the following set of voltage sources $E_{T_i} = u_{k_i}^0 - u_{m_i}^0, i = 1, 2, \dots, M$ is obtained.

In the second step vectors \mathbf{r}_i are calculated according to (2.38) and calculation have to be repeated for each pair of nodes for different vectors \mathbf{p}_i in the right side of (2.38). Most complex calculations are carried out in the third step since the set of nonlinear equations has to be solved for all nonlinear elements in the network. The significant simplification of those calculations can be obtained if the characteristics on nonlinear elements are given in linear piecewise approximation form.

The final form of the node voltage vector is obtained in the fourth step of the algorithm but (2.39) must be updated for all nonlinear branches:

$$\mathbf{u} = \mathbf{u}^0 - \mathbf{r}_1 i_{k_1 m_1} - \mathbf{r}_2 i_{k_2 m_2} - \dots - \mathbf{r}_M i_{k_M m_M} \quad (2.40)$$

Matrix \mathbf{G}_{km}^0 should be non-singular in all stages of calculation process. Otherwise the network with removed nonlinear branches cannot be solved. Problem may also appear if nonlinear elements are located in adjacent branches. However, this problem can be solved by separation of adjacent nonlinear branches by one calculation step delay using the long line element).

Another problem which may appear in modelling of nonlinear networks is related to unwanted oscillations caused by dummy hysteresis (Fig. 2.12) especially in nonlinear inductances [23]. To limit this negative effect the calculation step should be sufficiently small.

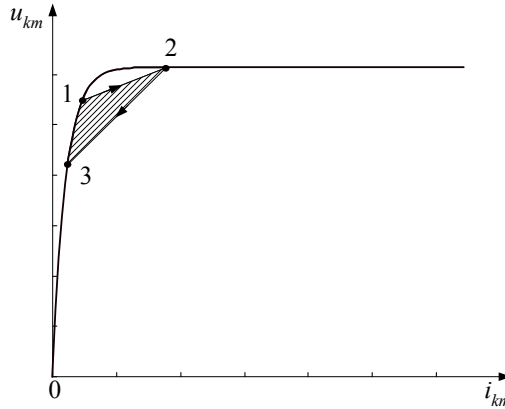


Fig. 2.12 Dummy hysteresis (shaded area)

2.3.3. Piecewise approximation method

Effective calculation methods used for linear networks can be applied to the nonlinear ones if characteristics of nonlinear elements can be represented by their linear piecewise approximations. In general case a nonlinear characteristic can be approximated by an arbitrary number of straight line segments thus making the network linear in intervals. The basic problem which appears in this approach concerns calculations in points located on the boundary of two adjacent segments of the approximated nonlinear characteristic since the solution obtained in a given calculation step may go off the characteristic. The problem mainly concerns vast networks comprising of many nonlinear elements [18, 23, 85].

In EMTP program the nonlinear elements are of monotonic type (magnetizing characteristic, nonlinear characteristic of MOV and others) so further simplifications increasing calculation effectiveness can be applied. The basic limitations which have to be controlled by the program user are:

- the calculation step as well as the characteristic approximating segments should be selected in such way that the solutions obtained in consecutive steps do not lay outside the adjacent segments of the characteristic ('off characteristic' solution). Warning is displayed if it happens so - Fig. 2.13.
- the 'off characteristic' solutions have to be neglected (solution k'' in Fig. 2.13).

Thus the approximated characteristic should not comprise of too many segments if the calculation step value is to be reasonable [29]. Change of conductance in nonlinear elements and new factorization of matrix \mathbf{G} is carried out in the consecutive calculation step [52].

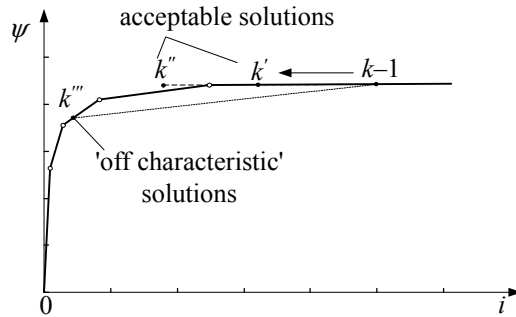


Fig. 2.13. Illustration of solutions which can be obtained in two consecutive steps for piecewise approximated characteristic

Such simplification (small number of linear segments in piecewise approximation of the nonlinear characteristic) does not significantly affect the accuracy of calculations thus making the piecewise approximation very attractive in design of simulation programs. It is illustrated by waveforms in Fig. 2.14 – $i_2(k)$ and $i_3(k)$ are practically identical even though the current $i_2(k)$ was calculated for accurate nonlinear magnetizing characteristic and $i_3(k)$ (dotted line) for the approximated one comprising of 2 segments only.

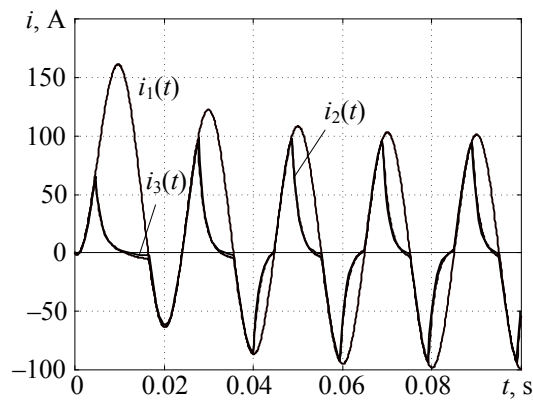


Fig. 2.14. Results of transients simulation in CT: the primary current $i_1(k)$; the secondary current for accurate magnetizing characteristic ($i_2(k)$); the secondary current for two-segmented piecewise approximation of the characteristic ($i_3(k)$)

Exercises

- 2.1. Using the Newton's method determine the current i in the nonlinear circuit shown in Fig. Z2.1. Resistance R_w is described by the function: $i = 10(u_w)^3$. The supply voltage: $u = 100$ V, $R = 5$ Ω .

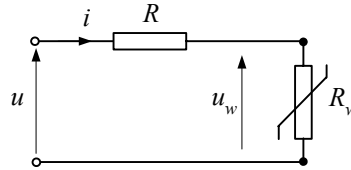


Fig. Z2.1

- 2.2. In the circuit shown in Fig. Z2.2 the input voltage is applied at the instant $t = 0$ with the zero initial conditions. Using the nodal method formulate the dynamic equations of the circuit taking the trapezoidal integration model of inductance. Show the algorithm for solution of the derived equations. Implement the algorithm in MATLAB environment. Data: $L = 100$ mH, the rest like in problem 2.1.

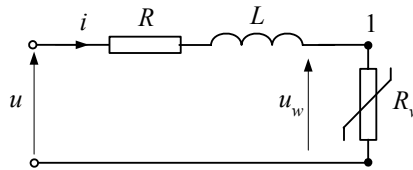


Fig. Z2.2

- 2.3. Consider the network shown in Fig. Z2.3a. The piecewise approximation of the nonlinear resistance characteristic is like in Fig. Z2.3b. Show the way of the current i calculation, and determine the value of this current for $R_1 = 1$ Ω and $u_1 = 20$ V.

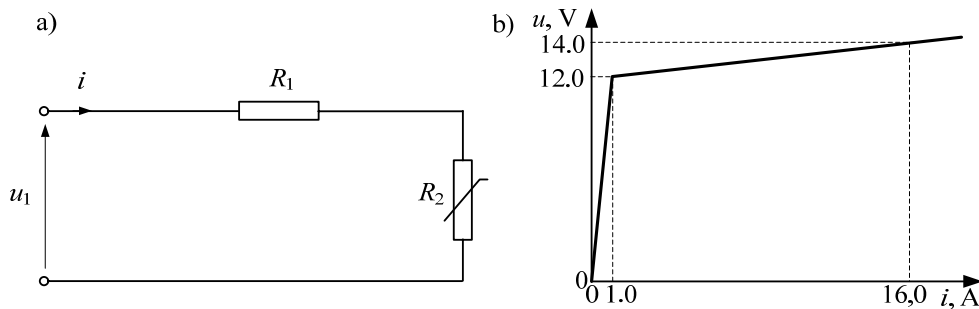


Fig. Z2.3

3. STATE-VARIABLES METHOD

3.1. Introduction

This method is based on the mathematical model of a network in which vector of input variables $\mathbf{f}(t)$ (sources) is related with the output variable vector $\mathbf{y}(t)$ (selected currents and voltages) by the fundamental equations [21, 36, 70, 80]:

$$\begin{aligned}\dot{\mathbf{x}}(t) &= \mathbf{A}\mathbf{x}(t) + \mathbf{B}\mathbf{f}(t) \\ \mathbf{y}(t) &= \mathbf{C}\mathbf{x}(t) + \mathbf{D}\mathbf{f}(t)\end{aligned}\tag{3.1}$$

where: $\mathbf{A}_{n \times n}$, $\mathbf{B}_{n \times r}$, $\mathbf{C}_{m \times n}$, $\mathbf{D}_{m \times r}$ - matrixes of parameters, $\mathbf{x}(t)$ - state vector.

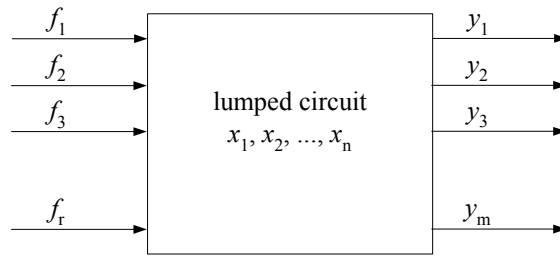


Fig. 3.1. Network state variable representation

In general the matrices of parameters can change in time (time-variant network) or can be functions of the state variables (non-linear network).

The first equation in (3.1) is called the state equation and the second one is the output equation. The state variables in (3.1) are related with energy preserving elements (inductances, capacitances) for which:

$$\frac{d}{dt}(Cu_C(t)) = i_C(t)\tag{3.2}$$

and

$$\frac{d}{dt}(Li_L(t)) = u_L(t)\tag{3.3}$$

so the voltages on capacitances and currents flowing through inductances are always selected as state variables. Thus any network can be represented as it is shown in Fig. 3.2. Parameters L , C can be nonlinear.

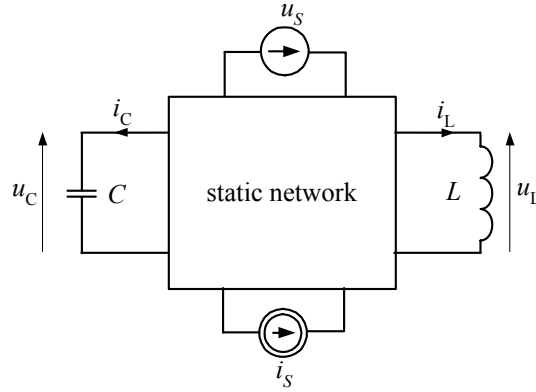


Fig. 3.2. Network represented by state variables

The energy preserving elements (Fig. 3.2) can be described by the following general equations:

$$\begin{aligned} \mathbf{i}_C(t) &= \mathbf{g}_C(\mathbf{u}_C, \mathbf{i}_L, \mathbf{u}_S, \mathbf{i}_S, t) \\ \mathbf{u}_L(t) &= \mathbf{g}_L(\mathbf{u}_C, \mathbf{i}_L, \mathbf{u}_S, \mathbf{i}_S, t) \end{aligned} \quad (3.4)$$

which lead to the state equation.

The number of state variable doesn't always have to be equal to the sum of capacitors and inductors in the network since all loop and node equations should be linearly independent. That is why, in some network configurations, one voltage across capacitor in circuit loop or one coil current in the node can be eliminated from the state variable equation as it is shown in Fig. 3.3.

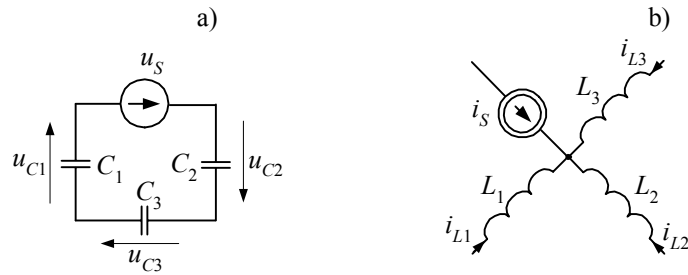


Fig. 3.3. Example of independent loop CE (a) and independent node LJ (b)

For the circuit loop in Fig. 3.3a there is:

$$u_S(t) + u_{C1}(t) + u_{C2}(t) + u_{C3}(t) = 0 \quad (3.5)$$

To make the circuit loop equations independent one of the prospective state variables in (3.5) should be eliminated.

The same concerns the node in Fig. 3.3b for which:

$$i_S(t) + i_{L1}(t) + i_{L2}(t) + i_{L3}(t) = 0 \quad (3.6)$$

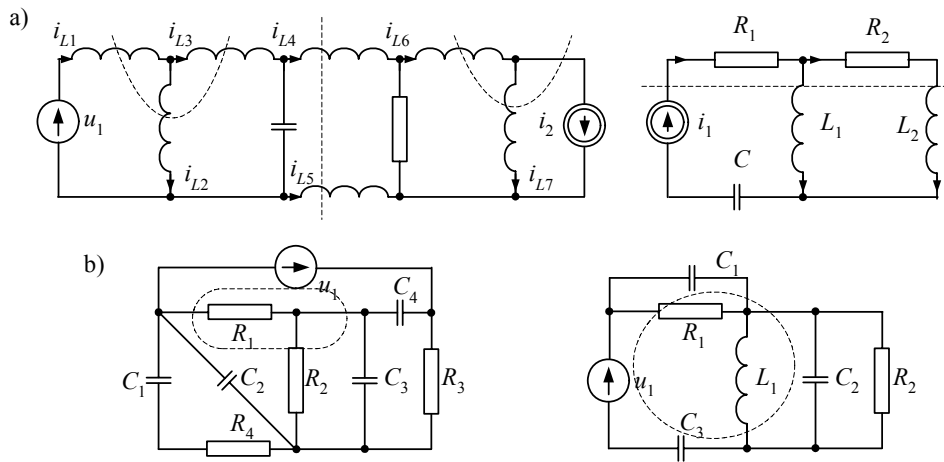


Fig. 3.4. Examples of independent nodes LJ a) and circuit loops CE b)

In case of linear, time invariant lumped networks the number of indispensable state variables n can be determined from the equation [18, 80]:

$$n = n_{LC} - (n_{CE} + n_{LJ}) \quad (3.7)$$

where:

n_{LC} - the number of all condensers and coils in the network

n_{CE} - the number of independent circuit loops CE in the network

n_{LJ} - the number of independent circuit nodes LJ in the network

Examples of independent nodes LJ and loops CE are shown in Fig. 3.4.

Reduction of state variable number according to (3.7) results in the presence of input sources derivatives in the input vector [18].

3.2. Derivation of state-variables equations

State space representation of an electric network is obtained by application of Kirchhoff's rules to the network diagram for state variables assigned to reactive

elements (condensers, coils) in the number selected according to (3.7). It is illustrated by the following example:

Example 3.1. Determine the state space representation of the circuit shown in Fig. 3.5. Assign state variables to energy preserving elements.

The circuit contains 3 LC ($n_{LC} = 3$) components but $n_{CE} = 1$ since one loop (e , C_1 , C_2) is linearly dependent and $n_{LJ} = 0$. Thus the number of independent equations in overall state equation is $n = 2$. The selected state variables are the current i_L and the voltage u_{C2} . As the output variables the currents i_L , i_{C1} and i_{C2} are selected.

The respective circuit equations are:

$$j - i_L - i_{R2} = 0, \quad C_1 \frac{du_{R1}}{dt} + i_{R1} - i = 0,$$

$$e - u_{R1} - u_{C2} = 0, \quad L \frac{di_L}{dt} - R_2 i_{R2} = 0, \quad R_1 i_1 - u_{R1} = 0.$$

Eliminating all variables, save for selected state variables i_L , u_{C2} and excitation sources e and j , we get:

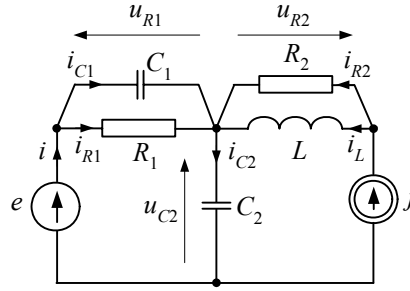


Fig. 3.5. The circuit diagram of considered network

$$\frac{di_L}{dt} = -\frac{R_2}{L} i_L + \frac{R_2}{L} j, \quad \frac{du_{C2}}{dt} = -\frac{1}{R_1(C_1 + C_2)} u_{C2} + \frac{1}{C_1 + C_2} j + \frac{1}{R_1(C_1 + C_2)} e + \frac{C_1}{C_1 + C_2} \frac{de}{dt}.$$

The output variables (aside of i_L) are:

$$i_{C1} = \frac{C_1}{R_1(C_1 + C_2)} u_{C2} - \frac{C_1}{C_1 + C_2} j - \frac{C_1}{R_1(C_1 + C_2)} e + \frac{C_1^2}{C_1 + C_2} \frac{de}{dt},$$

$$i_{C2} = -\frac{C_2}{R_1(C_1 + C_2)} u_{C2} + \frac{C_2}{C_1 + C_2} j + \frac{C_2}{R_1(C_1 + C_2)} e + \frac{C_1 C_2}{C_1 + C_2} \frac{de}{dt}.$$

In matrix notation:

$$\frac{d}{dt} \begin{bmatrix} i_L \\ u_{C2} \end{bmatrix} = \begin{bmatrix} -\frac{R_2}{L} & 0 \\ 0 & -\frac{1}{R_1(C_1+C_2)} \end{bmatrix} \begin{bmatrix} i_L \\ u_{C2} \end{bmatrix} + \begin{bmatrix} \frac{R_2}{L} & 0 \\ \frac{1}{C_1+C_2} & \frac{1}{R_1(C_1+C_2)} \end{bmatrix} \begin{bmatrix} j \\ e \end{bmatrix} + \begin{bmatrix} 0 & 0 \\ 0 & \frac{C_1}{C_1+C_2} \end{bmatrix} \frac{d}{dt} \begin{bmatrix} j \\ e \end{bmatrix}$$

$$= \mathbf{Ax} + \mathbf{Bf} + \mathbf{B}_1 \frac{d}{dt} \mathbf{f},$$

$$\begin{bmatrix} i_L \\ i_{C1} \\ i_{C2} \end{bmatrix} = \begin{bmatrix} 1 & 0 \\ 0 & \frac{C_1}{R_1(C_1+C_2)} \\ 0 & -\frac{C_2}{R_1(C_1+C_2)} \end{bmatrix} \begin{bmatrix} i_L \\ u_{C2} \end{bmatrix} + \begin{bmatrix} 0 & 0 \\ -\frac{C_1}{C_1+C_2} & -\frac{C_1}{R_1(C_1+C_2)^2} \\ \frac{C_2}{C_1+C_2} & \frac{C_2}{R_1(C_1+C_2)^2} \end{bmatrix} \begin{bmatrix} j \\ e \end{bmatrix} + \begin{bmatrix} 0 & 0 \\ 0 & \frac{C_1^2}{C_1+C_2} \\ 0 & \frac{C_1 C_2}{C_1+C_2} \end{bmatrix} \frac{d}{dt} \begin{bmatrix} j \\ e \end{bmatrix}$$

$$= \mathbf{Cx} + \mathbf{Df} + \mathbf{D}_1 \frac{d}{dt} \mathbf{f}.$$

Elimination of source variable derivatives from the state equation can be obtained by substitution:

$$u_e = u_{C2} - \frac{C_1}{C_1+C_2} e.$$

As a result the state equation takes the form (3.1) in which:

$$\mathbf{x} = \begin{bmatrix} i_L \\ u_e \end{bmatrix}, \mathbf{A} = \begin{bmatrix} -\frac{R_2}{L} & 0 \\ 0 & -\frac{1}{R_1(C_1+C_2)} \end{bmatrix}, \mathbf{B} = \begin{bmatrix} \frac{R_2}{L} & 0 \\ \frac{1}{C_1+C_2} & \frac{C_2}{R_1(C_1+C_2)^2} \end{bmatrix}, \mathbf{f} = \begin{bmatrix} j \\ e \end{bmatrix}, \mathbf{y} = \begin{bmatrix} i_L \\ i_{C1} \\ i_{C2} \end{bmatrix},$$

$$\mathbf{C} = \begin{bmatrix} 1 & 0 \\ 0 & \frac{C_1}{R_1(C_1+C_2)} \\ 0 & -\frac{C_2}{R_1(C_1+C_2)} \end{bmatrix}, \mathbf{D} = \begin{bmatrix} 0 & 0 \\ -\frac{C_1}{C_1+C_2} & -\frac{C_1 C_2}{R_1(C_1+C_2)^2} \\ \frac{C_2}{C_1+C_2} & \frac{C_2^2}{R_1(C_1+C_2)^2} \end{bmatrix}, \mathbf{D}_1 = \begin{bmatrix} 0 & 0 \\ 0 & \frac{C_1^2}{C_1+C_2} \\ 0 & \frac{C_1 C_2}{C_1+C_2} \end{bmatrix}.$$

In general, the derivatives of excitation signals can be eliminated from the state equation (but not from the output one) by use of suitable substitution.

In general form the state equations are:

$$\dot{\mathbf{x}}(t) = \mathbf{Ax}(t) + \mathbf{Bf}(t) + \mathbf{B}_1 \frac{d}{dt} \mathbf{f}(t) + \dots + \mathbf{B}_p \frac{d^p}{dt^p} \mathbf{f}(t) \quad (3.8)$$

$$\mathbf{y}(t) = \mathbf{Cx}(t) + \mathbf{Df}(t) + \mathbf{D}_1 \frac{d}{dt} \mathbf{f}(t) + \dots + \mathbf{D}_p \frac{d^p}{dt^p} \mathbf{f}(t) \quad (3.9)$$

where $0 \leq p \leq n_{CE} + n_{LJ}$.

Applying subsequent substitutions:

$$\mathbf{z}(t) = \mathbf{x}(t) - \mathbf{B}_p \frac{d^{p-1}}{dt^{p-1}} \mathbf{f}(t) \quad (3.10)$$

(like in Example 3.1) the derivatives can be eliminated from the state equation (3.8). The output equation in general form may contain derivatives of excitation sources.

State variable equations can be formulated for a given network diagram automatically by use of dedicate computer programs [18].

3.3. Solution of state-variables equations

The intrinsic feature of the state variables approach is that the transients in all nodes and branches of the network considered can uniquely and entirely be determined by solution of the state equation (3.1). In case of linear networks the accurate solution of the state equation is possible and relatively simple.

By analogy to the method of the first order linear differential equation solution first the solution of homogenous differential equation written in vector (multivariable) notation:

$$\dot{\mathbf{x}}(t) = \mathbf{A}\mathbf{x}(t) \quad (3.11)$$

has to be determined and this solution, as it can easily be checked by simple substitution to (3.11), is given by the equation:

$$\mathbf{x}(t) = e^{\mathbf{A}t} \mathbf{k}(t) \quad (3.12)$$

where: $\mathbf{k}(t)$ is a certain functional vector which should also satisfy the non-homogenous solution (3.1).

To substitute (3.12) into (3.1) the derivative of (3.12) should be determined first:

$$\dot{\mathbf{x}}(t) = \mathbf{A}e^{\mathbf{A}t} \mathbf{k}(t) + e^{\mathbf{A}t} \dot{\mathbf{k}}(t) \quad (3.13)$$

After substitution we get:

$$\mathbf{A}e^{\mathbf{A}t} \mathbf{k}(t) + e^{\mathbf{A}t} \dot{\mathbf{k}}(t) = \mathbf{A}e^{\mathbf{A}t} \mathbf{k}(t) + \mathbf{B}\mathbf{f}(t) \quad (3.14)$$

and, noting that [18]:

$$\mathbf{A}e^{\mathbf{A}t} = e^{\mathbf{A}t} \mathbf{A} = \frac{d}{dt} e^{\mathbf{A}t} \quad (3.15)$$

we get finally:

$$\dot{\mathbf{k}}(t) = \mathbf{e}^{-\mathbf{A}t} \mathbf{B} \mathbf{f}(t) \quad (3.16)$$

Solution of the above equation can be obtained by integration so that:

$$\mathbf{k}(t) = \int_{t_0}^t \mathbf{e}^{-\mathbf{A}\tau} \mathbf{B} \mathbf{f}(\tau) d\tau + \mathbf{k}(t_0) \quad (3.17)$$

Substituting the result to (3.12), we get:

$$\mathbf{x}(t) = \mathbf{e}^{\mathbf{A}t} \left(\int_{t_0}^t \mathbf{e}^{-\mathbf{A}\tau} \mathbf{B} \mathbf{f}(\tau) d\tau + \mathbf{k}(t_0) \right) \quad (3.18)$$

Now the initial value of the state equation solution can be determined. By substitution of $t = t_0$, into (3.18) we get: $\mathbf{x}(t_0) = \mathbf{e}^{\mathbf{A}t_0} \mathbf{k}(t_0)$, and finally:

$$\mathbf{k}(t_0) = \mathbf{e}^{-\mathbf{A}t_0} \mathbf{x}(t_0) \quad (3.19)$$

Thus the final solution of the state equation (3.1) is given by the formula:

$$\mathbf{x}(t) = \mathbf{e}^{\mathbf{A}t} \int_{t_0}^t \mathbf{e}^{-\mathbf{A}\tau} \mathbf{B} \mathbf{f}(\tau) d\tau + \mathbf{e}^{\mathbf{A}(t-t_0)} \mathbf{x}(t_0) \quad (3.20)$$

Having the state variables determined the solution of the output equation (3.9) is obtained as a linear combination on of respective state variables and excitation sources according to the output equation form.

The solution (3.20) is valid for the continuous time domain. To get the solution in discrete form integration (3.20) should be carried out by use of one of the numerical integration methods [32, 83].

To calculate the exponential function in (3.20) the expansion into power series can be used:

$$\mathbf{e}^{\mathbf{A}t} = \mathbf{1} + \mathbf{A}t + \frac{1}{2!}(\mathbf{A}t)^2 + \dots + \frac{1}{m!}(\mathbf{A}t)^m + \dots \quad (3.21)$$

Unfortunately, to get the sufficient accuracy of calculation remarkable number of terms in the series has to be calculated (slowly convergent series). However, there are some other much more effective approximations of $\mathbf{e}^{\mathbf{A}t}$, for instance, the Pade approximation [18].

Exercises

3.1. Formulate the state variable equations (in minimal form) for the given (Fig Z3.1) electric circuits. Assign outputs to voltage drops across resistors

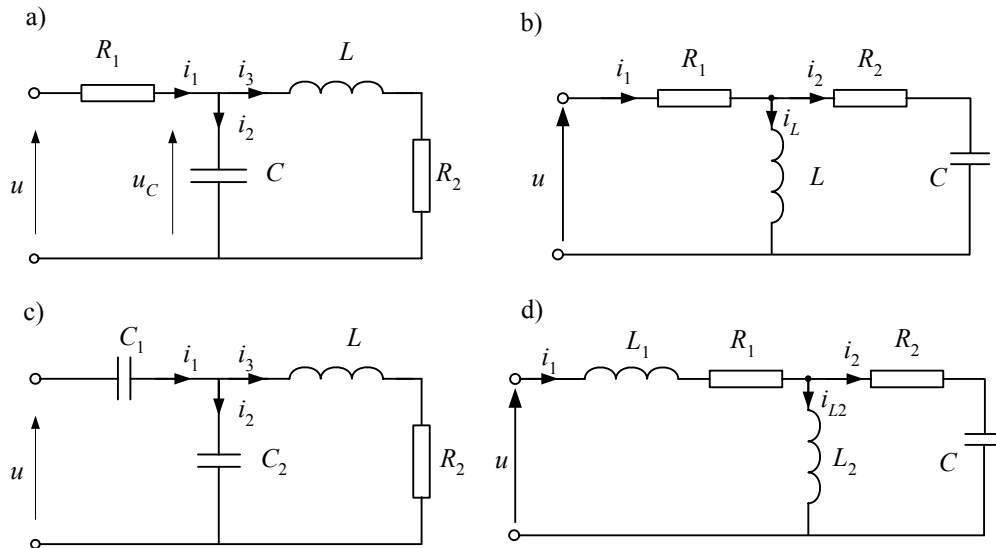


Fig. Z3.1

3.2. Determine the initial conditions ($t = 0$) for state equations in problem 3.1 assuming the following inputs:

- a) $u = 10 \text{ V}$,
- b) $u = 10 \sin(\omega t + \varphi) \text{ V}$, $\omega = 100\pi$, $\varphi = 0$.

3.3. Determine the state variable model for the network with CT in Example 2.6. Carry out transient simulation for conditions as specified in the Example. Use the R-K IV algorithm for digital integration [83].

Note: After reduction the network is described by a single differential equation.

4. OVER-HEAD LINE MODELS

4.1. Single-phase Line Model

The fundamentals of a distributed parameter line modelling are shown in sect. 1.3.6. In this Chapter various detailed problems related to a single phase power line modelling are presented including the basic information on application of geometrical parameters to the line modelling. The frequency dependent model of the line is considered in detail. The discussed approach to modelling is then extended to the multi-phase line case.

4.1.1. Line Parameters

In general the electric parameters of overhead lines and cable feeders depend on geometrical dimensions, physical properties of design materials and surrounding environment. The parameters can be calculated from fundamental equations [3, 14, 24]. The equations are used by special parameters calculating procedures provided by most of professional transient simulation programs. However, to apply those procedures the program user needs many, sometimes very detailed, data of the line or cable modelled. It is illustrated by the following example:

Example 4.1. Using the geometrical parameters and the respective material constants determine the electric parameters of the overhead 400 kV line. Use the LINE CONSTANTS procedure available in ATP-EMTP [7].

The geometrical dimensions of the line are shown in Fig. 4.1. The midspan data are shown under the bar. The relevant entries are formatted as shown below:

```
BEGIN NEW DATA CASE
C Line 400 kV
LINE CONSTANTS
METRIC
C Data for LINE CONSTANTS
C 34567890123456789012345678901234567890123456789012345678901234567890
1 .231 .0564 4 3.15 -10.3 24.5 12.0 40.0 0.0 2
2 .231 .0564 4 3.15 0.0 24.5 12.0 40.0 0.0 2
3 .231 .0564 4 3.15 10.3 24.5 12.0 40.0 0.0 2
0 0.5 .2388 4 1.565 -6.87 31.0 23.5
0 0.5 .2388 4 1.565 6.87 31.0 23.5
BLANK CARD ENDING CONDUCTOR CARDS OF "LINE CONSTANTS" CASE
```

```

C      1      2      3      4      5      6      7      8
C 34567890123456789012345678901234567890123456789012345678901234567890
C      >< Freq  >< FCar  > <ICPR> <IZPR> =< DIST > <PP>==< >< >< ><>>
      100.0    50.0                1  1  0  180.0                0
BLANK CARD ENDING FREQUENCY CARDS
BLANK CARD ENDING "LINE CONSTANTS"
BEGIN NEW DATA CASE
BLANK

```

Due to the program requirements (data format) it is assumed that the line length is 180 km.

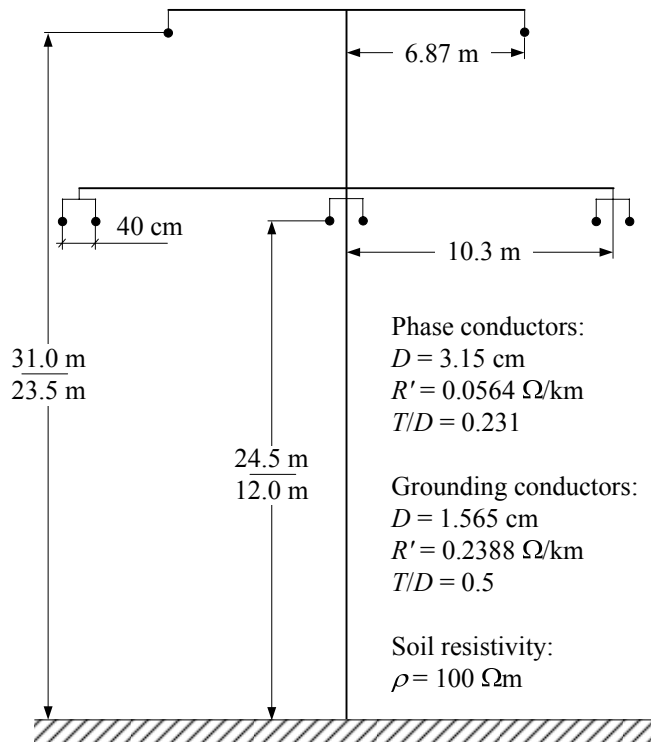


Fig. 4.1. Geometrical data of the line considered

The results obtained refer to positive and zero sequence symmetrical components. The parameter T/D is discussed in Example 4.2.

The respective line parameters calculation results for the fundamental frequency $f_1 = 50 \text{ Hz}$ are as follows:

$$R'_0 = 0.1576 \text{ } \Omega/\text{km} \quad L'_0 = 2.2966 \text{ mH/km} \quad C'_0 = 0.007729 \text{ } \mu\text{F/km}$$

$$R'_1 = 0.0291 \text{ } \Omega/\text{km} \quad L'_1 = 1.0296 \text{ mH/km} \quad C'_1 = 0.01123 \text{ } \mu\text{F/km}.$$

Similarly the wave travelling speed and the surge impedance values are:

$$v_0 = 235968 \text{ km/s} \quad v_1 = 293798 \text{ km/s} \quad Z_{0c} = 548.3 \text{ } \Omega \quad Z_{1c} = 302.8 \text{ } \Omega.$$

Parameters for zero and positive symmetrical components differ since the physical parameters of the earthing conductor and phase conductors are different. The transverse line conductivity G' is usually neglected in such calculations.

4.1.2. Frequency-dependent Model

The frequency dependence of the conductor electric parameters is the result of the skin effect which is caused by pushing of the electromagnetic field outside the conductor when the frequency of the current grows. As a result the effective current conducting cross-section of the wire decreases and the wire resistance grows. Decreasing current reduces the magnetic flux ψ around the conductor thus decreasing the conductor inductance L ($L = \psi / i$) [24].

The frequency dependant parameters depend upon many factors and the most important of them are: the distance between phase and earth conductors and the applied model of the earth which is also the current conductor. The phase conductors in the overhead line can be bundled thus comprising of many wires in various geometrical arrangements being spaced by few tens of centimetres. Also the models of the earth used in calculations may differ significantly since the earth is non-homogenous conducting environment. Thus the calculation of frequency dependent parameters becomes a complex task.

The next example shows how the input data are prepared for subroutine of frequency dependent parameters calculation which is available in ATP-EMTP.

Example 4.2. Determine the frequency dependent parameters of 400 kV line from Example 4.1. Coefficient T/D (*Thickness/Diameter*) is necessary for calculation of the skin effect (Fig. 4.1) since the conductor is represented by a pipe of external diameter D and thickness T . For the homogenous wire $T/D = 0.5$.

Again the LINE CONSTANTS procedure is used and the input data are arranged as follows:

```
BEGIN NEW DATA CASE
C Line 400 kV
C
LINE CONSTANTS
METRIC
FREQUENCY
C Data for LINE CONSTANTS
C 34567890123456789012345678901234567890123456789012345678901234567890
1 .231 .0564 4 3.15 -10.3 24.5 12.0 40.0 0.0 2
2 .231 .0564 4 3.15 0.0 24.5 12.0 40.0 0.0 2
3 .231 .0564 4 3.15 10.3 24.5 12.0 40.0 0.0 2
0 0.5 .2388 4 1.565 -6.87 31.0 23.5
0 0.5 .2388 4 1.565 6.87 31.0 23.5
BLANK CARD ENDING CONDUCTOR CARDS OF LINE CONSTANTS CASE
C 34567890123456789012345678901234567890123456789012345678901234567890
```

```

100.0      0.1      1
BLANK CARD ENDING FREQUENCY CARDS
BLANK CARD ENDING "LINE CONSTANTS"
BEGIN NEW DATA CASE
BLANK

```

5 5

The parameters versus frequency characteristics obtained are shown in Fig. 4.2. The plots show that the zero sequence parameters (R'_0 – Fig. 4.2a and L'_0 – Fig. 4.2b) change more intensively with frequency than the positive sequence ones (R'_1 – Fig. 4.2a and L'_1 – Fig. 4.2b).

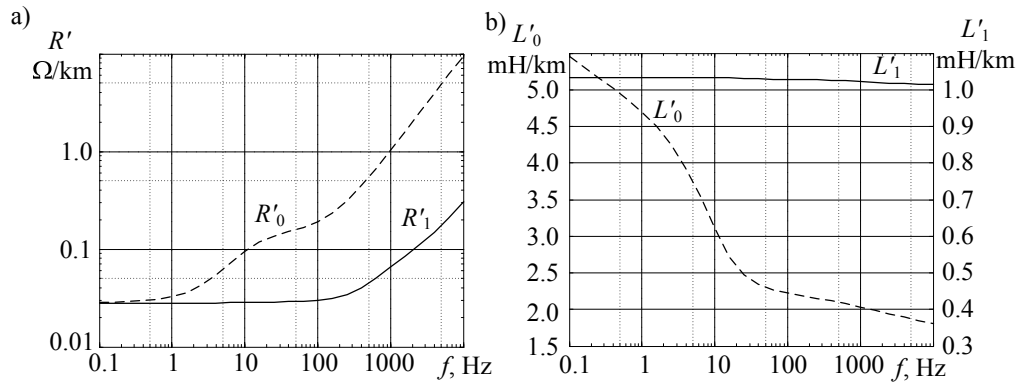


Fig. 4.2. Frequency characteristics of the 400 kV line:
a) resistance and b) inductance

The difference can be attributed to the fact that the skin effect in return (earthing) wire which is of much greater diameter than the phase wires is much more effective.

The transverse parameters (capacitances and conductances) are practically frequency independent. However for the sake of calculation stability usually the small value of one of those parameters is used for instance $G' = 0.03 \mu\text{S}/\text{km}$ [3].

Application of frequency dependent parameters to the line model setup is not simple since equations (1.75) are functions of time. Thus the frequency dependent model must be based on Fourier transform.

The Fourier transform of (1.75) can be determined by use of the following fundamental relations:

$$\int_0^{\infty} \frac{\partial u(x,t)}{\partial x} e^{-j\omega t} dt = \frac{d}{dx} \int_0^{\infty} u(x,t) e^{-j\omega t} dt = \frac{dU(x, j\omega)}{dx} \quad (4.1)$$

$$\int_0^{\infty} \frac{\partial u(x,t)}{\partial t} e^{-j\omega t} dt = \partial u(x,t) e^{-j\omega t} \Big|_{-\infty}^{\infty} + j\omega \int_0^{\infty} u(x,t) e^{-j\omega t} dt = j\omega U(x, j\omega) \quad (4.2)$$

The function $U(x, j\omega)$ is complex. For fixed frequency $U(x, j\omega)$ is the voltage phasor as used in steady state analysis of electric networks.

Formulas (4.1) (4.2) can also be applied to the current equations in (1.75). Thus the line equations (1.75) in frequency domain are now:

$$\begin{aligned} -\frac{dU(x, j\omega)}{dx} &= (R' + j\omega L')I(x, j\omega) \\ -\frac{dI(x, j\omega)}{dx} &= (G' + j\omega C')U(x, j\omega) \end{aligned}$$

and using the substitution:

$$\begin{aligned} Z'(j\omega) &= R' + j\omega L' \\ Y'(j\omega) &= G' + j\omega C' \end{aligned} \quad (4.3)$$

finally:

$$\begin{aligned} -\frac{dU(x, j\omega)}{dx} &= Z'(j\omega)I(x, j\omega) \\ -\frac{dI(x, j\omega)}{dx} &= Y'(j\omega)U(x, j\omega) \end{aligned} \quad (4.4)$$

The first of the above equations describe the longitudinal line model. Impedance $Z'(j\omega)$ is frequency-dependent since $R' = R'(\omega)$ and $L' = L'(\omega)$. The second equation describes the line model for transverse parameters. Usually the components of the admittance $Y'(j\omega)$ are frequency independent.

The equation (4.4) can also be split into the current and voltage parts. Differentiating the first equation in (4.4) with respect to x and applying the result to the second one we get:

$$\frac{d^2U(x, j\omega)}{dx^2} = Z'(j\omega)Y'(j\omega)U(x, j\omega) \quad (4.5)$$

Using notation $\gamma^2 = Z'(j\omega)Y'(j\omega)$ the final form of (4.5) is:

$$\frac{d^2U(x, j\omega)}{dx^2} = \gamma^2 U(x, j\omega) \quad (4.6)$$

The general solution of (4.6) is as below [77]:

$$U(x, j\omega) = A_1 \cosh(\gamma x) + B_1 \sinh(\gamma x) \quad (4.7)$$

where: A_1, B_1 – constants calculated from boundary conditions and

$$\gamma = \sqrt{Y'(j\omega)Z'(j\omega)} = \alpha + j\beta \quad (4.8)$$

Out of the two the square root values only the one for which $\alpha \geq 0$ is valid. The parameter γ [1/km] is known as the line propagation velocity constant; α is the line attenuation constant (Np/km)¹ and β is the phase propagation constant (rad/km).

Substituting (4.7) into the second equation in (4.4) we get:

$$I(x, j\omega) = -\frac{1}{Z_f} (A_1 \sinh(\gamma x) + B_1 \cosh(\gamma x)) \quad (4.9)$$

where:
$$Z_f = Z_f(j\omega) = \sqrt{\frac{Z'(j\omega)}{Y'(j\omega)}} = \frac{Z'(j\omega)}{\gamma} \quad (4.10)$$

is the complex surge impedance of the line.

Constants A_1 B_1 can be determined from the boundary conditions: at beginning of the line $x=0$ (subscript 1) and at the end $x=l$ (subscript 2) and in such case (4.7) (4.9) are as follows:

$$U_1(j\omega) = U(x, j\omega)|_{x=0} = A_1 \cosh(\gamma x) + B_1 \sinh(\gamma x)|_{x=0} = A_1 \quad (4.11)$$

$$U_2(j\omega) = U(x, j\omega)|_{x=l} = A_1 \cosh(\gamma l) + B_1 \sinh(\gamma l)|_{x=l} = A_1 \cosh(\gamma l) + B_1 \sinh(\gamma l) \quad (4.12)$$

$$I_1(j\omega) = I(x, j\omega)|_{x=0} = -\frac{1}{Z_f} (A_1 \sinh(\gamma x) + B_1 \cosh(\gamma x))|_{x=0} = -\frac{B_1}{Z_f} \quad (4.13)$$

$$\begin{aligned} I_2(j\omega) &= I(x, j\omega)|_{x=l} = -\frac{1}{Z_f} (A_1 \sinh(\gamma l) + B_1 \cosh(\gamma l))|_{x=l} \\ &= -\frac{1}{Z_f} (A_1 \sinh(\gamma l) + B_1 \cosh(\gamma l)) \end{aligned} \quad (4.14)$$

Assuming that the voltage and current at the end of the line are known and $U_1(j\omega)$ $I_1(j\omega)$ are to be determined then the respective solution, for the line output currents flowing in directions as shown in Fig. 4.3, is:

$$\begin{bmatrix} U_1(j\omega) \\ I_1(j\omega) \end{bmatrix} = \begin{bmatrix} \cosh(\gamma l) & Z_f(j\omega) \sinh(\gamma l) \\ \frac{1}{Z_f(j\omega)} \sinh(\gamma l) & \cosh(\gamma l) \end{bmatrix} \begin{bmatrix} U_2(j\omega) \\ -I_2(j\omega) \end{bmatrix} \quad (4.15)$$

¹ Np (neper) is the unit of attenuation. 1 Np = 8.686 dB.

Equation (4.15) describes the l km long line segment model for steady state with input-output nodes denoted by 1 and 2 respectively. The model can be represented by Π -cell (Fig. 4.3) having the following parameters:

$$\begin{aligned} Z_w &= Zl \frac{\sinh(\gamma l)}{\gamma l} = R_w(\omega) + j\omega L_w(\omega) \\ Y_p &= Yl \frac{\tanh(\gamma l/2)}{\gamma l/2} = G_2(\omega) + j\omega C_w(\omega) \end{aligned} \quad (4.16)$$

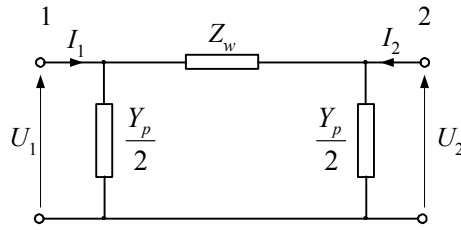


Fig. 4.3. Π -cell representation of the long line in steady-state

The model can easily be extended to the multiphase line case. For this purpose the single phase line parameters should be replaced by the respective matrices of multiphase line ones.

Writing (4.15) for the first line end and assuming that the second end (subscript 2) is located in distance x the equation for voltage at any point in the line can be obtained:

$$U(x, j\omega) = U_1(j\omega) \cosh(\gamma x) - Z_f(j\omega) I_1(j\omega) \sinh(\gamma x) \quad (4.17)$$

Changing the hyperbolic functions into the exponential ones we get:

$$U(x, j\omega) = U_a(j\omega) e^{-\gamma x} + U_b(j\omega) e^{\gamma x} = A(x, j\omega) U_a(j\omega) + \frac{1}{A(x, j\omega)} U_b(j\omega) \quad (4.18)$$

$$\text{where: } U_a(j\omega) = \frac{1}{2} (U_1(j\omega) + Z_f(j\omega) I_1(j\omega)) \quad U_b(j\omega) = \frac{1}{2} (U_1(j\omega) - Z_f(j\omega) I_1(j\omega))$$

$$A(x, j\omega) = e^{-\gamma x}.$$

$U_a(j\omega)$ and $U_b(j\omega)$ represent complex amplitudes of the primary ($U_a(j\omega)$) and the reflected ($U_b(j\omega)$) waves which are distributed along the line according to the propagation constant γ given by $A(x, j\omega)$. Since the harmonic components of distorted voltage signal are suppressed and shifted according to the propagation constant then for a given distance x the function can be considered as the filter

transmittance of frequency response determined by $|A(x, j\omega)| = e^{-\alpha x}$ and the phase response given by $\arg(A(x, j\omega)) = e^{-j\beta x}$. In case of the overall line ($x = l$) we get:

$$A(j\omega) = A(l, j\omega) = e^{-\gamma l} \quad |A(j\omega)| = e^{-\alpha l} \quad \arg(A(j\omega)) = e^{-j\beta l} \quad (4.19)$$

The next example explains the discussed line characteristics.

Example 4.3. Analyse the considered frequency characteristics for the 400 kV line from Example 4.1.

The example of imaginary component distribution for wave of frequency $f_p = 2000$ Hz in the $l = 300$ km long 400 kV line is shown in Fig. 4.4. Two standing waves for positive and zero sequence voltage components are presented for comparison. The waveforms correspond to the following functions::

$$U_1(x) = \operatorname{Re}(A_1(x, j\omega_p) U_{a1}(j\omega_p)) \quad U_0(x) = \operatorname{Re}(A_0(x, j\omega_p) U_{a0}(j\omega_p))$$

and: $A_1(x, j\omega_p) = e^{-(\alpha_{p1} + j\beta_{p1})x}$ $A_0(x, j\omega_p) = e^{-(\alpha_{p0} + j\beta_{p0})x}$ $|U_{a1}(j\omega_p)| = |U_{a0}(j\omega_p)| = 1$; subscript p refers to the selected frequency while respective components are denoted by 0 and 1. The line parameters for frequency $f_p = 2000$ Hz (Example 4.1) are given in Table 4.1.

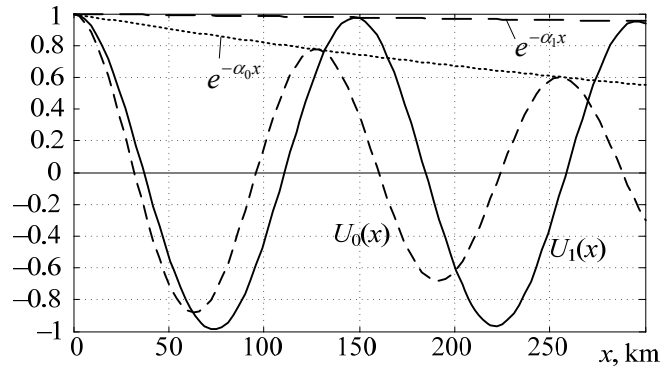


Fig. 4.4. Distribution of the wave along the line

Table 4.1. 400 kV line parameters for frequency 2 kHz

Parameter	Positive sequence component	Zero sequence component
$R' \ \Omega/\text{km}$	0.09619	2.0075
$L' \ \text{mH}/\text{km}$	1.0194	1.968
$C' \ \mu\text{F}$	0.01123	0.00779
$\alpha \ \text{Np}/\text{km}$	$1.596 \cdot 10^{-4}$	0.0020
$\beta \ \text{rad}/\text{km}$	0.0425	0.0491

The wavelength can be determined by examination of arguments of functions $A_1(x, j\omega_p)$ and $A_0(x, j\omega_p)$. The resulting general relation is: $\lambda = \frac{2\pi}{\beta}$, which for the considered example yields: $\lambda_0 = 128.097$ km and $\lambda_1 = 147.776$ km.

According to the known relation the wave propagation velocity is:

$$v = \lambda f = \frac{\omega}{\beta} \text{ and: } v_0 = 2.562 \cdot 10^5 \text{ km/s } v_1 = 2.955 \cdot 10^5 \text{ km/s.}$$

The wave propagation velocity depends mainly on the line parameters. The attenuation of the phase-phase loop is much lower than for phase–earth one (zero sequence component).

Multiplying the current equation in (4.15) by Z_f and subtracting it from the first (voltage) one we get:

$$U_1(j\omega) - Z_f(j\omega)I_1(j\omega) = (U_2(j\omega) + Z_f(j\omega)I_2(j\omega))e^{-\gamma l} \quad (4.20)$$

or in alternative voltage and current notations:

$$U_1(j\omega) = Z_f(j\omega)I_1(j\omega) + (U_2(j\omega) + Z_f(j\omega)I_2(j\omega))A(j\omega) \quad (4.21)$$

$$I_1(j\omega) = U_1(j\omega)/Z_f(j\omega) - (U_2(j\omega)/Z_f(j\omega) + I_2(j\omega))A(j\omega) \quad (4.22)$$

where: $A(j\omega)$ is like in (4.19).

If (4.20) is applied to the lossless line with frequency independent parameters then we have:

$$Z_f(j\omega) = Z_f = \sqrt{L'/C'} \quad \gamma = j\omega\sqrt{L'C'} \quad e^{-\gamma l} = e^{-j\omega\tau}$$

After inverse Fourier transformation of (4.20) we get:

$$u_1(t) - Z_f i_1(t) = u_2(t - \tau) + Z_f i_2(t - \tau)$$

$$\text{and: } \mathcal{F}\{x(t - \tau)\} = X(j\omega)e^{-j\omega\tau}.$$

being is the same as (1.83) which describes the lossless line in time domain. Thus (4.21) can be considered as an operator equation in the line model. Parameters $Z_f(j\omega)$ and $A(j\omega)$ are now the filter transmittances revealing the respective frequency responses. The complex propagation function $A(j\omega)$ can be deemed as a product of lumped parameter transmittance $P(j\omega)$ and the delay line so that:

$$A(j\omega) = P(j\omega)e^{-j\omega\tau_f} \quad (4.23)$$

where: τ_f is the propagation time of the fastest wave component.

The delay τ_f can be determined from the equation:

$$\omega\tau_f = \arg(P(j\omega)) - \arg(A(j\omega)) = \arg(P(j\omega)) + \beta l \quad (4.24)$$

and $P(j\omega)$ comes from (4.19) and (4.23):

$$|P(j\omega)| = |A(j\omega)| = e^{-\alpha l} \quad (4.25)$$

The filters based on the above equations represent the frequency dependent line model with parameters expressed by functions $Z_f(j\omega)$ and $A(j\omega)$ in (4.21) (4.22). The frequency properties of those functions are illustrated by the following example.

Example 4.4. Examine the frequency characteristics of positive and zero sequence components for 400 kV line discussed in Example 4.1. Assume that the line is 180 km long.

Like in Example 4.1 calculations have been carried out by use of the LINE CONSTANTS auxiliary program in ATP-EMTP for the frequency range 0.001 Hz–1 MHz. The frequency response of the propagation function $A(j\omega)$ is shown in Fig. 4.5. The continuous line (1) denotes the positive sequence component and the dotted line (2) – refers to the zero sequence one. The phase displacement of the function $\arg(A(j\omega)) = -l\beta$ is nearly linear since $\beta = \omega/v$ and the propagation velocity v is practically constant in the considered frequency range so the coefficient $l\beta$ (the total phase displacement between the line input and output) is proportional to the wave length.

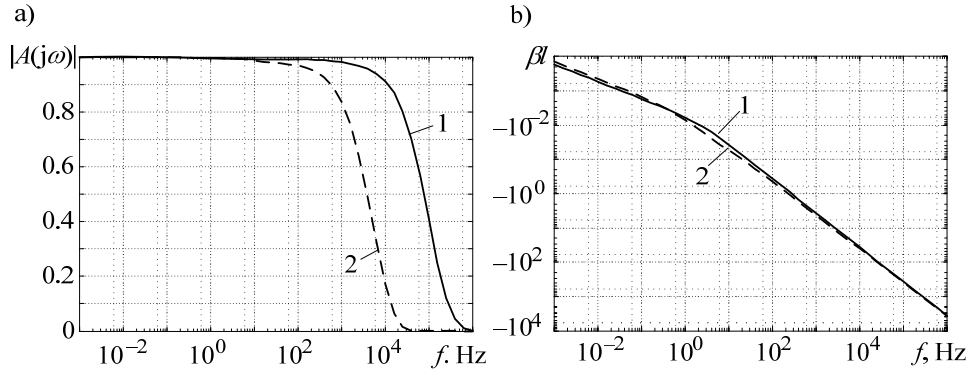


Fig. 4.5. Frequency characteristic of the propagation function $A(j\omega)$:
a) frequency response b) phase response

For the lossless line there is $\gamma = \alpha + j\beta = j\omega/v = j\omega\sqrt{L'C'}$ that implies $A(j\omega) = e^{-j\omega\sqrt{L'C'}}$ and the function $A(j\omega)$ represents the signal distortion caused by the frequency dependent line parameters.

The phase characteristic comprises of two parts. The first part is related to the phase response of the filter and the second one reflects the phase displacement $\omega\tau_f$ caused by wave propagation time (delay) (4.23).

The propagation time τ_f should have the least value which corresponds to the highest frequency in the considered frequency range [58]. The phase response $\arg\{P(j\omega)\} = \omega\tau_f - \beta l$ of the function $P(j\omega)$ for positive sequence (curve 1) and zero sequence (2) component of the line considered are shown in Fig. 4.6.

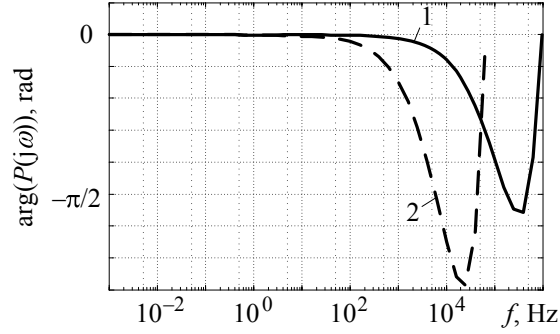


Fig. 4.6. Phase response of $P(j\omega)$ for 400 kV line:
1 – positive sequence component 2 – zero sequence component

The values of propagation time τ_f for both components have been estimated for the frequency f_{gr} for which $|P(j\omega)|$ drops below 0.01 (Fig. 4.5a) according to the relation: $\tau_f = (l/v)|_{f=f_{gr}} = (\beta l / \omega)|_{f=f_{gr}}$. The respective frequency response of wave impedance is shown in Fig. 4.7. Thus the equivalent wave impedance can be considered as the lumped element of adequate frequency response.

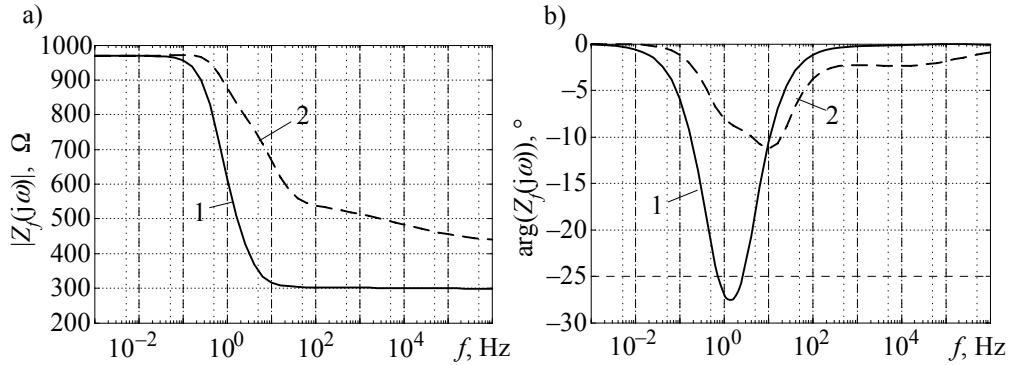


Fig. 4.7. Frequency characteristics of the line surge impedance a) frequency response
b) phase characteristic; 1 – for positive sequence 2 – for zero sequence

The respective filter transmittances in Laplace sense corresponding to line parameters $Z_f(s) = Z_f(j\omega)|_{j\omega=s}$ and $P(s) = P(j\omega)|_{j\omega=s}$ can be determined by rules of minimum-phase system design known from the control system theory [21, 24] if the frequency response $|Z_f(j\omega)|$ and $|P(j\omega)|$ are known (they can be determined as in Example 4.1). If the transmittance considered can be expressed in the factor form which, for instance, in case of wave impedance is:

$$Z_f(s) = \frac{L(s)}{M(s)} = \frac{a_0 s^{k_n} + a_1 s^{k_n-1} + \dots + a_{k_n}}{b_0 s^{k_m} + b_1 s^{k_m-1} + \dots + b_{k_m}} = k_Z \frac{(s-z_1)(s-z_2)\dots(s-z_{k_n})}{(s-b_1)(s-b_2)\dots(s-b_{k_m})} \quad (4.26)$$

then zeroes and poles of such a transmittance can be determined by use of the Bode plot (logarithmic) method [58].

Then the transmittance can be implemented by chain of parallel RC cells. The conditions of such implementation is that poles and zeros alternate on the real axis of the s plane and one pole is located closest to the origin as it is shown in Example 4.5.

Example 4.5. Design the chain of parallel RC cells which approximate the wave impedance of 400 kV line for zero sequence component $Z_{f0}(j\omega)$. The line parameters are as in Example 4.1.

The frequency response of the wave impedance considered is shown in Fig. 4.7 plot 2. The following transmittance is obtained (calculated in MATLAB) [66] for the fifth order approximation:

$$Z_{f0}(s) = k_Z \frac{(s-z_1)(s-z_2)(s-z_3)(s-z_4)(s-z_5)}{(s-b_1)(s-b_2)(s-b_3)(s-b_4)(s-b_5)}$$

where:

$$\begin{aligned} k_Z &= 446.15 & z_1 &= -37112 & z_2 &= -1266.4 & z_3 &= -18.708 & z_4 &= -4.469 & z_5 &= -1.088 \\ b_1 &= -33789 & b_2 &= -1165.5 & b_3 &= -14.013 & b_4 &= -3.929 & b_5 &= -0.9057. \end{aligned}$$

The implementation requirements are met so after partial fraction decomposition of $Z_{f0}(s)$ we get:

$$Z_{f0}(s) = k_Z + \frac{K_1}{s-b_1} + \frac{K_2}{s-b_2} + \frac{K_3}{s-b_3} + \frac{K_4}{s-b_4} + \frac{K_5}{s-b_5} \quad \text{where: } K_i = Z_{f0}(s)(s-b_i)|_{s=b_i}.$$

and also:

$$K_1 = 1.478 \cdot 10^6 \quad K_2 = 4.935 \cdot 10^4 \quad K_3 = 2335.2 \quad K_4 = 396.0 \quad K_5 = 155.86.$$

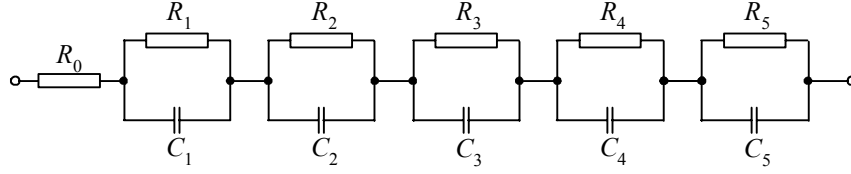
Now using the Foster's method the required RC circuit is obtained (Fig. 4.8) for which the respective parameters are [66]:

$$R_0 = k_Z \quad R_i = -K_i / b_i \quad C_i = 1 / K_i \quad i = 1 \dots 5.$$

After relevant substitution we get:

$$R_0 = 44615 \, \Omega \quad R_1 = 43738 \, \Omega \quad R_2 = 42345 \, \Omega \quad R_3 = 16665 \, \Omega \quad R_4 = 10078 \, \Omega \quad R_5 = 17210 \, \Omega$$

$$C_1 = 06766 \, \mu\text{F} \quad C_2 = 2026 \, \mu\text{F} \quad C_3 = 4282 \, \mu\text{F} \quad C_4 = 2525 \, \mu\text{F} \quad C_5 = 6416 \, \mu\text{F}.$$

Fig. 4.8. The RC chain representing transmittance $Z_{f0}(j\omega)$

Comparison of wave impedance frequency response obtained from calculations and from the RC model is shown in Fig. 4.9.

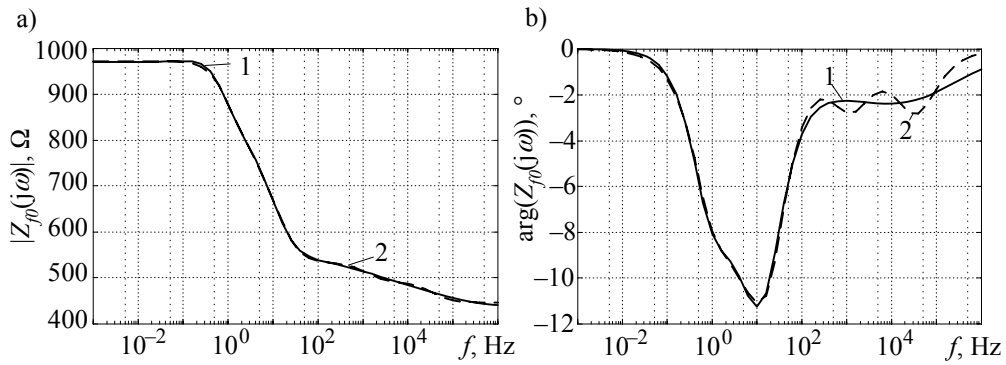


Fig. 4.9. Frequency response of zero sequence wave impedance $Z_{f0}(j\omega)$: a) magnitude; b) phase 1 – calculations 2 – frequency response of the RC model

The numerical model of the equivalent RC circuit can be derived using the model setup rules for lumped element circuit. A single i -th RC cell in the chain is described by the following continuous differential equation:

$$\frac{du_i(t)}{dt} = -\frac{1}{R_i C_i} u_i(t) + \frac{1}{C_i} i_{Z_f}(t) \quad (4.27)$$

and the known solution of the equation is:

$$u_i(t) = e^{-\alpha_i(t-t_0)} u_i(t_0) + \frac{1}{C_i} \int_{t_0}^t e^{-\alpha_i(t-\tau)} i_{Z_f}(\tau) d\tau \quad (4.28)$$

where: $\alpha_i = 1/R_i C_i$ t_0 denotes calculation starting time.

Using the trapezoidal integration method we get ($t - t_0 = T$ – calculation step):

$$u_i(k) = e^{-\alpha_i T} u_i(k-1) + \frac{T}{2C_i} (e^{-\alpha_i T} i_{Z_f}(k-1) + i_{Z_f}(k))$$

and after rearrangement:

$$u_i(k) = R_{ei} i_{Z_f}(k) + v_i(k-1) \quad (4.29)$$

$$\text{where: } R_{ei} = \frac{T}{2C_i} = \frac{TK_i}{2} \quad v_i(k-i) = e^{-\alpha_i T} (u_i(k-1) + R_{ei} i_{Z_f}(k-1)).$$

Series connection of m RC cells along with resistance R_0 results in the following numerical model:

$$u(k) = R_{Z_f} i_{Z_f}(k) + v_{Z_f}(k-1) \quad (4.30)$$

$$\text{where: } R_{Z_f} = R_0 + \sum_{i=1}^{k_m} R_{ei} \quad v_{Z_f}(k-1) = \sum_{i=1}^{k_m} e^{-\alpha_i T} (u_i(k-1) + R_{ei} i_{Z_f}(k-1)).$$

Writing (4.30) in alternative current form we get:

$$i_{Z_f}(k) = G_f u(k) + j_{Z_f}(k-1) \quad (4.31)$$

$$\text{where: } G_f = 1/R_{Z_f} \quad j_{Z_f}(k-1) = -G_f v_{Z_f}(k-1).$$

In case of propagation function $A(j\omega)$ the model can be applied to approximation of $P(j\omega)$ (4.23) as it is illustrated by the following example.

Example 4.6. Design the numerical model of function $P_0(j\omega)$ (zero sequence component) for 400 kV line considered in Example 4.4.

The frequency response of $P_0(j\omega)$ is shown in Fig. 4.5a plot 2. Again applying the fifth order approximation we get:

$$P_0(s) = k_p \frac{(s-z_1)(s-z_2)(s-z_3)(s-z_4)}{(s-b_1)(s-b_2)(s-b_3)(s-b_4)(s-b_5)}$$

where:

$$\begin{aligned} k_p &= 0.0465 & z_1 &= -29424 & z_2 &= -659.99 & z_3 &= -12.89 & z_4 &= -0.1915 \\ b_1 &= -9842.8 & b_2 &= -3089.5 & b_3 &= -569.4 & b_4 &= -12.58 & b_5 &= -0.1908. \end{aligned}$$

Partial fraction decomposition leads to the equation:

$$P_0(s) = k_p + \frac{K_1}{s-b_1} + \frac{K_2}{s-b_2} + \frac{K_3}{s-b_3} + \frac{K_4}{s-b_4} + \frac{K_5}{s-b_5}$$

$$\text{where: } K_i = P_0(s)(s-b_i) \Big|_{s=b_i},$$

and:

$$K_1 = -2372.6 \quad K_2 = 3106.3 \quad K_3 = 92.41 \quad K_4 = 0.2916 \quad K_5 = 6.0 \cdot 10^{-4}.$$

The approximation of the logarithmic frequency response used [34] yields the negative K_1 so the in RC circuit model cannot be applied. However calculations can be carried out according to (4.27)–(4.30) for $\alpha_i = -b_i$. (4.31) can be written in changed form for the current excitation $i_{P_w}(k)$ (the input current):

$$i_p(k) = i_{pw}(k) + j_p(k-1)$$

where: $j_p(k-1) = G_p v_p(k-1) = \sum_{i=1}^5 i_{pi}(k-1)$ and by analogy to (4.30):

$$G_p = \frac{2}{2k_p + T \sum_{i=1}^5 K_i} \quad v_p(k-1) = \sum_{i=1}^5 e^{-\alpha_i T} \left(u_i(k-1) + \frac{TK_i}{2} i_{pw}(k-1) \right).$$

After simplification the equation for the current $i_{pi}(k)$ is:

$$i_{pi}(k) = L_i i_{pw}(k) + j_{pi}(k-1) \quad i = 1 \dots 5$$

where: $j_{pi}(k-1) = e^{b_i T} i_{pi}(k-1) + L_i(k-1) i_{pw}(k-1)$ $L_i = \frac{T}{2} G_p K_i$.

Comparison of respective frequency responses is shown in Fig. 4.10.

Relatively big difference in phase characteristics (Fig. 4.10b) can be attributed to large error in estimation of the original characteristic for high frequency. If $P(s)$ is the correct representation of $P(j\omega)$ then τ_f can be determined from (4.24). Referring calculations to the fundamental frequency ω_1 and using (4.8) we get:

$$\tau_f = \frac{1}{\omega_1} \left(\arg(P(j\omega_1)) + l \arg \left(\sqrt{Z'(j\omega_1) Y'(j\omega_1)} \right) \right) \quad (4.32)$$

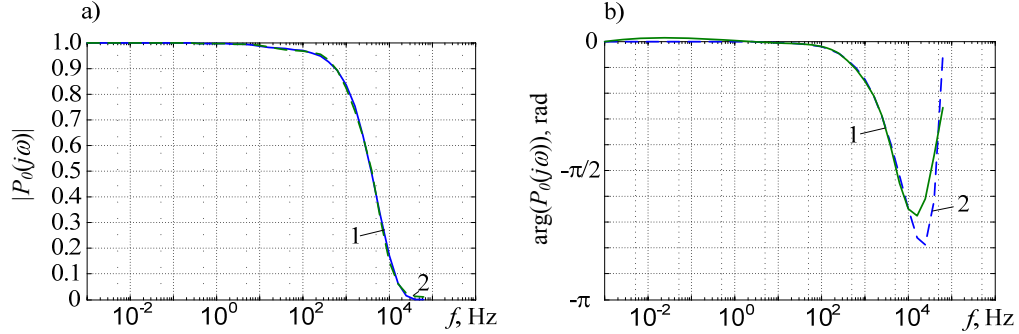


Fig. 4.10. Frequency response of zero sequence surge impedance $P_0(j\omega)$: a) magnitude; b) phase 1 – calculations 2 – frequency response of the fifth order model

Both functions $Z_f(j\omega)$ and $A(j\omega)$ can now be represented by the equivalent lumped parameter circuits described by the respective transmittances $Z_f(s)$ $P(s)$ and time delay τ_f . The equation (4.22) takes the following form in time domain:

$$i_1(k) = i_{1Z_f}(k) + j_1(k-m) \quad (4.33)$$

where: i_{1Z_f} corresponds to (4.31) for node 1; $j_1(k-m)$ is the current 'seen' from the other end of the line; m is the discrete time delay calculated from τ_f .

Taking into account (4.31) the value of excitation in node 2 of the line is given by the following sum of currents:

$$i_{2Pw}(k) = i_{2Z_f}(k) + i_2(k) = G_f u_2(k) + i_2(k) + j_{2Z_f}(k-1) \quad (4.34)$$

Introducing the delay m and including $P(s)$ we get (see Example 4.6):

$$j_1(k-m) = i_{2Pw}(k-m) + j_{2P}(k-m-1) \quad (4.35)$$

where: $j_{2P}(k-m-1) = \sum_{i=1}^{k_m} i_{2Pi}(k-m-1)$

$$i_{2Pi}(k) = L_i i_{2Pw}(k) + j_{2Pi}(k-1) \quad i=1, \dots, k_m$$

$$j_{2Pi}(k-1) = e^{b_i T} i_{2Pi}(k-1) + L_i i_{2Pw}(k-1) \quad L_i = \frac{T}{2} G_p K_i \quad G_p = \frac{2}{2k_p + T \sum_{i=1}^{k_m} K_i}.$$

k_m denotes the number of poles b_i in $P(s)$ while k_p and K_i come from the partial fraction decomposition.

Relations (4.31)–(4.35) describe the digital model of the line with frequency dependent parameters. (Fig. 4.11).

The currents $j_1(k-m)$ $j_2(k-m)$ 'seen' from the other side of the line should be calculated from (4.34) (4.35).

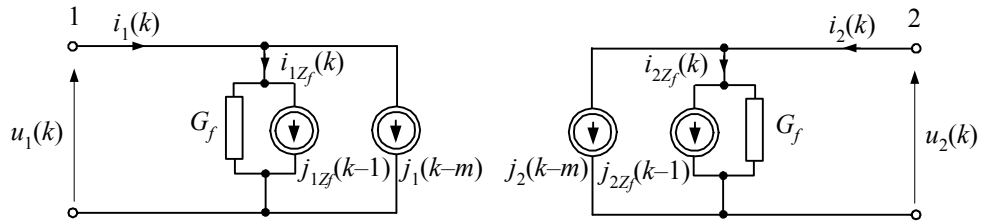


Fig. 4.11. The equivalent circuit of the line with frequency dependent parameters.

The currents $j_{1Z_f}(k-1)$ $j_{2Z_f}(k-1)$ along with the conductance G_f represent the wave impedance $Z_f(j\omega)$ according to (4.31).

4.2. Multi-phase Line Model

4.2.1. Lumped Parameter Model

The generalized model of multi-phase line was developed by Carson [14]. In the model the multi-conductor arrangement of phase wires along with equivalent arrangement of identical and symmetrical with respect to earth surface return wires (Fig. 4.12) is considered.

Parameters of the equivalent line circuit can be determined under assumption that the sum of currents in all conductors (Fig. 4.122) is equal to zero. The equivalent circuit of the considered line segment is shown in Fig. 4.13. Vector of voltage drop across that segment is given by the following equation:

$$\begin{bmatrix} \Delta U_A \\ \Delta U_B \\ \Delta U_C \\ 0 \\ 0 \\ \vdots \\ 0 \end{bmatrix} = (\mathbf{R} + j\omega\mathbf{L}) \begin{bmatrix} I_A \\ I_B \\ I_C \\ I_{N1} \\ I_{N2} \\ \vdots \\ I_{NM} \end{bmatrix} \quad (4.36)$$

where:

$$\mathbf{R} = \begin{bmatrix} R_A + R_D & R_D & R_D & R_D & \cdots & R_D \\ R_D & R_B + R_D & R_D & R_D & \cdots & R_D \\ R_D & R_D & R_C + R_D & R_D & \cdots & R_D \\ R_D & R_D & R_D & R_{N1} + R_D & \cdots & R_D \\ \vdots & \vdots & \vdots & \vdots & \vdots & \vdots \\ R_D & R_D & R_D & R_D & \cdots & R_{NM} + R_D \end{bmatrix} \quad \mathbf{L} = \{L_{km}\}$$

$R_A \dots R_{NM}$ – conductor resistances (in general temperature, frequency and current dependent)

$R_D = 9.869 \times 10^{-7} f \cdot l$ (Ω) f – frequency (Hz) l – conductor length (m);

$L_{km} = \frac{\mu_0 l}{2\pi} \ln \frac{D_{km}}{d_{km}}$ (H) $\mu_0 = 4\pi \times 10^{-7}$ H/m – magnetic permeability k, m – conductor

numbers d_{kk} – conductor radius (equivalent for bunch wires).

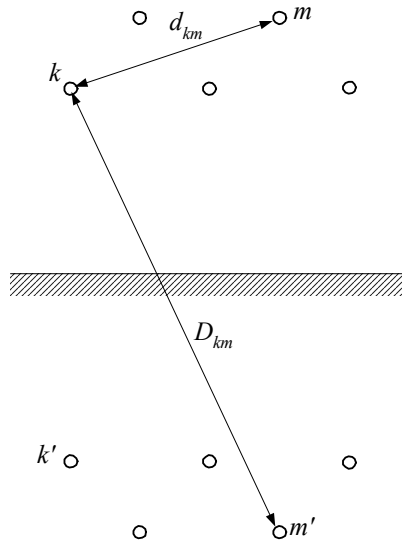


Fig.. 4.12. Conductor arrangement for equivalent overhead line

In analysis of three-phase lines the simplified line model is applied in which M return conductors is replaced by one equivalent wire.

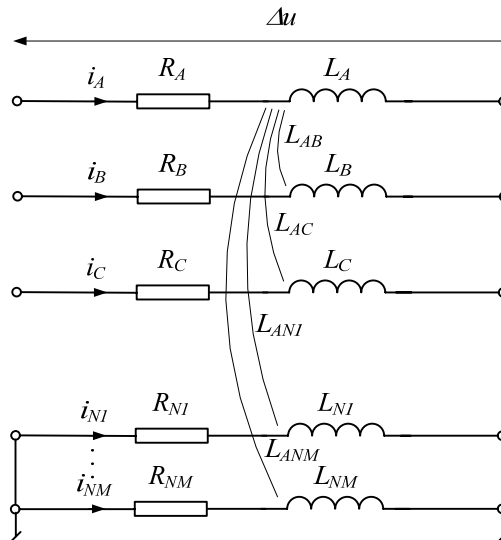


Fig 4.13. The equivalent circuit of the multiphase line

In more detailed notation (4.36) takes the form:

$$\begin{bmatrix} \Delta \underline{U}_A \\ \Delta \underline{U}_B \\ \Delta \underline{U}_C \\ 0 \\ \vdots \\ 0 \end{bmatrix} = \begin{bmatrix} \underline{Z}_{11} & \underline{Z}_{12} & \underline{Z}_{13} & \underline{Z}_{14} & \cdots & \underline{Z}_{1(3+M)} \\ \underline{Z}_{21} & \underline{Z}_{22} & \underline{Z}_{23} & \underline{Z}_{24} & \cdots & \underline{Z}_{2(3+M)} \\ \underline{Z}_{31} & \underline{Z}_{32} & \underline{Z}_{33} & \underline{Z}_{34} & \cdots & \underline{Z}_{3(3+M)} \\ \underline{Z}_{41} & \underline{Z}_{42} & \underline{Z}_{43} & \underline{Z}_{44} & \cdots & \underline{Z}_{4(3+M)} \\ \vdots & \vdots & \vdots & \vdots & \vdots & \vdots \\ \underline{Z}_{(3+M)1} & \underline{Z}_{(3+M)2} & \underline{Z}_{(3+M)3} & \underline{Z}_{(3+M)4} & \cdots & \underline{Z}_{M(3+M)} \end{bmatrix} \begin{bmatrix} \underline{I}_A \\ \underline{I}_B \\ \underline{I}_C \\ \underline{I}_{N1} \\ \vdots \\ \underline{I}_{NM} \end{bmatrix} \quad (4.37)$$

where:

$$\underline{Z}_{kk} = R_k + R_D + j\omega L_{kk} \quad \underline{Z}_{km} = R_D + j\omega L_{km}.$$

The equation (4.37) can be written in compact form as:

$$\begin{bmatrix} \Delta \underline{U} \\ \mathbf{0} \end{bmatrix} = \begin{bmatrix} \underline{Z}_A & \underline{Z}_B \\ \underline{Z}_C & \underline{Z}_D \end{bmatrix} \begin{bmatrix} \underline{I}_f \\ \underline{I}_N \end{bmatrix} \quad (4.38)$$

Basing on (4.38) the following equations can be written:

$$\begin{aligned} \Delta \underline{U} &= \underline{Z}_A \underline{I}_f + \underline{Z}_B \underline{I}_N \\ \mathbf{0} &= \underline{Z}_C \underline{I}_f + \underline{Z}_D \underline{I}_N \end{aligned} \quad (4.39)$$

The second equation yields:

$$\underline{I}_N = -\underline{Z}_D^{-1} \underline{Z}_C \underline{I}_f \quad (4.40)$$

Substituting (4.40) to the first equation in (4.39) we get:

$$\Delta \underline{U} = \underline{Z}_f \underline{I}_f \quad (4.41)$$

where:

$$\underline{Z}_f = \underline{Z}_A - \underline{Z}_B \underline{Z}_D^{-1} \underline{Z}_C = \begin{bmatrix} \underline{Z}_{AA} & \underline{Z}_{AB} & \underline{Z}_{AC} \\ \underline{Z}_{AB} & \underline{Z}_{BB} & \underline{Z}_{BC} \\ \underline{Z}_{AC} & \underline{Z}_{BC} & \underline{Z}_{CC} \end{bmatrix} \quad (4.42)$$

is the parameter matrix of the equivalent three-phase line (Fig. 4.14).

The following relations are valid for transposed line in frequency domain:

$$\underline{Z}_{AA} = \underline{Z}_{BB} = \underline{Z}_{CC} = \underline{Z}_S \quad \underline{Z}_{AB} = \underline{Z}_{AC} = \underline{Z}_{BC} = \underline{Z}_M.$$

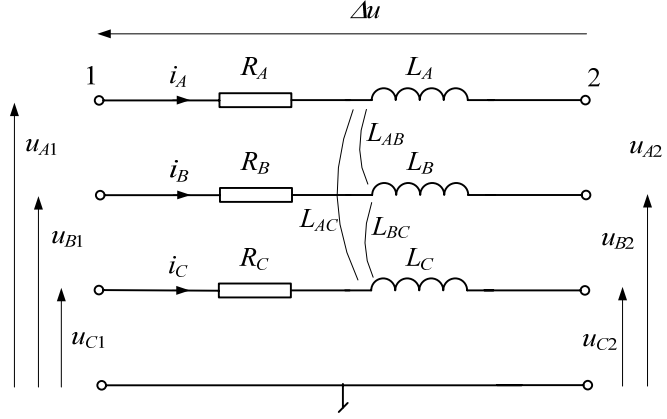


Fig. 4.14. Simplified circuit of three-phase line

In time domain voltage drop across the considered line segment is given by:

$$\Delta \mathbf{U}(t) = \mathbf{R}_f \mathbf{I}_f(t) + \mathbf{L}_f \frac{d}{dt} \mathbf{I}_f(t) \quad (4.43)$$

where:

$$\Delta \mathbf{U}(t) = \begin{bmatrix} u_{A1}(t) - u_{A2}(t) \\ u_{B1}(t) - u_{B2}(t) \\ u_{C1}(t) - u_{C2}(t) \end{bmatrix} \quad \mathbf{I}_f(t) = \begin{bmatrix} i_A(t) \\ i_B(t) \\ i_C(t) \end{bmatrix}$$

$$\mathbf{R}_f = \begin{bmatrix} R_{AA} & R_{AB} & R_{AC} \\ R_{AB} & R_{BB} & R_{BC} \\ R_{AC} & R_{BC} & R_{CC} \end{bmatrix} \quad \mathbf{L}_f = \begin{bmatrix} L_{AA} & L_{AB} & L_{AC} \\ L_{AB} & L_{BB} & L_{BC} \\ L_{AC} & L_{BC} & L_{CC} \end{bmatrix}.$$

Using the generalized line model (Fig 4.12) the equivalent transverse line model can be derived under general assumption that all conductors are isolated one from each other entirely. The electric charges q in physical conductors and in the equivalent ones located under the earth (mirror reflection) are equal and opposite so it can be assumed that the voltage between k -th conductor and the earth surface is equal to the half of the voltage between the conductor and its mirror reflection under the earth [36]. If so then:

$$U_{kN} = \frac{1}{2} U_{km} = \frac{1}{2\pi\epsilon_0} \sum_{i=1}^{3+M} q_i \ln \frac{D_{km}}{d_{km}} \quad (4.44)$$

where: $\epsilon_0 = \frac{1}{\mu_0 c^2} = 8.854 \times 10^{-12}$ F/m – electric permeability, q_i – charge in i -th conductor (C/m), c – light velocity (m/s).

Similar equations can be written for each isolated phase conductor while the other conductors are earthed and connected to the zero reference potential. Using the matrix-vector notation the equations take the form:

$$\begin{bmatrix} U_A \\ U_B \\ U_C \\ 0 \\ \vdots \\ 0 \end{bmatrix} = \begin{bmatrix} P_{11} & P_{12} & P_{13} & P_{14} & \cdots & P_{1(3+M)} \\ P_{21} & P_{22} & P_{23} & P_{24} & \cdots & P_{2(3+M)} \\ P_{31} & P_{32} & P_{33} & P_{34} & \cdots & P_{3(3+M)} \\ \hline P_{41} & P_{42} & P_{43} & P_{44} & \cdots & P_{4(3+M)} \\ \vdots & \vdots & \vdots & \vdots & \vdots & \vdots \\ P_{(3+M)1} & P_{(3+M)2} & P_{(3+M)3} & P_{(3+M)4} & \cdots & P_{M(3+M)} \end{bmatrix} \begin{bmatrix} q_A \\ q_B \\ q_C \\ q_{N1} \\ \vdots \\ q_{NM} \end{bmatrix} \quad (4.45)$$

where:

$$P_{km} = \frac{1}{2\pi\epsilon_0} \ln \frac{D_{km}}{d_{km}} \quad (\text{m/F}) \quad (4.46)$$

P_{km} is known as Maxwell coefficient.

Similarly to (4.37) the equation (4.45) can be simplified and:

$$\begin{bmatrix} \mathbf{U}_f \\ \mathbf{0} \end{bmatrix} = \begin{bmatrix} \mathbf{P}_A & \mathbf{P}_B \\ \mathbf{P}_C & \mathbf{P}_D \end{bmatrix} \begin{bmatrix} \mathbf{q}_f \\ \mathbf{q}_N \end{bmatrix} \quad (4.47)$$

from which:

$$\mathbf{U}_f = (\mathbf{P}_A - \mathbf{P}_B \mathbf{P}_D^{-1} \mathbf{P}_C) \mathbf{q}_f \quad (4.48)$$

or alternatively

$$\mathbf{q}_f = (\mathbf{P}_A - \mathbf{P}_B \mathbf{P}_D^{-1} \mathbf{P}_C)^{-1} \mathbf{U}_f = \mathbf{C}_f \mathbf{U}_f \quad (4.49)$$

where:

$$\mathbf{C}_f = (\mathbf{P}_A - \mathbf{P}_B \mathbf{P}_D^{-1} \mathbf{P}_C)^{-1} = \begin{bmatrix} C_{AA} & C_{AB} & C_{AC} \\ C_{AB} & C_{BB} & C_{BC} \\ C_{AC} & C_{BC} & C_{CC} \end{bmatrix} \quad (\text{F/m}) \quad (4.50)$$

is the capacitance matrix of the equivalent three-phase system.

Conductance is an active element of the transverse line model. Confining considerations to linear case the corresponding model will be described by the following equation:

$$\mathbf{I}_G = \mathbf{G}_f \mathbf{U}_f, \quad \mathbf{G}_f = \begin{bmatrix} G_{AA} & G_{AB} & G_{AC} \\ G_{AB} & G_{BB} & G_{BC} \\ G_{AC} & G_{BC} & G_{CC} \end{bmatrix} \text{ (S/m)} \quad (4.51)$$

In power line models conductance is not taken into account as being negligibly small with respect to line susceptance. Thus the line model looks like it is shown in Fig. 4.15.

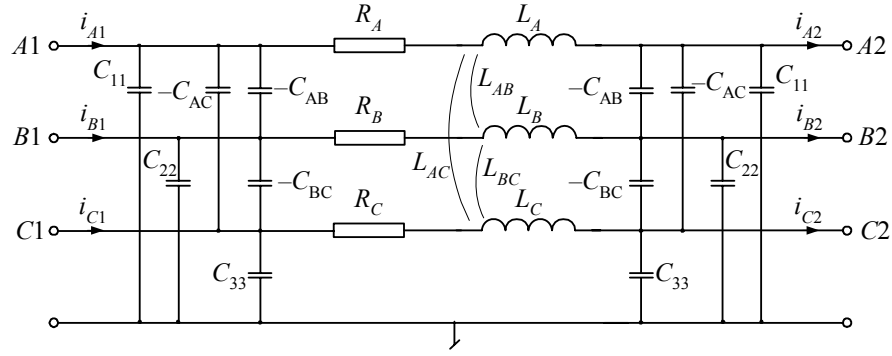


Fig. 4.15. The equivalent circuit of the three-phase line

The current flowing through the transverse elements at any side of the three-phase line model can be determined by the following equation:

$$\mathbf{I}_Y = \mathbf{Y}_f \mathbf{U}_f, \quad \mathbf{Y}_f = \mathbf{G}_f + j\omega \mathbf{C}_f \text{ (S/m)} \quad (4.52)$$

in frequency domain or by:

$$\mathbf{I}_Y(t) = \mathbf{G}_f \mathbf{U}_f(t) + \mathbf{C}_f \frac{d}{dt} \mathbf{U}_f(t) \quad (4.53)$$

in time domain.

It should be noted that the respective capacitances in the line model are divided into two equal parts connected to each end of the line. The values of phase-to-phase capacitances are negative while the respective phase-to-ground capacitance values are:

$$C_{11} = C_{AA} - C_{AB} - C_{AC},$$

$$C_{22} = C_{BB} - C_{AB} - C_{BC},$$

$$C_{33} = C_{CC} - C_{AC} - C_{BC}.$$

and if the line is transposed then:

$$C_{AA} = C_{BB} = C_{CC} = C_S \quad C_{AB} = C_{AC} = C_{BC} = C_M .$$

In the model of transposed line the parameters in all phases can be assumed as being equal and then the line parameters for symmetrical components can be used. The respective relations can be obtained after transformation of phase coordinates into the symmetrical ones by use of the fundamental formula:

$$\mathbf{U}_f = \mathbf{S} \mathbf{U}_s \quad (4.54)$$

for voltages (the same formula holds for currents) where:

$$\mathbf{S} = \frac{1}{3} \begin{bmatrix} 1 & 1 & 1 \\ 1 & a & a^2 \\ 1 & a^2 & a \end{bmatrix} \quad a = e^{j2\pi/3} = \frac{-1}{2} + j \frac{\sqrt{3}}{2} \quad (4.55)$$

$$\mathbf{U}_s = \begin{bmatrix} \underline{U}_0 \\ \underline{U}_1 \\ \underline{U}_2 \end{bmatrix} - \text{symmetrical voltage(current) component vector.}$$

Applying transformation (4.54) to (4.41) the relation between phase \mathbf{Z}_f and symmetrical \mathbf{Z}_s component impedance matrices is obtained and:

$$\mathbf{Z}_s = \mathbf{S}^{-1} \mathbf{Z}_f \mathbf{S} \quad (4.56)$$

If the three-phase system is transposed then the matrix of symmetrical impedance components is diagonal:

$$\mathbf{Z}_s = \begin{bmatrix} Z_0 & & \\ & Z_1 & \\ & & Z_2 \end{bmatrix} \quad (4.57)$$

In case of power line: $\underline{Z}_1 = \underline{Z}_2$,

and (4.56) shows that for the transposed line the following relations hold:

$$\begin{aligned} Z_0 &= Z_S + 2Z_M & Z_1 &= Z_S - Z_M \\ Z_S &= \frac{Z_0 + 2Z_1}{3} & Z_M &= \frac{Z_0 - Z_1}{3} . \end{aligned}$$

It should be born in mind that transformation into symmetrical components refers to complex vectors of currents and voltages which represent fixed frequency harmonic functions of time in steady state. Therefore the transformation is not applied directly to transient analysis of electric networks. However all the relations shown are important

for the model setup since line and cable parameters are very frequently available in symmetrical component form.

4.2.2. Distributed Parameters Model

Derivations of the multi-phase distributed parameter line model and of the single phase one are very much alike. In case of n phases (1.75) takes the form:

$$\begin{aligned} -\frac{\partial \mathbf{U}(x,t)}{\partial x} &= \mathbf{R}'\mathbf{I}(x,t) + \mathbf{L}'\frac{\partial \mathbf{I}(x,t)}{\partial t} \\ -\frac{\partial \mathbf{I}(x,t)}{\partial x} &= \mathbf{G}'\mathbf{U}(x,t) + \mathbf{C}'\frac{\partial \mathbf{U}(x,t)}{\partial t} \end{aligned} \quad (4.58)$$

where:

$$\mathbf{U}(x,t) = \begin{bmatrix} u_1(x,t) \\ u_2(x,t) \\ \vdots \\ u_n(x,t) \end{bmatrix} \quad \mathbf{I}(x,t) = \begin{bmatrix} i_1(x,t) \\ i_2(x,t) \\ \vdots \\ i_n(x,t) \end{bmatrix} \quad \text{-- voltages and currents of } n\text{-phase line;}$$

$$\mathbf{R}' = \begin{bmatrix} R'_{11} & R'_{12} & \cdots & R'_{1n} \\ R'_{12} & R'_{22} & \cdots & R'_{2n} \\ \vdots & \vdots & \cdots & \vdots \\ R'_{n1} & R'_{n2} & \cdots & R'_{nn} \end{bmatrix} \quad (\Omega/\text{km}) \quad \text{-- matrix of 'per unit' line resistance (similarly to } \mathbf{G}' \text{ } \mathbf{L}' \text{ } \mathbf{C}').$$

In general, parameters in (4.58) are frequency dependent but for the sake of model simplicity this effect can be neglected.

a) Constant Parameters Model

In case of lossless multiphase line (4.58) can be written as (by analogy to (1.79)):

$$\begin{aligned} \frac{\partial^2 \mathbf{U}}{\partial x^2} - \mathbf{L}'\mathbf{C}'\frac{\partial^2 \mathbf{U}}{\partial t^2} &= 0 \\ \frac{\partial^2 \mathbf{I}}{\partial x^2} - \mathbf{C}'\mathbf{L}'\frac{\partial^2 \mathbf{I}}{\partial t^2} &= 0 \end{aligned} \quad (4.59)$$

The matrices:

$$\mathbf{A}_u = \mathbf{L}'\mathbf{C}' \quad \mathbf{A}_i = \mathbf{C}'\mathbf{L}'$$

are complete and symmetrical. Therefore:

$$\mathbf{A}_i = (\mathbf{A}_u)^T \quad (4.60)$$

Subscripts i and u indicate either current or voltage matrix in (4.59).

The line model will be simplified significantly if the matrices in (4.59) are diagonal since in such case the multiphase system gets uncoupled and the model of n -phase line splits into n single phase ones.

Diagonalization of matrix \mathbf{A}_i is described by the equation:

$$\mathbf{A}_{i\text{mod}} = \mathbf{T}_i^{-1} \mathbf{A}_i \mathbf{T}_i \quad (4.61)$$

where: \mathbf{T}_i is the square eigenvalue matrix in which the k -th column \mathbf{s}_k (the eigenvector² of \mathbf{A}_i) is the function of k -th eigenvalue λ_k of the matrix \mathbf{A}_i so that the following equation is satisfied [21]:

$$(\mathbf{A}_i - \lambda_k \mathbf{1}) \mathbf{s}_k = 0 \quad (4.62)$$

Relation (4.61) is known as similarity transformation in which the eigenvalues of \mathbf{A}_i and $\mathbf{A}_{i\text{mod}}$ are the same. For the voltage equation in (4.59) we get similarly:

$$\mathbf{A}_{u\text{mod}} = \mathbf{T}_u^{-1} \mathbf{A}_u \mathbf{T}_u \quad (4.63)$$

The respective inverse transformations yield:

$$\begin{aligned} \mathbf{A}_u &= \mathbf{L}' \mathbf{C}' = \mathbf{T}_u \mathbf{A}_{u\text{mod}} \mathbf{T}_u^{-1} \\ \mathbf{A}_i &= \mathbf{C}' \mathbf{L}' = \mathbf{T}_i \mathbf{A}_{i\text{mod}} \mathbf{T}_i^{-1} \end{aligned} \quad (4.64)$$

Substitution of (4.64) to (4.59) results in multiphase line equation for modal components:

$$\begin{aligned} \frac{\partial^2 \mathbf{U}_{\text{mod}}}{\partial x^2} - \mathbf{A}_{u\text{mod}} \frac{\partial^2 \mathbf{U}_{\text{mod}}}{\partial t^2} &= 0 \\ \frac{\partial^2 \mathbf{I}_{\text{mod}}}{\partial x^2} - \mathbf{A}_{i\text{mod}} \frac{\partial^2 \mathbf{I}_{\text{mod}}}{\partial t^2} &= 0 \end{aligned} \quad (4.65)$$

where:

$$\mathbf{I}_{\text{mod}} = \mathbf{T}_i^{-1} \mathbf{I} = \mathbf{T}_i^{-1} \mathbf{I}_f \quad \mathbf{U}_{\text{mod}} = \mathbf{T}_u^{-1} \mathbf{U} = \mathbf{T}_u^{-1} \mathbf{U}_f ;$$

subscript f indicates phase components.

Further, using (4.60) and (4.64) we can write:

$$\mathbf{T}_u \mathbf{A}_{u\text{mod}} \mathbf{T}_u^{-1} = (\mathbf{T}_i \mathbf{A}_{i\text{mod}} \mathbf{T}_i^{-1})^T = (\mathbf{T}_i^{-1})^T \mathbf{A}_{i\text{mod}}^T \mathbf{T}_i^T \quad (4.66)$$

and:

² Eigenvalues of the square matrix \mathbf{A} are equal to the roots of the equation: $\det(\mathbf{A} - \lambda \mathbf{1}) = 0$; Eigenvector \mathbf{x} is related to the eigenvalue λ by equation: $\mathbf{A}\mathbf{x} = \lambda\mathbf{x}$ [21, 83].

$$\mathbf{A}_{u \text{ mod}} = \mathbf{T}_u^{-1} (\mathbf{T}_i^{-1})^T \mathbf{A}_{i \text{ mod}}^T \mathbf{T}_i^T \mathbf{T}_u = \mathbf{D}^{-1} \mathbf{A}_{i \text{ mod}} \mathbf{D} = \mathbf{A}_{i \text{ mod}} \quad (4.67)$$

where:

$$\mathbf{D} = \mathbf{T}_i^T \mathbf{T}_u = d \mathbf{1} \quad d \neq 0 \quad (4.68)$$

is the diagonal matrix of identical elements and $\mathbf{A}_{i \text{ mod}}^T = \mathbf{A}_{i \text{ mod}}$.

In many cases it can be assumed that $d = 1$ and as implication: $\mathbf{T}_i^T = \mathbf{T}_u^{-1}$.

If matrix \mathbf{A}_i (\mathbf{A}_u) is real (like in (4.59)) the eigenvalue matrices \mathbf{T}_i (\mathbf{T}_u) are also real. Moreover if the parameter matrix is symmetrical then the following relation holds:

$$\mathbf{T}_i^T \mathbf{T}_i = \mathbf{1} \quad \text{and:} \quad \mathbf{T}_i^{-1} = \mathbf{T}_i^T \quad (4.69)$$

The same applies to matrix \mathbf{T}_u . Matrix which satisfies (4.69) is said to be orthogonal³. In such case for $d = 1$ both matrices are equal:

$$\mathbf{T}_i = \mathbf{T}_u = \mathbf{T} \quad (4.70)$$

The condition is also satisfied for transposed lines.

If the current and voltage transformation matrices satisfy (4.69) then current and voltage wave propagation velocities are identical and

$$\mathbf{A}_{u \text{ mod}} = \mathbf{A}_{i \text{ mod}} = \begin{bmatrix} \frac{1}{v_1^2} & & & \\ & \frac{1}{v_2^2} & & \\ & & \ddots & \\ & & & \frac{1}{v_n^2} \end{bmatrix} \quad (4.71)$$

$v_k = \frac{1}{\sqrt{L'_k C'_k}}$ – wave propagation velocity for the k -th mode,

L'_k C'_k – parameters of the k -th mode.

Similar relations are valid for wave impedance (1.82).

To include resistance into the line model the line equation in frequency domain can be used (for steady state – see (4.5)):

³ In case of complex form the orthogonal matrix is called the unitary one.

$$\begin{aligned}\frac{d^2 \mathbf{U}}{dx^2} - \mathbf{Z}' \mathbf{Y}' \mathbf{U} &= 0 \\ \frac{d^2 \mathbf{I}}{dx^2} - \mathbf{Y}' \mathbf{Z}' \mathbf{I} &= 0\end{aligned}\quad (4.72)$$

where:

$\mathbf{Z}' = \mathbf{R} + j\omega \mathbf{L}$ $\mathbf{Y}' = \mathbf{G} + j\omega \mathbf{C}$ (conductance \mathbf{G} usually neglected),
vectors \mathbf{U} and \mathbf{I} are function of distance x and by analogy to (4.4):

$$\begin{aligned}-\frac{d\mathbf{U}}{dx} &= \mathbf{Z}' \mathbf{I} \\ -\frac{d\mathbf{I}}{dx} &= \mathbf{Y}' \mathbf{U}\end{aligned}\quad (4.73)$$

For complex model (4.72) eigenvalue matrices \mathbf{T}_u and \mathbf{T}_i are, generally, also complex and:

$$\begin{aligned}\mathbf{A}_{u \text{ mod}} &= \mathbf{T}_u^{-1} \mathbf{A}_u \mathbf{T}_u \\ \mathbf{A}_{i \text{ mod}} &= \mathbf{T}_i^{-1} \mathbf{A}_i \mathbf{T}_i\end{aligned}\quad (4.74)$$

where: $\mathbf{A}_u = \mathbf{Z}' \mathbf{Y}'$ $\mathbf{A}_i = \mathbf{Y}' \mathbf{Z}'$.

Using the diagonal matrices of parameters (4.72) takes the form:

$$\begin{aligned}\frac{d^2 \mathbf{U}_{\text{mod}}}{dx^2} - \mathbf{A}_{u \text{ mod}} \mathbf{U}_{\text{mod}} &= 0 \\ \frac{d^2 \mathbf{I}_{\text{mod}}}{dx^2} - \mathbf{A}_{i \text{ mod}} \mathbf{I}_{\text{mod}} &= 0\end{aligned}\quad (4.75)$$

Interpretation of parameters located in the matrix diagonal is the same as for (4.6):

$$\mathbf{A}_{u \text{ mod}} = \mathbf{A}_{i \text{ mod}} = \begin{bmatrix} \gamma_1^2 & & & \\ & \gamma_2^2 & & \\ & & \ddots & \\ & & & \gamma_n^2 \end{bmatrix}\quad (4.76)$$

where: $\gamma_k = \sqrt{Z'_k(j\omega)Y'_k(j\omega)} = \alpha_k + j\beta_k$ is the propagation constant for the k -th mode.

Comparison of (4.71) and (4.76) yields $\beta_k = \omega v_k$. Substitution of (4.74) to (4.4) leads to the following relations:

$$\begin{aligned}\mathbf{Z}_{\text{mod}} &= \mathbf{T}_u^{-1} \mathbf{Z}' \mathbf{T}_i \\ \mathbf{Y}_{\text{mod}} &= \mathbf{T}_i^{-1} \mathbf{Y}' \mathbf{T}_u\end{aligned}\quad (4.77)$$

The matrices \mathbf{T}_u and \mathbf{T}_i in (4.77) are usually complex what makes further calculations cumbersome. To avoid this drawback the matrices are approximated by the respective real ones. This is usually obtained by rotation of the complex matrix to minimize the imaginary parts of complex elements. The respective algorithm of such approximation is shown in [24]:

1. Determine the matrix $\mathbf{T}_{uw} = \mathbf{T}_u$ (the matrix is complex) assuming that the admittance matrix \mathbf{Y}' comprises of reactance (imaginary elements) only.
2. Calculate $\mathbf{Y}_{w\text{mod}} = \mathbf{T}_{uw}^T \mathbf{Y}' \mathbf{T}_{uw}$ using (4.77) for $T_{uw}^T = T_{iw}^{-1}$ ($d = 1$ in (4.68)).
3. Since the matrix \mathbf{T}_{uw} is complex the real parts appear in elements of $\mathbf{Y}_{w\text{mod}}$. Such elements can be written as: $j\omega C_{k\text{mod}} e^{j\alpha_k}$. To get the normalized (rotated) form of the matrix $\mathbf{T}_{uw} \rightarrow \mathbf{T}_u$ the columns should be multiplied by the complex operator $e^{j\alpha_k/2}$. As a result the imaginary elements of the new matrix \mathbf{Y}_{mod} become very small and can be neglected.

It must be stressed that the line model in frequency domain (4.72) is meant for determination of the model parameters and the eigenvalue matrices only while the modelling algorithm remains the same as for the lossless line and can be complemented by the lumped resistance model if necessary (in EMTP the total line resistance is divided into four parts— see Fig. 4.10b). The diagram of the model considered is shown in Fig. 4.16.

The model is realized for each mode according to the algorithm discussed in sect. 1.3.6. The phase vectors of currents and voltages at both sides of the line are transformed into the modal ones in each calculation step. Then after processing by (1.91) and (1.92) the original phase voltages and currents are recovered.

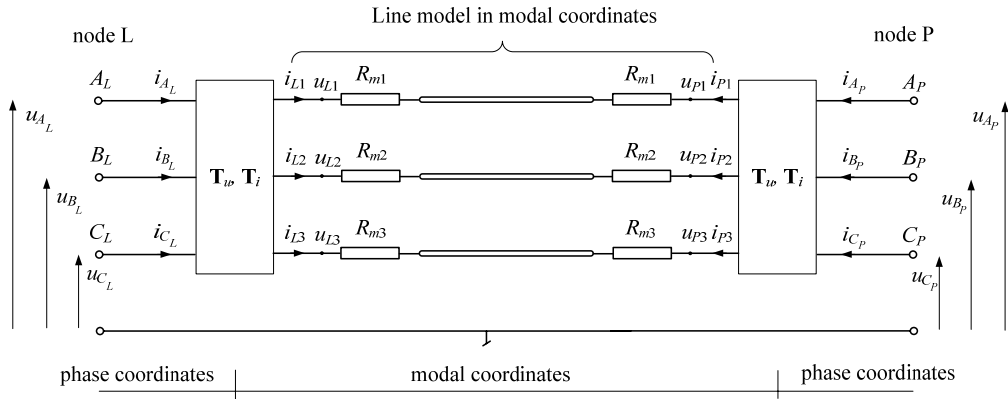


Fig 4.16. Multiphase line in modal arrangement

The following example illustrates how the diagonal matrices are calculated in ATP-EMTP.

Example 4.7. Calculate the line parameters of the line in Example 4.1 for phase and modal components assuming that the line is untransposed. Use the LINE CONSTANTS supporting program available in ATP-EMTP.

The line cross section (Fig. 4.1) indicates that the parameters of the middle phase (capacitance and inductance) (B) differ from the parameters of other phases. The input file for parameter calculating subroutine in ATP-EMTP is also different as compared to the file used in Example 4.1 (the bold typed control line) The control lines read as follows:

col. 34: 1 – calculate capacitances for the equivalent three-phase system.

col. 38: 1 – calculate impedances for the equivalent system

col. 44: 1 – capacitance in (F) units not as ωC (S) – like before;

col. 70: 1 – line is untransposed – the current eigenvalue matrix \mathbf{T}_i must be calculated

```
BEGIN NEW DATA CASE
C Line 400 kV
LINE CONSTANTS
METRIC
C Data for LINE CONSTANTS
C 34567890123456789012345678901234567890123456789012345678901234567890
1 .231 .0564 4 3.15 -10.3 24.5 12.0 40.0 0.0 2
2 .231 .0564 4 3.15 0.0 24.5 12.0 40.0 0.0 2
3 .231 .0564 4 3.15 10.3 24.5 12.0 40.0 0.0 2
0 0.5 .2388 4 1.565 -6.87 31.0 23.5
0 0.5 .2388 4 1.565 6.87 31.0 23.5
BLANK CARD ENDING CONDUCTOR CARDS OF "LINE CONSTANTS" CASE
C 1 2 3 4 5 6 7 8
C 34567890123456789012345678901234567890123456789012345678901234567890
C >< Freq >< FCar > <ICPR> <IZPR> =< DIST > <PP>==< >< >< >< ><
100.0 50.0 1 1 1 180.0 1
BLANK CARD ENDING FREQUENCY CARDS
BLANK CARD ENDING "LINE CONSTANTS"
BEGIN NEW DATA CASE
BLANK
```

The relevant fragment of the output file is shown in the next page. Here comes the short comment of results:

Capacitance matrix refers to the phase-to- earth capacitances \mathbf{C}_f (F) (4.50). The lower part of these matrices is given only since the matrix is symmetrical. The same refers to the *impedance matrix* $\mathbf{R}_f + j\omega\mathbf{L}_f$ (Ω).

Further the *modal parameters* are printed: resistance, reactance, wave impedance propagation velocity v : in lossless actual line α (attenuation). All three modal components are of different values. The current eigenvector matrix \mathbf{T}_i is complex but in this case the normalized imaginary form is given.

It can be verified that \mathbf{T}_i is not orthogonal: $\mathbf{T}_i^T \mathbf{T}_i \neq \mathbf{1}$ so equation (4.70) does not hold.

Assuming $d = 1$ calculation of: $\mathbf{T}_u = (\mathbf{T}_i^T)^{-1}$ yields:

$$\mathbf{T}_u = \begin{bmatrix} 5.802174291013298\text{e-}01 & -7.071067811865468\text{e-}01 & -3.760128057084046\text{e-}01 \\ 5.737902829739805\text{e-}01 & -2.248770831006496\text{e-}15 & 8.483917484204246\text{e-}01 \\ 5.802174291013300\text{e-}01 & 7.071067811865482\text{e-}01 & -3.760128057084001\text{e-}01 \end{bmatrix}.$$

Let's follow – using MATLAB - calculation of the eigenvalue matrices \mathbf{T}_u \mathbf{T}_i The matrix $\mathbf{A}_u = \mathbf{Z}'\mathbf{Y}'$ is:

$$\mathbf{Z}'\mathbf{Y}' = \begin{bmatrix} -0.1353\text{E-}5 + \text{j}0.0197\text{E-}5 & -0.0195\text{E-}5 + \text{j}0.0085\text{E-}5 & -0.0205\text{E-}5 + \text{j}0.0100\text{E-}5 \\ -0.0218\text{E-}5 + \text{j}0.0095\text{E-}5 & -0.1310\text{E-}5 + \text{j}0.0192\text{E-}5 & -0.0218\text{E-}5 + \text{j}0.0095\text{E-}5 \\ -0.0205\text{E-}5 + \text{j}0.0100\text{E-}5 & -0.0195\text{E-}5 + \text{j}0.0085\text{E-}5 & -0.1353\text{E-}5 + \text{j}0.0197\text{E-}5 \end{bmatrix}.$$

The function *eig()* calculates eigenvalues and eigenvectors of $\mathbf{Z}'\mathbf{Y}'$:

[TuV]=eig(ZY)

where: Tu is the desired matrix \mathbf{T}_u and V (=V) is the diagonal eigenvalue matrix:

$$\mathbf{V} = \begin{bmatrix} -0.1751 \cdot 10^{-5} + \text{j}0.0383 \cdot 10^{-5} & & \\ & -0.1148 \cdot 10^{-5} + \text{j}0.0097 \cdot 10^{-5} & \\ & & -0.1118 \cdot 10^{-5} + \text{j}0.0108 \cdot 10^{-5} \end{bmatrix}.$$

Columns \mathbf{s}_k $k = 1 \ 2 \ \dots \ n$ of the eigenvector matrix $\mathbf{T}_u = [\mathbf{s}_1 \ \mathbf{s}_2 \ \dots \ \mathbf{s}_n]$ are obtained by solution of the following equations (4.62):

$$(\mathbf{A}_i - \lambda_k \mathbf{1})\mathbf{s}_k = 0$$

where: λ_k $k = 1 \ 2 \ \dots \ n$ are the subsequent eigenvalues of $\mathbf{Z}'\mathbf{Y}'$.

MATLAB returns the following result:

$$\mathbf{T}_u = \begin{bmatrix} 0.5792 - \text{j}0.0179 & -0.7071 - \text{j}0.0003 & 0.3754 + \text{j}0.0105 \\ 0.5727 - \text{j}0.0195 & 0.0000 + \text{j}0.0000 & -0.8469 - \text{j}0.0280 \\ 0.5792 - \text{j}0.0179 & 0.7071 + \text{j}0.0003 & 0.3754 + \text{j}0.0105 \end{bmatrix}.$$

which is different from that obtained in ATP-EMTP (different sign in the last column).

Now the modal admittance matrix \mathbf{Y}_{mod} can be calculated:

$$\mathbf{Y}_{\text{mod}} = \mathbf{T}_u^T \mathbf{Y}' \mathbf{T}_u = \begin{bmatrix} 0.0000 + \text{j}0.2429 & 0.0000 + \text{j}0.0000 & 0.0011 + \text{j}0.0001 \\ 0.0000 + \text{j}0.0000 & 0.0000 + \text{j}0.3270 & 0.0000 + \text{j}0.0000 \\ -0.0011 + \text{j}0.0001 & 0.0000 + \text{j}0.0000 & 0.0000 + \text{j}0.3769 \end{bmatrix} \cdot 10^{-5} \text{ (S/km)}.$$

The matrix is not diagonal and not entirely reactive due to the calculation errors and needs to be normalized [24]. Further we skip this stage assuming that the matrix is diagonal and reactive:

$$\mathbf{Y}_{\text{mod}} = \begin{bmatrix} \text{j}0.2429 \cdot 10^{-5} & & \\ & \text{j}0.3270 \cdot 10^{-5} & \\ & & \text{j}0.3769 \cdot 10^{-5} \end{bmatrix} \text{ (S/km)}.$$

Fragment of output file L400_PAR_PH.LIS.

...
Capacitance matrix, in units of [farads/kmeter] for the system of equivalent phase conductors.
Rows and columns proceed in the same order as the sorted input.

```

1  9.962258E-09
2 -1.526980E-09  1.026383E-08
3 -4.467067E-10 -1.526980E-09  9.962258E-09

```

Impedance matrix, in units of [ohms/kmeter] for the system of equivalent phase conductors.
Rows and columns proceed in the same order as the sorted input.

```

1  7.161787E-02
4.594878E-01
2  4.331943E-02  7.258155E-02
1.448813E-01  4.494188E-01
3  4.185105E-02  4.331943E-02  7.161787E-02
1.082764E-01  1.448813E-01  4.594878E-01

```

Modal parameters at frequency FREQ = 5.00000000E+01 Hz

Mode	Resistance ohms/km	Reactance ohms/km	Susceptance s/km	The surge impedance in units of [ohms] real	imag	lossless	Lossless and actual velocity in [km/sec]	Attenuation nepers/km
1	1.570727E-01	7.187872E-01	2.435554E-06	5.464474E+02	-5.900984E+01	5.432519E+02	2.374383E+05	2.360498E+05
2	2.976682E-02	3.512114E-01	3.270073E-06	3.280156E+02	-1.387556E+01	3.277220E+02	2.931480E+05	2.928856E+05
3	2.846724E-02	2.958356E-01	3.778321E-06	2.801410E+02	-1.344745E+01	2.798181E+02	2.971497E+05	2.968071E+05

Eigenvector matrix [Ti] for current transformation: I-phase = [Ti]*I-mode. First the real part, row by row:

```

5.991431833176021E-01 -7.071067811865462E-01 -4.052167378310909E-01
5.310884029689407E-01 -2.670468863295909E-15  8.195113121629626E-01
5.991431833176025E-01  7.071067811865489E-01 -4.052167378310873E-01

```

Finally, the imaginary part, row by row:

```

0.000000000000000E+00 0.000000000000000E+00 0.000000000000000E+00
0.000000000000000E+00 0.000000000000000E+00 0.000000000000000E+00
0.000000000000000E+00 0.000000000000000E+00 0.000000000000000E+00

```

The modal impedance matrix can be calculated using the eigenvalue matrix \mathbf{V} and the relation $\mathbf{V} = \mathbf{Z}_{\text{mod}} \mathbf{Y}_{\text{mod}}$:

$Z_{k \text{ mod}} = \frac{\lambda_k}{Y_{k \text{ mod}}}$ where subscript k indicates the mode number λ_k is the k -th element of the matrix \mathbf{V} . Thus we get:

$$\mathbf{Z}_{\text{mod}} = \begin{bmatrix} 0.1575 + j0.7206 & & \\ & 0.0298 + j0.3512 & \\ & & 0.0285 + j0.2966 \end{bmatrix} (\Omega/\text{km}).$$

The modal wave impedance (4.10) is:

$$Z_{fk \text{ mod}} = \sqrt{\frac{Z_{k \text{ mod}}}{Y_{k \text{ mod}}}} \text{ and further:}$$

$$\mathbf{Z}_{f \text{ mod}} = \begin{bmatrix} 547.83 - j59.16 & & \\ & 328.02 - j13.88 & \\ & & 280.85 - j13.48 \end{bmatrix} (\Omega).$$

The matrix $\mathbf{Z}_{f \text{ mod}}$ elements should be real since they are physical parameters of the actual line. so their imaginary parts can be neglected as coming from the calculation errors. [24].

Now the wave impedance matrix in phase coordinates can be determined using (4.77):

$$\mathbf{Z}_f = \mathbf{T}_u \mathbf{Z}_{f \text{ mod}} \mathbf{T}_i^{-1} = \begin{bmatrix} 387.58 & 92.56 & 59.56 \\ 92.56 & 381.55 & 92.55 \\ 59.56 & 92.55 & 387.58 \end{bmatrix} (\Omega)$$

The eigenvalue matrix \mathbf{T} can be calculated using algorithms available in many software packages [66]. The eigenvalue matrices are always real for transposed lines and the relations (4.69) (4.70) hold. Then one of the known from the three-phase circuit theory transformations can be applied for the purpose.

In Clarke transformation⁴ (also known as $0\alpha\beta$ transformation) the following matrices are applied [19]:

$$\mathbf{T} = \frac{1}{2} \begin{bmatrix} 2 & 2 & 0 \\ 2 & -1 & \sqrt{3} \\ 2 & -1 & -\sqrt{3} \end{bmatrix} \quad \mathbf{T}^{-1} = \frac{1}{3} \begin{bmatrix} 1 & 1 & 1 \\ 2 & -1 & -1 \\ 0 & \sqrt{3} & -\sqrt{3} \end{bmatrix} \quad (4.78)$$

which after normalization to (4.69) yield the following transformation pair:

⁴ Edith Clarke (1883–1959).

$$\mathbf{T} = \frac{1}{\sqrt{3}} \begin{bmatrix} 1 & \sqrt{2} & 0 \\ 1 & \frac{-1}{\sqrt{2}} & \frac{\sqrt{3}}{\sqrt{2}} \\ 1 & \frac{-1}{\sqrt{2}} & \frac{-\sqrt{3}}{\sqrt{2}} \end{bmatrix} \quad \mathbf{T}^{-1} = \frac{1}{\sqrt{3}} \begin{bmatrix} 1 & 1 & 1 \\ \sqrt{2} & \frac{-1}{\sqrt{2}} & \frac{-1}{\sqrt{2}} \\ 0 & \frac{\sqrt{3}}{\sqrt{2}} & \frac{-\sqrt{3}}{\sqrt{2}} \end{bmatrix} \quad (4.79)$$

The parameters of line models derived for $(0\alpha\beta)$ modal coordinates and for symmetrical components are the same. If, for instance, matrices (4.79) are used for transformation of transposed line resistance matrix then the result according to (4.77) and (4.69) is:

$$\mathbf{R}_{0\alpha\beta} = \begin{bmatrix} R_0 & & \\ & R_1 & \\ & & R_1 \end{bmatrix} = \mathbf{T}^{-1} \begin{bmatrix} R_S & R_M & R_M \\ R_M & R_S & R_M \\ R_M & R_M & R_S \end{bmatrix} \mathbf{T} \quad (4.80)$$

and similarly for the other parameters. Moreover the components $\alpha\beta$ are orthogonal in steady state. The $\alpha\beta$ coordinates make the base for definition of the space vector [76]:

$$\underline{f}_s = f_\alpha + j f_\beta = \sqrt{\frac{3}{2}} (\underline{f}_1 + \underline{f}_2^*) \quad (4.81)$$

which relates the modal coordinates (via (4.79)) with the phase ones (ABC):

$$\begin{bmatrix} f_0 \\ f_\alpha \\ f_\beta \end{bmatrix} = \mathbf{T}^{-1} \begin{bmatrix} f_A \\ f_B \\ f_C \end{bmatrix}$$

and also with the symmetrical components: positive- \underline{f}_1 i and negative - \underline{f}_2 ; superscript * denotes the complex conjugate function.

The space vector plays an important role in analysis of three-phase AC circuits [24, 76].

b) Frequency-dependent Line Model

There are many algorithms applied to modelling of multiphase circuits with frequency dependent distributed parameters.

All of them employ of two basic methods of transients representation in the long line:

- calculation of transients by use of the Bergeron's model (see sect. 1.3.7 that refers to the lossless line),

- application of the line model in frequency domain and return to the time domain by use of the inverse Fourier transform.

In case of multiphase line the mutual coupling between particular phases have to be taken into account. To solve this problem one of the following techniques is used:

1. By diagonalization of the multiphase line parameters the line model splits into many uncoupled single line modal models (the aforementioned approach).
2. The line model is derived for phase coordinates with full parameter matrices under assumption that the line is untransposed [3 24 58 87].

Below the approach to frequency dependent model of the multiphase line setup as used in ATP–EMTP is discussed. Application of this approach to a single-phase line is shown sect. 4.1.2.

The multi-phase line model is as shown in Fig. 4.18) and the constant resistances in particular models for modal coordinates are replaced by filters of frequency responses $Z_f(j\omega)$ and $A(j\omega)$ – like in (4.20) and (4.21) – which are represented by in series connected linear RC cells of transmittances $Z_f(s)$ and $A(s)$ respectively.

The models for particular modal components are as shown in Fig. 4.10. The following example shows how the line parameters are calculated.

Example 4.8. Calculate phase and modal parameters of the line in Example 4.1 Assume that the line is untransposed and the line parameters are frequency dependent. Use the JMARTI SETUP procedure available in ATP–EMTP [3].

Model of the frequency dependent long line offered by ATP–EMTP is known as JMARTI [24 58]. The input data for the model are calculated by MARTI SETUP support along with LINE CONSTANTS procedure (Example 4.7) which calculates the basic line parameters. The respective input file is shown below.

```
BEGIN NEW DATA CASE
JMARTI SETUP 1.0           {Note use of PDT0 = 1 to allow reduction of order
$ERASE
C Line 400 kV
BRANCH  PA    KA    PB    KB    PC    KC
LINE CONSTANTS
METRIC
C   Data for LINE CONSTANTS
C 34567890123456789012345678901234567890123456789012345678901234567890
1 .231 .0564 4          3.15 -10.3 24.5 12.0 40.0 0.0 2
2 .231 .0564 4          3.15  0.0 24.5 12.0 40.0 0.0 2
3 .231 .0564 4          3.15 10.3 24.5 12.0 40.0 0.0 2
0 0.5 .2388 4          1.565 -6.87 31.0 23.5
0 0.5 .2388 4          1.565  6.87 31.0 23.5
BLANK CARD ENDING CONDUCTOR CARDS OF "LINE CONSTANTS" CASE
C      1      2      3      4      5      6      7      8
C 34567890123456789012345678901234567890123456789012345678901234567890
C      >> Freq  >> FCar  > <ICPR> <IZPR> =< DIST > <PP>==< >< ><>>
```

```

100.0    5000.0                                180.0    1          1
100.0      50.0                                180.0    1          1
100.0      .01                                 180.0    1    3    4    1
BLANK CARD ENDING FREQUENCY CARDS
BLANK CARD ENDING "LINE CONSTANTS"
DEFAULT
$PUNCH
BLANK card ending JMARTI SETUP data cases
BEGIN NEW DATA CASE
BLANK

```

The file is very much alike to that in Example 4.7. The notable differences are:

- Template JMARTI SETUP indicates the procedure type.
- Declaration of nodes for both sides of the line (BRANCH).
- Declaration of frequencies (5000, 50 and 0.01 Hz) for which the frequency response is to be calculated.
- The numbers 3 (col. 62) and 4 (col. 65) in the last line. The former indicates that the frequency response is to be limited to 3 decades on the logarithmic frequency scale and the latter means that the frequency response will be approximated in 4 points within each decade (the numbers should be much greater, say 9, 10; here the small values are used to reduce the output file size).
- Line: \$PUNCH means request for the output file *.PCH printout.

The output file obtained is as below:

```

-1 PA    KA                                2.  1.00                                -2 3
    9                                7.3615544019279970000E+02
    5.16160970375891200E+03    -4.62836678876982000E+03    2.34908920073601300E+02
    2.21428884708777900E+02    4.37807446832278400E+02    3.04928174781558700E+02
    2.24591087014093900E+02    4.55263702130293400E+02    1.02771805987124600E+03
    2.54324867047940400E-01    2.58267247958202700E-01    4.75266615734256900E-01
    7.43821799922729000E-01    1.32805685385736000E+00    1.97949231121861500E+00
    2.90622851912841100E+00    6.69971775060332200E+00    1.50030074511141000E+01
    1                                1.0175027775544130000E-03
    4.96285426218186400E+02
    4.96823791675659200E+02
-2 PB    KB                                2.  1.00                                -2 3
    9                                3.4134523824302410000E+02
    5.30870510194876300E+02    2.02556181590067800E+01    2.68086180404834000E+02
    3.50337060561525300E+02    6.29292421363313800E+02    4.27034282349728200E+02
    2.48049348808883800E+03    -1.24353670385984700E+03    3.20930281998335600E+02
    1.97752951677736800E-01    2.77134426872770100E-01    5.53515928524456700E-01
    1.06867294826728000E+00    2.21360731622174100E+00    3.74655773786376000E+00
    8.95197627537033100E+00    9.97585888710791700E+00    1.65795393675722400E+01
    1                                6.2796878107565830000E-04
    4.68508344800458900E+02
    4.69023674409433600E+02
-3 PC    KC                                2.  1.00                                -2 3
    12                                2.9404800772668510000E+02
    4.05546694218969000E+02    5.42993557914113500E+01    -1.04056571557813800E+02

```

```

1.28675981115441400E+02  3.02482667071249200E+02  3.59727123238581600E+02
3.84565069398721800E+02  7.79608344392276500E+02  2.12278761695224800E+03
-1.19401802383945500E+03  1.92613893168671900E+02  2.99694164961513600E+02
1.75763316432903900E-01  2.65010489469351300E-01  2.77287520425178000E-01
2.19898614965812600E-01  5.56134028988414100E-01  1.08558003958717100E+00
2.02757957168211700E+00  4.44555679851210300E+00  9.65825030962793800E+00
1.10764943326363400E+01  1.13569798059043500E+01  1.81281850219694700E+01
1 6.2206229083791410000E-04
4.22175997238486200E+02
4.22644824279796200E+02
0.58407538 -0.70710678 -0.41958805
0.00000000 0.00000000 0.00000000
0.56365939 0.00000000 0.80491722
0.00000000 0.00000000 0.00000000
0.58407538 0.70710678 -0.41958805
0.00000000 0.00000000 0.00000000

```

The file comprises of three parts which refer to the modal components of the line model and are numbered -1 ... -2 ... -3 ... respectively.

In the subsequent line in each part the order of $Z_f(s)$ transmittance (9 for the first and the second mode and 12 for the third one) and the limit value of the respective impedance for infinite frequency is printed.

The subsequent three lines show zeroes of the approximating function (9 in total) and in the next three lines the poles of that function are shown.

Further the information about parameters of $A(s)$ transmittance which approximates the propagation function for the first mode is shown including the order of the transmittance (1 in this case) and the wave propagation time for infinite frequency.

The next 2 lines show zeroes and poles of $A(s)$ respectively (in this case it is the first order function).

In the last part of the output file the eigenvector matrix \mathbf{T}_i is printed.

The essential simplification of the line model discussed in the example shown is that the transformation between phase and modal coordinates is assumed to be frequency independent. In fact if the line parameters depend upon frequency then the eigenvector matrix $\mathbf{T}_i = \mathbf{T}_i(\omega)$ becomes frequency dependent too (4.74). This dependence is particularly strong for cable feeder models [62]. The solution to the problem is based on representation of the eigenvector matrix elements by respective transmittances as it is applied in case of wave impedance and propagation function. Such approximation is possible after normalization of the diagonalization matrix. [62].

The most adequate is the model based on direct solution of (4.72). In application to multi-phase line the equations yield:

$$\begin{aligned} \mathbf{U}_1(j\omega) &= \mathbf{Z}_f(j\omega)\mathbf{I}_1(j\omega) + \mathbf{A}(j\omega)(\mathbf{Z}_f\mathbf{I}_2(j\omega) + \mathbf{U}_2(j\omega)) \\ \mathbf{I}_1(j\omega) &= \mathbf{Z}_f^{-1}(j\omega)\mathbf{U}_1(j\omega) - \mathbf{A}(j\omega)(\mathbf{Z}_f^{-1}\mathbf{U}_2(j\omega) + \mathbf{I}_2(j\omega)) \end{aligned} \quad (4.82)$$

where by analogy to (4.19): $\mathbf{A}(j\omega) = e^{-\sqrt{\mathbf{Y}'\mathbf{Z}'}l}$ and the wave impedance matrix (4.10) is:

$$\mathbf{Z}_f(j\omega) = \sqrt{\mathbf{Z}'(\mathbf{Y}')^{-1}}.$$

The subscripts 1, 2 refer to the respective line ends.

The parameters of the frequency model obtained (matrices $\mathbf{Z}_f(j\omega)$ and $\mathbf{A}(j\omega)$) must be determined for the specified frequencies so that they can be approximated in the considered frequency range [71]. The model excitation functions (input – output) should be transformed into frequency domain [72].

Exercises

- 4.1. Check that the equivalent long line Π circuit shown in Fig 4.3 and the equations (4.16) correspond to the line model described by equations (4.15).
- 4.2. In Example 4.3 the 400 kV line is analysed for the fortieth harmonic (at fundamental 50 Hz) for which the respective wavelength is $\lambda_1 = 147.776$ km. Determine the steady state output current for the metallic short-circuit at the end of the line if the positive sequence line input voltage is:

$$u_1(t) = \sqrt{\frac{2}{3}} 400 \cos(40\omega_1 t) \text{ kV}.$$

Repeat calculations for two values of the line length: a) $l = \lambda_1$ b) $l = 0.75 \lambda_1$.

Hint: Write the input voltage as a phasor and use (4.15) assuming that the output voltage is equal to zero. Note that voltage U_1 waveform in Fig. 4.4 shows the envelope of the steady state AC voltage.

- 4.3. In three-phase transposed line models the parameter matrices comprise of two different elements – those located in the matrix diagonal and those located aside. The matrices can be transformed in many different ways including the symmetrical component transformation. In practice only the matrices with real elements are used, like (4.79), or the Karrenbauer's transformation [29, 78]:

$$\mathbf{T} = \begin{bmatrix} 1 & 1 & 1 \\ 1 & -2 & 1 \\ 1 & 1 & -2 \end{bmatrix} \quad \mathbf{T}^{-1} = \frac{1}{3} \begin{bmatrix} 1 & 1 & 1 \\ 1 & -1 & 0 \\ 1 & 0 & -1 \end{bmatrix}.$$

Check that in all cases the obtained diagonal matrices for modal components are the same.

5. TRANSFORMER MODEL

5.1. Introduction

The transformer is a device in which the electric power is conveyed between two electric circuits by means of magnetic induction. The magnetic circuit of the transformer comprises the ferromagnetic core with nonlinear characteristic of magnetic induction B versus inducing magnetic field H , whose characteristic feature is the hysteresis loop. In such a circuit, aside of losses related to heat dissipation in windings resistance, the magnetic losses caused by the core hysteresis loop (magnetization of the transformer core) and the losses due to eddy currents which heat the transformer core are observed.

The electric and magnetic circuits of power transformers may have various designs depending on purpose which the transformer unit is applied for. Thus we have: the single phase transformers (usually used as measuring CTs and VTs or the auxiliary transformers) and three-phase two- and multi-winding ones. The windings in three phase transformers can be connected in Δ or Y arrangement so that many various groups of connections are possible.

The windings at both sides of the transformer can be separated or connected – the latter arrangement is characteristic for autotransformers.

Making the transformer model the frequency range in which the transformer works must be taken into account. From this point of view the low and the high frequency models are considered. For the latter the turn-to turn and turn-to ground capacitances as well as the frequency dependence of the transformer parameters (the skin effect) must be taken into account when formulating the model equations.

Another classification is related to the structure of the transformer models. Here the two approaches are applied. In the first one the windings create the ideal transformer in required connection arrangement and the magnetizing branch is connected to one of the windings. In the second the transformer model is represented as multi- terminal circuit.

In this Chapter the various aspects of power transformers computer modelling are presented.

5.2. Single-phase Transformer

5.2.1. Equivalent Scheme

The basic diagram of the single phase two-winding transformer is shown in Fig 5.1 where the main magnetic flux ϕ_M along with the stray fluxes ϕ_1 and ϕ_2 related to transformer windings of turn numbers N_1 and N_2 , respectively, are marked. The fluxes induced by the currents in the windings (i_1 , i_2) have the same direction so they add since the winding direction is also the same. The beginnings of the respective windings are marked with asterisks. In this respect the common rule is applied: if the current flows towards the asterisk in one of the winding then it must flow out of the asterisk in the second one (Fig. 5.1).

Let's recall the basic equations of the transformer equations.

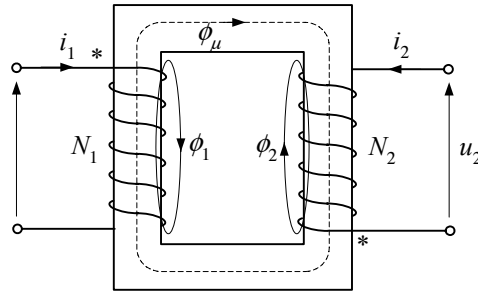


Fig. 5.1. The single phase two-winding transformer

The voltages at both sides of the ideal transformer for which the stray fluxes and winding resistances are neglected, i.e.: $\phi_1 = \phi_2 = 0$ and $R_1 = R_2 = 0$, are described by the following equations:

$$u_1(t) = N_1 \frac{d\phi_\mu(t)}{dt}, \quad u_2(t) = N_2 \frac{d\phi_\mu(t)}{dt} \quad (5.1)$$

from which the transformer turn ratio is obtained and: $\frac{u_1}{u_2} = \frac{N_1}{N_2} = \vartheta$

The magnetic force related to the winding currents is given by [8]:

$$F = N_1 i_1 + N_2 i_2 = R_m \phi_\mu \quad (5.2)$$

where R_m is the reluctance of the magnetic circuit. In an ideal transformer the reluctance is infinite due to the infinite value of magnetic permeability assumed. In such case we have:

$$\frac{-i_2}{i_1} = \frac{N_1}{N_2} = \vartheta \quad (5.3)$$

and this means that in the ideal transformer the current and voltage transformations remain in inversely proportional relation.

If the winding resistances and the stray fluxes are taken into account the transformer terminal voltage equations are:

$$\begin{aligned} u_1(t) &= R_1 i_1(t) + \frac{d\psi_{1M}(t)}{dt} \\ u_2(t) &= R_2 i_2(t) + \frac{d\psi_{2M}(t)}{dt} \end{aligned} \quad (5.4)$$

where: $\psi_{1M} = \psi_M + \psi_1 = N_1(\phi_M + \phi_1)$ – for electromagnetic flux (Wb) coupled with the first winding and, similarly: $\psi_{2M} = \psi_M + \psi_2 = N_2(\phi_M + \phi_2)$ for the second one.

Moreover, noting that:

$$\psi = Li \quad (5.5)$$

L – inductance (H), and splitting in (5.4) terms related to the main and mutual flux ϕ_M we get:

$$\begin{aligned} u_1(t) &= R_1 i_1(t) + L_1 \frac{di_1(t)}{dt} + N_1 \frac{d\phi_M(t)}{dt} \\ u_2(t) &= R_2 i_2(t) + L_2 \frac{di_2(t)}{dt} + N_2 \frac{d\phi_M(t)}{dt} \end{aligned} \quad (5.6)$$

After further manipulations we get finally:

$$u_1(t) = R_1 i_1(t) + L_1 \frac{di_1(t)}{dt} + \vartheta u_2(t) - \vartheta^2 R_2 \frac{i_2(t)}{\vartheta} - \vartheta^2 L_2 \frac{d}{dt} \left(\frac{i_2(t)}{\vartheta} \right) \quad (5.7)$$

The equation (5.7) can also be written in the following form:

$$u_1(t) = R_1 i_1(t) + L_1 \frac{di_1(t)}{dt} + u'_2(t) - R'_2 i'_2(t) - L'_2 \frac{di'_2(t)}{dt} \quad (5.8)$$

where:

$$u'_2(t) = \vartheta u_2(t), \quad i'_2(t) = \frac{i_2(t)}{\vartheta}, \quad R'_2 = \vartheta^2 R_2, \quad L'_2 = \vartheta^2 L_2 \quad (5.9)$$

are the quantities and parameters at the secondary side of the transformer ‘seen’ from the primary side. The equivalent transformer circuit corresponding to (5.8) is shown in Fig. 5.2a while the circuit in Fig. 5.2b corresponds to (5.7).

In the next step towards the real transformer model formulation the reluctance in (5.2) is assumed to be finite and greater than zero: $R_m > 0$ (magnetic permeability is finite). In such case:

$$i_1 = \frac{R_m \phi_\mu}{N_1} - \frac{1}{\vartheta} i_2 = i_\mu - \frac{1}{\vartheta} i_2 \quad (5.10)$$

where: $i_\mu = \frac{R_m \phi_\mu}{N_1}$ is the magnetizing current inducing the flux in the transformer core.

The magnetizing current is related to voltage via flux (5.4) i.e.:

$$u_\mu(t) = N_1 \frac{d\phi_\mu(t)}{dt} = L_\mu \frac{di_\mu(t)}{dt} \quad (5.11)$$

where: $L_\mu = \frac{N_1^2}{R_m}$ (compare with (5.5)).

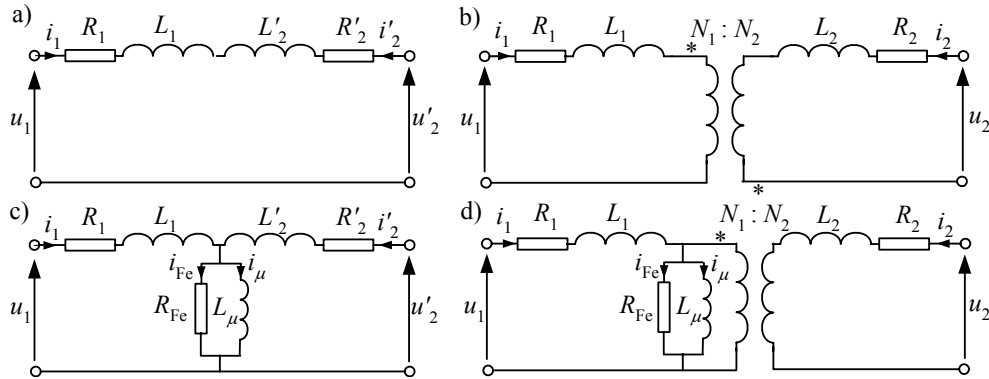


Fig. 5.2. The equivalent circuits of the single phase two-winding transformer:

a) calculated for the common voltage, b) with ideal transformer and c), d) with magnetizing branch

The eddy currents and the hysteresis losses are represented by the resistance R_{Fe} . (Fig. 5.2c and 5.2d).

5.2.2. Two-winding Transformer

a) The Equivalent Circuit

The equivalent diagram of the transformer considered (Fig 5.2) can be represented as the two-port circuit. Neglecting the resistance R_{Fe} the following relation between currents and voltages at the transformer terminals is valid (Fig. 5.2d):

$$\mathbf{u}(t) = \mathbf{R}\mathbf{i}(t) + \mathbf{L} \frac{d}{dt} \mathbf{i}(t) \quad (5.12)$$

where:

$$\mathbf{u}(t) = \begin{bmatrix} u_1(t) \\ u_2(t) \end{bmatrix}, \quad \mathbf{i}(t) = \begin{bmatrix} i_1(t) \\ i_2(t) \end{bmatrix}, \quad \mathbf{R} = \begin{bmatrix} R_1 & \\ & R_2 / \vartheta^2 \end{bmatrix}, \quad \mathbf{L} = \begin{bmatrix} L_1 + L_\mu & L_\mu / \vartheta \\ L_\mu / \vartheta & (L_2 + L_\mu) / \vartheta^2 \end{bmatrix}.$$

The respective digital model can be obtained by analogy to a single RL branch. Solving (5.12) for the derivative of current vector we get the equation:

$$\frac{d}{dt} \mathbf{i}(t) = \mathbf{L}^{-1} \mathbf{u}(t) - \mathbf{L}^{-1} \mathbf{R} \mathbf{i}(t) \quad (5.13)$$

which can be represented by use of one of the known digital models.

In some cases problems with determination of matrix \mathbf{L}^{-1} may appear since the inductance of magnetizing branch is much greater than the stray inductance of transformer windings: $L_\mu \gg L_1, L_2$ and, for $\vartheta=1$, all matrix \mathbf{L} elements are nearly identical. Thus very high accuracy of those parameters is required.

Matrix \mathbf{L} becomes singular if the magnetizing current is neglected (or is negligibly small - $L_\mu = \infty$) In order to avoid numerical problems the inverse matrix \mathbf{L}^{-1} ⁵ for nodes 1 and 2 can be determined directly, by analogy to the admittance matrix in nodal method [11, 24]:

$$\mathbf{L}^{-1} = \frac{1}{L_1 L_2 + (L_1 + L_2) L_\mu} \begin{bmatrix} L_2 + L_\mu & -\vartheta L_\mu \\ -\vartheta L_\mu & \vartheta^2 (L_1 + L_\mu) \end{bmatrix} \quad (5.14)$$

To relate the transformer parameters with the transformer 'plate data' solution of (5.12) for fundamental frequency in steady state is used:

$$\underline{\mathbf{U}} = \underline{\mathbf{Z}} \underline{\mathbf{I}} \quad (5.15)$$

⁵ In ATP-EMTP it is called AR notation in distinction to RL notation which refers to the inductance representation like in (5.12) [11, 24].

where: $\underline{\mathbf{U}} = \begin{bmatrix} U_1 \\ U_2 \end{bmatrix}$, $\underline{\mathbf{I}} = \begin{bmatrix} I_1 \\ I_2 \end{bmatrix}$, $\underline{\mathbf{Z}} = \begin{bmatrix} Z_{11} & Z_{12} \\ Z_{21} & Z_{22} \end{bmatrix} = \mathbf{R} + j\omega\mathbf{L}$,

or, in admittance form:

$$\underline{\mathbf{Y}}\underline{\mathbf{U}} = \underline{\mathbf{I}} \quad (5.16)$$

where: $\underline{\mathbf{Y}} = \underline{\mathbf{Z}}^{-1}$.

Due to the problems of inverse matrix \mathbf{L} calculation for coupled RL circuits which are encountered in computer programs the circuit parameters are represented by matrices \mathbf{R} and \mathbf{L}^{-1} instead of impedance and admittance ones. In such case only reactance (susceptance) appears in (5.15) and (5.16) and the resistance is processed separately. (The simplification is justified if the resistance is much smaller than the reactance) [24]. Neglecting resistance in (5.16) we get:

$$-j\mathbf{B}\underline{\mathbf{U}} = \underline{\mathbf{I}} \quad (5.17)$$

where: $\mathbf{B} = \frac{1}{\omega}\mathbf{L}^{-1} = \begin{bmatrix} B_1 + B_{12} & -B_{12} \\ -B_{12} & B_2 + B_{12} \end{bmatrix}$.

The equation is represented by the Π circuit as in Fig 5.3. with parameters ((5.14) and (5.17)):

$$B_1 = \frac{1}{\omega} \frac{L_2 + (1 - \vartheta)L_\mu}{L_1 L_2 + (L_1 + L_2)L_\mu}, \quad B_2 = \frac{1}{\omega} \frac{\vartheta^2 L_1 + (\vartheta^2 - \vartheta)L_\mu}{L_1 L_2 + (L_1 + L_2)L_\mu}, \quad B_{12} = \frac{1}{\omega} \frac{\vartheta L_\mu}{L_1 L_2 + (L_1 + L_2)L_\mu}.$$

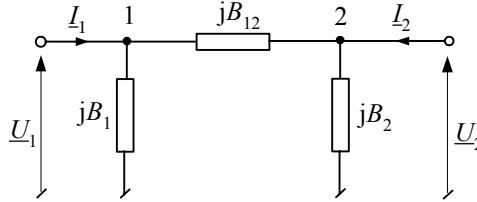


Fig. 5.3. The equivalent Π circuit of the transformer

The values of those parameters can be determined from the ‘plate data’ of the transformer:

$$R_1 = \frac{1}{2} \frac{\Delta P_{Cu} U_{r1}^2}{S_{r1}^2} \quad (\text{under assumption that } R_1 = \vartheta^2 R_2),$$

$$Z_1 = \frac{1}{2} \frac{u_k U_{r1}^2}{100 \cdot S_{r1}} = \sqrt{R_1^2 + X_1^2}, \quad X_1 = \sqrt{Z_1^2 - R_1^2} = \omega L_1 \quad (\text{under assumption that } X_1 = \vartheta^2 X_2),$$

The transverse (magnetizing) branch parameters (referred to the primary side1):

$$R_{Fe} = \frac{U_{r1}^2}{\Delta P_{Fe}}, \quad Z_p = \frac{100 \cdot U_{r1}^2}{i_0 \cdot S_{r1}}, \quad X_\mu = \frac{R_{Fe} Z_p}{\sqrt{R_{Fe}^2 - Z_p^2}} = \omega L_\mu,$$

where: S_{r1} – nominal power for the side 1, (MVA),

U_{r1} – nominal voltage –side 1, (kV),

ΔP_{Cu} – active(dissipation) losses at both sides, (kW),

ΔP_{Fe} – active losses in the core, (kW),

i_0 – the idle current, (%) referred to the nominal one.

In more general approach the two-winding transformer is represented by the five-terminal element. The fifth terminal is earth. This terminal is necessary in case of multi-winding or multiphase transformers since any winding can be connected to earth.

The extended representation of the transformer with the earth terminal is shown in Fig. 5.4. The circuit is said to have the primary form [11, 24]. The resulting conductance matrix is singular and the circuit can be solved if one of the two-terminal circuit nodes is earthed.

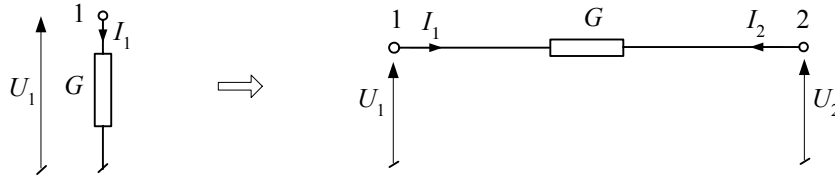


Fig. 5.4. Illustration of extended transformer representation

By analogy, (5.17) can be extended to the following form:

$$GU_1 = I_1 \quad \rightarrow \quad \begin{bmatrix} G & -G \\ -G & G \end{bmatrix} \begin{bmatrix} U_1 \\ U_2 \end{bmatrix} = \begin{bmatrix} I_1 \\ I_2 \end{bmatrix}$$

$$-j \left[\begin{array}{cc|cc} B_1 + B_{12} & -B_{12} & -B_1 - B_{12} & B_{12} \\ -B_{12} & B_2 + B_{12} & B_{12} & -B_2 - B_{12} \\ \hline -B_1 - B_{12} & B_{12} & B_1 + B_{12} & -B_{12} \\ B_{12} & -B_2 - B_{12} & -B_{12} & B_2 + B_{12} \end{array} \right] \begin{bmatrix} \underline{U}_1 \\ \underline{U}_2 \\ \underline{U}_3 \\ \underline{U}_4 \end{bmatrix} = \begin{bmatrix} \underline{I}_1 \\ \underline{I}_2 \\ \underline{I}_3 \\ \underline{I}_4 \end{bmatrix} \quad (5.18)$$

The corresponding equivalent circuit is shown in Fig. 5.5. Terminals 1–2 refer to the primary winding and 3–4 – to the secondary one. Also in this case the circuit can not be solved without additional earthing which is realized by admittances marked with dotted line. The admittance values have to be added to the respective elements located in the diagonal of the conductance matrix in (5.18). This way the winding-to-earth capacitances or other resistive earthing can be included into the transformer model [6].

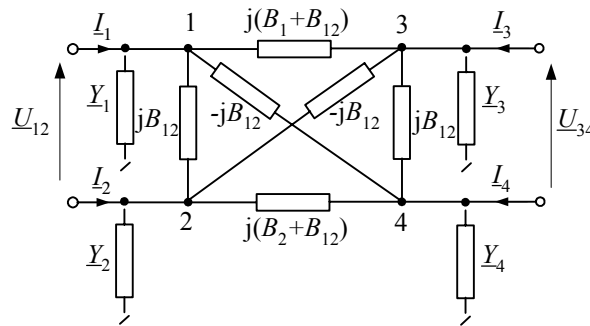


Fig 5.5. 5-terminal equivalent circuit of the two winding transformer

The resistance representing the losses in the core is not included into the transformer model discussed. Also, the magnetizing inductance is usually neglected ($L_\mu = \infty$) and the transverse branches of the circuit in Fig. 5.2 are connected to one of the two sides of the circuit in Fig. 5.5. In ATP–EMTP the discussed transformer model is realized by BCTRAN procedure [7].

b) Structural Model

In another approach to the transformer model setup the circuit in Fig. 5.2d is split into two equal parts as shown in Fig. 5.6.

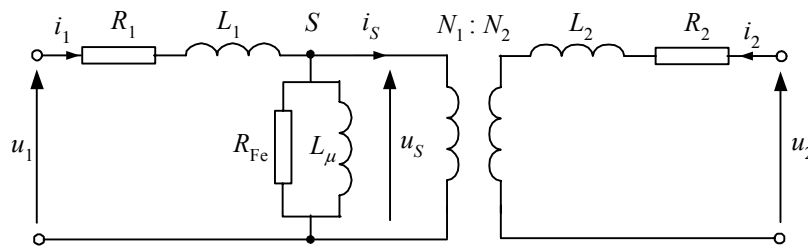


Fig. 5.6. The equivalent circuit of the structural transformer model

The first part which includes the transverse (magnetizing) branch is represented by the Γ -type circuit described by the equation:

$$\frac{d}{dt} \begin{bmatrix} i_1(t) \\ i_s(t) \end{bmatrix} = \begin{bmatrix} \frac{1}{R_1} & \frac{-1}{R_1} \\ \frac{1}{R_1} & -\frac{R_1 + R_{Fe}}{R_1 R_{Fe}} \end{bmatrix} \begin{bmatrix} u_1(t) \\ u_s(t) \end{bmatrix} - \begin{bmatrix} \frac{1}{L_1} & \frac{-1}{L_1} \\ \frac{1}{L_1} & -\frac{L_1 + L_\mu}{L_1 L_\mu} \end{bmatrix} \begin{bmatrix} i_1(t) \\ i_s(t) \end{bmatrix} \quad (5.19)$$

while the equation of the second one with connected ideal transformer is [24]:

$$\frac{d}{dt} \begin{bmatrix} i_s(t) \\ i_2(t) \end{bmatrix} = \frac{1}{L_2} \begin{bmatrix} \frac{1}{\vartheta^2} & \frac{-1}{\vartheta} \\ \frac{-1}{\vartheta} & 1 \end{bmatrix} \begin{bmatrix} u_s(t) \\ u_2(t) \end{bmatrix} - \begin{bmatrix} \frac{R_2}{L_2} & 0 \\ 0 & \frac{R_2}{L_2} \end{bmatrix} \begin{bmatrix} i_s(t) \\ i_2(t) \end{bmatrix} \quad (5.20)$$

The resistance R_{Fe} is included into the model.

The presented approach can easily be extended for the multi-winding transformer model in which (5.19) refers to the primary side (High Side) while the particular secondary (Low Side) windings are represented by (5.20). In the model the additional node S appears (Fig. 5.6).

The discussed equations describe linear and continuous transformer model. The digital model can be obtained using one of the derivative numerical approximation methods. The following example illustrates the transformer parameters calculation.

Example 5.1. A three phase transformer 400/15.75 kV comprises of the three single phase units. Determine the digital model of the single phase unit and simulate the short-circuit at the HS

Parameters of the three phase transformer:

Nominal power $S_r = 250$ MVA, the short-circuit voltage $u_k = 12\%$, the active losses $\Delta P_{Cu} = 500$ kW, losses in the core $\Delta P_{Fe} = 240$ kW, the idle current $i_0 = 0.7\%$, nominal turn ratio of the single unit $\vartheta_r = 400/\sqrt{3}/15.75$ kV/kV.

We assume that the magnetizing branch is connected the HS winding. and the transformer parameters have to be determined for both HS and LS. The HS parameters can be calculated from the following equations:

$$R_H = \frac{1}{2} \frac{\Delta P_{Cu} U_{rH}^2}{(S_r/3)^2} = \frac{1}{2} \frac{0.5 \cdot (400/\sqrt{3})^2}{(250/3)^2} = 1.92 \, \Omega,$$

$$Z_H = \frac{1}{2} \frac{u_k U_{rH}^2}{100 \cdot S_r/3} = \frac{1}{2} \frac{12 \cdot (400/\sqrt{3})^2}{100 \cdot 250/3} = 38.4 \, \Omega,$$

$$X_H = \sqrt{Z_H^2 - R_H^2} = \sqrt{38.4^2 - 1.92^2} = 38.35 \Omega.$$

The coefficients $\frac{1}{2}$ indicate that the longitudinal transformer parameters are divided into two equal parts for both sides of the transformer. The same parameters as ‘seen’ from the LS are:

$$R_L = R_H / \vartheta^2 = 0.0089 \Omega,$$

$$X_L = X_H / \vartheta^2 = 0.178 \Omega.$$

The transverse (magnetizing) branch parameters at the HS:

$$R_{Fe} = \frac{U_{rH}^2}{\Delta P_{Fe}} = \frac{(400/\sqrt{3})^2}{0.24} = 222.2 \text{ k}\Omega,$$

$$Z_p = \frac{100 \cdot U_{rH}^2}{i_0 \cdot S_r / 3} = \frac{100(400/\sqrt{3})^2}{0.7 \cdot 250 / 3} = 91.43 \text{ k}\Omega,$$

$$X_\mu = \frac{R_{Fe} Z_p}{\sqrt{R_{Fe}^2 - Z_p^2}} = 100.3 \text{ k}\Omega.$$

To simulate the short-circuit let's assume that the supply source of source impedance $Z_S = 0.008 + j0.069 \Omega$ is connected to the LS of the transformer and short-circuit via resistance $R_F = 0.5 \Omega$ is incepted at the HS. In normal operating conditions the transformer is loaded by impedance $Z_o = 610 + j450 \Omega$ (Fig. 5.7).

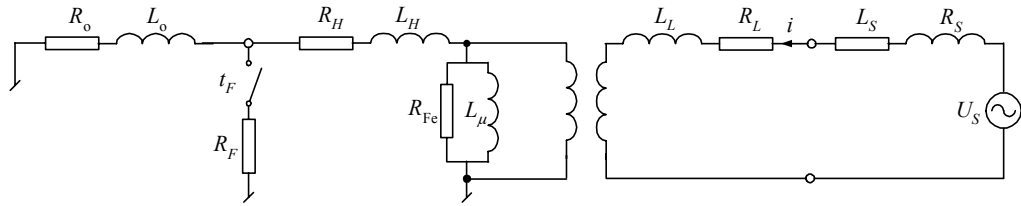


Fig. 5.7. The analysed circuit diagram

The short-circuit current waveform at the LS of the transformer is shown in Fig. 5.8. The short-circuit occurs at the time instant $t_F = 25$ ms when the instantaneous value of the supply voltage is equal to zero. In such case the large decaying DC. component appears in the short-circuit current.

The circuit modelled by use of ATPDraw program is shown in Fig. 5.9. The linear transformer model is applied for which inductance L_μ is determined by only one point on the linear magnetizing characteristic $\psi - i_\mu$: $\psi = 15971$ Vs, $i_\mu = 1$ A (another point is located at the origin 0,0). The absolute values of that point coordinates are not essentially important - the important thing is that the value of the inductance L_μ (5.5) obtained satisfies the relation:

$$X_\mu = \omega L_\mu.$$

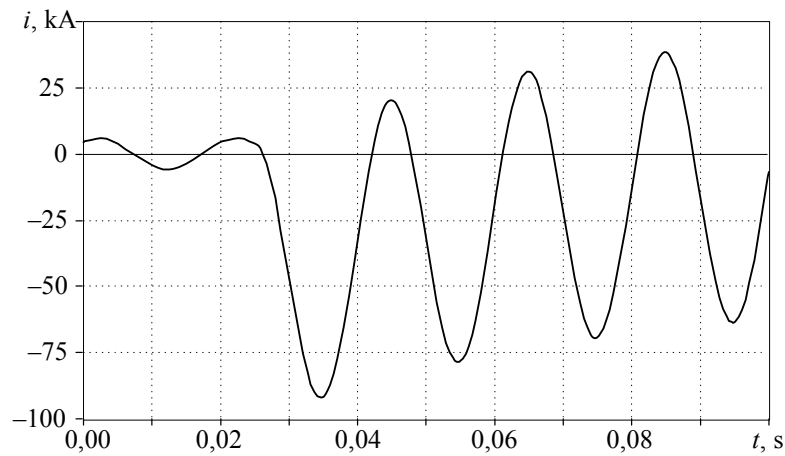


Fig. 5.8. The current waveform at the LS of the transformer

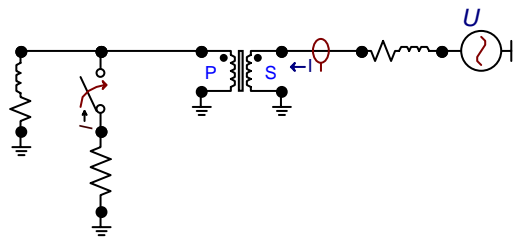


Fig. 5.9. ATPDraw diagram of the circuit model

The magnetizing branch in ATP-EMTP model is always connected to the primary (HS) side of the transformer (P in Fig. 5.9).

5.2.3. Three-winding Transformer

The three winding transformer circuit is usually presented as it is shown in Fig. 5.10. The magnetizing branch model can be assigned to any of the three transformer windings. All windings are magnetically coupled by the transformer core.

The subscript digits in Fig. 5.10 refer to the winding numbers. (P, S, T (*tertiary*) or H, L, M (*medium*) notations are also used).

Parameters of the equivalent circuit are determined experimentally from idle run and from short-circuit tests of the transformer. Power and highest winding voltage are usually the base values.

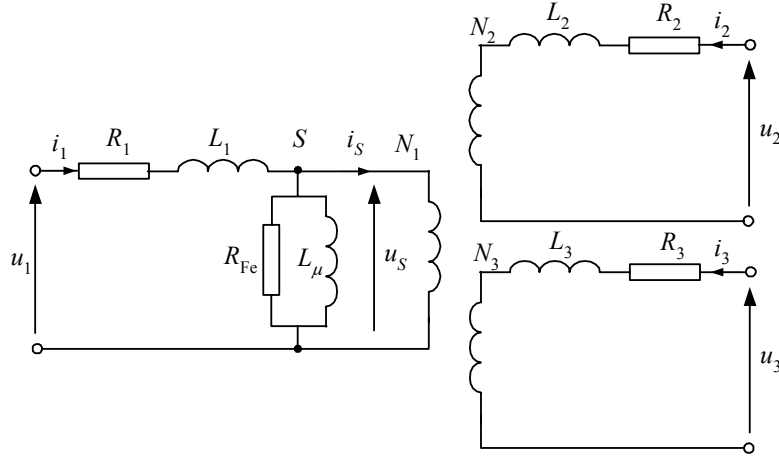


Fig. 5.10. The equivalent circuit diagram of the three winding transformer

The equivalent transformer circuit for longitudinal parameters is shown in Fig. 5.11a. The respective impedances are determined from the equations

$$Z_{HL} = \frac{u_{KHL} U_{rH}^2}{100 \cdot S_r}, \quad Z_{HT} = \frac{u_{KHT} U_{rH}^2}{100 \cdot S_r}, \quad Z_{LL} = \frac{u_{KLT} U_{rL}^2}{100 \cdot S_r}, \quad (5.21)$$

where: u_{KHL} , u_{KHT} , u_{KLT} are the respective short-circuit voltages (%); U_{rH} , U_{rL} , U_{rT} are the nominal voltages across the respective windings (kV); S_r is the base nominal power (MVA) (usually at the HS).

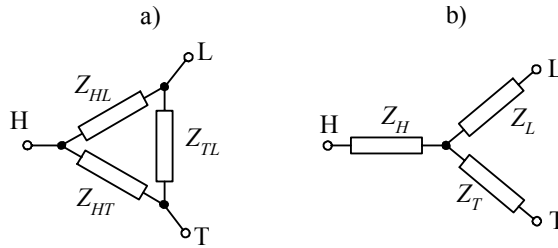


Fig. 5.11. The equivalent circuit of the three winding transformer a) in Δ arrangement and b) in Y arrangement

Similarly, knowing the power dissipated in the transformer windings their resistances can be calculated from the equations:

$$R_{HL} = \frac{\Delta P_{CuHL} U_{rH}^2}{S_r^2}, \quad R_{HT} = \frac{\Delta P_{CuHT} U_{rH}^2}{S_r^2}, \quad R_{LT} = \frac{\Delta P_{CuLT} U_{rL}^2}{S_r^2} \quad (5.22)$$

Using (5.21) and (5.22) the reactance of the respective windings can be determined. Note that Z_{LT} and R_{LT} refer to the low side (LS) voltage. The respective HS values can be obtained from:

$$Z_{HT} = \vartheta^2 Z_{LT} \quad (5.23)$$

and in the same way for resistances.

The parameters of the circuit in Fig. 5.10 can be determined by transformation of the diagram in Fig. 5.11a into Y arrangement (Fig. 5.11b):

$$\begin{aligned} Z_H &= 0,5(Z_{HL} + Z_{HT} - Z'_{LT}) \\ Z_L &= 0,5(Z_{HL} + Z'_{LT} - Z'_{HT}) \\ Z_T &= 0,5(Z_{HT} + Z'_{LT} - Z'_{HL}) \end{aligned} \quad (5.24)$$

and all impedance values refer to the HS.

The transverse (magnetizing) branch parameters are determined like for the two-winding transformer from the transformer idle run test results:

$$R_{Fe} = \frac{U_{rH}^2}{\Delta P_{Fe}}, \quad Z_p = \frac{100 \cdot U_{rH}^2}{i_0 \cdot S_r}, \quad X_\mu = \frac{R_{Fe} Z_p}{\sqrt{R_{Fe}^2 - Z_p^2}} \quad (5.25)$$

for the branch connected to the HS of the transformer.

5.2.4. Autotransformer Model

Taking into account the equivalent circuit diagrams the autotransformer and the transformer are very much alike. In this case the LS winding is the part of the HS one (Fig. 5.12a) thus reducing the autotransformer unit size and production cost. Both windings have galvanic connection. The magnetizing branch model can be connected to any side of the equivalent circuit.

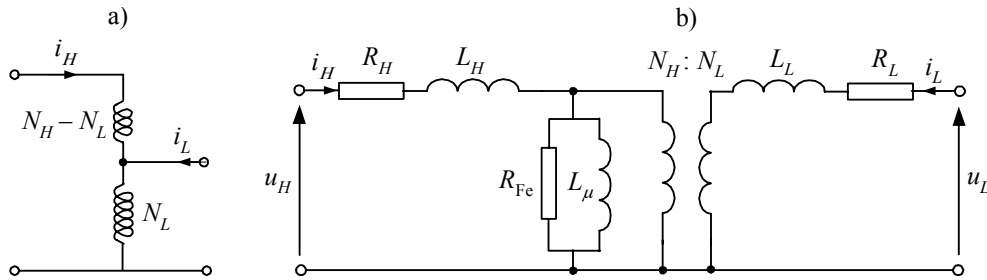


Fig. 5.12. The equivalent circuit diagram of the autotransformer: a) winding configuration and b) the equivalent circuit

5.2.5. Model of Magnetic Circuit

In the presented considerations it was assumed that the magnetic circuit and active losses in the core are linear and, as a consequence, the branch parameters are constant. In fact such assumption can be applied in very low number of cases. That is why the EMTP offers more adequate models of the effects observed in the transformer magnetic core. Further the basic models of nonlinear inductance are presented.

Magnetizing Characteristic

The magnetizing characteristic of ferromagnetic material is determined by the relation between magnetic field intensity H (A/m) and the magnetic induction B (T): $H = f(B)$ ⁶. The relation is nonlinear with hysteresis loop (Fig. 5.13a). The loop size is determined by the maximal magnetic remnant induction B_r and the magnetic coercion H_c .

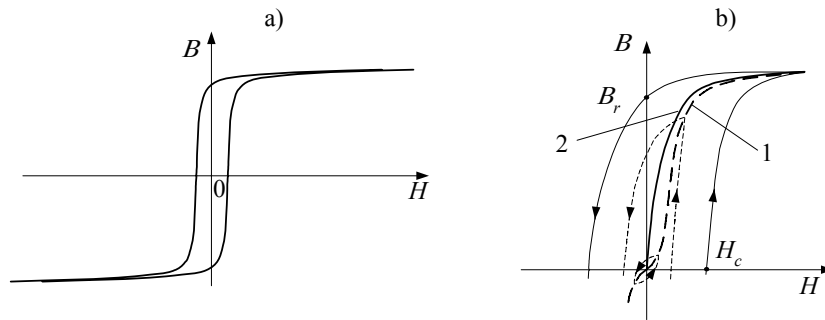


Fig. 5.13. The magnetizing characteristic with hysteresis loop: a) limit loop and b) inner loops

At slow and symmetrical changes of the magnetic field the magnetizing characteristic takes the shape of many inner loops whose width is determined by the magnitude of the magnetic field H (Fig. 5.13b). The inner loop vertices determine the magnetizing characteristic of the magnetic core material (curve 1) [20]. In many cases the hysteresis loop can be neglected and then the magnetizing characteristic is represented by the function which is equal to the mean value of the limit hysteresis loop (curve 2).

To relate the magnetizing characteristic with the electric quantities in the transformer windings let's recall some basic equations. The electric current i flowing through the coil of N_c turns wound around the core of the mean length l induces the magnetic field of intensity H (A/m) and:

⁶ $1 \text{ T} = 1 \text{ Wb/m}^2 = 1 \text{ Vs/m}^2$.

$$H = \frac{N_c}{l} i \quad (5.26)$$

in which the stray flux is neglected and i is called the magnetizing current. The magnetizing current and magnetic field intensity can be functions of time: $i = i(t)$, $H = H(t)$.

The corresponding magnetic induction $B = f(H)$ is uniquely identified by the magnetic flux ψ (Wb) in the N_c turn coil whose mean value can be calculated from the equation⁷:

$$\psi = N_c S B = N_c \phi \quad (5.27)$$

where S (m²) is the core cross-section.

The magnetic flux is related to the voltage drop across the coil (5.4) so:

$$\psi(t) = \int_{t_0}^t u(\tau) d\tau + \psi_0 \quad (5.28)$$

The similar relation holds for the magnetic inductance B (with coil parameters like in (5.27)).

In case of alternate voltage the magnetizing flux strongly depends upon the voltage initial value. The steady state flux for the sinusoidal voltage of frequency ω is (5.28):

$$\Psi = \frac{1}{\omega} U \quad (5.29)$$

The properties of the core magnetic material are characterized by the magnetic permeability μ (H/m):

$$\mu = \frac{dB}{dH} \quad (5.30)$$

which is related to the inductance L by the coil the core size:

$$L = \frac{d\psi}{di} = \frac{N_c^2 S}{l} \mu \quad (5.31)$$

In practice it is much easier to use the characteristic $\psi = f(i_\mu)$ (instead of $B = f(H)$) where the subscript μ indicates that the magnetizing current induces the magnetic field H .

There are many representations of the core magnetizing characteristic used for choke and transformer models. Some of them are shown in Fig. 5.14.

⁷ 1 Wb = 1 Vs.

In simplest case the piecewise approximation of the magnetizing characteristic comprises of three segments for which (Fig. 5.14a): $L_\mu = 0$ (the segment lies on ψ axis) and $L_\mu = L$ (two segments for positive and negative values of the magnetizing current). The greater number of segments (Fig. 5.14b) results in the better approximation of the characteristic. The ideal one is the continuous characteristic (Fig. 5.14c).

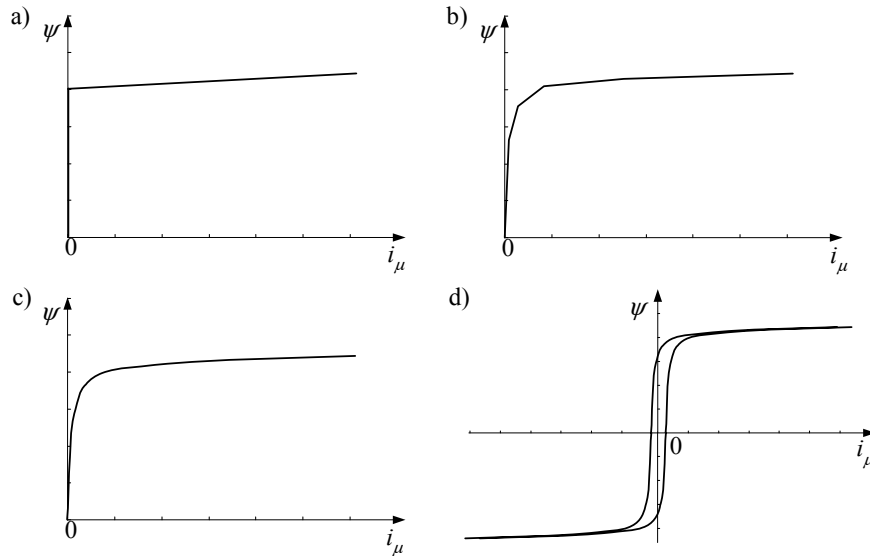


Fig. 5.14. Some representations of the core magnetizing characteristic

The magnetizing characteristic can be approximated by a continuous function and resulting model is called a *true type* one. The approximation is obtained by use of odd functions, for instance:

$$\psi(i_\mu) = a_1 i_\mu + a_3 i_\mu^3 + a_5 i_\mu^5 + \dots, \quad (5.32)$$

and good result is obtained of the first two terms of the series ($a_1 \neq 0$ and $a_2 \neq 0$).

Inclusion of losses due to the hysteresis and more accurate approximation of losses in the core can be obtained for the characteristic with the hysteresis loop (Fig. 5.14d), which can also have the piecewise approximation. The function like in (2.41) can be used for this purpose:

$$\psi(i_\mu) = a_1 \cdot \text{arctg}(a_2(i_\mu \pm I_c)) + a_3 i_\mu \quad (5.33)$$

where I_c denotes the magnetizing current corresponding to coercion H_c . If $I_c > 0$, then the function enables the coarse approximation of the hysteresis loop including the inner loops (the sign depends upon the sign of ψ/dt).

Accurate approximation of effects in the ferromagnetic core in transient state is difficult [15, 85] and it is important that the model includes the initial conditions for induction (B_0) or the flux (ψ_0).

The initial value of the flux determines the point on the inner loop (Fig. 5.15a).

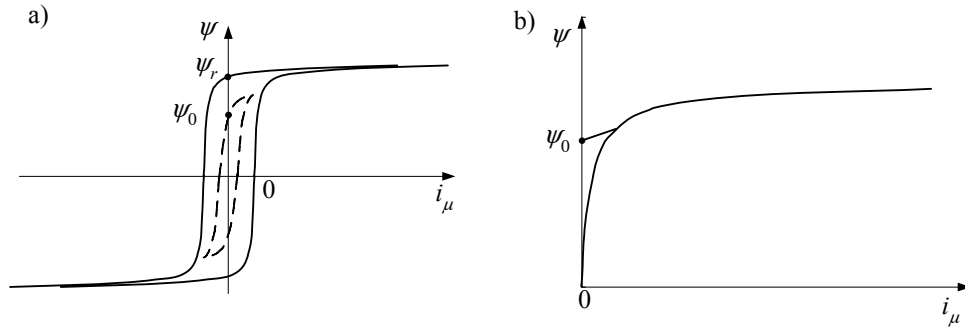


Fig. 5.15. Initial condition in the model: a) with hysteresis and b) without hysteresis

In the model without hysteresis the initial conditions can not be set directly (the magnetizing characteristic passes through the origin – Fig. 5.15b). The problem can be solved by introduction of the voltage source which is active in the first calculation step. The following example shows how the problem is solved in ATP–EMTP.

Example 5.2. Using the ATPDraw interface set up the protection CT model in which the magnetizing characteristic is represented by 98 (*pseudo-nonlinear*) element with the option of setting the flux initial value.

Let's consider the 5P20⁸ type CT of the following parameters:

nominal power: $S_n = 20 \text{ VA}$ ($S_n = I_{2n}^2 Z_{obcn}$),

nominal load impedance: $Z_{obcn} = 20 \Omega$, $\cos \varphi = 0.5$,

current ratio: 500:1 ($I_{1n} : I_{2n}$) A/A, winding turn ratio: 500:1 ($N_2 : N_1$),

the core cross-section: $S = 28.8 \text{ cm}^2 = 2.88 \cdot 10^{-3} \text{ m}^2$, the length of magnetic loop: $l = 0.675 \text{ m}$,

the secondary resistance winding: $R_2 = 4.5 \Omega$.

The magnetizing characteristic is shown in Fig. 5.16. The characteristic has been obtained experimentally (by measurement) for sinusoidal excitation and the respective values are the peak ones. It must be noted that such a characteristic is not accurate for large values of inductance since the corresponding magnetic field intensity H is calculated for r.m.s. values of current which is strongly distorted; the professional computer programs use the special correcting procedures [24].

⁸ Protection CT of composite error 5% at rated accuracy limit primary current and Standard Accuracy Limit Factor 20 [46, 47].

In ATP–EMTP the magnetizing characteristic of the 98 element is represented by the function $\psi = f(i)$ (for peak values). Transformation of this characteristic can be effected by use of

$$(5.26) \text{ and } (5.27): i_\mu = \frac{l}{N_2} H, \quad \psi = N_2 S B.$$

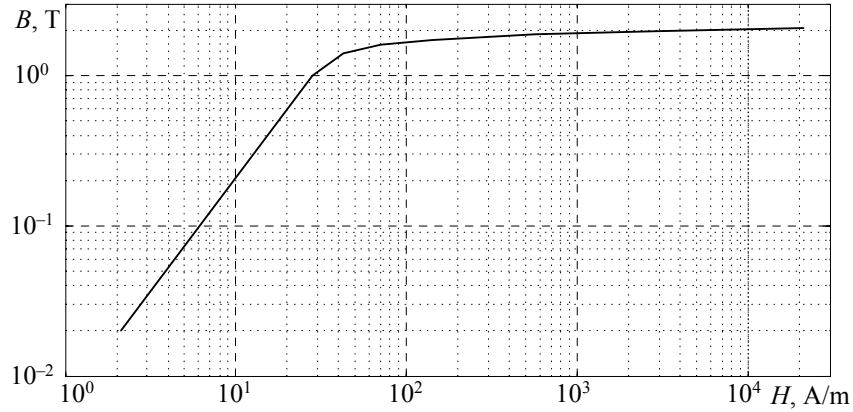


Fig. 5.16. CT's magnetizing characteristic

Substituting the values taken from Fig. 5.16 the following data (Table 5.1) are obtained which can be used for type 98 element set up.

Table 5.1. CT's magnetizing characteristic: $\psi = f(i_\mu)$

i_μ , A	ψ , Vs
0.0143	0.1440
0.0382	1.4400
0.0573	2.0160
0.0955	2.3184
0.1909	2.4912
0.7637	2.6928
3.8184	2.8368
28.6378	2.9664

The calculation step $T=10^{-5}$ s has been selected and the respective ATPDraw diagram is shown in Fig. 5.17. The dotted line denotes the CT's elements; the other ones are: the source impedance (Z_S) and the load impedance (Z_{obc}).

The nominal CT's load is $Z_{obcn} = 10 + j17.3 \, \Omega$ and the excitation source allows obtaining the over-current ratio equal to 20.

The CT's magnetizing branch comprises of element 98 connected in series with the DC voltage (source 11) which is used for setting of the inductance ψ . initial value.

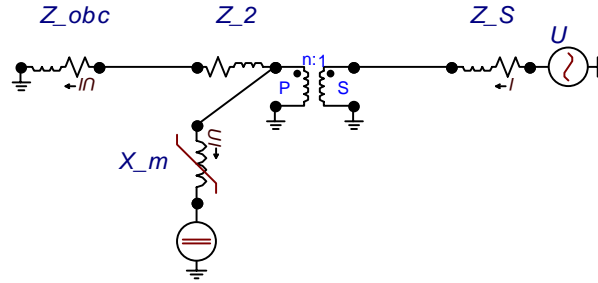


Fig. 5.17. The circuit with the CT model

The secondary current i_2 waveform along with the magnetizing current i_μ and the flux ψ waveforms are shown in Fig. 5.18 for two values of the remnant flux: $\psi_0 = 2$ Vs (Fig. 5.18a) and $\psi_0 = 0$ (Fig. 5.18b).

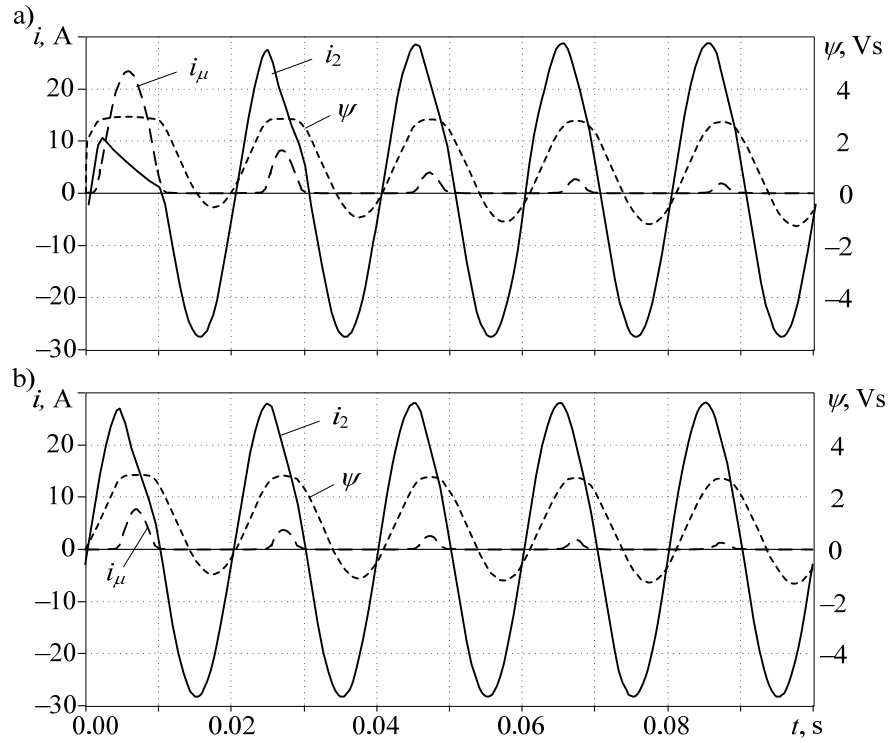


Fig. 5.18. The result of CT's switch-on: a) for remnant flux $\psi_0 = 2$ Vs and b) for zero remnant flux

Basing on (5.28) the external voltage source is switched on at $t_{\text{on}} = 0$ (TSTART = 0) and switched off after one calculation step at $t_{\text{off}} = t_{\text{on}} + T$ (TSTOP = $T + \varepsilon$, where ε is the fraction

of T — the declared time interval of the voltage source activation must be slightly longer than T ; otherwise the source will not be switched on. The peak value of U is calculated from (5.28) written in discrete form for one calculation step: $\psi = UT$ from which: $U = \psi_r / T$ where: ψ_r — the initial value of the remnant flux.

5.3. Three-phase Transformer

5.3.1. Two-winding Transformer

The properties of the three-phase transformer depend on arrangement of the windings connection which is called the winding connection group and on the transformer core design. In majority of applications the transformer windings are connected in Δ or in Y arrangement.

The transformer windings are assumed to be symmetrical that implies the identical winding equivalent parameters. Moreover, in the low frequency range (up to 2000 Hz) the transformer capacitances (phase-to-phase and phase-to-ground) as well as the skin effect can be neglected.

Just like for the single phase transformer the three-phase unit can be considered as a multi-terminal element or as the circuit corresponding to the transformer design with distinguished primary and secondary side. Further, the multi-terminal approach to the transformer winding connection will be presented.

The transformer winding connections are normalized according to respective standards and, generally, different winding connection groups are applied to different power networks [36, 91]. Some of them are shown in Table 5.2.

Knowing the transformer winding arrangement the transformer model can easily be developed. The equivalent circuit of the transformer in Yd11 connection is shown in Fig. 5.19a. The equivalent circuits of the respective winding pairs are the same as for the single-phase transformer. Due to the LS winding connection the LS voltage vectors lead the HS voltage vectors by 30° . The Y side voltage is equal to the phase one while the Δ side voltage is the phase-to-phase one. Thus, the winding turn ratio is $\sqrt{3}$ times greater.

The transverse (magnetizing) branch can be connected to any side of the transformer. In ATP–EMTP the magnetizing branch is always connected to the primary side of the transformer model.

The considered representation of the three phase transformer is acceptable if the magnetic circuit configuration allows splitting of the transformer into three separate phase units. It can be done for units with magnetic core as shown in Fig. 5.20b.

The magnetic core design in the three phase transformer determines the transformer properties, in particular, the equivalent representation for the zero sequence component. This component produces the magnetic flux which has the same

sign in all transformer columns. In case of the three column unit (Fig. 5.20a) this flux loop closes only via external environment (oil, air) which has very high reluctance.

Table 5.2 Selected winding connections of the two-winding transformers

Item	Connection group	Diagram	Voltage vectors	Remarks*
1	Yy0			$\underline{U}_{1y} = \underline{U}_{1Y} / \vartheta$
2	Dy5			$\underline{U}_{1y} = \frac{-\underline{U}_{1\Delta}}{\sqrt{3}\vartheta}$
3	Yd11			$\underline{U}_{1\Delta} = \underline{U}_{1Y} / \vartheta$
4	Yd1			$\underline{U}_{1\Delta} = \underline{U}_{1Y} / \vartheta$
5	Yz5			$\underline{U}_{1L} = \frac{\underline{U}_{2Y} - \underline{U}_{1Y}}{\sqrt{3}\vartheta}$
6	Dz0			$\underline{U}_{1L} = \underline{U}_{1H} / \vartheta$

* $\vartheta = U_H / U_L$, $U_{1Y} = U_{1H}$, $U_{1y} = U_{1L}$.

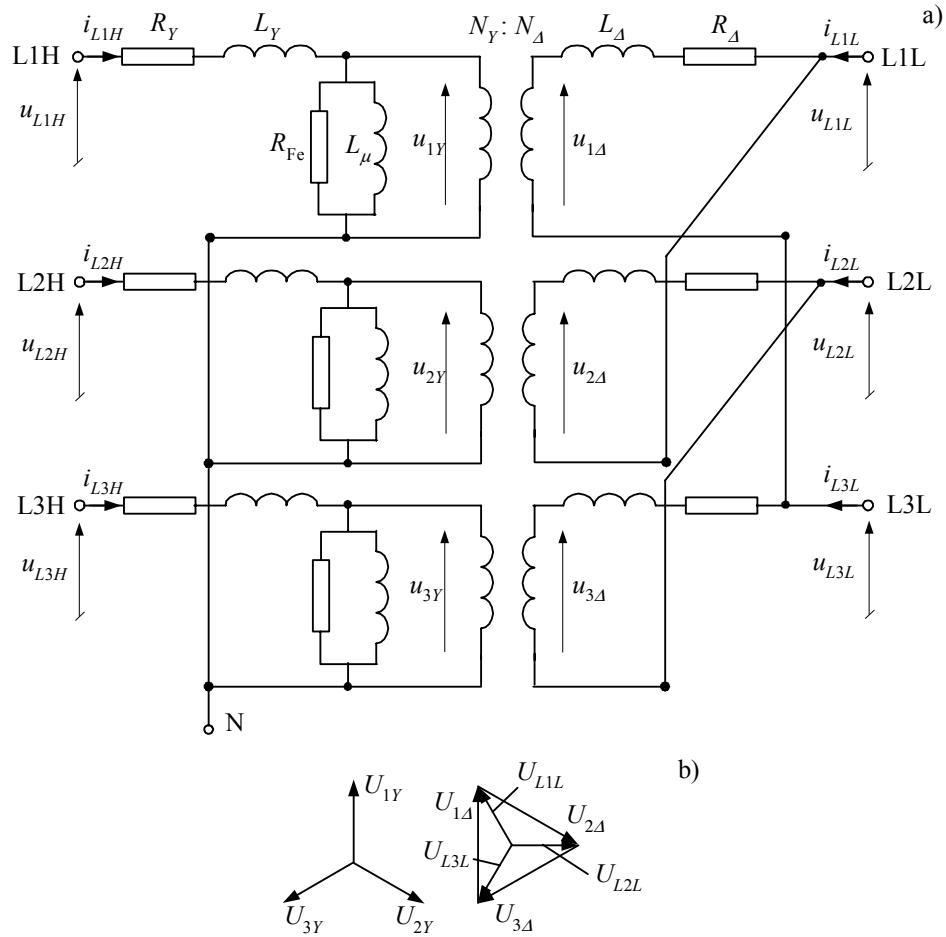


Fig. 5.19. The equivalent circuit of the Yd11 transformer

The magnetizing characteristic of such magnetic loop is more flat as compared to the ferromagnetic core characteristic and the nonlinearity effect is reduced. In effect the magnetizing inductance for zero sequence component $L_{0\mu}$ is much lower. The four and five column transformers (Fig. 5.20b) are devoid of this effect since the zero sequence flux loop closes via additional columns.

Similarly to the single phase transformer the magnetizing circuit can be represented by the nonlinear magnetizing branch as shown in Fig. 5.20 [87]. In case of the three column transformer the effect of the zero sequence flux loop can be modelled by additional circuit as shown in Fig. 5.21.

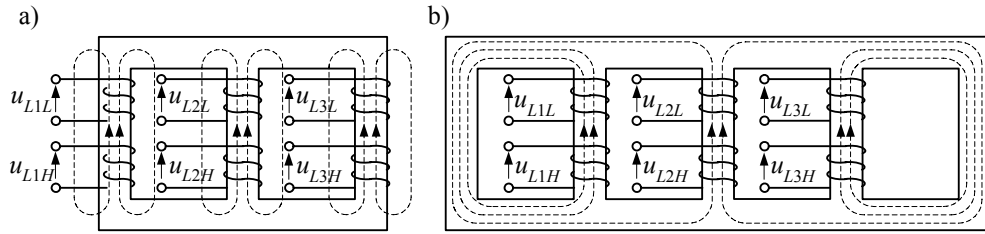


Fig. 5.20. The three phase transformer cores: a) three column, b) five column

Due to the different magnetic loops for the positive and zero sequence flux components the three column transformer impedance for the latter is 3 – 5 times greater [8].

Using two extra ideal transformer of 1:1 turn ratio (Fig. 5.21) the triple value of the zero sequence voltage $3u_{0H\mu}$ at transformer HS is obtained. The triple nonlinear inductance represents the magnetic circuit for the zero sequence flux component.

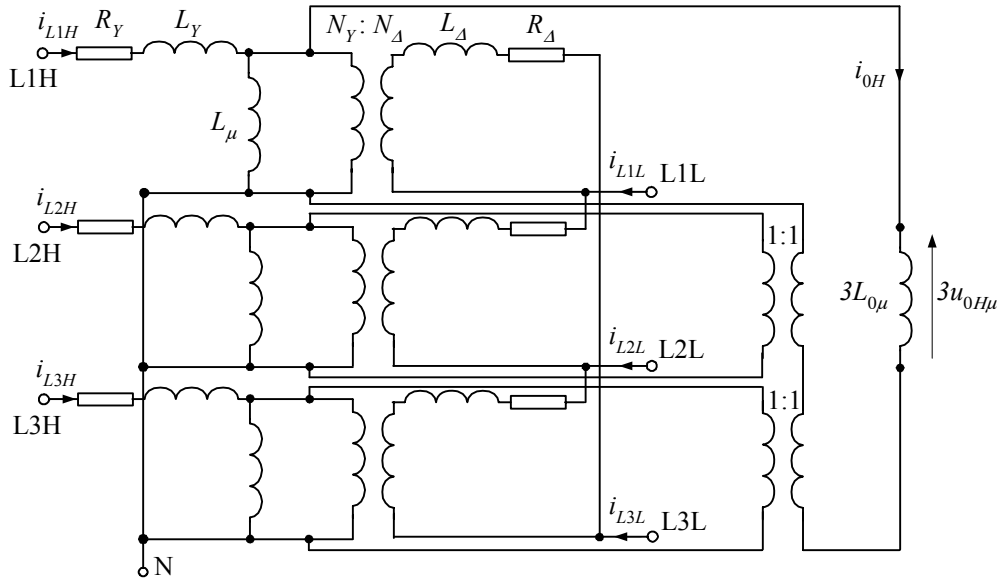


Fig. 5.21. The equivalent circuit of the Yy0 transformer with the three column core

In ATP-EMTP the input data format for this model is determined by *TRANSFORMER THREE PHASE (TRAYYH 3* in ATPDraw interface). The relevant details are illustrated by the following example.

Example 5.3. Using the ATPDraw graphical interface set up the model of the 110/20 kV power system fragment with 40 MVA Yn0y0 three column transformer (Y/Y with earthed HS and unearthened LS - Fig. 5.22).

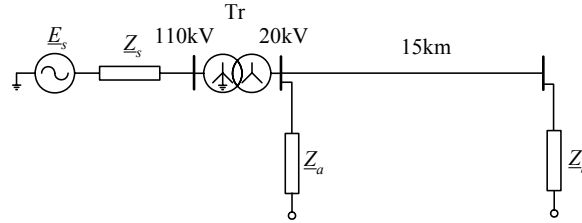


Fig. 5.22. The diagram of the modelled power system fragment

The transformer parameters:

nominal power: $S_n = 40 \text{ MV}\cdot\text{A}$;

nominal voltage: 115/22 kV.

the following parameters have been measured at the transformer LS:

For the positive sequence component:

losses in the core: $\Delta P_{\text{Fep}} = 32 \text{ kW}$;

magnetizing current: $I_{\mu p} = 11.4 \text{ A}$;

magnetizing voltage $U_{\mu p} = 19.0 \text{ kV}$;

load losses in windings: $\Delta P_{\text{Cu}} = 205 \text{ kW}$;

short-circuit current: $I_z = I_{NH} = 200.8 \text{ A}$;

short-circuit voltage: $U_z = 12.07 \text{ kV}$;

For the zero sequence component:

losses in the core: $\Delta P_{\text{Fe0p}} = 168.1 \text{ kW}$;

magnetizing current: $I_{\mu 0 p} = 280 \text{ A}$;

magnetizing voltage: $U_{\mu 0 p} = 1.636 \text{ kV}$ (voltage at the short-circuited LS terminals);

load losses in windings: $\Delta P_{\text{Cu0p}} = 12.5 \text{ kW}$;

short-circuit current: $I_{z0p} = 95 \text{ A}$;

source impedance: $Z_{1s} = 0.15 + j2.5 \Omega$, $Z_{0s} = 0.26 + j3.4 \Omega$;

loading power: $S_{\text{obc}_a} = 25.4 + j15.8 \text{ VA}$, $S_{\text{obc}_b} = 4.5 + j2.2 \text{ MVA}$.

The magnetizing characteristic for LS is shown in Table 5.3).

The 20 kV overhead line:

The line length $l = 15 \text{ km}$; $R_1 = 0.36 \Omega/\text{km}$; $X_1 = 0.38 \Omega/\text{km}$; $R_0 = 0.60 \Omega/\text{km}$;

$X_0 = 1.55 \Omega/\text{km}$; $C_1 = 10.5 \text{ nF/km}$; $C_0 = 4.2 \text{ nF/km}$.

The data are necessary to set up the transformer model (*TRAYH_3* in ATPDraw). The following calculations are automatically carried out by the program:

$$I_{\mu} = I_{\mu p} \frac{U_N}{U_{\mu p}} = 11.4 \frac{22}{19} = 13.2 \text{ A}, \quad \Delta P_{Fe} = \Delta P_{Fep} \left(\frac{U_N}{U_{\mu p}} \right)^2 = 32 \left(\frac{22}{19} \right)^2 = 42.9 \text{ kW}.$$

Subscript p indicates that the measurements were not taken in nominal conditions so, assuming that the circuit is linear, the nominal values are recovered.

Table 5.2. The magnetizing characteristic $\psi = f(i_{\mu})$ for LS (22kV)

i_{μ} , A	ψ , Vs
18.62	57.20
38.95	64.56
367.6	75.27
1121.0	77.97
3587.0	80.43

The same for the zero sequence:

$$I_{\mu 0} = \frac{I_{\mu 0 p}}{3} \frac{U_N}{\sqrt{3} U_{\mu 0 p}} = \frac{280}{3} \frac{22}{1.636\sqrt{3}} = 724.6 \text{ A},$$

$$\Delta P_{Fe0} = \Delta P_{Fe0 p} \left(\frac{U_N}{\sqrt{3} U_{\mu 0 p}} \right)^2 = 168.1 \left(\frac{22}{1.636\sqrt{3}} \right)^2 = 10133 \text{ kW}.$$

The measured magnetizing current $I_{\mu p}$ and magnetizing voltage $U_{\mu p}$ determine the linear part of the magnetizing characteristic $\psi = f(i_{\mu})$. The respective values are:

$$i_{\mu} = \sqrt{2} I_{\mu p} = 11.4\sqrt{2} = 16.12 \text{ A}, \quad \psi = \sqrt{2} U_{\mu p} / (\sqrt{3}\omega) = 19000\sqrt{2} / (314\sqrt{3}) = 49.38 \text{ Vs}.$$

The values are used for calculation of the magnetizing branch reactance:

$$X_{\mu} = \frac{\omega\psi}{i_{\mu}},$$

which, in turn, is used for calculation of the initial steady state of the network.

The transformer impedance can be determined from measurement data obtained in the short-circuit conditions:

$$R_T = \frac{\Delta P_{Cu}}{3I_z^2} = \frac{205000}{3 \cdot 200.8^2} = 1.695 \Omega, \quad Z_T = \frac{U_z}{\sqrt{3}I_z} = \frac{12,07}{0.2008\sqrt{3}} = 34.7 \Omega,$$

$$X_T = \sqrt{Z_T^2 - R_T^2} = \sqrt{34.7^2 - 1.695^2} = 34.66 \Omega.$$

and the respective winding parameters are:

$$R_H = R_T / 2 = 0.8475 \Omega, \quad X_H = X_T / 2 = 17.35 \Omega,$$

$$R_L = R_H \left(\frac{22}{115} \right)^2 = 0.031 \Omega, \quad X_L = X_H \left(\frac{22}{115} \right)^2 = 0.635 \Omega.$$

As the losses in iron for positive and zero components are different they can not be represented by the resistor connected in parallel with the inductance L_μ (Fig. 5.21). The losses can be represented by the external three phase element of mutually coupled resistors connected to the transformer terminals. The resistance matrix of that element can be determined from the symmetrical components relation:

$$R_{FeS} = \frac{R_{Fe0} + 2R_{Fe1}}{3}, \quad R_{FeM} = \frac{R_{Fe0} - R_{Fe1}}{3},$$

$$\text{where: } R_{Fe0} = \frac{3U_{\mu0p}^2}{\Delta P_{Fe0p}} = \frac{3 \cdot 1.636^2}{168.1} 1000 = 48 \, \Omega, \quad R_{Fe1} = \frac{U_{\mu p}^2}{\Delta P_{Fep}} = \frac{19^2}{32} 1000 = 11281 \, \Omega.$$

$$\text{Thus: } R_{FeS} = \frac{48 + 2 \cdot 11281}{3} = 7536.8 \, \Omega, \quad R_{FeM} = \frac{48 - 11281}{3} = -3744.0 \, \Omega.$$

These resistances are calculated with respect to the L-side and form the following matrix:

$$R_{Fe} = \begin{bmatrix} R_{FeS} & R_{FeM} & R_{FeM} \\ R_{FeM} & R_{FeS} & R_{FeM} \\ R_{FeM} & R_{FeM} & R_{FeS} \end{bmatrix} = \begin{bmatrix} 7536.8 & -3744.0 & -3744.0 \\ -3744 & 7536.8 & -3744.0 \\ -3744.0 & -3744.0 & 7536.8 \end{bmatrix} \Omega.$$

Using the ATPDraw interface the coupled resistors in form of the type 51, 52, 53 elements are connected to the transformer model by default [7].

The constant zero sequence inductance $L_{0\mu}$ is represented by the reluctance at the LS of the transformer:

$$R_{m0} = \frac{(U_{NL} / \sqrt{3})^2}{3L_{0\mu}}.$$

The inductance $L_{0\mu}$ can be estimated from the equation:

$$L_{0\mu} = \frac{U_{\mu0p} \left(1 - \frac{I_{\mu0}}{I_{NL}} \frac{Z_T}{Z_{NH}} \right)}{\omega I_{\mu0p} / 3}, \quad \text{where } I_{NL} = \frac{S_N}{\sqrt{3}U_{NL}}, \quad Z_{NH} = \frac{U_{NH}^2}{S_N} \text{ represent the base values at the}$$

primary and the secondary side of the transformer, respectively (Fig. 5.21).

Substituting the necessary data we get:

$$L_{0\mu} = \frac{1636 \left(1 - \frac{724.6}{1049.7} \frac{34.7}{330.6} \right)}{100\pi \cdot 280 / 3} = 0.0517 \, \text{H}, \quad \text{and: } R_{m0} = \frac{(22 / \sqrt{3})^2}{3L_{0\mu}} = \frac{22^2}{9 \cdot 0.0517} = 1039 \, \Omega.$$

The neutral point earthing resistance R_{Ng} is determined as the difference between power losses for zero and positive sequence components measured in the transformer winding:

$$\Delta P_{Ng} = \Delta P_{Cu0} - \Delta P_{Cu}, \quad \text{where } \Delta P_{Cu0} = \Delta P_{Cu0p} \left(\frac{I_z}{I_{z0} / 3} \right)^2 = 12.5 \left(\frac{200.8}{95/3} \right)^2 = 502.57 \, \text{kW} \text{ (referred to}$$

the nominal current). Thus:

$$\Delta P_{Ng} = 502.27 - 205.0 = 297.27 \, \text{kW}.$$

The earthing resistance value is:

$$R_{Ng} = \frac{\Delta P_{Ng}}{(3I_{NH})^2} = R_{Ng} = \frac{297270}{(3 \cdot 200.8)^2} = 0.82 \text{ } \Omega.$$

In ATPDraw interface the resistance is included by default.

The load impedance is calculated from the equation:

$$\underline{Z}_O = \frac{U_N^2}{S_0^*} \text{ (the asterisk denotes the conjugate value). Further:}$$

$$\underline{Z}_{abc_a} = \frac{20^2}{25.4 - j15.8} = 11.35 + j7.06 \text{ } \Omega, \quad \underline{Z}_{abc_b} = \frac{20^2}{4.5 - j2.2} = 71.74 + j35.07 \text{ } \Omega.$$

The load impedance is represented by the RLCY3 element while the line is modelled by use of the three phase Π circuit with the following matrices \mathbf{R} , \mathbf{X} , \mathbf{C} :

$$R_S = \frac{R_0 + 2R_1}{3}, \quad R_M = \frac{R_0 - R_1}{3}, \text{ where: } R_0 = 15 \cdot 0.6 = 9.0 \text{ } \Omega, \quad R_1 = 15 \cdot 0.36 = 5.4 \text{ } \Omega. \text{ From that:}$$

$$R_S = 6.6 \text{ } \Omega, \quad R_M = 1.2 \text{ } \Omega.$$

Similarly, the line reactance is:

$$X_0 = 15 \cdot 1.55 = 23.25 \text{ } \Omega, \quad X_1 = 15 \cdot 0.38 = 5.7 \text{ } \Omega, \quad X_S = 11.55 \text{ } \Omega, \quad X_M = 5.85 \text{ } \Omega.$$

The line capacitances are represented by the respective susceptances ($B = \omega C = 2\pi fC$, $f = 50 \text{ Hz}$):

$$B_0 = 100\pi \cdot 15 \cdot 4.2 \cdot 10^{-3} = 19.79 \text{ } \mu\text{S}, \quad B_1 = 100\pi \cdot 15 \cdot 10.5 \cdot 10^{-3} = 49.48 \text{ } \mu\text{S}.$$

$$B_S = \frac{B_0 + 2B_1}{3} = \frac{19.79 + 2 \cdot 49.48}{3} = 39.58 \text{ } \mu\text{S}, \quad B_M = \frac{B_1 - B_0}{3} = \frac{49.48 - 19.79}{3} = 9.97 \text{ } \mu\text{S}.$$

The ATPDraw model of the system considered is shown in Fig. 5.23. The primary side current waveforms calculated for the transformer switch-on in ‘no load’ conditions are presented in Fig. 5.24. The highest voltage in phase L1 results in very small value of the magnetizing current in this phase. The currents in other phases are biased in the same direction (positive or negative half-waves) so the content of the second harmonic is very large in these currents.

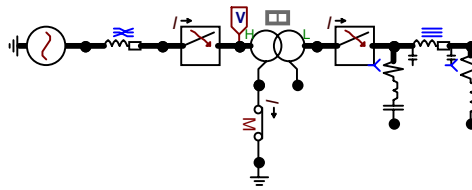


Fig. 5.23. ATPDraw model of the system considered

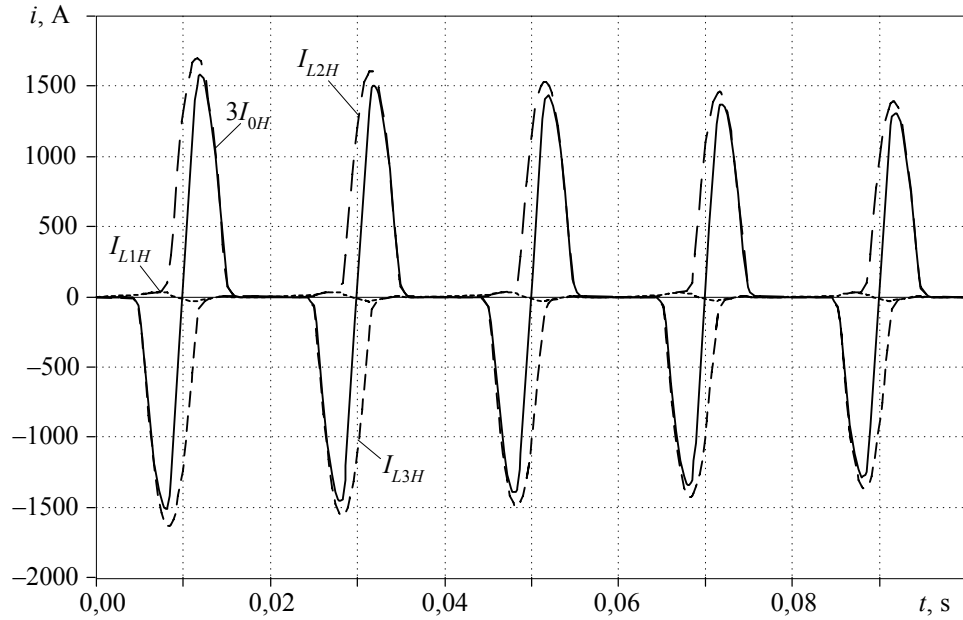


Fig. 5.24. The current waveforms during switch-on of the unloaded transformer

Large zero sequence current $3I_{0H}$ flows through the earthed neutral point at the transformer primary side.

5.3.2. Multi-winding Transformer

Three winding transformers are applied in power systems very frequently. The third winding, if connected in Δ arrangement (mostly in autotransformers), effectively reduces the transformer zero sequence impedance in networks operating with the earthed neutral point. Transformers with greater than three number of windings are used rarely.

Some examples of winding arrangement in three winding transformers are shown in Fig. 5.25. The tertiary winding is denoted by T.

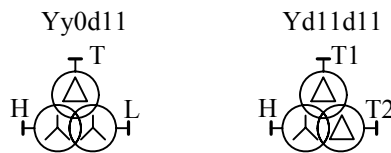


Fig. 5.25. Examples of winding arrangement in three winding transformers

The three phase three winding transformer model can be obtained by connection of three single winding three phase transformer models (s. 123). If one of the windings is in Δ arrangement then the impact of the zero sequence component flux can be neglected⁹. The example 5.4 shows how the three winding transformer model is realized in ATP–EMTP.

Example 5.4. Using the ATPDraw interface set up the model of the 220/110/10 kV power system fragment with Yn0yn0d11 160 MVA transformer (Fig. 5.26). The load at MV side (10 kV) is $S_o = 32 + j18$ MV·A. and the secondary winding load is $S_2 = 105 + j28$ MV·A. The other system parameters are as below.

The transformer parameters:

nominal power: $S_{rH} / S_{rL} / S_{rT} = 160/160 / 50$ MV·A;

nominal voltage: 230/120/10,5 kV;

short-circuit voltage: $u_{kHL} = 10\%$, $u_{KHT} = 33.5\%$, $u_{KLT} = 20.8\%$ (referred to HS);

idle current: $i_0 = 0.5\%$;

losses in the core: $\Delta P_{Fe} = 0.25\%$;

winding resistance: 320/80/2.4 m Ω ;

source impedance: $Z_{1sH} = 0.35 + j3.77 \Omega$, $Z_{0sH} = 1.16 + j10.42 \Omega$; $Z_{1sL} = 0.18 + j1.55 \Omega$, $Z_{0sL} = 0.56 + j2.75 \Omega$.

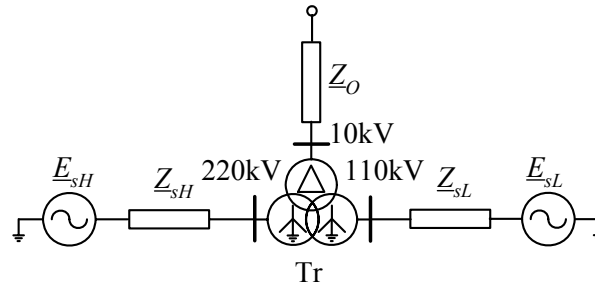


Fig. 5.26. The system diagram

The magnetizing characteristic (the relative values) is as in Table 5.4.

The turn ratio calculation:

$$\vartheta_{HT} = \frac{U_{rH}}{U_{rT}} = \frac{230}{10,5} = 21.9, \quad \vartheta_{HL} = \frac{U_{rH}}{U_{rL}} = \frac{230}{120} = 1.92.$$

⁹ The zero sequence voltage at the Y side which induces the flux is small since the Δ winding enhances the zero sequence current flow at the YN side.

Table 5.3. The transformer magnetizing characteristic

$i_\mu / i_{\mu 0}$	ψ / ψ_0
1.0	1.0
1.4259	1.2285
4.0846	1.5015
74.517	1.7745
322.0	1.911

The transformer short-circuit impedance:

$$Z_{HL} = \frac{u_{KHL}}{100} \frac{U_{rH}^2}{S_{rH}} = \frac{10}{100} \frac{230^2}{160} = 33.06 \, \Omega, \quad Z_{HT} = \frac{u_{KHT}}{100} \frac{U_{rH}^2}{S_{rH}} = \frac{33.5}{100} \frac{230^2}{160} = 110.76 \, \Omega,$$

$$Z_{LT} = \frac{u_{KLT}}{100} \frac{U_{rH}^2}{S_{rH}} = \frac{20.8}{100} \frac{230^2}{160} = 68.77 \, \Omega.$$

The calculations refer to the HS. The winding impedances (Fig. 5.25) are (for the HS):

$$Z_H = 0.5(Z_{HL} + Z_{HT} - Z_{LT}) = 0.5(33.06 + 110.76 - 68.77) = 37.52 \, \Omega,$$

$$Z'_L = 0.5(Z_{HL} + Z_{LT} - Z_{HT}) = 0.5(33.06 + 68.77 - 110.76) = -4.46 \, \Omega,$$

$$Z'_T = 0.5(Z_{HT} + Z_{LT} - Z_{HL}) = 0.5(110.76 + 68.77 - 33.06) = 73.23 \, \Omega,$$

$$\text{and: } Z_L = Z'_L / \vartheta_{HL}^2 = -4.46 / 1.92^2 = -1.21 \, \Omega, \quad Z_T = Z'_T / \vartheta_{HT}^2 = 73.23 / 21.9^2 = 0.153 \, \Omega.$$

Knowing the resistance values the winding reactance can be calculated:

$$X_H = \sqrt{Z_H^2 - R_H^2}$$

Assuming the magnetizing characteristic is determined for the HS the relative values (Table 5.4) must be multiplied by the nominal ones:

$$\psi_0 = \frac{\sqrt{2} U_{rH}}{\sqrt{3} \cdot 2\pi f} = \frac{\sqrt{2} \cdot 230000 / \sqrt{3}}{314.16} = 597.77 \, \text{Vs},$$

$$i_{\mu 0} = \sqrt{2} I_{rH} i_0 / 100 = \sqrt{2} \cdot \frac{160000}{\sqrt{3} \cdot 230} \cdot 0.005 = 2.84 \, \text{A},$$

As a result the magnetizing characteristic for the $230 / \sqrt{3}$ kV winding as in Table 5.4 is obtained. Resistance representing the losses in the core at the HS:

$$R_{Fe} = \frac{U_{rH}^2}{\Delta P_{Fe}} = \frac{100 U_{rH}^2}{\Delta P_{Fe} S_{rH}} = \frac{100 \cdot 230^2}{0.25 \cdot 160} = 132 \, \text{k}\Omega.$$

Table 5.4. The magnetizing characteristic for the $230 / \sqrt{3}$ kV winding: $\psi = f(i_\mu)$

i_μ, A	ψ, Vs
2.84	597.8
4.05	734.4
11.6	897.6
211.6	1060.7
914.50	1142.3

The load impedance for MV (10 kV) network (Δ arrangement):

$$\underline{Z}_o = \frac{U_{rT}^2}{S_o} = \frac{10.5^2}{32 + j18} = 2.62 + j1.47 \, \Omega.$$

In case of the three winding transformer the reactance of one winding is negative what may bring about the numerical stability problems. That is why the magnetizing branch should be connected to one of the transformer terminals but to the neutral point (Fig. 5.19). In our case this is HS winding [17]. The considered model diagram is shown in Fig. 5.27. The transverse branches are represented by TYPE-98 (*pseudo-nonlinear reactor*) elements which in ATPDraw are denoted as NLININD.

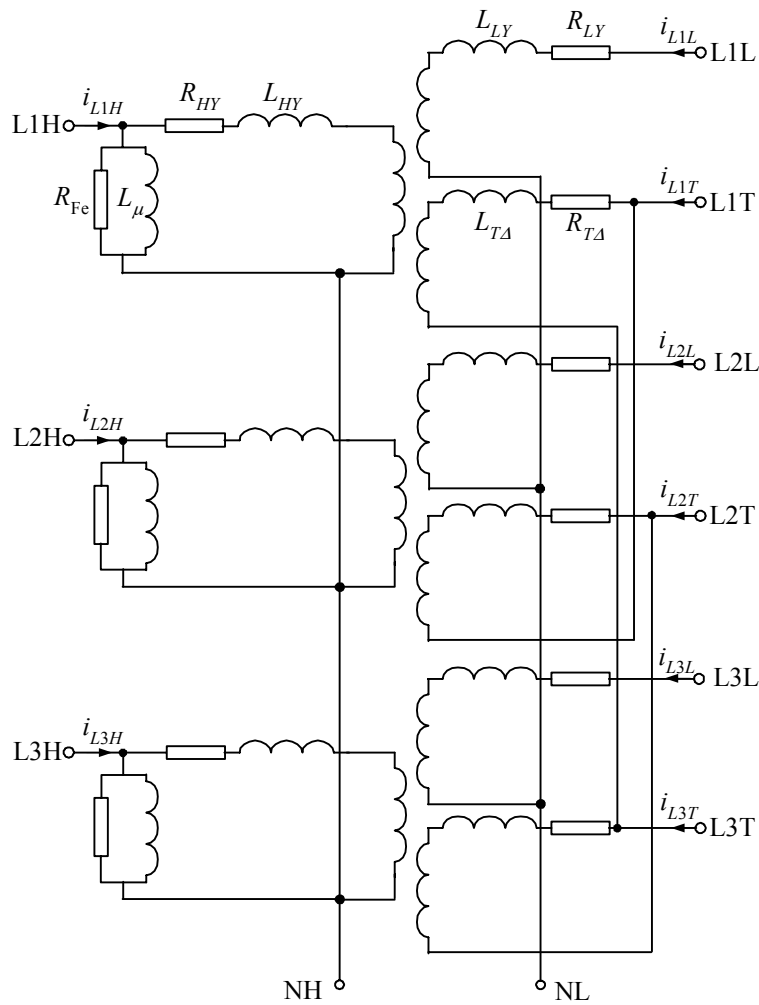


Fig. 5.27. The considered transformer model

The power system model is shown in Fig. 5.28. To stabilize the model the unearthed 10 kV winding is connected to the earth via 10 nF capacitors (corresponding susceptance $10.87 \mu\text{S}$) in each phase. Being equivalent to few tens of meters of cable feeder the capacitors do not essentially change the system operating conditions.

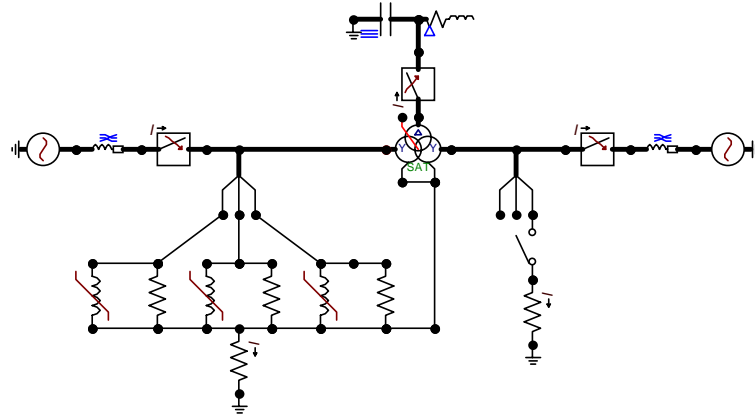


Fig. 5.28. The ATPDraw model of the analysed system

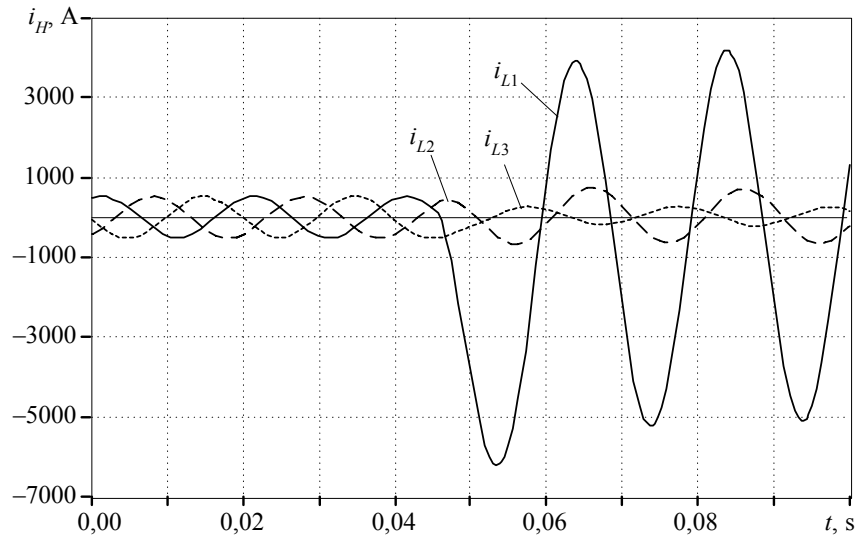


Fig. 5.29. Current waveforms at the HS of the transformer

The magnetizing branches are connected to the earthing resistor $R_N = 1.0 \Omega$ at the HS of the transformer.

The L1–G fault at the 110 kV bus-bar was simulated via fault resistance $R_z = 0.5 \Omega$. For this purpose the splitter was used. The respective current waveforms are shown in Fig. 5.29.

The multi winding transformer model can be applied to modelling of winding internal faults. In such case the faulty winding is divided into two parts and fault model is connected to the winding fault location. Using the ATPDraw interface transformer models the faulty winding division must be done in all three phases. Thus modelling the internal winding fault in two winding transformer the three phase one must be used in which two in series connected windings make one winding of the two winding transformer.

5.3.3. Z (zig-zag)-connected Transformer

The HV/MV transformers usually operate in Yd arrangement with adequate phase shift. In order to get the possibility of MV side neutral point earthing (for instance, via Peterson coil or resistor) the special earthing transformers are used. In such transformers the earthing windings are connected in Z arrangement (zig-zag – Table 5.2) in order to minimize the transformer zero sequence impedance value. The windings connection can provide positive or negative phase shift (Fig. 5.30). In general, Z connected windings may have different number of turns and the resulting relations are [40, 41]:

- turn ratio:

$$\vartheta_z = \frac{N_y}{N_z} = \frac{U_y}{U_z} = \frac{\sin \alpha}{\sin(\pi/3 - \alpha)} \quad (5.34)$$

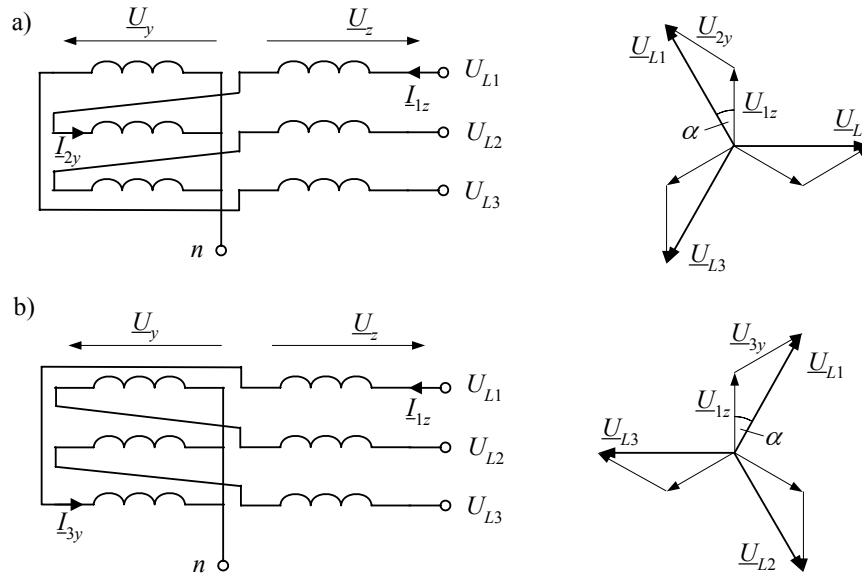


Fig. 5.30. Zig-zag connections

- voltage vector relation in the first phase:

$$\underline{U}_{1z} = \frac{\underline{U}_{1L}}{1 + \vartheta_z e^{jp\pi/3}} \quad (5.35)$$

$$\underline{U}_{ky} = \frac{\underline{U}_{1L} \vartheta_z e^{jp\pi/3}}{1 + \vartheta_z e^{jp\pi/3}} \quad (5.36)$$

where p denotes the sign which for positive phase shift (Fig. 5.30a) is also positive ($p = 1$, index $k = 2$). For negative phase shift (Fig. 5.30b) $p = -1$, index $k = 3$.

In the equivalent circuit the winding resistance is proportional to the turn number and the reactance of in series connected winding is proportional to the squared turn number. Thus, ($R = R_z + R_y$, $X = X_z + X_y$):

$$R_z = \frac{R}{1 + \vartheta_z}, \quad R_y = \frac{R \vartheta_z}{1 + \vartheta_z}, \quad (5.37)$$

$$X_z = \frac{X}{1 + \vartheta_z^2}, \quad X_y = \frac{X \vartheta_z^2}{1 + \vartheta_z^2} \quad (5.38)$$

The magnetizing current is measured for unloaded transformer and can be determined for any winding. In case of the first phase the magnetizing current is related to the first core column and can be determined from the equation $\underline{I}_\mu = \underline{U}_{1L} / jX_\mu$. The losses in core iron can be neglected. Using the first part of the winding the magnetizing current is:

$$\underline{I}_\mu = \underline{I}_{\mu z} = \frac{\underline{U}_{1z}}{jX_{\mu z}} \quad (5.39)$$

The second winding on the same column refers to the phase L3 and the related magnetizing current is:

$$\underline{I}_{\mu y} = \frac{\underline{U}_{1y}}{jX_{\mu y}} = \underline{I}_{\mu z} e^{j2\pi/3} \quad (5.40)$$

Equations (5.39) and (5.40) are valid for the transformer with positive phase shift (Fig. 5.30a). For negative phase shift the sign of power in (5.40) must be changed. Multiplying (5.40) by ϑ_z and subtracting (5.39) from (5.40) we get:

$$\underline{I}_{\mu z} (1 - \vartheta_z e^{j2\pi/3}) = \frac{\underline{U}_{1z}}{jX_{\mu z}} - \vartheta_z \frac{\underline{U}_{1y}}{jX_{\mu y}} \quad (5.41)$$

where: $X_{\mu y} = \vartheta_z^2 X_{\mu z}$. Applying this relation along with (5.35), (5.36) and (5.38) to (5.41) we get the final formulas [40]:

$$X_{\mu z} = \frac{X_{\mu}}{1 + \vartheta_z + \vartheta_z^2}, \quad X_{\mu y} = \frac{X_{\mu} \vartheta_z^2}{1 + \vartheta_z + \vartheta_z^2} \quad (5.42)$$

which enable to calculate the magnetizing branch reactance from the measured reactance X_{μ} .

In similar way the magnetizing reactance for zero sequence component can be determined. The zero sequence currents in windings on the same column flow in the same direction and bear the opposite signs so, by analogy to (5.39) and (5.40), equation (5.41) takes the form:

$$\underline{I}_0(1 - \vartheta_z) = \frac{\underline{U}_{z0}}{jX_{\mu z0}} - \vartheta_z \frac{\underline{U}_{y0}}{jX_{\mu y0}} \quad (5.43)$$

where: \underline{U}_{z0} , \underline{U}_{y0} – the zero sequence voltage on the respective windings; $X_{\mu z0}$, $X_{\mu y0}$ – the respective zero sequence magnetizing reactances.

Equations analogous to (5.35), (5.36) and (5.38) applied to (5.43) yield:

$$X_{\mu z0} = \frac{U_0}{I_0} \frac{2}{(1 - \vartheta_z)^2}, \quad X_{\mu y0} = \frac{U_0}{I_0} \frac{2\vartheta_z^2}{(1 - \vartheta_z)^2} \quad (5.44)$$

where: U_0 , I_0 – the r.m.s. values of the zero sequence voltage and current at the transformer Z terminals.

Note that for $\vartheta_z = 1$ (both windings have the same number of turns) the zero sequence magnetizing reactance tends to infinity (no magnetizing branch). The transformer impedance, as ‘seen’ from point n (Fig. 5.30), is very small (equal to the winding resistance and the stray reactance only).

The phase shift $\alpha = \pm\pi/6$ of the earthing transformer can be adjusted in ‘hour’ steps (0, 6, 5, 11, ...) depending on how the third winding is connected.

Changing the ratio ϑ_z the phase shift α of any arbitrary value can be obtained.

This property is applied in design of three winding Zdy transformers which supply the electronic power converters. In such application the transformer is supplied from the Z winding side and the phase shift value between Δ and Y windings is selected to minimize ripples in the 12-pulse converter d.c. output current. [40]. The winding connection diagram of such a transformer along with the vector diagram are shown in Fig. 5.31. In ATPDraw interface such a transformer is modelled by use of SATTRAFO block and the input data can be calculated from equations presented in this paragraph.

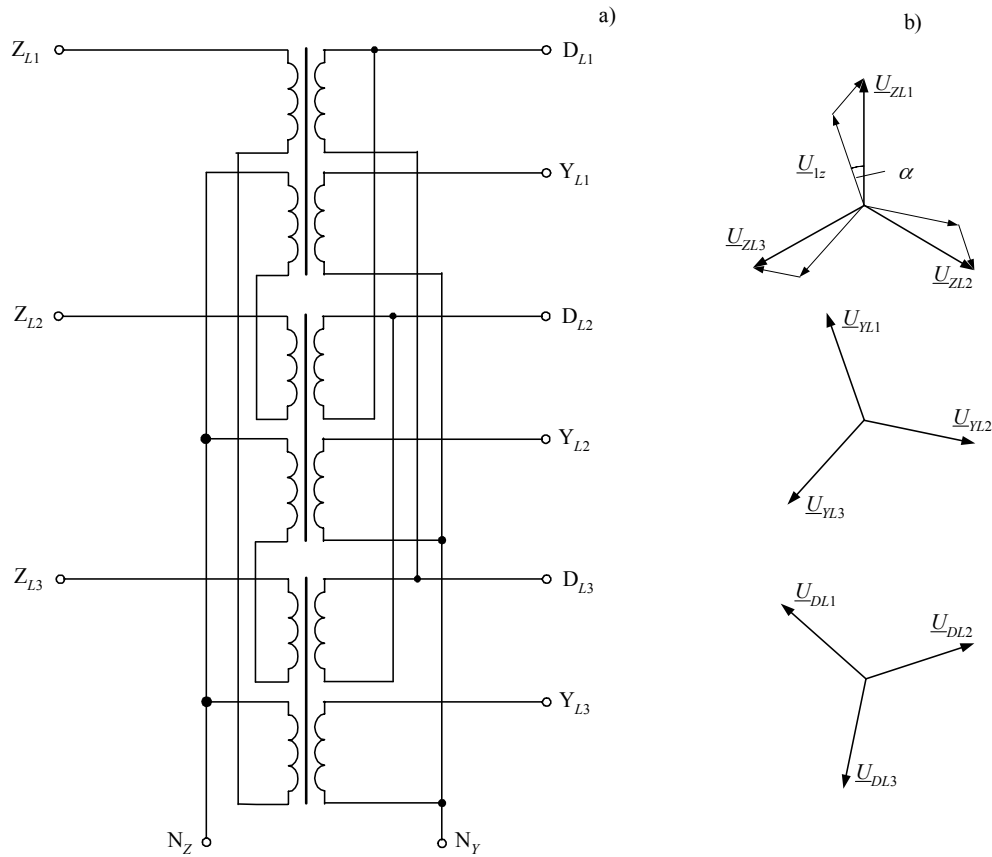


Fig. 5.31. Transformer ZNd11y: a) wiring diagram, b) voltage vector diagram

Exercises

- 5.1. Show the winding connection diagrams for the two winding transformers in the following connection groups:
a) Yd5 b) Zy5 c) Zy11 d) Dz6 e) Dd6 f) Yy6 g) Dd0 h) Dy11
- 5.2. In Example 5.3 the modelling procedure for the three column Yy0 transformer is shown. The presented magnetizing characteristic (Table 5.3) refers to the LS (22 kV) of the transformer. Rescale that characteristic for the HS (115 kV) of the transformer.
- 5.3. The LS winding of the Yy0 transformer in Example 5.3 has been rearranged into Δ connection thus making the new Yd1 unit. Calculate the LS nominal voltage of the new transformer for which the original magnetizing characteristic doesn't have to be re-scaled. Set up the ATPDraw model of the new transformer using the original transformer data. Carry out the relevant comparison tests.

- 5.4. Below the results of the magnetizing characteristic measurement for the LS winding of the Yd1 transformer are shown. The transformer parameters are:

$$S_r = 6.3 \text{ MVA}, U_r = 115/11 \text{ kV}, \Delta P_{Cu} = \text{kW}, \Delta P_{Fe} = \text{kW}, i_0 = 0.8\%.$$

Measurement results:

$I, \text{ A}$	$U, \text{ kV}$
1.53	11.0
2.86	12.1
9.55	13.2
28.6	13.7
107.9	14.3

Determine the characteristic $\psi = f(i_\mu)$ which can be used in ATP–EMTP (peak values).

Note: In ATP–EMTP such calculations can be carried out using *SATURA* subroutine. As the input data the relative values of the original characteristic (as above) must be entered (voltage and current referred to the nominal values for the winding considered)– see file *satur1.dat*.

- 5.5. Set up and examine the transformer Zy5 20/0,5kV model of the following parameters: $S_{rH} = 630 \text{ kV}\cdot\text{A}$, $S_{rL} = 100 \text{ kV}\cdot\text{A}$, $u_k = 4.5\%$, $\Delta P_{Cu} = 1.5\%$ (referred to S_{rL}). The short-circuit power at the 20 kV busbar $S_z = 6000 \text{ MV}\cdot\text{A}$. The neutral point at the SN side is earthed via resistor and at the LS is earthed solidly. Determine by experiment the earthing resistance value for which the short-circuit current at the 20 kV busbar for the phase-to-ground fault is equal to 100 A r.m.s.

6. MODELLING OF ELECTRIC MACHINES

In this Chapter rotating electric machines are analysed. It is assumed that the Reader knows the basic theory of electric machines design and operation. Electric machines, due to the magnetic coupling between the stator and the rotor windings, are similar to the transformer. However, since the rotor winding is in continuous motion with respect to the stator ones the analysis of the electric machine is more complex.

The presented here analysis is limited to the synchronous and the AC induction (asynchronous) electric machines operating as electric motors or as power generators.

6.1. Synchronous Machines

The basic functional diagram of an electric machine is shown Fig. 6.1. The electric machine design details may differ significantly depending mainly on the applied rotating velocity of the machine rotor. This velocity is related to the power network frequency f_1 by the following equation:

$$f_1 = \frac{np}{60} \text{ (Hz)}, \quad (6.1)$$

where: n – the rotating velocity of the rotor, (1/min), p – the number of pole pairs.

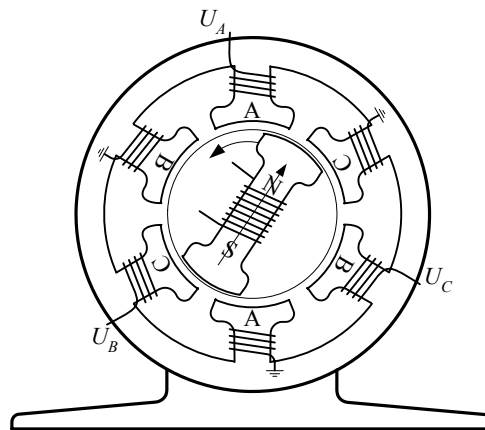


Fig. 6.1. The functional diagram of a three phase rotating electric machine; $p = 1$

The factor $n/60$ (Hz) in (6.1) is the rotating velocity of the electric machine shaft. Multiplication of the machine pole pair number results in adequate increase of the electric and magnetic quantities related to the rotating magnetic field produced by the machine rotor. For example, if the angular speed of the magnetic field in the machine γ_e changes p times faster than the angular speed of the rotor γ_r then:

$$\gamma_e = p\gamma_r \quad (6.2)$$

In case of cylindrical rotor with a single pair of poles (as in turbo generators) the rotor speed is equal to 3000 rotates/min (for the network fundamental frequency of 50 Hz). The power generators driven by the water turbines (hydro generators) usually rotate with the lower speed so they must have the greater number pole pairs.

6.1.1. Model in $0dq$ Coordinates

a) Electric Part

The machine shown in Fig. 6.1 can be represented by the equivalent diagram comprising of four separate circuits as shown in Fig. 6.2. The three-phase circuit represents the stator windings. If the stator windings are connected in star arrangement the neutral point can be earthed directly or via impedance. The excitation winding is represented by the circuit of the equivalent parameters r_f , L_f and is supplied by the external d.c. voltage u_f .

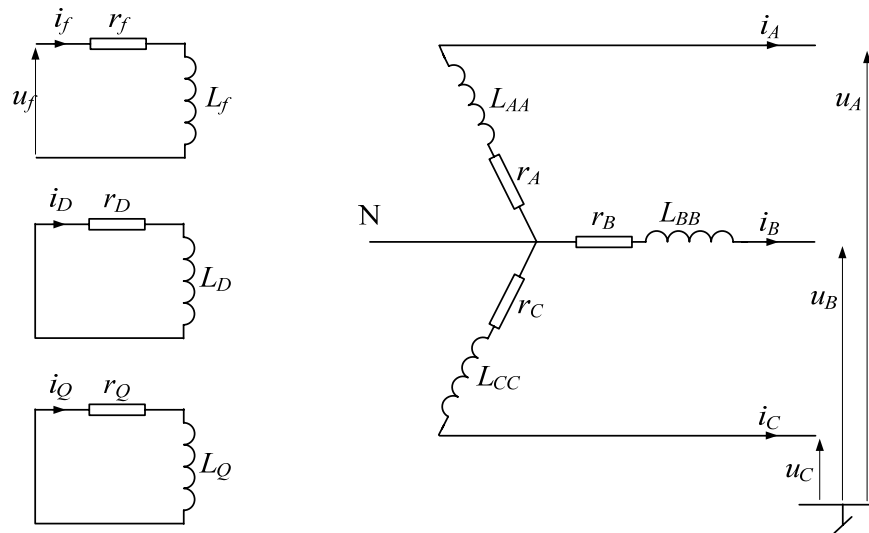


Fig. 6.2. The equivalent circuits of the synchronous machine

The other two circuits represent the damping windings located at the machine rotor. The damping windings are meant for suppression of the rotor oscillatory swings which occur in transient states. These equivalent (and in fact dummy) circuits are located in the main rotor (r_D , L_D) axis and in the vertical one (r_Q , L_Q). In case of relatively low power units (up to a few MVA) the excitation flux is generated by permanent magnet rotors thus improving the machine reliability and efficiency.

The stator windings can be connected in star or in delta arrangement. The three following circuits are related with the machine stator: the excitation circuit driven by the external source to produce the magnetic field and the two equivalent D and Q circuits. The current and voltage directions (arrows) are shown in Fig. 6.2 for the stator and rotor windings.

All the circuits are mutually coupled (the equivalent damping circuits are short-circuited) and represent sort of a transformer which can be described by the following equations [10, 24]:

$$\mathbf{u} = -\mathbf{R}\mathbf{i} - \frac{d\boldsymbol{\psi}}{dt} \quad (6.3)$$

where:

$$\mathbf{u} = \begin{bmatrix} u_A \\ u_B \\ u_C \\ -u_f \\ 0 \\ 0 \end{bmatrix}, \quad \mathbf{i} = \begin{bmatrix} i_A \\ i_B \\ i_C \\ i_f \\ i_D \\ i_Q \end{bmatrix}, \quad \boldsymbol{\psi} = \begin{bmatrix} \psi_A \\ \psi_B \\ \psi_C \\ \psi_f \\ \psi_D \\ \psi_Q \end{bmatrix}, \quad \mathbf{R} = \begin{bmatrix} r_A & & & & & \\ & r_B & & & & \\ & & r_C & & & \\ \text{---} & & & r_f & & \\ & & & & r_D & \\ & & & & & r_Q \end{bmatrix},$$

and, assuming that the circuit is linear, the particular fluxes are proportional to the values of currents:

$$\begin{bmatrix} \psi_A \\ \psi_B \\ \psi_C \\ \psi_f \\ \psi_D \\ \psi_Q \end{bmatrix} = \begin{bmatrix} L_{AA} & L_{AB} & L_{AC} & L_{Af} & L_{AD} & L_{AQ} \\ L_{BA} & L_{BB} & L_{BC} & L_{Bf} & L_{BD} & L_{BQ} \\ L_{CA} & L_{CB} & L_{CC} & L_{Cf} & L_{CD} & L_{CQ} \\ \text{---} & \text{---} & \text{---} & \text{---} & \text{---} & \text{---} \\ L_{fA} & L_{fB} & L_{fC} & L_{ff} & L_{fD} & L_{fQ} \\ L_{DA} & L_{DB} & L_{DC} & L_{Df} & L_{DD} & L_{DQ} \\ L_{QA} & L_{QB} & L_{QC} & L_{Qf} & L_{QD} & L_{QQ} \end{bmatrix} \begin{bmatrix} i_A \\ i_B \\ i_C \\ i_f \\ i_D \\ i_Q \end{bmatrix} \quad (6.4)$$

or, in compact form:

$$\begin{bmatrix} \Psi_{ABC} \\ \Psi_{fDQ} \end{bmatrix} = \begin{bmatrix} \mathbf{L}_s & \mathbf{L}_{sr} \\ \mathbf{L}_{rs} & \mathbf{L}_r \end{bmatrix} \begin{bmatrix} \mathbf{i}_{ABC} \\ \mathbf{i}_{fDQ} \end{bmatrix} \quad (6.5)$$

in which the quantities related to the rotor and stator are separated. However, since the rotor turns, reluctances for particular magnetic fluxes change. In effect the inductances in the machine equations depend on the rotor angle position γ (Fig. 6.3):

$$\Psi = \mathbf{L}(\gamma) \mathbf{i} \quad (6.6)$$

and:

$$\gamma = \gamma_e = \int_0^t \omega d\tau + \gamma_0 \quad (6.7)$$

where: $\omega = \omega_e = \omega(t)$ – electric angular velocity, γ_0 – the initial value of γ_e .

It should be noted that the rotor angular velocity depends on the pole pair number and, by analogy to (6.2):

$$\omega_r = \frac{\omega_e}{p} \quad (6.8)$$

The equation (6.8) is characteristic for synchronous machines in which the rotor and stator magnetic field rotation velocities are the same in the steady state. The rotor synchronous rotation velocity is p times lesser.

Analysis of the diagram in Fig. 6.3 leads to the following equations for the stator inductance matrix \mathbf{L}_s elements:

$$\begin{aligned} L_{AA} &= L_s + L_M \cos 2\gamma, L_{BB} = L_s + L_M \cos\left(2\gamma - \frac{2\pi}{3}\right), L_{CC} = L_s + L_M \cos\left(2\gamma + \frac{2\pi}{3}\right), \\ L_{AB} &= L_{BA} = -\left(M_s + L_M \cos\left(2\gamma + \frac{\pi}{6}\right)\right), \\ L_{BC} &= L_{CB} = -\left(M_s + L_M \cos\left(2\gamma - \frac{\pi}{2}\right)\right), \\ L_{CA} &= L_{AC} = -\left(M_s + L_M \cos\left(2\gamma + \frac{5\pi}{6}\right)\right), \end{aligned}$$

where: L_M , L_s , M_s are the constant inductances; γ is the angle between the rotor main axis d and the magnetic field axis of A taken as the reference.

In dq coordinates the axis d leads the axis q and such arrangement is in accordance with the adopted standards of synchronous machine analysis [10, 24].

Inductance L_M appears in model of machines with salient poles; for machines with cylindrical rotors $L_M = 0$.

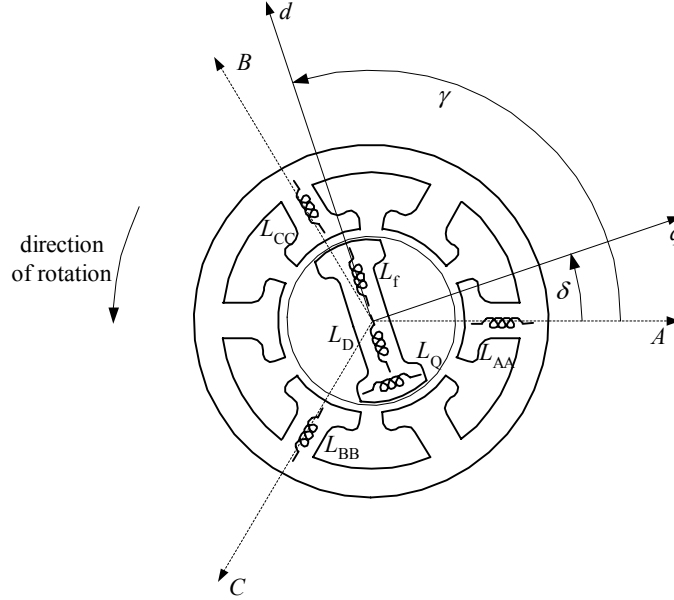


Fig. 6.3. the equivalent diagram of synchronous machine

The stator and rotor mutual inductances can be determined in the similar way:

$$L_{Af} = L_{fA} = M_f \cos \gamma, \quad L_{Bf} = L_{fB} = M_f \cos \left(\gamma - \frac{2\pi}{3} \right), \quad L_{Cf} = L_{fC} = M_f \cos \left(\gamma + \frac{2\pi}{3} \right),$$

$$L_{AD} = L_{DA} = M_D \cos \gamma, \quad L_{BD} = L_{DB} = M_D \cos \left(\gamma - \frac{2\pi}{3} \right),$$

$$L_{CD} = L_{DC} = M_D \cos \left(\gamma + \frac{2\pi}{3} \right),$$

$$L_{AQ} = L_{QA} = M_Q \sin \gamma, \quad L_{BQ} = L_{QB} = M_Q \sin \left(\gamma - \frac{2\pi}{3} \right), \quad L_{CQ} = L_{QC} = M_Q \sin \left(\gamma + \frac{2\pi}{3} \right).$$

The self- and mutual inductances of the rotor do not depend upon its angular position and the inductances of vertically laid windings are equal to zero:

$$L_{fD} = L_{Df} = M_R, \quad L_{fQ} = L_{Qf} = 0,$$

$$L_{DQ} = L_{QD} = 0.$$

The parameter matrix in (6.4) and (6.5) is symmetrical ($\mathbf{L}_{sr} = \mathbf{L}_{rs}^T$).

The machine model described by (6.3)–(6.7) is called the natural one or the machine model in phase coordinates. The model parameters are time-varying what is clearly noticeable after substitution of (6.6) into (6.3):

$$\mathbf{u} = -\mathbf{R}\mathbf{i} - \frac{d\mathbf{L}(\gamma)}{dt}\mathbf{i} - \mathbf{L}(\gamma)\frac{d\mathbf{i}}{dt} \quad (6.9)$$

Numerical solution of (6.9) is cumbersome and sometimes essential for the natural machine model feasibility.

Simplification of the problem is obtained by replacement of coordinates attached to the machine stator by the coordinates attached to the revolving rotor. The coordinates are determined by mutually vertical axes d - q . This approach is known as the Park's transformation. The third coordinate is related to the zero sequence component and is taken into account if the stator windings neutral point is earthed. The stator currents and voltages are transformed into $0dq$ coordinates in the following way:

$$\begin{aligned} \mathbf{i}_{0dq} &= \mathbf{P}^{-1}(\gamma)\mathbf{i}_{ABC} \\ \mathbf{u}_{0dq} &= \mathbf{P}^{-1}(\gamma)\mathbf{u}_{ABC} \end{aligned} \quad (6.10)$$

$$\text{where: } \mathbf{i}_{0dq} = \begin{bmatrix} i_0 \\ i_d \\ i_q \end{bmatrix}, \quad \mathbf{u}_{0dq} = \begin{bmatrix} u_0 \\ u_d \\ u_q \end{bmatrix}.$$

The same relation can be written for the magnetic flux.

Matrix $\mathbf{P}(\gamma)$ contains coefficients which project the stator phase quantities onto d - q axes of the revolving rotor. The zero sequence components are like in standard symmetrical component transformation:

$$\mathbf{P}^{-1}(\gamma) = \sqrt{\frac{2}{3}} \begin{bmatrix} \frac{1}{\sqrt{2}} & \frac{1}{\sqrt{2}} & \frac{1}{\sqrt{2}} \\ \cos \gamma & \cos\left(\gamma - \frac{2\pi}{3}\right) & \cos\left(\gamma + \frac{2\pi}{3}\right) \\ \sin \gamma & \sin\left(\gamma - \frac{2\pi}{3}\right) & \sin\left(\gamma + \frac{2\pi}{3}\right) \end{bmatrix} \quad (6.11)$$

The constant normalizing coefficient has been introduced to make the matrices orthogonal:

$$\mathbf{P}(\gamma) = [\mathbf{P}^{-1}(\gamma)]^T = \sqrt{\frac{2}{3}} \begin{bmatrix} \frac{1}{\sqrt{2}} & \cos \gamma & \sin \gamma \\ \frac{1}{\sqrt{2}} & \cos\left(\gamma - \frac{2\pi}{3}\right) & \sin\left(\gamma - \frac{2\pi}{3}\right) \\ \frac{1}{\sqrt{2}} & \cos\left(\gamma + \frac{2\pi}{3}\right) & \sin\left(\gamma + \frac{2\pi}{3}\right) \end{bmatrix} \quad (6.12)$$

and to simplify the inverse transformation:

$$\begin{aligned}\mathbf{i}_{ABC} &= \mathbf{P}(\gamma)\mathbf{i}_{0dq} \\ \mathbf{u}_{ABC} &= \mathbf{P}(\gamma)\mathbf{u}_{0dq}\end{aligned}\quad (6.13)$$

since now the normalizing coefficients used for both transformations are the same.

Substitution of (6.13) into (6.3) with reference to (6.4) and (6.5) leads to the following equation:

$$\begin{bmatrix} \mathbf{P}(\gamma) & \\ & \mathbf{1} \end{bmatrix} \begin{bmatrix} \mathbf{u}_{0dq} \\ \mathbf{u}_{fDQ} \end{bmatrix} = - \begin{bmatrix} \mathbf{r}_{ABC} & \\ & \mathbf{r}_{fDQ} \end{bmatrix} \begin{bmatrix} \mathbf{P}(\gamma) & \\ & \mathbf{1} \end{bmatrix} \begin{bmatrix} \mathbf{i}_{0dq} \\ \mathbf{i}_{fDQ} \end{bmatrix} - \frac{d}{dt} \left\{ \begin{bmatrix} \mathbf{P}(\gamma) & \\ & \mathbf{1} \end{bmatrix} \begin{bmatrix} \boldsymbol{\Psi}_{0dq} \\ \boldsymbol{\Psi}_{fDQ} \end{bmatrix} \right\} \quad (6.14)$$

and further:

$$\begin{bmatrix} \mathbf{u}_{0dq} \\ \mathbf{u}_{fDQ} \end{bmatrix} = - \begin{bmatrix} \mathbf{r}_{ABC} & \\ & \mathbf{r}_{fDQ} \end{bmatrix} \begin{bmatrix} \mathbf{i}_{0dq} \\ \mathbf{i}_{fDQ} \end{bmatrix} - \frac{d}{dt} \left\{ \begin{bmatrix} \boldsymbol{\Psi}_{0dq} \\ \boldsymbol{\Psi}_{fDQ} \end{bmatrix} \right\} + \begin{bmatrix} \boldsymbol{\Omega} & \\ & \mathbf{0} \end{bmatrix} \begin{bmatrix} \boldsymbol{\Psi}_{0dq} \\ \boldsymbol{\Psi}_{fDQ} \end{bmatrix} \quad (6.15)$$

where matrix:

$$\boldsymbol{\Omega} = \frac{d\mathbf{P}^{-1}(\gamma)}{dt} \mathbf{P}(\gamma) = \omega \begin{bmatrix} 0 & 0 & 0 \\ 0 & 0 & -1 \\ 0 & 1 & 0 \end{bmatrix} \quad (6.16)$$

is the rotation matrix [30].

Note that resistance matrix \mathbf{R} being diagonal remains unchanged after transformation. Moreover, it can be assumed that resistances in all phases are identical:

$$r_A = r_B = r_C = r_s.$$

To facilitate calculations (6.15) is represented using the machine resistance and inductance \mathbf{R} \mathbf{L} parameters. Substituting (6.13) into (6.5) we get:

$$\begin{bmatrix} \mathbf{P}(\gamma) & \\ & \mathbf{1} \end{bmatrix} \begin{bmatrix} \boldsymbol{\Psi}_{0dq} \\ \boldsymbol{\Psi}_{fDQ} \end{bmatrix} = \begin{bmatrix} \mathbf{L}_s & \mathbf{L}_{sr} \\ \mathbf{L}_{rs} & \mathbf{L}_r \end{bmatrix} \begin{bmatrix} \mathbf{P}(\gamma) & \\ & \mathbf{1} \end{bmatrix} \begin{bmatrix} \mathbf{i}_{0dq} \\ \mathbf{i}_{fDQ} \end{bmatrix}, \text{ and further:} \quad (6.17)$$

$$\begin{bmatrix} \boldsymbol{\Psi}_{0dq} \\ \boldsymbol{\Psi}_{fDQ} \end{bmatrix} = \begin{bmatrix} \mathbf{P}^{-1}(\gamma)\mathbf{L}_s\mathbf{P}(\gamma) & \mathbf{P}^{-1}(\gamma)\mathbf{L}_{sr} \\ \mathbf{L}_{sr}^T\mathbf{P}(\gamma) & \mathbf{L}_r \end{bmatrix} \begin{bmatrix} \mathbf{i}_{0dq} \\ \mathbf{i}_{fDQ} \end{bmatrix}$$

The inductance matrix in (6.17):

$$\mathbf{L}_E = \begin{bmatrix} \mathbf{P}^T(\gamma)\mathbf{L}_s\mathbf{P}(\gamma) & \mathbf{P}^T(\gamma)\mathbf{L}_{sr} \\ \mathbf{L}_{sr}^T\mathbf{P}(\gamma) & \mathbf{L}_r \end{bmatrix} = \begin{bmatrix} L_0 & 0 & 0 & 0 & 0 & 0 \\ 0 & L_d & 0 & k_1 M_f & k_1 M_D & 0 \\ 0 & 0 & L_q & 0 & 0 & k_1 M_Q \\ 0 & k_1 M_f & 0 & L_f & M_R & 0 \\ 0 & k_1 M_D & 0 & M_R & L_D & 0 \\ 0 & 0 & k_1 M_Q & 0 & 0 & L_Q \end{bmatrix} \quad (6.18)$$

is constant and time invariant and:

$$L_0 = L_s - 2M_s, \quad L_d = L_s + M_s + k_1^2 L_M, \quad L_q = L_s + M_s - k_1^2 L_M, \quad k_1 = \sqrt{3/2}.$$

Moreover, the normalized form of matrix $\mathbf{P}(\gamma)$ makes the inductance matrix symmetrical thus facilitating the respective numerical calculation procedures.

Finally, (6.17) can be written in the following compact form:

$$\boldsymbol{\Psi}_E = \mathbf{L}_E \mathbf{i}_E \quad (6.19)$$

$$\text{where: } \boldsymbol{\Psi}_E = \begin{bmatrix} \Psi_{0dq} \\ \Psi_{fDQ} \end{bmatrix}, \quad \mathbf{i}_E = \begin{bmatrix} \mathbf{i}_{0dq} \\ \mathbf{i}_{fDQ} \end{bmatrix}.$$

Relations between electric quantities in $0dq$ model of electric machine are presented graphically in Fig. 6.4.

In similar compact form (6.15) can be written:

$$\frac{d\boldsymbol{\Psi}_E}{dt} = -\mathbf{R}\mathbf{i}_E - \mathbf{u}_E + \mathbf{u}_\omega \quad (6.20)$$

or:

$$\frac{d\mathbf{i}_E}{dt} = \mathbf{L}_E^{-1}(-\mathbf{R}\mathbf{i}_E - \mathbf{u}_E + \mathbf{u}_\omega), \quad (6.21)$$

where:

$$\mathbf{u}_E = \begin{bmatrix} \mathbf{u}_{0dq} \\ \mathbf{u}_{fDQ} \end{bmatrix}, \quad \mathbf{u}_\omega = \begin{bmatrix} 0 \\ -\omega\psi_q \\ \omega\psi_d \\ \mathbf{0} \end{bmatrix},$$

$$\psi_q = L_q i_q + k_1 M_Q i_Q, \quad \psi_d = L_d i_d + k_1 (M_f i_f + M_D i_D).$$

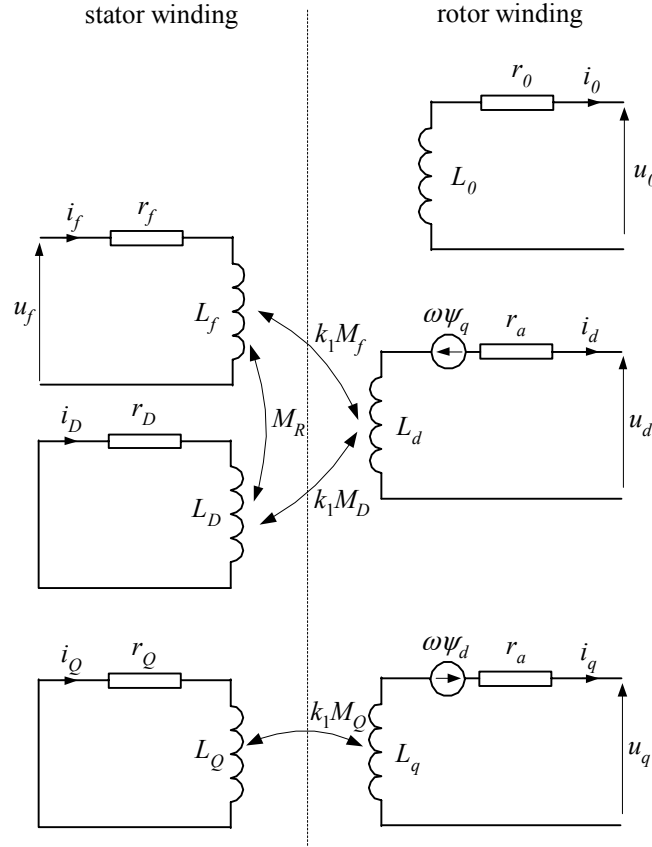


Fig. 6.4. Graphical representation of synchronous machine for $0dq$ coordinates

Equations (6.20) – in flux notation or (6.21) – in voltage notation, along with (6.10) and (6.13), define the electric part of the synchronous machine for $0dq$ coordinates (Fig. 6.4). The angular velocity ω in (6.21) refers to magnetic field changes and is related to the rotor angular velocity according to (6.8) which describes the coupling between electrical and mechanical part of the machine model.

The presented model can be modified according to actual needs (simplification of calculations, better representation of electromagnetic effects). In order to obtain the identical coefficients of mutual inductance the transformation ratios between windings in d axis can be modified [24]:

$$\sqrt{3/2}M_f = \sqrt{3/2}M_D = M_R = L_{ad}.$$

The modification is effective for correct turn numbers in particular windings. The first equation ($M_f = M_D$) can easily be satisfied since the damping winding is

dummy. The second one is true for corrected turn number of the excitation winding which can be calculated from the following relations:

$$i_{fm} = \frac{1}{k_1 k_m} i_f, \quad \psi_{fm} = k_1 k_m \psi_f, \quad u_{fm} = k_1 k_m u_f, \quad (6.22)$$

where: $k_m = \frac{M_f}{M_R}$.

The modification also requires the adequate rescaling of the excitation current value what can be done outside of the model.

Due to the modification the equivalent voltages in the coupled magnetic circuits (Fig. 6.4) are the same so the circuits can be directly connected. As a result the equivalent circuits as shown in Fig. 6.5 are obtained. Splitting (6.21) into three parts respectively related to $0dq$ coordinates we get:

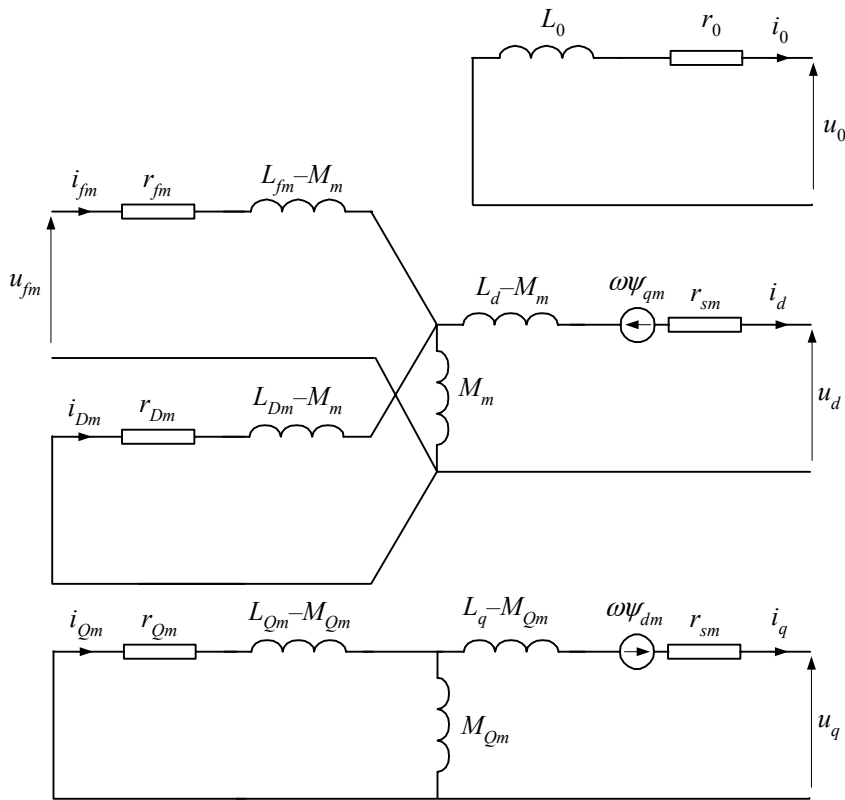


Fig. 6.5. The equivalent circuit diagram of the synchronous machine for $0dq$ coordinates

$$\frac{d}{dt} \begin{bmatrix} i_d \\ i_{fm} \\ i_{Dm} \end{bmatrix} = \begin{bmatrix} L_d & M_m & M_m \\ M_m & L_{fm} & M_m \\ M_m & M_m & L_{Dm} \end{bmatrix}^{-1} \left(- \begin{bmatrix} r_s & & \\ & r_{fm} & \\ & & r_{Dm} \end{bmatrix} \begin{bmatrix} i_d \\ i_{fm} \\ i_{Dm} \end{bmatrix} - \begin{bmatrix} u_d \\ -u_{fm} \\ 0 \end{bmatrix} + \begin{bmatrix} -\omega\psi_{qm} \\ 0 \\ 0 \end{bmatrix} \right) \quad (6.23)$$

$$\frac{d}{dt} \begin{bmatrix} i_q \\ i_{Qm} \end{bmatrix} = \begin{bmatrix} L_q & M_{Qm} \\ M_{Qm} & L_{Qm} \end{bmatrix}^{-1} \left(- \begin{bmatrix} r_s & \\ & r_{Qm} \end{bmatrix} \begin{bmatrix} i_q \\ i_{Qm} \end{bmatrix} - \begin{bmatrix} u_q \\ 0 \end{bmatrix} + \begin{bmatrix} \omega\psi_{dm} \\ 0 \end{bmatrix} \right) \quad (6.24)$$

$$\frac{di_0}{dt} = -\frac{r_0}{L_0} i_0 - \frac{u_0}{L_0}, \quad (6.25)$$

where:

$$\begin{aligned} \psi_q &= L_q i_q + M_{Qm} i_{Qm}, & \psi_d &= L_d i_d + M_m (i_{fm} + i_{Dm}), & M_m &= k_1^2 k_m M_f, & L_{fm} &= k_1^2 k_m^2 L_f, \\ L_{Dm} &= k_1^2 k_m^2 L_D, & L_{Qm} &= k_1^2 k_m^2 L_Q, & M_{Qm} &= k_1^2 k_m M_Q, & r_{fm} &= k_1^2 k_m^2 r_f, & r_{Dm} &= k_1^2 k_m^2 r_D, \\ r_{Qm} &= k_1^2 k_m^2 r_Q. \end{aligned}$$

The coefficient k_m in (6.22) can be determined by measurements for idle (no load) run of the machine [24] when $i_d = i_q = i_D = 0$ and $u_q = \omega M_m i_{fm}$. Then, using (6.22), we can write:

$$k_m = \frac{\omega_{1N} M_m i_{f0}}{\sqrt{3} k_1 U_G} = \frac{\sqrt{3} U_G r_{fm}}{k_1 \omega_{1N} M_m}, \quad (6.26)$$

where: U_G – the nominal voltage of the generator (r.m.s. phase-to-phase value for stator windings in delta arrangement or r.m.s. phase-to-ground value for stator windings in star arrangement), i_{f0} – the excitation current for machine idle run.

It is assumed that the machine model parameters in q axis can be modified by use of the same coefficient k_m .

More accurate modelling of the machine operation in transient states can be achieved if the greater number of the dummy short-circuited windings is included into the machine model in both (d and q) axes. Having different parameters the windings can model the effects in the machine iron that have different time constants [4, 8, 57].

The parameters r_{fm} i M_m in (6.26) as well as the other ones are determined according to the specified standards [64]. The machine parameters measurements can be carried out both in short-circuit and in idle run conditions. Usually the following machine parameters are deemed to be the basic ones [24, 64]:

- R_s – stator winding resistance;
- X_l – stator winding stray reactance;
- X_0 – zero sequence reactance of the machine;

X'_d, X'_q – transient reactance: series and transverse, respectively;

X''_d, X''_q – sub-transient reactance: series and transverse, respectively;

τ'_d, τ'_q – transient time constants: series and transverse, respectively;

τ''_d, τ''_q – sub-transient time constant: series and transverse, respectively.

The reactances in the list above refer to the nominal frequency, for example, $X_l = \omega_{1N} L_l$ while the time constants determine the transient d.c. components decay rate:

$$\tau = \frac{L}{R} = \frac{X}{\omega_{1N} R}.$$

Parameters which refer to the open generator circuits (idle run) are denoted by extra 'o' in the subscript, for example: τ'_{do} denotes the time constant in d axis for the idly running generator.

The further details concerning the machine model parameters determination can be found in [4, 24, 64].

b) Saturation Consideration

Accurate modelling of magnetic circuit saturation effect in rotating machines is a complex problem which requires the cumbersome analysis of the machine magnetic core design by use of advanced numerical methods like Finite Element Method [123]. Therefore the commonly applied methods of transient state analysis in electric machines are based on the following simplifying assumptions [24, 60]:

- the overall magnetic flux produced by a given winding comprises of the basic and the stray flux only; the saturation intensity of the magnetic material depends upon the value of the overall magnetic flux;
- the stray flux does not get saturated;
- the mutual inductance of the rotor is sinusoidal;
- the hysteresis and the eddy currents effects are negligible.

The magnetizing characteristic of the idly running generator (open stator circuit while the excitation current is changed at nominal rotation velocity) is necessary for inclusion of the saturation effect into the machine model (see Fig. 6.6 [53]). The characteristic can be continuous or piecewise approximated.

Calculation of saturation effect impact is carried out by iteration process in which the new points on magnetizing characteristics are calculated for all generators present in the analysed network. The process is illustrated in Fig. 6.6. The reference base for inductance calculation is the linear part of the magnetizing characteristic whose slope $m_l = \tan(\alpha_l)$. Let's assume that the machine working point A_1 has been determined in

the current calculation step. The point is located on the linear characteristic whose slope $m_2 = \tan(\alpha_2)$. In the next calculation step the new operating point A_2 located on the same linear characteristic is determined along with the new value of the magnetizing current i_{m2} . Using this new excitation current value the corrected flux B_2 is calculated from the nonlinear magnetizing characteristic.

The resulting inductance correction ratio is: $\chi_2 = m_2/m_l$. According to the simplifying assumptions correction concerns the main flux only, for example:

$$L_{d_nas} = L_{dl} + \chi_2 k_1 M_f, \quad (6.27)$$

where: L_{dl} – stray inductance along d axis or:

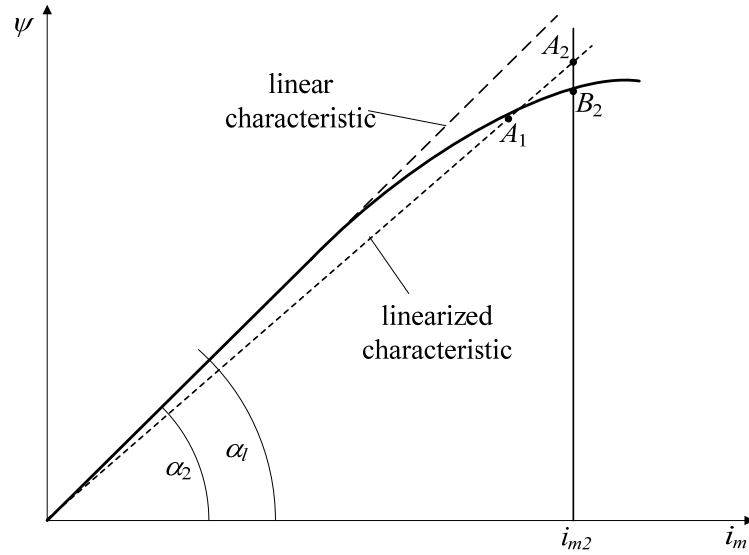


Fig. 6.6. Idle run magnetizing characteristic of the generator

$$M_{R_nas} = \chi_2 M_R \quad (6.28)$$

for the mutual inductance f - D (Fig. 6.4).

The algorithm can be modified according to the numerical methods being used for calculations [24, 53, 60].

c) Mechanical Model

The basic dynamic equation of the machine rotor mechanical balance is as follows:

$$J \frac{d^2 \gamma_r}{dt^2} + D \frac{d\gamma_r}{dt} = T_t - T_e, \quad (6.29)$$

where: J – inertia torque of the rotating mass, $(\text{kg}\cdot\text{m}^2)^{10}$; D – damping factor, $(\text{N}\cdot\text{m}/(\text{rad}/\text{s}))$; T_t , T_e – turbine (mechanical) and generator (electromechanical) torque, respectively, $(\text{N}\cdot\text{m})$.

The angle γ_r is related to ω_r by (6.7). In case of power generator $-T_t > T_e$ – turbine energy is transmitted to power system.

Electromagnetic torque of the machine can be determined from (6.9). For $\mathbf{i} = \mathbf{i}(t)$, $\gamma = \gamma(t)$ and for $\mathbf{L} = \mathbf{L}(i_L, \gamma)$, where i_L – the current in inductance which is an element of matrix \mathbf{L}^{11} we get:

$$\mathbf{u} = -\mathbf{R}\mathbf{i} - \left(\frac{\partial \mathbf{L}}{\partial i_L} \frac{di_L}{dt} + \frac{\partial \mathbf{L}}{\partial \gamma} \frac{d\gamma}{dt} \right) \mathbf{i} - \mathbf{L} \frac{d\mathbf{i}}{dt} \quad (6.30)$$

Multiplying (6.30) by vector \mathbf{i}^T the instantaneous machine power is obtained:

$$P_G = -P_R - P_L - P_e \quad (6.31)$$

where:

$$P_G = \mathbf{i}^T \mathbf{u} \text{ – output power,} \quad (6.32)$$

$$P_R = \mathbf{i}^T \mathbf{R} \mathbf{i} \text{ – power loss in windings,} \quad (6.33)$$

$$P_L = \frac{\partial E_L}{\partial t} = \frac{\partial}{\partial t} \left(\frac{1}{2} \mathbf{i}^T \mathbf{L} \mathbf{i} \right) = \mathbf{i}^T \left(\mathbf{L} \frac{d\mathbf{i}}{dt} + \frac{\partial \mathbf{L}}{\partial i_L} \frac{di_L}{dt} \mathbf{i} + \frac{1}{2} \frac{\partial \mathbf{L}}{\partial \gamma} \frac{d\gamma}{dt} \mathbf{i} \right) \text{ – magnetizing power,} \quad (6.34)$$

E_L – energy of electromagnetic field,

$$P_e = \frac{1}{2} \mathbf{i}^T \frac{\partial \mathbf{L}}{\partial \gamma} \frac{d\gamma}{dt} \mathbf{i} = \frac{p}{2} \mathbf{i}^T \frac{\partial \mathbf{L}}{\partial \gamma} \mathbf{i} \omega_r = T_e \omega_r \text{ – electromagnetic power.} \quad (6.35)$$

The electromagnetic torque in the air slot between stator and rotor is given by the equation:

$$T_e = \frac{p}{2} \mathbf{i}^T \left(\frac{d\mathbf{L}}{d\gamma} \right) \mathbf{i} \quad (6.36)$$

where \mathbf{i} is the vector of phase currents in stator and rotor and \mathbf{L} is like in (6.6).

Using $0dq$ coordinates (6.36) reduces to [9]:

$$T_e = p(\psi_d i_q - \psi_q i_d) \quad (6.37)$$

¹⁰ Inertia torque is also expressed in $(\text{N}\cdot\text{m}\cdot\text{s}^2)$; $1 \text{ kg}\cdot\text{m}^2 = 1 \text{ N}\cdot\text{m}\cdot\text{s}^2$.

¹¹ Important for nonlinear magnetic circuits where inductance is a function of current.

The remarks concerning the physical interpretation of discussed relations are:

- Signs of particular powers in (6.31) correspond to current and voltage notation in Fig. 6.5.
- The magnetizing power P_L is produced by each magnetic field change while P_e is related to the rotor rotation (changing angle γ).
- The zero sequence component (6.37) does not affect the electromagnetic torque.

Sometimes, instead of inertia torque, the inertia constant H is used and:

$$H = \frac{E_N}{S_N}, 1 \frac{\text{W} \cdot \text{s}}{\text{VA}} = 1 \frac{\text{MW} \cdot \text{s}}{\text{MVA}} \quad (6.38)$$

where:

$$E_N = \frac{1}{2} J \omega_{rN}^2 \times 10^{-6} \text{ (MW} \cdot \text{s)} - \text{energy of rotating mass}^{12};$$

ω_{rN} – nominal (synchronous) rotor angle velocity (1/s);

S_N – nominal apparent power (MVA).

Thus:

$$H = \frac{0.5 J \omega_{rN}^2 \times 10^{-6}}{S_N} = 5.4831 \times 10^{-9} \frac{J \cdot n_N^2}{S_N} \text{ (s)} \quad (6.39)$$

where $n_N = \frac{60 \omega_{rN}}{2\pi}$ – nominal rotating velocity (rot/min).

Equation (6.29) and definition (6.38) show that for nominal driving torque $T_t = T_{tN}$ (N·m) at $D = 0$ machine will attain the nominal rotation velocity after time $\tau_m = 2H$ (s) (parameter τ_m is sometimes called the mechanical time constant [57] or the running in time. The inertia torque J in (6.29) can be expressed by parameters which are easier to obtain:

$$J = \frac{\tau_m \cdot S_N}{\omega_{rN}^2} \times 10^6 = \frac{2H \cdot S_N}{\omega_{rN}^2} \times 10^6 = \frac{182.378 \cdot H \cdot S_N}{n_N^2} \times 10^6 \quad (6.40)$$

and the dynamic equation of the machine can be rewritten as:

$$\frac{H \cdot S_N}{\pi f_{rN}} \frac{d^2 \gamma_r}{dt^2} + \omega_{rN} D \frac{d\gamma_r}{dt} = P_t - P_g \quad (6.41)$$

where: f_{rN} – nominal rotor frequency (Hz); P_t , P_g – turbine and generator power (MW), respectively.

¹² 1 W·s = 1 N·m = 1 J.

The time constant τ_m takes the values from the range 1–20 s depending on the size and the nominal power of the machine.

If the rotating system contains several masses linked by resilient couplings then the mechanical torque conveyed is proportional to the angle displacement between particular elements (Fig. 6.7). In such a multi-section arrangement couplings convey the resilience torque T_s to adjacent elements so the torque signs have to be differentiated accordingly. In general case we have [24]:

$$T_{s,i-1} = K_{i-1,i}(\gamma_{i-1} - \gamma_i) = -T_{s,i} \quad (6.42)$$

where: $K_{i-1,i}$ – the resilience coefficient between rotating masses $i-1, i$.

The damping in particular elements also has to be differentiated as the 'self-' and the mutual one. The latter represents losses caused by the resilient link swings and can be expressed by the following equation:

$$T_{d,i} = D_i \frac{d\gamma_i}{dt} + D_{i-1,i} \frac{d}{dt}(\gamma_i - \gamma_{i-1}) + D_{i,i+1} \frac{d}{dt}(\gamma_i - \gamma_{i+1}) \quad (6.43)$$

where: $D_{i-1,i}$, $D_{i,i+1}$ – damping coefficients in couplings between respective masses.

In the system shown in Fig 6.7 sections 1–3 generate the driving torque (in direction of the system rotation) while sections 4–5 are those driven ones.

Using (6.42) and (6.43) the multi-mass system equation takes the form:

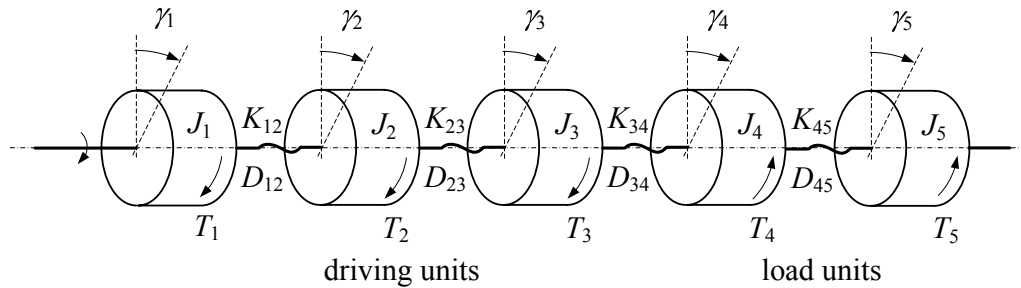


Fig. 6.7. Diagram of the multi-stage rotating system

$$\mathbf{J} \frac{d^2}{dt^2} \boldsymbol{\gamma} + \mathbf{D} \frac{d}{dt} \boldsymbol{\gamma} + \mathbf{K} \boldsymbol{\gamma} = \mathbf{T}_t - \mathbf{T}_e, \quad (6.44)$$

where:

\mathbf{J} – diagonal matrix of inertia torque (J_1, J_2, \dots, J_n) for particular elements;

$\boldsymbol{\gamma}$ – vector of angles ($\gamma_1, \gamma_2, \dots, \gamma_n$) for particular elements;

\mathbf{K} – matrix of the resilience coefficients;

$$\mathbf{K} = \begin{bmatrix} K_{12} & -K_{12} & & & \vdots & & \\ -K_{12} & K_{12} + K_{23} & -K_{23} & & \vdots & & \\ & -K_{23} & K_{23} + K_{34} & -K_{34} & \vdots & & \\ \dots & \dots & \dots & \dots & \vdots & \dots & \dots \\ & & & & \vdots & -K_{n-1,n} & K_{n-1,n} \end{bmatrix},$$

\mathbf{D} – matrix of damping coefficients:

$$\mathbf{D} = \begin{bmatrix} D_1 + D_{12} & -D_{12} & & & \vdots & & \\ -D_{12} & D_{12} + D_2 + D_{23} & -D_{23} & & \vdots & & \\ & -D_{23} & D_{23} + D_3 + D_{34} & -D_{34} & \vdots & & \\ \dots & \dots & \dots & \dots & \vdots & \dots & \dots \\ & & & & \vdots & -D_{n-1,n} & D_{n-1,n} + D_n \end{bmatrix}$$

\mathbf{T}_t – vector of turbine driving torques;

\mathbf{T}_e – vector of electric driving torques

Since (6.44) refers to the generator so the rotor angle $\gamma = \gamma_4$ in Fig. 6.7. Parameters required in (6.44) are usually difficult to obtain so the model can be applied to special cases only.

In EMTP the mechanical part model of synchronous machine is combined with the electrical part model by default so user should only enter the necessary data.

d) Calculation Algorithms

In complex power system simulation models the generator equations should be solved along with the equations of the other system elements. However, due to the specific form of the generator equations the direct representation of the system equations (for instance, the use of the nodal voltage method) becomes difficult. Therefore, in practice, the generator models and the models of the other system elements are processed as separated subsystems. To ensure the electric balance between particular subsystems (voltages and currents in common nodes and branches must be the same) the adequate numerical methods of simultaneous calculations for all subsystems have to be applied. For this purpose one of the following methods is used:

1. Direct *iteration method* of the system balance calculation in each simulation step. Solving the generator equations for specified initial conditions (calculated in previous iteration step) the new current values at the generator output terminals are determined which, in turn, are used for calculation of voltages in the other subsystems which become the corrected generator output voltages. The calculation process is continued until the assumed convergence of results is obtained [57].
2. Representation of the network by the equivalent voltage (Thévenin's theorem) or current (Norton's theorem) source. The equivalent circuit is connected to the

generator and solved along with the machine equations. This approach is called the *compensation method*¹³ [12, 24].

3. Representation of electric machines by the equivalent voltage or current sources connected to the system model. The method is known as *prediction method* [12, 24, 60]. Common calculations ensure balance between both subsystems but some machine quantities must be predicted.

The direct *iteration method* is accurate and stable but due to iterations applied in each simulation step makes the calculations time-consuming.

The *compensation method* is also accurate but the subsystem with generators must not contain any true type nonlinear element. In ATP–EMTP this method is used by the model of Universal Machine (UM) [7, 12].

The *prediction method* is applied in EMTP to simulation of complex networks (Type 59 model) [24].

6.1.2. Model in Phase Coordinates

The basic drawback of the synchronous machine representation in $0dq$ coordinates is the lack of direct transformation between $0dq$ and phase coordinates since transformation coefficients depend upon solution which is unknown and use of extrapolations may result in instability of the network model [12].

The generator model in phase coordinates is as follows:

$$\frac{d}{dt} \begin{bmatrix} \mathbf{L}_s(\gamma) & \mathbf{L}_{sr}(\gamma) \\ \mathbf{L}_{rs}(\gamma) & \mathbf{L}_r(\gamma) \end{bmatrix} \begin{bmatrix} \mathbf{i}_{ABC} \\ \mathbf{i}_{jDQ} \end{bmatrix} = - \begin{bmatrix} \mathbf{r}_{ABC} & \\ & \mathbf{r}_{jDQ} \end{bmatrix} \begin{bmatrix} \mathbf{i}_{ABC} \\ \mathbf{i}_{jDQ} \end{bmatrix} - \begin{bmatrix} \mathbf{u}_{ABC} \\ \mathbf{u}_{jDQ} \end{bmatrix} \quad (6.45)$$

where the notation is like in (6.3)–(6.7) and usually $\mathbf{L}_r(\gamma) = \mathbf{L}_r$.

On the basis of (6.3) the digital model of the generator is developed and is directly connected to the network model. Both models are solved together. Calculations are carried out according to the following algorithm [12, 13]:

1. Predict the rotor angular velocity ω and the rotor angle position γ . Determine the equivalent parameters of the generator.
2. Calculate the rotor currents and the electric torque using (6.36). Solving the equations of the mechanical model the new values of ω and γ are obtained.
3. Check the solution convergence with respect to ω . In case of unacceptable discrepancy return to p. 2.

In EMTP the method is applied in Type-58 generator model [13]. The method is stable and the nonlinear elements in the network model are acceptable [53, 60].

¹³ Compare with p. 2.3.2.

6.2. Induction Machines

6.2.1. General Notes

The name *induction machine* refers to the wide group of rotating electric machines in which electromagnetic (generators) or electrodynamic (motors) force is produced by magnetic fields induced in stator and rotor. The rotor magnetic field is produced by the current induced in the rotor windings (or short-circuited cages) when the rotor moves in the stator magnetic field. Contrary to synchronous machines the rotor and stator magnetic field frequencies are different and that is why the induction machines are also called the asynchronous ones.

Taking into account the design features induction machines of the following types are used in practice:

1. **Cage (or squirrel-cage) rotor electric machines** in which the rotor winding is made of copper or aluminium rods connected at their ends (Fig. 6.8). In case of the cage machine the alternate stator magnetic field induces electric current in the rotor cage and the resulting rotor magnetic flux produces the rotation torque.

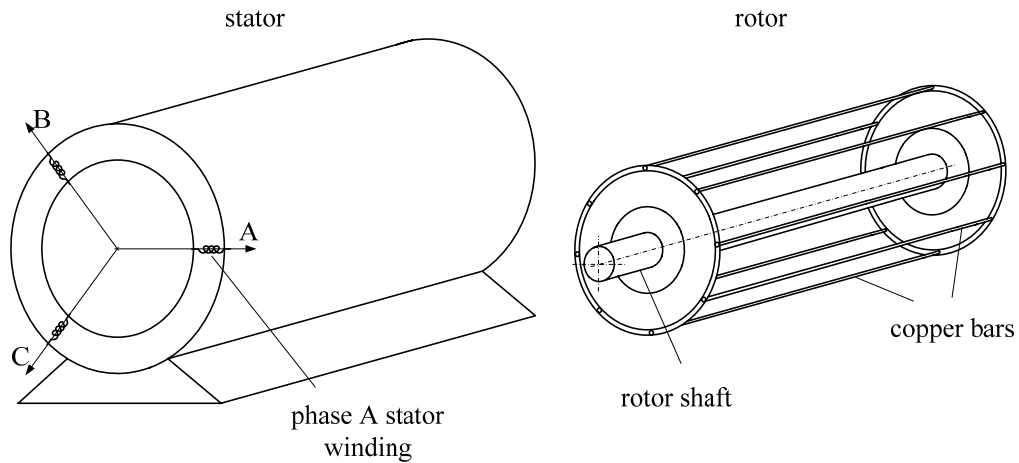


Fig. 6.8. Squirrel-cage induction machine model

Stator and rotor magnetic fields rotate in the same direction so the current in rotor cage can be induced when the stator and rotor rotation velocities are different. The difference is defined as the slip s and:

$$s = \frac{n_1 - n_e}{n_1} = \frac{\omega_1 - \omega_e}{\omega_1} \quad (6.46)$$

where: n_1 – synchronous rotation velocity (angular velocity ω_1), n_e – rotor field rotation velocity (rotor field angular velocity ω_e).

In the machine with pole pairs number $p > 1$:

$$\omega_e = p\omega_r \quad (6.47)$$

where ω_r - rotor angular velocity and:

$$\omega_r = \frac{\omega_1(1-s)}{p} \quad (6.48)$$

The current in symmetrical rotor winding has the frequency:

$$f_r = \frac{sf_1}{p} = \frac{s}{1-s} \frac{n_r}{60} \text{ (Hz)} \quad (6.49)$$

where $n_r = n$ – rotation velocity (rot/min).

The value of slip depends upon machine operating state. At the beginning of machine starting $s=1$ and decreases gradually to the value $s > 0$ which depends on machine load. In case of induction power generator $s < 0$.

To facilitate the machine starting (to get the greater torque for reduced inrush current) the machine rotors are modified by application of *multi-cage* and *deep bar* rotor designs (Fig. 6.9).

Such designs take advantage of the skin effect properties to increase the rotor resistance during machine inrush when the machine slip is big.

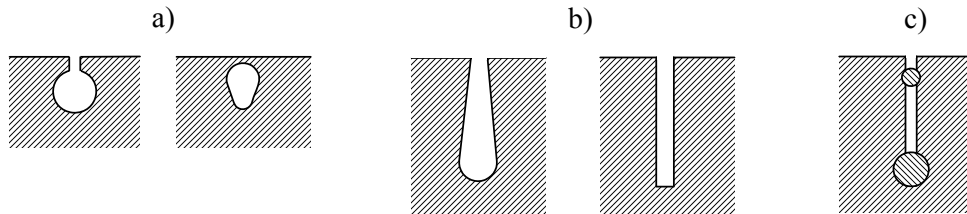


Fig. 6.9. Examples of rotor design: a) normal, b) deep, c) double cage

2. **Wound-rotor machines** in which standard windings (in star or delta arrangement) are connected to *slip rings* (Fig. 6.10).

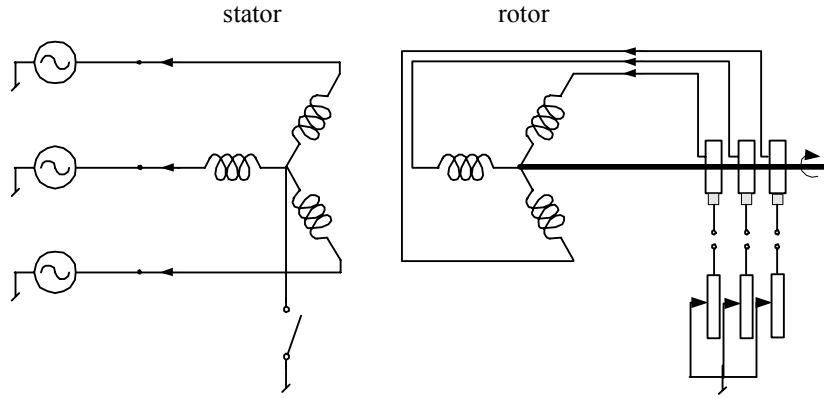


Fig. 6.10. Slip ring machine model.

Such design essentially facilitates the machine inrush process since the external variable resistances can be connected in series with the rotor windings. The value of the start controlling resistances, being large at the beginning of machine starting, is gradually reduced to zero when machine rotation speed increases [6, 10].

3. **Doubly-fed induction machine** design is similar to the wound-rotor machine one; here the slip rings are used for connection of external excitation source of specified frequency so the machine rotation speed (in motor) or the output voltage frequency (in generator) can be controlled [9]. In some conditions the doubly-fed machines behave like the synchronous ones. Mutual reaction of rotor and stator magnetic fields of frequencies f_{rs} and f_r , respectively, fixes the ‘synchronous’ rotation speed at the value determined by slip according to (6.46).

6.2.2. Mathematical Model

Induction and synchronous machine models are very much alike. The voltage equation in phase coordinates for a single three phase rotor winding is like in (6.3):

$$\begin{bmatrix} \mathbf{u}_{ABC(s)} \\ -\mathbf{u}_{ABCr(r)} \end{bmatrix} = - \begin{bmatrix} \mathbf{R}_s & \\ & \mathbf{R}_{rr} \end{bmatrix} \begin{bmatrix} \mathbf{i}_{ABC(s)} \\ \mathbf{i}_{ABCr(r)} \end{bmatrix} - \frac{d}{dt} \begin{bmatrix} \boldsymbol{\Psi}_{ABC(s)} \\ \boldsymbol{\Psi}_{ABCr(r)} \end{bmatrix} \quad (6.50)$$

where the extra ‘ r ’ subscript indicates the rotor winding.

The rotor winding voltages can be different from zero in doubly-fed machines. Magnetic fluxes produced by stator (s) and rotor windings (r) can be determined by the following equation:

$$\begin{bmatrix} \Psi_{ABC(s)} \\ \Psi_{ABCr(r)} \end{bmatrix} = \begin{bmatrix} \mathbf{L}_s & \mathbf{L}_{sr} \\ \mathbf{L}_{rs} & \mathbf{L}_r \end{bmatrix} \begin{bmatrix} \mathbf{i}_{ABC(s)} \\ \mathbf{i}_{ABCr(r)} \end{bmatrix} \quad (6.51)$$

where the inductance matrices comprise of the following sub-matrices:

$$\mathbf{L}_s = \begin{bmatrix} L_{ss} & -\frac{L_{Ms}}{2} & -\frac{L_{Ms}}{2} \\ -\frac{L_{Ms}}{2} & L_{ss} & -\frac{L_{Ms}}{2} \\ -\frac{L_{Ms}}{2} & -\frac{L_{Ms}}{2} & L_{ss} \end{bmatrix}, \quad \mathbf{L}_r = \begin{bmatrix} L_{rr} & -\frac{L_{Mr}}{2} & -\frac{L_{Mr}}{2} \\ -\frac{L_{Mr}}{2} & L_{rr} & -\frac{L_{Mr}}{2} \\ -\frac{L_{Mr}}{2} & -\frac{L_{Mr}}{2} & L_{rr} \end{bmatrix},$$

$$\mathbf{L}_{sr} = L_{sr} \begin{bmatrix} \cos \gamma & \cos\left(\gamma + \frac{2\pi}{3}\right) & \cos\left(\gamma - \frac{2\pi}{3}\right) \\ \cos\left(\gamma - \frac{2\pi}{3}\right) & \cos \gamma & \cos\left(\gamma + \frac{2\pi}{3}\right) \\ \cos\left(\gamma + \frac{2\pi}{3}\right) & \cos\left(\gamma - \frac{2\pi}{3}\right) & \cos \gamma \end{bmatrix}, \quad \mathbf{L}_{rs} = \mathbf{L}_{sr}^T,$$

and:

$$L_{Ms} = L_{sr} \frac{N_s}{N_r}, \quad L_{Mr} = L_{sr} \frac{N_r}{N_s}, \quad L_{ss} = L_{sl} + L_{Ms}, \quad L_{rr} = L_{rlr} + L_{Mr},$$

L_{sl} , L_{rlr} – stator and rotor stray inductance, respectively,

L_{sr} – magnitude of mutual inductance between stator and rotor windings,

N_s , N_r – number of turns in stator and rotor, respectively,

$\gamma = \gamma_e$ – electric angle between stator and rotor coordinates.

To simplify the machine equivalent model the rotor circuit voltages can be transformed to the level of the stator windings ones. The relevant transformation formulas are [10]:

$$k_{sr} = \frac{L_{sr}}{L_{Ms}}, \quad k_{sr}^2 = \frac{L_{Mr}}{L_{Ms}}, \quad L_{rl} = \frac{L_{rlr}}{k_{sr}^2}, \quad R_r = \frac{R_{rr}}{k_{sr}^2} \quad (6.52)$$

$$\mathbf{u}_{ABC(r)} = \frac{1}{k_{sr}} \mathbf{u}_{ABCr(r)}, \quad \mathbf{i}_{ABC(r)} = k_{sr} \mathbf{i}_{ABCr(r)}$$

The next step towards the induction machine model simplification is the transformation of the stator and rotor phase coordinates into the $0dq$ ones:

$$\begin{bmatrix} \mathbf{u}_{0dq(s)} \\ -\mathbf{u}_{0dq(r)} \end{bmatrix} = - \begin{bmatrix} \mathbf{R}_{0dq(s)} & \\ & \mathbf{R}_{0dq(r)} \end{bmatrix} \begin{bmatrix} \mathbf{i}_{0dq(s)} \\ \mathbf{i}_{0dq(r)} \end{bmatrix} - \frac{d}{dt} \left\{ \begin{bmatrix} \Psi_{0dq(s)} \\ \Psi_{0dq(r)} \end{bmatrix} \right\} + \begin{bmatrix} \boldsymbol{\Omega} & \\ \mathbf{0} & \end{bmatrix} \begin{bmatrix} \Psi_{0dq(s)} \\ \Psi_{0dq(r)} \end{bmatrix} \quad (6.53)$$

where the angular velocity in the matrix $\mathbf{\Omega}$ (6.16) is the rotor electric velocity: $\omega = p\omega_r$; $\Psi_{0dq(s)}$, $\Psi_{0dq(r)}$ denote the stator (s) and rotor (r) magnetic fluxes in $0dq$ coordinates – like in (6.17):

$$\begin{bmatrix} \Psi_{0dq(s)} \\ \Psi_{0dq(r)} \end{bmatrix} = \begin{bmatrix} \mathbf{P}^{-1}(\gamma) & 0 \\ 0 & \mathbf{C} \end{bmatrix} \begin{bmatrix} \mathbf{L}_s & \mathbf{L}_{sr} \\ \mathbf{L}_{sr}^T & \mathbf{L}_r \end{bmatrix} \begin{bmatrix} \mathbf{P}(\gamma) & 0 \\ 0 & \mathbf{C}^{-1} \end{bmatrix} \begin{bmatrix} \mathbf{i}_{0dq(s)} \\ \mathbf{i}_{0dq(r)} \end{bmatrix} \quad (6.54)$$

in which matrix \mathbf{C} represents relation between phase (ABC) and $0dq$ rotor coordinates.

Elements of vector $\mathbf{u}_{0dq(r)}$ are different from zero for the slip-ring machines (Fig. 6.10); in cage machines the rotor circuits are short-circuited. The transformation matrix $\mathbf{P}(\gamma)$ is like in (6.11); γ is the electric angle and can be calculated from (6.7) for $\omega = p\omega_r$ so, that:

$$\frac{d\gamma}{dt} = p\omega_r = \omega_e \quad (6.55)$$

Matrix \mathbf{C}^{-1} transforms the three phase quantities in the rotor winding into $0dq$ coordinates and is related to the matrix $\mathbf{P}(\gamma)$ by the following equation:

$$\mathbf{P}(\gamma) = \mathbf{C} \cdot \mathbf{E}(\gamma) = \sqrt{\frac{2}{3}} \begin{bmatrix} \frac{1}{\sqrt{2}} & 1 & 0 \\ \frac{1}{\sqrt{2}} & -\frac{1}{2} & \frac{\sqrt{3}}{2} \\ \frac{1}{\sqrt{2}} & -\frac{1}{2} & -\frac{\sqrt{3}}{2} \end{bmatrix} \cdot \begin{bmatrix} 1 & 0 & 0 \\ 0 & \cos \gamma & \sin \gamma \\ 0 & \sin \gamma & -\cos \gamma \end{bmatrix} \quad (6.56)$$

Matrix \mathbf{C} is known as the transformation matrix between three phase and $0\alpha\beta$ coordinates in normalized form (4.81). Matrix $\mathbf{E}(\gamma)$ represents the angular displacement (rotation) of stator coordinates with respect to the rotor ones - axis d leads the axis q – like in the synchronous machine model (Fig. 6.3). Transformation of three phase stator and rotor quantities into $0dq$ coordinates is given by the equations:

$$\begin{aligned} \mathbf{i}_{0dq(s)} &= \mathbf{P}^{-1} \cdot \mathbf{i}_{ABC(s)} = \mathbf{E}^{-1}(\gamma) \cdot \mathbf{C}^{-1} \cdot \mathbf{i}_{ABC(s)} \\ \mathbf{i}_{0dq(r)} &= \mathbf{C}^{-1} \cdot \mathbf{i}_{ABC(r)} \end{aligned} \quad (6.57)$$

for currents and, by strict analogy, for other quantities.

Substituting (6.57) to (6.54) we get:

$$\begin{bmatrix} \Psi_{0dq(s)} \\ \Psi_{0dq(r)} \end{bmatrix} = \begin{bmatrix} \mathbf{L}_{0dq(s)} & \mathbf{L}_{0dq(sr)} \\ \mathbf{L}_{0dq(sr)}^T & \mathbf{L}_{0dq(r)} \end{bmatrix} \begin{bmatrix} \mathbf{i}_{0dq(s)} \\ \mathbf{i}_{0dq(r)} \end{bmatrix} \quad (6.58)$$

where:

$$\mathbf{L}_{0dq(s)} = \begin{bmatrix} L_{0s} & & \\ & L_{ds} & \\ & & L_{qs} \end{bmatrix}, \mathbf{L}_{0dq(r)} = \begin{bmatrix} L_{0r} & & \\ & L_{dr} & \\ & & L_{qr} \end{bmatrix}, \mathbf{L}_{0dq(sr)} = \begin{bmatrix} 0 & & \\ & L_{dsr} & \\ & & L_{qsr} \end{bmatrix}.$$

Taking into account the assumed symmetry of stator and rotor windings the equality of the model parameters can be verified:

$$L_{dsr} = L_{qsr} = L_m, L_{ds} = L_{qs} = L_s = L_{sl} + L_m, L_{dr} = L_{qr} = L_r = L_{rl} + L_m \quad (6.59)$$

where: L_{sl} , L_{rl} – stray inductances of the stator and rotor windings unified to the common level.

Resistance matrices in 6.53) can be determined using the transformation matrices $\mathbf{P}(\gamma)$ and \mathbf{C} . Symmetry of the stator and rotor windings implies that:

$$\mathbf{R}_{0dq(s)} = \begin{bmatrix} R_s & & \\ & R_s & \\ & & R_s \end{bmatrix}, \mathbf{R}_{0dq(r)} = \begin{bmatrix} R_r & & \\ & R_r & \\ & & R_r \end{bmatrix} \quad (6.60)$$

where: $R_{A(s)} = R_{B(s)} = R_{C(s)} = R_s$, $R_{A(r)} = R_{B(r)} = R_{C(r)} = R_r$.

Equations (6.53) and (6.54) describe the induction machine model in $0dq$ coordinates attached to rotor. The machine equations for particular coordinates are simple (diagonal parameter matrices) since d i q coordinates are mutually vertical.

Let's consider in more detail the voltage equations of the equivalent stator and rotor circuits for d coordinate:

$$\begin{aligned} u_{ds} &= -R_s i_{ds} - (L_{sl} + L_m) \frac{di_{ds}}{dt} - L_m \frac{di_{dr}}{dt} + \omega((L_{sl} + L_m)i_{qs} + L_m i_{qr}) \\ u_{dr} &= R_r i_{dr} + (L_{rl} + L_m) \frac{di_{dr}}{dt} + L_m \frac{di_{ds}}{dt} \end{aligned} \quad (6.61)$$

Subtraction of (6.61) results in the voltage equation of the equivalent machine circuit along d axis:

$$\begin{aligned} u_{ds} &= -R_s i_{ds} - R_r i_{dr} - L_{sl} \frac{di_{ds}}{dt} - L_{rl} \frac{di_{dr}}{dt} + \omega((L_{sl} + L_m)i_{qs} + L_m i_{qr}) + u_{dr} \\ &= -R_s i_{ds} - R_r i_{dr} - L_{sl} \frac{di_{ds}}{dt} - L_{rl} \frac{di_{dr}}{dt} + \omega(L_s i_{qs} + L_m i_{qr}) + u_{dr} \end{aligned} \quad (6.62)$$

In the similar way the voltage equation along q axis can be derived:

$$u_{qs} = -R_s i_{qs} - R_r i_{qr} - L_{sl} \frac{di_{qs}}{dt} - L_{rl} \frac{di_{qr}}{dt} - \omega(L_s i_{ds} + L_m i_{dr}) + u_{qr} \quad (6.63)$$

and also for zero sequence component:

$$u_{0s} = -R_s i_{0s} - L_{sl} \frac{di_{0s}}{dt}, \quad u_{0r} = -R_r i_{0r} - L_{rl} \frac{di_{0r}}{dt} \quad (6.64)$$

The respective equivalent circuit diagrams are shown Fig. 6.11 in which:

$$i_{dm} = i_{ds} - i_{dr}, \quad i_{qm} = i_{qs} - i_{qr} \quad (6.65)$$

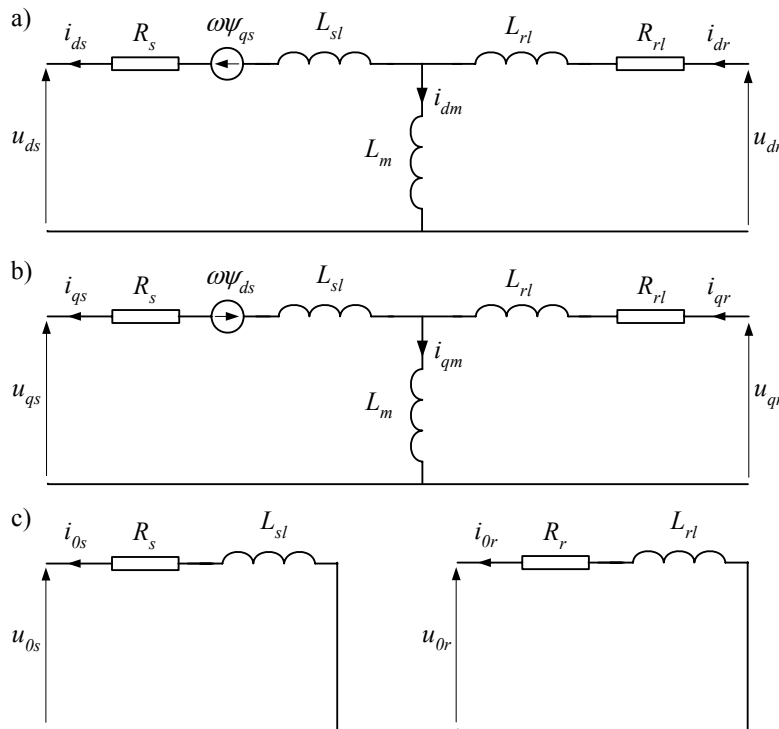


Fig. 6.11. Equivalent circuit diagram of induction machine:
a) for d axis, b) for q axis and c) for zero sequence components

Connection of the discussed model to the model of the external network requires inverse transformation of calculated quantities into phase coordinates as ‘seen’ at the real machine terminals in each simulation step.

In case of slip-ring machines the starting resistance has to be included into the overall rotor resistance. The model equations have to be modified for other than considered number of rotor windings [10, 30].

6.2.3. Electro-mechanical Model

The basic dynamic equation of the rotor mechanical balance is as follows: (compare with (6.29)):

$$J \frac{d\omega_r}{dt} + D\omega_r = T_e - T_m \quad (6.66)$$

where: J – inertia torque of rotating system, ($\text{kg}\cdot\text{m}^2$); D – damping coefficient, ($\text{N}\cdot\text{m}/(\text{rad/s})$); T_m – mechanical torque, ($\text{N}\cdot\text{m}$); ω_r – rotor angular velocity, (rad/s); T_e – electromagnetic torque, ($\text{N}\cdot\text{m}$) (in the air slot).

The electromechanical torque can be determined using (6.36), where: \mathbf{i} denotes vector of stator and rotor phase currents while \mathbf{L} is the complete inductance matrix like in (6.51). In the $0dq$ model the moment can be calculated using the stator and rotor quantities:

$$T_e = p(\psi_{ds}i_{qs} - \psi_{qs}i_{ds}) = p(\psi_{dr}i_{qr} - \psi_{qr}i_{dr}) \quad (6.67)$$

or, after relevant transformation to $0dq$ coordinates, from (6.37). Power transmitted from stator to rotor in induction motor (or in reverse direction in generator) is related to the electromechanical torque by the following equation:

$$P_e = T_e \omega_r = T_e \frac{(1-s)\omega_1}{p} \quad (6.68)$$

The rotor angular position can be determined from the equation:

$$\gamma_r = \int_0^t \omega_r d\tau + \gamma_{r0} \quad (6.69)$$

$T_m > T_e$ for power generator and $T_m < T_e$ if the machine is used as the electric motor.

If the electric motor drives a machine via resilient coupling or elastic shaft then the torque T_w conveyed to the machine being driven is:

$$T_w = T_w(t) = K_w(\gamma_r(t) - \gamma_m(t)) = K_w \int_0^t (\omega_r(\tau) - \omega_m(\tau)) d\tau + T_{w0} \quad (6.70)$$

where: γ_r, γ_m – angular position of rotor and a lumped mass of the machine driven, respectively; K_w – the resilience coefficient of the shaft; $T_{w0} = T_w(0)$.

In such case the compact mechanical system described by (6.66) can be split into two rotating mechanical devices linked by the shaft (Fig. 6.12). Dynamics of the particular devices are then described by the two following equations:

$$J_r \frac{d\omega_r}{dt} + D_r \omega_r = T_e - T_w \quad (6.71)$$

$$J_m \frac{d\omega_m}{dt} + D_m \omega_m = T_w - T_m \quad (6.72)$$

where T_w is like in (6.66).

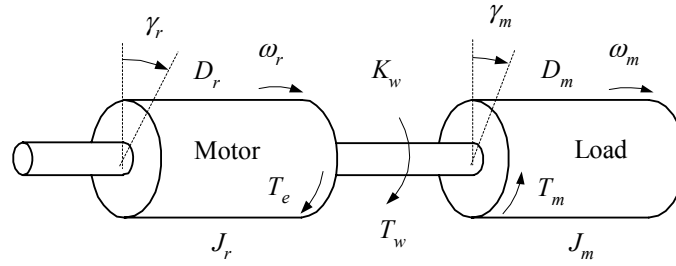


Fig. 6.12. Mechanical system with two rotating masses

In this arrangement the mechanical model of the driving system ‘motor–load’ with elastic link is described by (6.71)–(6.72) and can be extended to the greater number of elements as it is shown for the synchronous generator (6.44). Assuming that the link is stiff ($K_w \rightarrow \infty$) the single mass model is obtained which is described by (6.66) where: $D = D_r + D_m$, $J = J_r + J_m$, $\omega = \omega_r = \omega_m$.

As the model of the electric part of the machine is represented by the adequate electric circuit the same representation can be applied to the mechanical part¹⁴. Note that (6.71)–(6.72) have the same form as the equations of the equivalent electric circuits:

$$C_r \frac{du_r}{dt} + \frac{1}{R_r} u_r = i_e - i_w \quad (6.73)$$

$$C_m \frac{du_m}{dt} + \frac{1}{R_m} u_m = i_w - i_m \quad (6.74)$$

The electric equivalence of (6.70) is obtained in the following way:

$$\frac{1}{K_w} \frac{dT_w}{dt} = \omega_r - \omega_m \leftrightarrow L_w \frac{di_w}{dt} = u_r - u_m \quad (6.75)$$

The analogy between variables and constants in mechanical and the equivalent electrical circuit equations is as shown below:

¹⁴ This approach is applied in ATP–EMTP

inertia torque	J (kg·m ²)	\leftrightarrow	capacitance	C (F);
damping coefficient	D (N·m/(rad/s))	\leftrightarrow	conductance	$1/R$ (1/Ω);
rotation torque	T (N·m)	\leftrightarrow	current	i (A);
angular velocity	ω (rad/s)	\leftrightarrow	voltage	u (V);
resilience coefficient	K (N·m/rad)	\leftrightarrow	1/inductance	$1/L$ (1/H);
angular displacement	γ (rad)	\leftrightarrow	magnetic flux	ψ (V·s).

Thus, the equations (6.73)–(6.75) can be modelled by the electric circuit shown in Fig. 6.13. The current source T_e represents the electric torque which in mechanical model of the machine is described by (6.37) while T_m is the DC current source which corresponds to the constant load torque (1 A = 1 N·m). The values of voltage in the electric circuit correspond to rotation velocities ω_r , ω_m , according to analogy: 1 V \leftrightarrow 1 rad/s.

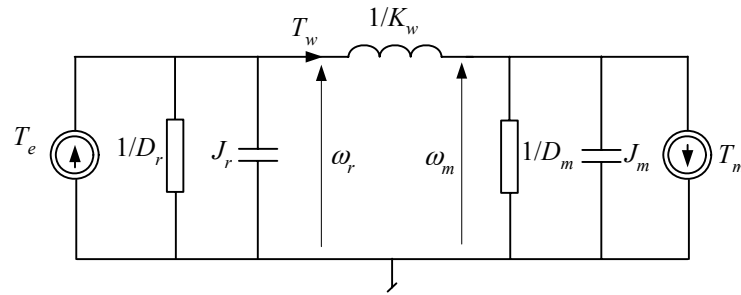


Fig. 6.13. The equivalent electric circuit of the mechanical part of the machine

Example 6.5. Set up the model of the slip-ring induction motor including the equivalent supply network. Examine transients in the motor windings for a single phase break in the supplying network for nominal load conditions.

The motor parameters: $U_N = 6$ kV, 50 Hz, $P_N = 420$ KM¹⁵, $n = 1458$ rot/min (at the nominal load) $\cos\varphi = 0.84$, $s_N = 2.8\%$, $\eta = 97\%$ (power efficiency); the initial torque $T_m = 0.95$ p.u.; inrush current $I_r = 6$ p.u.; $H = 1.1$ s.

The pole pairs number can be calculated from the equation:

$$p = \frac{n_l}{n_e} = \frac{f_1 \cdot 60}{n_e} = \frac{50 \cdot 60}{1500} = 2.$$

In case of electric motors the load torque, the damping coefficient or the inertial torque can be estimated from the motor plate data [33]:

$$T_m = \frac{P}{\omega} = \frac{7023.5 \cdot P(\text{KM})}{n} = \frac{9549.3 \cdot P(\text{kW})}{n} = 2024 \text{ N·m}, \quad n - \text{nominal rotation speed (rot/min)}.$$

¹⁵ 1 KM = 0.73549875 kW for $g = 9.80665$ m/s².

To calculate the detailed motor parameters the Windsyn program can be applied [33]. Using this program for the motor considered we get (notation as in ATPDraw):

LMUD = LMUQ = 0.913927 H (magnetizing inductance for d and q axes),

Lsd = Lsq = Lrd = Lrq = 0.031485 H (stator and rotor inductance for d and q axes),

Rsd = Rsq = 0.613031 Ω (stator resistance for d and q axes),

Rrd = Rrq = 2.33505 Ω (rotor resistance for d and q axes).

$J = 30.06 \text{ kgm}^2$, $D = 1/2.91 \text{ N}\cdot\text{m}/(\text{rad/s})$.

The ATPDraw model of the system considered is shown in Fig. 6.14. The capacitor $30.06 \cdot 10^6 \mu\text{F}$ in the model of the mechanical part represents J , and the voltage drop across the capacitor corresponds to the angular velocity. If the initial rotation velocity is nominal then the initial capacitor voltage is:

$$u(0) = \frac{(1-s)}{p} \omega_1 = \frac{(1-0.028)}{2} 100\pi = 152.7 \text{ V}.$$

The parallel resistor of the value $1/D$ represents the mechanical damping.

Since the motor parameters are determined for the nominal load the current source representing the machine load can be neglected. The current source of very small value is used in the model to meet the calculation procedure requirements only.

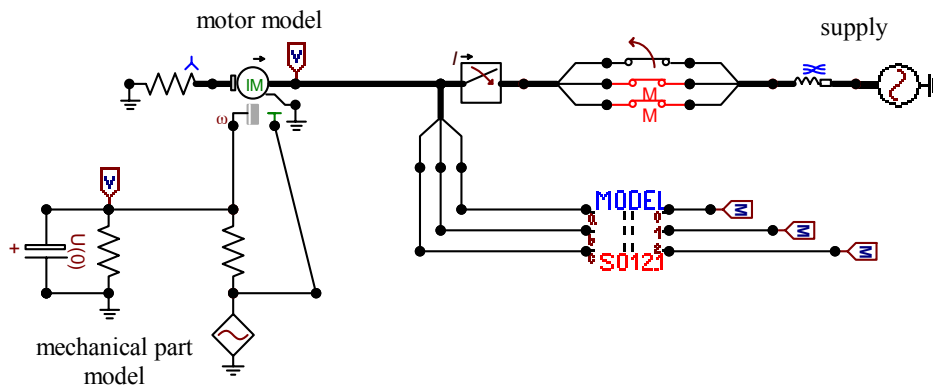


Fig. 6.14. The ATPDraw model of the considered system

The block MODEL (implemented by use of MODELS) is applied to calculation of the motor current symmetrical components.

The rotor current in phase A is shown in Fig. 6.155. The beginning of the waveform refers to the normal operating conditions of the motor (Fig. 6.15a). The rotor current is sinusoidal and has the frequency (1,4 Hz) determined by the slip $(\omega_s - \omega_r)$ value.

When the break in phase A occurs at $t_p = 3 \text{ s}$ the stator electromagnetic field gets distorted due to the supply asymmetry and comprises of two components which rotate in mutually reverse directions. It is the well known effect which is manifested by sudden increase of the r.m.s. value of the rotor current (Fig. 6.15a). The component of double fundamental frequency appears in the rotor current (Fig. 6.15b) and the remarkable increase of the negative sequence

current at the motor terminals is observed (Fig. 6.16b). Practically, the machine slows down (Fig. 6.16a), gets abnormally heated and weaker and can get damaged if not switched off on time.

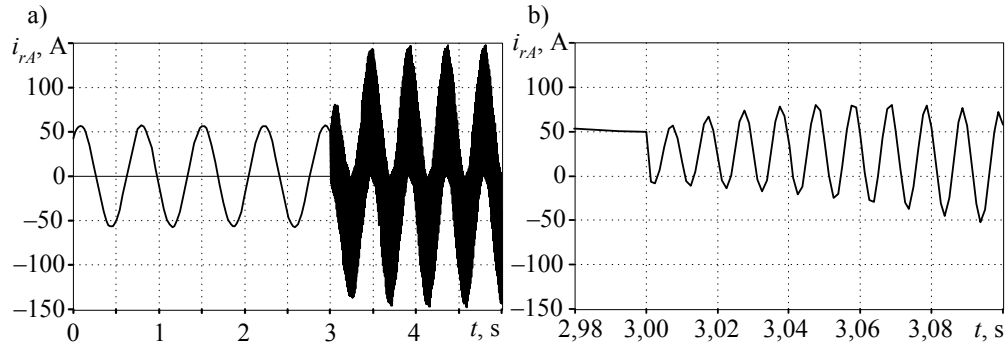


Fig. 6.15. The rotor current waveform: a) in full simulation time span b) right after the phase break occurrence

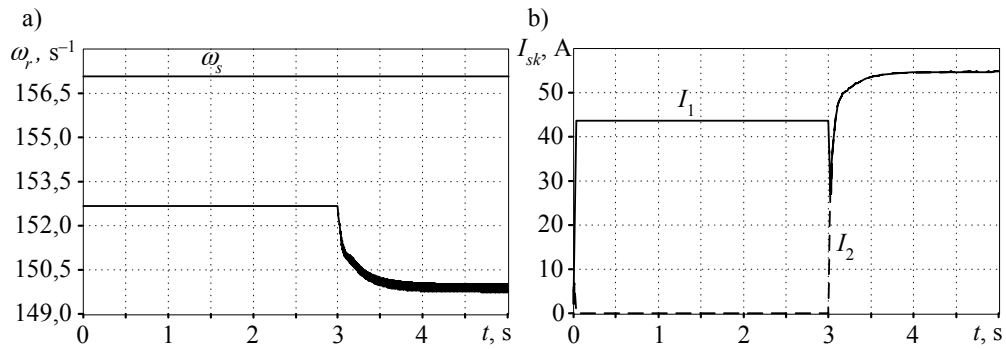


Fig. 6.16. Rotor angular velocity change (a) and the stator current positive I_1 and negative I_2 symmetrical components (b)

6.2.4. Numerical Models

The induction machine models, just like the synchronous ones, can be represented in $0dq$ coordinates (6.53)–(6.54) or in the natural (phase) ones. The same concerns the common solution of the machine and the network equations – the compensation and the prediction method can also be applied for the purpose.

In ATP-EMTP the induction machine models represented in $0dq$ coordinates are implemented in universal machine model. The Type-56 model is the implementation of the machine model in phase coordinates.

6.3. Universal Machine

The Universal Machine term (UM) refers to the general model of the rotating electric machine. The UM concept combines many electric machines which have similar or identical mathematical models. Such an approach results in significant reduction of computer program blocks meant for implementation of numerous machine types. The attached to UM auxiliary programs unify the representation of mechanical devices which cooperate with electric machines and also facilitate the external control of UM. [54].

In ATP–EMTP the block UM contains models of twelve machine types, namely, [7]:

- Synchronous:
 1. 3-phase armature,
 2. 2-phase armature;
- Induction:
 3. 3-phase armature, cage rotor,
 4. 3-phase armature, 3-phase field,
 5. 2-phase armature, cage rotor;
- Single-phase a.c.:
 6. – 1-phase field,
 7. – 2-phase field;
- Direct Current:
 8. – separate excitation,
 9. – series compound field,
 10. – series field,
 11. – parallel compound field,
 12. – parallel field (self-excitation).

The number of item position in the list is also the UM type code, e.g.: UM-3 means 3-phase cage rotor induction machine.

Despite of unified mathematical model the particular implementations may differ in input data format representation and in the initial conditions determination procedures. In ATP–EMTP the UM model connection to the electric network model can be based on compensation or prediction method – the choice is up to the user [7, 24].

Excercises

- 6.1 Basing on the induction machine model operating in steady state (Fig. 6.11)) calculate the equivalent circuit parameters for the cage induction motor. Use the following data:

Nominal power	1.8 MW
Nominal voltage	6 kV
Pole pairs number	4
Power factor	0.9
Nominal slip	1%
Neglect losses.	

- 6.2 Power in stator and rotor for vector model of electric machine are given by:

$$P_s = \frac{2}{3} (u_{sx} i_{sx} + u_{sy} i_{sy}) \approx \frac{2L_s}{3L_m} u_s i_{ry}$$

$$Q_s = \frac{2}{3} (u_{sy} i_{sx} - u_{sx} i_{sy}) \approx \frac{2L_s}{3L_m} u_s (i_{rx} - i_m)$$

for stator and for rotor:

$$P_r = \frac{2}{3} (u_{rx} i_{rx} + u_{ry} i_{ry})$$

$$Q_r = \frac{2}{3} (u_{ry} i_{rx} - u_{rx} i_{ry})$$

Using the relevant model equations estimate how the active rotor power depends on the stator one. Neglect losses.

REFERENCES

1. ALEXANDER R., *Diagonally implicit Runge–Kutta methods for stiff O.D.E.'s*, SIAM Journal on Numerical Analysis, Vol. 14, No. 6 (Dec., 1977), p. 1006–1021.
2. ALVARADO F.L., LASSETER R.H., SANCHEZ J.J., *Testing of trapezoidal integration with damping for the solution of power transient problems*, IEEE Transactions on Power Apparatus and Systems, Vol. PAS-102, No.12, December 1983, p. 3783–3790.
3. AMETANI A. BABA Y., *Frequency-dependent line and cable modeling*, EEUG Course, 27-th September 2000, Wrocław, Poland.
4. ANDERSON P.M., FOUAD A.A., *Power system control and stability*, The Iowa State University Press, Iowa, 1977.
5. ANNAKKAGE U.D., MCLAREN P.G., DIRKS E., JAYASINGHE R.P., PARKER A.D., *A current transformer model based on the Jiles-Atherton theory of ferromagnetic hysteresis*, IEEE Transactions on Power Delivery, Vol. 15, No. 1, January 2000, p. 57–61.
6. ARRILLAGA J., WATSON N., *Computer modeling of electrical power systems*, John Wiley & Sons, Ltd, Chichester, 2001
7. *ATP–EMTP Rule Book*, Canadian/American EMTP User Group, 1987–92.
8. BERGEN A.R., VITTAL V., *Power systems analysis*, Prentice Hall, Upper Saddle River, N.J., 2000.
9. BOLDEA I., *Variable speed generators*, Taylor & Francis Group, Boca Raton, 2006.
10. BOLDEA I., NASAR S.A., *The induction machine handbook*, CRC Press LLC, Boca Raton, 2002.
11. BRANDWAJN V., DOMMEL H.W., DOMMEL I.I., *Matrix representation of three-phase n-winding transformers for steady-state and transient studies*, IEEE Transactions on Power Apparatus and Systems, Vol. PAS-101, No. 6, 1982, p. 1369–178.
12. CAO X., KURITA A., TADA Y., OKAMOTO H., *Type-58 synchronous machine model and related modifications*, EMTP Journal, Vol. 11, 2006, p. 78–84.
13. CAO X., KURITA A., MITSUMA H., TADA Y., OKAMOTO H., *Improvements of Numerical Stability of Electromagnetic Transient Simulation by Use of Phase-Domain Synchronous Machine Models*, Electrical Engineering in Japan, Vol. 128, No. 3, 1999, p. 53–62.
14. CARSON J.R., *Wave propagation in overhead wires with ground return*, Bell Syst. Tech. Journal, Vol. 5, 1926, p. 539–554.
15. CHANDRASENA W., MCLAREN P.G., ANNAKKAGE U.D., JAYASINGHE R.P., MUTHUMUNI D., DIRKS E., *Simulation of hysteresis and eddy current effects in a power transformer*, Proc. Int. Conf. on Power System Transients, IPST 2003, New Orleans, paper 9a-3.
16. CHAUDHARY A.K.S., TAM K.S., PHADKE A.G., *Protection System Representation in the Electromagnetic Transients Program*, IEEE Transactions Power Delivery, Vol. 9, No. 2, April 1994, p. 700–711.
17. CHEN X., *Negative inductance and numerical instability of saturable transformer component in EMTP*, IEEE Transactions on Power Delivery, Vol. 15, No. 4, October 2000, p. 1199–1204.
18. CHUA L.O., LIN P.M., *Computer-Aided Analysis of Electronic Circuits. Algorithms and Computational Techniques*, Prentice-Hall, Inc. Englewood Cliffs, New Jersey, 1975.

19. CLARKE E., *Circuit Analysis of AC Power Systems*, Vol. I. New York, Wiley, 1950.
20. DENNETIÈRE S., MAHSEREDJIAN J., MARTINEZ M., RIOUAL M., XÉMARD A., *On the implementation of a hysteretic reactor model in EMTP*, Proc. Int. Conf. on Power System Transients, IPST 2003, New Orleans, paper 9d-3.
21. DIRECTOR S.W., ROHRER R.A., *Introduction to System Theory*, McGraw-Hill.
22. DOMMEL H.W., *Digital computer solution of electromagnetic transients in single- and multiphase networks*, IEEE Transactions on Power Apparatus and Systems, Vol. PAS-88, April 1969, p. 388–399.
23. DOMMEL H.W., *Nonlinear and time-varying elements in digital simulation of electromagnetic transients*, IEEE Transactions on Power Apparatus and Systems, Vol. PAS-90, November 1971, p. 2561–2567.
24. DOMMEL H.W., *Electromagnetic Transients Program. Reference Manual (EMTP theory book)*, Bonneville Power Administration, Portland, 1986.
25. DOMMEL H.W., *Introduction to the use of MicroTran® and other EMTP versions, Notes used in Graduate Course ELEC 553 'Advanced Power Systems Analysis'*, in: <http://www.ece.ubc.ca/power/e553data/e553.pdf>.
26. DUBÉ L., *Models in ATP. Language manual*, Feb. 1996.
27. DUBÉ L., BONFANTI I., *MODELS. A new simulation tool in the EMTP*, European Transactions on Electrical Power Engineering, Vol. 2, No. 1, January/February 1992, p. 45–50.
28. ДЖУВАРЛЫ Ч.М., ДМИТРИЕВ Е.В., *Применение метода характеристик к решению т-проводной линии электропередач*, Изв. АН СССР, Энергетика и Транспорт, № 1, 1967, p. 48–53 (in Russian).
29. *Electromagnetic Transients Program (EMTP) Workbook*, Electric Power Research Institute, Palo Alto 1986. EL-4651, Research Project 2149-6.
30. FITZGERALD A.E., KINGSLEY C., JR., UMANS S.D., *Electric machinery*, McGraw-Hill, New York, 2003.
31. FORSYTHE G.E., MALCOLM M.A., MOLER C.B., *Computer methods for mathematical computations*, Englewood Cliffs, N.J., Prentice-Hall, Inc., 1977.
32. FORTUNA Z., MACUKOW B., WĄSOWSKI J., *Metody numeryczne*, Warszawa, WNT, 1993.
33. FURST G., *Induction and synchronous motor simulation using ATP/U.M. type 1, 3 and 4. A brief review*, European ATP–EMTP Users Group e.V Meeting, Wrocław, 2000.
34. GALAS G.J., DOYLE J.C., GLOVER K., PACKARD A., SMITH R., *μ -Analysis and Synthesis Toolbox For Use with MATLAB. User's Guide*, The MathWorks, Inc. 1998.
35. GÓMEZ P., URIBE F.A., *The numerical Laplace transform: An accurate technique for analyzing electromagnetic transients on power system devices*, Electrical Power and Energy Systems, 31 (2009), 116–123.
36. GLOVER J.D., SARMA M.S., *Power system analysis and design*, Brooks/Cole, 2002.
37. GOLDBERG S., HORTON W.F., TZIOUVARAS D., *A computer model of the secondary arc in single phase operation of transmission line*, IEEE Transactions on Power Delivery, Vol. 4, No. 1, January 1989, p. 586–595.
38. HAGINOMORI E., *Highly Sophisticated Electric Power Systems*, Japanese ATP User Group, w: <http://gundam.eei.eng.osaka-u.ac.jp/hseps/index.html>.
39. HENSCHER S., IBRAHIM A.I., DOMMEL H.W., *Transmission line model for variable step size simulation algorithms*, Electrical Power and Energy Systems, 21 (1991), p. 191–198.
40. HØIDALEN H.K., SPORILD R., *Modeling of phase-shift zigzag transformers in ATP*, EEUG Meeting, Trondheim, 2004.

41. HØIDALEN H.K., SPORILD R., *Using Zigzag Transformers with Phase-shift to reduce Harmonics in AC-DC Systems*, Proc. Int. Conf. on Power System Transients, IPST 2005, Montreal, IPST05_Paper044.
42. HUMPAGE W.D., *Z-Transform Electromagnetic Transient Analysis in High-Voltage Networks*, Peter Peregrinus Ltd., London, 1982.
43. IBRAHIM A.I., *Frequency dependent network equivalents for electromagnetic transients studies: a bibliographical survey*, Electrical Power and Energy Systems, 25 (2003), p. 193–199.
44. IBRAHIM A.I., HENSCHER S., LIMA A.C., DOMMEL H.W., *Application of a new EMTP line model for short overhead lines and cables*, Electrical Power and Energy Systems, 24 (2002), p. 639–645.
45. *IEEE Standard Common Format for Transient Data Exchange (COMTRADE) for Power Systems*, IEEE Std C37.111–1999.
46. *IEEE Standard Requirements for Instrument Transformers*. IEEE Std C57.13™-2008.
47. *Instrument transformers - Part 1: Current transformers*. International Electrotechnical Commission, International Standard IEC 60044-1, 2003.
48. JACKSON L.B., *Digital filters and signal processing*, Kluwer Academic Publisher, Boston, 1986.
49. КАДОМСКАЯ К.П., ЛЕВИНШТЕЙН М.Л., ШТЕРЕНБЕРГ Г.П., *О решении уравнений длинной линии электропередачи на математических машинах непрерывного и дискретного действия*, Изв. АН СССР, Энергетика и Транспорт, № 4, 1963 (in Russian).
50. KASZTENNY B., ROSOŁOWSKI E., SAHA M.M., HILLSTROM B., *A power transformer model for investigation of protection schemes*, Proc. Int. Conf. on Power System Transients, IPST 1995, Lisbon, Portugal, p. 136–141.
51. KIZILCAY M., PNIOK T., *Digital simulation of fault arcs in power system*, European Transactions on Electric Power, Vol. 1, January 1991, p. 55–60.
52. KIZILCAY M., *Review of solution methods in ATP–EMTP*, EEUG News, Feb–May 2001, p. 25–36.
53. LAGACE P.J., VOUNG M.H., AL-HADDAD K., *A time domain model for transient simulation of synchronous machines using phase coordinates*, Power Engineering Society General Meeting, 2006. IEEE (2006), 6 p.
54. LAUW H.K., MEYER W.S., *Universal machine modeling for representation of rotating electric machinery in an electromagnetic transients program*, IEEE Transactions on Power Apparatus and Systems, Vol. PAS-101, No. 6, June 1982, p. 1342–1351.
55. LEON F.D., SEMLYEN A., *Complete transformer model for electromagnetic transients*, IEEE Transactions on Power Delivery, Vol. 9, No. 1, January 1994, p. 231–239.
56. LIN J., MARTI J.R., *Implementation of the CDA procedures in the EMTP*, IEEE Transactions on Power Systems, Vol. 5, No. 2, May 1990, p. 394–401.
57. MACHOWSKI J., BIALEK J., BUMBY J., *Power System Dynamics, Stability and Control*, New York, John Wiley & Sons, 2008.
58. MARTI J.R., *Accurate modelling of frequency-dependent transmission lines in electromagnetic transient simulations*, IEEE Transactions on Power Apparatus and Systems, Vol. PAS-101, No. 1, January 1982, p. 147–155.
59. MARTI J.R., LIN J., *Suppression of numerical oscillations in the EMTP*, IEEE Transactions on Power Systems, Vol. 4, No. 2, May 1989, p. 739–745.
60. MARTI J.R., LOUIE K.W., *A phase-domain synchronous generator model including saturation effect*, IEEE Transactions on Power Systems, Vol. 12, No. 1, February 1997, p. 222–227.
61. MARTI L., *Low-order approximation of transmission line parameters for frequency-dependent models*, IEEE Transactions on Power Apparatus and Systems, Vol. PAS-102, No. 11, November 1983, p. 3582–3589.

62. MARTI L., *Simulation of transients in underground cables with frequency-dependent modal transformation matrices*, IEEE Transactions on Power Delivery, Vol. 3, No. 3, July 1988, p. 1099–1106.
63. MARTINEZ J.A., *EMTP simulation of a digitally-controlled static var system for optimal load compensation*, IEEE Transactions on Power Delivery, Vol. 10, No. 3, July 1995, p. 1408–1415.
64. MARTINEZ J.A., JOHNSON B., GRANDE-MORAN C., *Parameter determination for modeling system transients – Part IV: Rotating machines*, IEEE Transactions on Power Delivery, Vol. 20, No. 3, July 2005, p. 2063–2072.
65. MARTINEZ J.A. (Ed.), *Power System Transients. Parameter Determination*, CRC Press, Boca Raton, London, 2009.
66. *MATLAB user's guide*, The Math Works Inc., Natick, MA, USA, 2000.
67. MENEMENLIS N., MAHARSI Y.H., *Real-time implementation of a CCVT including a noniterative dynamic hysteresis model*, Second International Conference on Digital Power System Simulators – ICDS '97, Montreal, May 28–30, 1997, p. 111–116.
68. MEYER W.S., DOMMEL H.W., *Numerical modelling of frequency-dependent transmission line parameters in an electromagnetic transients program*, IEEE Transactions on Power Apparatus and Systems, Vol. PAS-93, Sept./Oct. 1974, p. 1401–1409.
69. MORENO P., RAMIREZ A., *Implementation of the numerical Laplace transform: a review*, Task Force on Frequency Domain Methods for EMT Studies, IEEE Transactions on Power Delivery, Vol. 23, No. 4, October 2008, p. 2599–2609.
70. NAJIM F.N., *Circuit simulation*, Wiley-IEEE Press, 2010.
71. NGUYEN H.V., DOMMEL H.W., MARTI J.R., *Direct phase-domain modeling of frequency-dependent overhead transmission lines*, IEEE Transactions on Power Delivery, Vol. 12, No. 3, July 1997, p. 1335–1342.
72. NODA T., NAGAOKA N., AMETANI A., *Phase domain modeling of frequency-dependent transmission lines by means of an ARMA model*, IEEE Transactions on Power Delivery, Vol. 11, No. 1, January 1996, p. 401–411.
73. NODA T., TAKENAKA K., INOUE T., *Numerical integration by the 2-stage diagonally implicate Runge–Kutta method for Electromagnetic Transient Simulation*, IEEE Transactions on Power Delivery, Vol. 24, No. 1, 2009, p. 390–399.
74. OPPENHEIM A.V., SHAFER R.W., BUCK J.R., *Discrete-time Signal Processing*, Prentice-Hall, Inc. Englewood Cliffs, New Jersey, 1999.
75. PRIKLER L., HØIDALEN H.K., *ATPDRAW version 3.5 for Windows 9x/NT/2000/XP. Users' Manual*. SINTEF Energy Research, Norway, 2002.
76. ROSOŁOWSKI E., *Computer Methods for Electromagnetic Transients Analysis*, Oficyna Wydawnicza Politechniki Wrocławskiej, Wrocław 2009 (in Polish).
77. SACHDEV M.S., NAGPAL M., ADU T., *Interactive Software for Evaluating and Teaching Digital Relaying Algorithms*, IEEE Transactions on Power Systems, Vol. 5, No. 1, Feb. 1990, p. 346–352.
78. SAHA M.M., IŻYKOWSKI J., ROSOŁOWSKI E., *Fault Location on Power Networks*, Springer-Verlag London Limited 2010.
79. SIDHU T.S., HFUDA M., SACHDEV M.S., *Generating Relay Models for Protection Studies*, IEEE Computer Applications in Power, Vol. 11, No. 4, Oct. 1998, p. 33–38.
80. SHENKMAN A.L., *Transient Analysis of Electric Power Circuits Handbook*, Springer, Dordrecht 2005.
81. SONG Y.H., AGGARWAL R.K., JONES A.T., *Digital Simulation of Fault Arcs Long-Distance Compensated Transmission Systems with Particular Reference to Adaptive Autoreclose*, European Transactions on Electric Power, Vol. 5, No. 5, Sept/Oct 1995, p. 315–324.
82. STEIGLITZ K., *Introduction to Discrete Systems*, John Wiley & Sons Inc., 1974.

83. STOER J., BULRISCH R., *Introduction to Numerical Analysis*, Springer, New York, 2002.
84. TOKIC A., UGLESIC I., JAKL F., *An algorithm for calculations of low frequency transformer transients*, International Conference on Power Systems Transients – IPST 2003 in New Orleans, USA, paper 9a-2.
85. TRAN-QUOC T., PIERRAT L., MONTMEAT A., KUENY J.L., *Modeling of nonlinear elements in a digital simulator, Part I: Implementation*, Second International Conference on Digital Power System Simulators – ICDS '97, Montreal, May 28–30, 1997, p. 99–104.
86. *Tutorial on Electromagnetic Transient Program Applications to Power System Protection*, IEEE Power Engineering Society, 01TP150, 2000.
87. WATSON N., ARRILLAGA J., *Power systems electromagnetic transients simulation*, The Institution of Electrical Engineers, London, 2003.
88. WATSON N.R., IRWIN G.D., *Electromagnetic transient simulation of power systems using root-matching techniques*, IEE Proc.-Gener. Transm. Distrib. Vol. 145, No. 5, September 1998, p. 481–486.
89. WATSON N.R., IRWIN G.D., *Comparison of root-matching techniques for electromagnetic transient simulation*, IEEE Transactions on Power Delivery, Vol. 15, No. 2, April 2000, p. 629–634.
90. WEDEPOHL L.M., *Application of matrix methods to the solution of travelling wave phenomena in polyphase systems*, Proc. IEE, pt C, Vol. 110 (12) 1963, p. 2200–2212.
91. WEEDY B.M., CORY B.J., *Electric power systems*, John Wiley & Sons, Chichester, 1999.
92. WILCOX D.J., *Numerical Laplace transformation and inversion*, Int. J. Elect. Eng. Educ. 1978, 15, p. 247–265.

Home pages:

93. Alan Philips, <http://www.lancs.ac.uk/staff/steveb/cpaap/pfe/default.htm> – text editor PFE.
94. <http://www.ee.mtu.edu/atp/> – Canadian-American EMTP Users Group.
95. atp-empt@listserv.nodak.edu – ATP-EMTP list server.
96. <http://www.eeug.de> – European EMTP Users Group.
97. <http://www.emtp.org/> – Alternative Transients Program (ATP).
98. <http://www.elkraft.ntnu.no/atpdraw/> – home page of ATPDraw authors.
99. <http://www.emtp.com/> – CEATI International Inc. (EMTP–RV).
100. <http://www.microtran.com> – UBC version (University of British Columbia, Canada).
101. <http://www.pscad.com/> – PSCAD/EMTDC (Manitoba HVDC Research Centre).
102. <http://www.digsilent.de/> – DIGSILENT PowerFactory.
103. <http://etap.com/> – ETAP Enterprise Solution for Electrical Power Systems.
104. <http://www.netomac.com/index.html> – NETOMAC (Siemens).
105. <http://www.rtds.com/> – RTDS (Real Time Digital Simulator).
106. http://www.pes-psrc.org/Reports/APublications_new_format.htm – Publications sponsored by the Power System Relaying Committee IEEE PES (EMTP Tutorial).
107. <http://www.ece.uidaho.edu/ee/power/EE524/> – Johnson Brian K., lecture notes to EE524, ‘Transients in Power Systems’.
108. <http://users.ece.utexas.edu/~grady/courses.html> – Grady W.M., lecture notes and materials.
109. <http://www.pqsoft.com/top/index.htm> – TOP, The Output Processor®, Electrotek Concepts®.
110. <http://www.mathworks.com/> – The MathWorks, Inc.
111. <http://www.ipst.org/> – home page of the International Conference on Power Systems Transients (IPST), many useful publications.
112. <http://gundam.eei.eng.osaka-u.ac.jp/jaug/index-e.htm> – Japanese EMTP Users Group.

INDEX

B

bilinear transformation, 9

D

differential equation, 9

 Euler's approximation, 10

 explicit type algorithm, 10

 Gear algorithm, 11

 implicit type algorithm, 10

 s-domain, 8

 trapezoidal approximation, 11

 z-domain, 8

digital model

 complex branch, 17

 numerical stability, 35

 critical damping adjustment, 37

 root-matching method, 41

discrete model

 frequency properties, 19

E

electric machine, 151

 universal machine, 181

I

induction machine, 169

$0dq$ coordinates, 173

 deep bars rotor, 170

 double feed, 171

 electromechanical torque, 176

 equivalent circuit, 175

 inertia torque, 176

 mathematical model, 171

 mechanical balance, 176

 mechanical model, 177

 rotor angular velocity, 170

slip, 169

squirrel-cage, 169

wound rotor, 170

L

line model

$0\alpha\beta$ transformation, 106

 Bergeron's model, 25

 d'Alembert's solution, 24

 discrete model, 26

 distributed parameters, 98

 Fourier transform, 78, 83

 frequency dependent model, 78, 107

 geometrical data, 75

 lossless model, 25

 lumped parameter model, 91

 multi-phase line, 91

 propagation characteristics, 24

 propagation constants, 82

 steady-state model, 34, 81

 telegraph equations, 23

 transposed line, 93

 untransposed line, 108

long line element, 63

M

Maxwell coefficient, 95

modal components, 99

model

 controlled sources, 18

 lumped parameters, 8

 multi-mass system, 166

 state variables, 67

N

Newton's method, 50

Newton-Raphson's method, 53

nodal method, 28
 conductance matrix, 30
non-linear model, 53
 capacitance, 59
 compensation method, 60
 induction, 57
 network, 60
 piecewise approximation, 64

S

skin effect, 77
solution of the state equation, 72
space vector, 107
state-variable equations, 69
symmetrical components, 97
 impedance matrix, 97
synchronous machine
 inertia torque, 165
synchronous machine
 $0dq$ coordinates, 152, 159
 electromagnetic torque, 164
 functional diagram, 151
 inertia torque, 164
 Park transformation, 156
 saturation effect, 163

synchronous machine
 mechanical torque, 166
synchronous machine
 calculation algorithm, 167
synchronous machine
 phase coordinates model, 168

T

transformation matrix, 99
transformer
 autotransformer, 125
 equivalent circuit, 123
 hysteresis losses, 116
 magnetic circuit, 126
 magnetizing characteristic, 126
 model
 ATP-EMTP, 135
 multi-winding, 121, 140
 three winding, 123
 three-phase, 132
 winding arrangement, 132
 zig-zag, 145
 two-port circuit, 117
 two-winding, 114

